# Patient-Specific Numerical Modeling in Transcatheter Aortic Valve Replacement: Towards a More Effective Treatment

## Patiëntspecifieke numerieke modellering voor minimaal invasieve aortaklepvervangingen: de weg naar een effectievere behandeling

Giorgia Rocatello

Promotoren: prof. dr. ir. P. Segers, dr. ir. P. Mortier
Proefschrift ingediend tot het behalen van de graad van
Doctor in de ingenieurswetenschappen: biomedische ingenieurstechnieken

UNIVERSITEIT
GENT

Vakgroep Elektronica en Informatiesystemen
Voorzitter: prof. dr. ir. K. De Bosschere
Faculteit Ingenieurswetenschappen en Architectuur
Academiejaar 2018 - 2019

ISBN 978-94-6355-225-7
NUR 954
Wettelijk depot: D/2019/10.500/33

**Supervisors:**

Prof. dr. ir Patrick Segers
Dr. ir. Peter Mortier

**Research Lab:**

Institute Biomedical Technology
Biofluid, Tissue and Solid Mechanics for Medical Application
(bioMMeda)
Ghent University
Corneel Heymanslaan 10 – Entrance 36
B-9000 Gent
Belgium

**Members of the exam committee:**

| | |
|---|---|
| *Chairman:* | |
| Ereprof. dr. ir. Ronny Verhoeven | Faculty of Engineering and Architecture, Ugent |
| *Secretary:* | |
| Prof. dr. ir. Pascal Verdonck | Faculty of Engineering and Architecture, Ugent |
| *Reading committee:* | |
| Prof. dr. ir. Wim Van Paepegem | Faculty of Engineering and Architecture, Ugent |
| Prof. dr. ir. Nele Famaey | Faculty of Engineering and Architecture, Ugent |
| Prof. dr. ir. Alberto Redaelli | Politecnico di Milano, Italy |
| Dr. ir. Monica Achiluzzi | LivaNova, Italy |
| Prof. dr. Peter de Jaegere | Erasmus Medical Center, Rotterdam |

# TABLE OF CONTENTS

**Table of contents** i

**List of Figures** vii

**List of Tables** xi

**Abbreviations and symbols** xiii

**Preface** xvii

**Samenvatting** xix

**Summary** xxv

**Introduction** xxxi

**I Background** 1

---

**1 Aortic valve: anatomy, pathology and treatments** 3
- 1.1 Anatomy and physiology of the aortic valve . . . . . . . . . . 3
  - 1.1.1 Bicuspid aortic valve . . . . . . . . . . . . . . . . . . . . 6
- 1.2 Aortic stenosis: a silent killer . . . . . . . . . . . . . . . . . . . 7
- 1.3 Treatment of aortic stenosis . . . . . . . . . . . . . . . . . . . . 10
  - 1.3.1 Surgical aortic valve replacement (SAVR) . . . . . . . 10
    - 1.3.1.1 Prosthetic aortic valves . . . . . . . . . . . 10
  - 1.3.2 Transcatheter aortic valve replacement (TAVR) . . . 13
    - 1.3.2.1 Prosthetic transcatheter aortic valves . . . 14
  - 1.3.3 TAVR versus SAVR: evidence of benefits in clinical trials . . . . . . . . . . . . . . . . . . . . . . . . . 17
    - 1.3.3.1 Randomized clinical trials . . . . . . . . . 17
    - 1.3.3.2 Other relevant clinical studies . . . . . . . 20
  - 1.3.4 To operate now or to wait? . . . . . . . . . . . . . . . 20
  - 1.3.5 TAVR Market Share . . . . . . . . . . . . . . . . . . . 21

2 **Insight into transcatheter aortic valve replacement: planning and complications** **23**

2.1 The crucial role of imaging techniques during TAVR . . . . . 23

2.1.1 Valve sizing . . . . . . . . . . . . . . . . . . . . . . . . . . 23

2.1.2 Pre-procedural imaging techniques . . . . . . . . . . 24

2.1.3 Peri-procedural imaging techniques . . . . . . . . . . 26

2.2 TAVR complications . . . . . . . . . . . . . . . . . . . . . . . . . 26

2.2.1 Conduction abnormalities: the first TAVR Achille's heel . . . . . . . . . . . . . . . . . . . . . . . . . . . . 32

2.2.1.1 Physiology of the conduction system of the heart . . . . . . . . . . . . . . . . . . . . . 32

2.2.1.2 Relationship between the aortic valve and the atrioventricular conduction system . . 32

2.2.1.3 Type of conduction abnormalities following TAVR . . . . . . . . . . . . . . . . . . 33

2.2.1.4 Diagnosis of conduction abnormalities . . 36

2.2.1.5 Management of conduction abnormalities: permanent pacemaker implantation . 39

2.2.1.6 Predictors for conduction abnormalities . 39

2.2.2 Aortic regurgitation: the second TAVR Achille's heel 40

2.2.2.1 Types of aortic regurgitation and main causes . . . . . . . . . . . . . . . . . . . . . 40

2.2.2.2 Diagnosis of residual paravalvular aortic regurgitation . . . . . . . . . . . . . . . . . 41

2.2.2.3 Management of paravalvular aortic regurgitation . . . . . . . . . . . . . . . . . . . . 44

2.2.2.4 Predictors for paravalvular aortic regurgitation . . . . . . . . . . . . . . . . . . . . 44

3 **Numerical simulations in TAVR** **47**

3.1 The role of numerical simulations . . . . . . . . . . . . . . . . 47

3.2 Building a patient-specific numerical simulation of TAVR . . 50

3.2.1 Geometry of the anatomy . . . . . . . . . . . . . . . . 50

3.2.2 Constitutive laws for the soft tissues . . . . . . . . . . 51

3.2.3 TAV devices . . . . . . . . . . . . . . . . . . . . . . . . 55

3.2.4 TAV deployment strategy . . . . . . . . . . . . . . . . 57

3.2.5 The fluid domain . . . . . . . . . . . . . . . . . . . . . 57

3.3 TAVR computer modelling and clinical consideration . . . . 59

3.4 TAVIguide . . . . . . . . . . . . . . . . . . . . . . . . . . . . . . 67

3.4.1 The patient-specific anatomy . . . . . . . . . . . . . . 67

3.4.2 Available TAVR devices . . . . . . . . . . . . . . . . . 67

3.4.3 FEA computer simulation and output variables . . . 68

3.4.4 CFD computer simulation and output variables . . . 68
3.4.5 TAVIguide studies outside the PhD thesis . . . . . . 68
3.4.6 Studies performed within the PhD thesis . . . . . . . 69

**II Computer simulation: prediction of TAVR complication 73**

**4 Patient-specific computer simulation to predict new conduction abnormalities after TAVR 75**
4.1 Introduction . . . . . . . . . . . . . . . . . . . . . . . . . . 75
4.2 Materials and methods . . . . . . . . . . . . . . . . . . . . 76
4.2.1 Study population . . . . . . . . . . . . . . . . . . . . 76
4.2.2 Computer simulations . . . . . . . . . . . . . . . . . . 76
4.2.3 Pressure analysis . . . . . . . . . . . . . . . . . . . . 77
4.2.4 Statistical analysis . . . . . . . . . . . . . . . . . . . 79
4.3 Results . . . . . . . . . . . . . . . . . . . . . . . . . . . . . 80
4.3.1 Mesh sensitivity analysis of the aortic root model . . 80
4.3.2 Clinical outcome . . . . . . . . . . . . . . . . . . . . 81
4.3.2.1 Contact pressure on the LVOT in the region of interest . . . . . . . . . . . . . . . . 83
4.4 Discussion . . . . . . . . . . . . . . . . . . . . . . . . . . . 88
4.5 Conclusions . . . . . . . . . . . . . . . . . . . . . . . . . . 90

**5 Effect of commissural alignment on paravalvular regurgitation after TAVR 91**
5.1 Introduction . . . . . . . . . . . . . . . . . . . . . . . . . . 91
5.2 Material and methods . . . . . . . . . . . . . . . . . . . . . 92
5.2.1 Study population . . . . . . . . . . . . . . . . . . . . 92
5.2.2 AR Assessment . . . . . . . . . . . . . . . . . . . . . 92
5.2.3 Analysis & Statistics . . . . . . . . . . . . . . . . . . 93
5.3 Results . . . . . . . . . . . . . . . . . . . . . . . . . . . . . 94
5.3.1 AR prediction . . . . . . . . . . . . . . . . . . . . . . 94
5.3.2 Frame deformation . . . . . . . . . . . . . . . . . . . 95
5.3.3 Frame alignment . . . . . . . . . . . . . . . . . . . . 97
5.4 Discussion . . . . . . . . . . . . . . . . . . . . . . . . . . . 99
5.5 Conclusions . . . . . . . . . . . . . . . . . . . . . . . . . . 100

**6 The impact of size and position of a mechanical expandable transcatheter aortic valve 101**
6.1 Introduction . . . . . . . . . . . . . . . . . . . . . . . . . . 101
6.2 Materials and methods . . . . . . . . . . . . . . . . . . . . 103
6.2.1 Study population . . . . . . . . . . . . . . . . . . . . 103

6.2.2 Computer modelling . . . . . . . . . . . . . . . . . . . 103
6.2.3 Data analysis . . . . . . . . . . . . . . . . . . . . . . 105
6.2.4 Statistical analysis . . . . . . . . . . . . . . . . . . . 106
6.3 Results . . . . . . . . . . . . . . . . . . . . . . . . . . . . 106
6.3.1 Postoperative AR . . . . . . . . . . . . . . . . . . . . 107
6.3.2 Postoperative conduction abnormalities . . . . . . . 107
6.3.3 Analysis of patients with equivocal aortic root dimensions . . . . . . . . . . . . . . . . . . . . . . . . . 108
6.4 Discussion . . . . . . . . . . . . . . . . . . . . . . . . . . 111
6.5 Conclusions . . . . . . . . . . . . . . . . . . . . . . . . . 115

**7 Optimization of a TAV frame using patient-specific computer simulations 117**
7.1 Introduction . . . . . . . . . . . . . . . . . . . . . . . . . 117
7.2 Material and methods . . . . . . . . . . . . . . . . . . . . 119
7.2.1 Patient-specific aortic root model . . . . . . . . . . . 119
7.2.2 Computer simulation strategy and output variables . 121
7.2.3 Experimental design . . . . . . . . . . . . . . . . . . 123
7.2.4 Response surface methodology . . . . . . . . . . . . 125
7.2.5 Optimization strategy . . . . . . . . . . . . . . . . . 126
7.3 Results . . . . . . . . . . . . . . . . . . . . . . . . . . . . 127
7.3.1 Mesh sensitivity analysis of the device model . . . . . 128
7.3.2 Goodness of fit . . . . . . . . . . . . . . . . . . . . . 129
7.3.3 Effects of the geometrical parameters . . . . . . . . . 130
7.3.4 Optimization results . . . . . . . . . . . . . . . . . . 132
7.4 Discussion . . . . . . . . . . . . . . . . . . . . . . . . . . 134
7.5 Conclusions . . . . . . . . . . . . . . . . . . . . . . . . . 137

**III Conclusions 139**

**8 Conclusions and future perspectives 141**
8.1 Conclusions . . . . . . . . . . . . . . . . . . . . . . . . . 141
8.1.1 Clinical investigation using computational modeling 142
8.1.2 Optimization of new devices . . . . . . . . . . . . . . 143
8.2 Considerations and future perspective . . . . . . . . . . . . 144

**IV Appendices 149**

**A Model implementation step-by-step 151**

**B Rationale behind the CoreValve System design** **157**

**Bibliography** **159**

# LIST OF FIGURES

1.1 Heart main components . . . . . . . . . . . . . . . . . . . . . . . . 4
1.2 Aortic root components . . . . . . . . . . . . . . . . . . . . . . . 5
1.3 Aortic valve leaflet structure . . . . . . . . . . . . . . . . . . . . 6
1.4 Classification of bicuspid aortic valve . . . . . . . . . . . . . . . 7
1.5 Healthy and stenotic aortic valve anatomy . . . . . . . . . . . . . 8
1.6 Curve of prognosis for aortic stenosis . . . . . . . . . . . . . . . 9
1.7 Steps of surgical aortic valve replacement . . . . . . . . . . . . . 11
1.8 Prosthetic aortic valves . . . . . . . . . . . . . . . . . . . . . . . 12
1.9 Steps of transcatheter aortic valve replacement . . . . . . . . . . 13
1.10 Prosthetic transcatheter aortic valves . . . . . . . . . . . . . . . 15
1.11 TAVR Market size . . . . . . . . . . . . . . . . . . . . . . . . . . 22
1.12 TAVR Market share . . . . . . . . . . . . . . . . . . . . . . . . . 22

2.1 Preprocedural imaging . . . . . . . . . . . . . . . . . . . . . . . . 26
2.2 Peri-procedural imaging . . . . . . . . . . . . . . . . . . . . . . . 27
2.3 Anatomy of the cardiac conduction system . . . . . . . . . . . . . 33
2.4 Schematic view of the Koch's triangle . . . . . . . . . . . . . . . . 34
2.5 Histological section and schematic view of the AV conduction system . . . . . . . . . . . . . . . . . . . . . . . . . . . . . . . . . 34
2.6 Schematic representation of the $1^{st}$ degree AVB . . . . . . . . . 35
2.7 Echocardiogram tracing . . . . . . . . . . . . . . . . . . . . . . . . 37
2.8 Normal and abnormal ECG tracing . . . . . . . . . . . . . . . . . . 38
2.9 Types of aortic regurgitation . . . . . . . . . . . . . . . . . . . . . 41
2.10 Imaging to assess the degree of aortic regurgitation . . . . . . . . 43

3.1 Reconstruction of native aortic valve leaflets . . . . . . . . . . . . 51
3.2 Reconstruction of device leaflets as proposed by Auricchio et al. [168] . . . . . . . . . . . . . . . . . . . . . . . . . . . . . . . . . 56
3.3 Reconstruction of device leaflets as proposed by Bailey et al. [172] 56
3.4 Effect of valve positioning on stress distribution . . . . . . . . . . 60
3.5 Summary of the CoreValve device positions within the patient's aortic valve model . . . . . . . . . . . . . . . . . . . . . . . . . . 61

3.6 Effect of valve positioning on stress distribution in the interleaflet triangle between RCC and NCC . . . . . . . . . . . . . . . . . . . 62
3.7 Paravalvular gaps between the SAPIEN device and the patient's aortic root anatomy . . . . . . . . . . . . . . . . . . . . . . . . . . 63
3.8 Blood flow after CoreValve implantation . . . . . . . . . . . . . . 65
3.9 Deformation of the CoreValve and SAPIEN device within the patient's aortic root model . . . . . . . . . . . . . . . . . . . . . . . . 70
3.10 Comparison between the predicted and the clinically assessed AR after implantation of a CoreValve device . . . . . . . . . . . . 71

4.1 Identification of anatomical landmarks and computer modelling workflow . . . . . . . . . . . . . . . . . . . . . . . . . . . . . . . 78
4.2 Anatomical variability of the IBMS . . . . . . . . . . . . . . . . . 79
4.3 Computational time vs mesh density . . . . . . . . . . . . . . . . 80
4.4 Histograms and box plot diagrams of valve implantation depth, maximum contact pressure and contact pressure index . . . . . . 83
4.5 Contact pressure: representative examples . . . . . . . . . . . . . 84
4.6 Correlation graph between predictors of new conduction abnormalities . . . . . . . . . . . . . . . . . . . . . . . . . . . . . . . . 85
4.7 Representative cases with no contact within the region of interest 86
4.8 ROC curves of maximum contact pressure and contact pressure index . . . . . . . . . . . . . . . . . . . . . . . . . . . . . . . . . 87
4.9 3D bar graph showing the prediction of conduction abnormalities according to the maximum contact pressure and contact pressure index . . . . . . . . . . . . . . . . . . . . . . . . . . . 87
4.10 Representative examples of high IBMS . . . . . . . . . . . . . . . 89

5.1 Description of the steps followed for prediction of AR . . . . . . 93
5.2 Alignment between bioprosthetic and native leaflets . . . . . . . 94
5.3 Comparison between predicted AR and AR based on echocardiography and angiography . . . . . . . . . . . . . . . . . . . . . . . 96
5.4 Frame deformation in four patients with moderate or severe AR post-TAVR . . . . . . . . . . . . . . . . . . . . . . . . . . . . . . . 96
5.5 frame eccentricity in patients with (a) angiography- and (b) echocardiography-based AR grade 0-I and AR grade II-III-IV . 98
5.6 Case illustration showing predicted AR in the align and misaligned scenario . . . . . . . . . . . . . . . . . . . . . . . . . . . . . 98

6.1 Computer modelling of the implantation of a Lotus valve . . . . 105
6.2 Study population . . . . . . . . . . . . . . . . . . . . . . . . . . . . 106
6.3 Box plot graphs of predicted AR, maximum contact pressure and contact pressure index . . . . . . . . . . . . . . . . . . . . . . . 107

6.4 3D bar graph representing the prediction of conduction abnormalities according to the maximum contact pressure and contact pressure index . . . 108
6.5 Impact of device positioning and device size on the contact pressure 109
6.6 Predicted AR, maximum contact pressure and contact pressure index distribution in case of high/low implantation depth or large/small valve size . . . 110
6.7 Representative example showing the impact of device size on the contact pressure . . . 111
6.8 Representative example of patients at risk of coronary occlusion 114

7.1 Parametric CoreValve-like design . . . 120
7.2 Computer simulation strategy . . . 122
7.3 Designs of the frame . . . 124
7.4 Qualitative RSM results . . . 125
7.5 Pipeline of this study. . . . 127
7.6 Radial force nitinol frame . . . 128
7.7 Quality RSM models . . . 130
7.8 RSM contour plots . . . 131
7.9 Representative examples . . . 131
7.10 Optimization history of the objectives-function. . . . 133
7.11 Optimal frame design. . . . 134
7.12 Comparison of performance between the optimized and initial designs. . . . 134

A.1 Diagram representing the iterative process of material calibration 153

B.1 Rationale of the CoreValve design . . . 158
B.2 Target position of the CoreValve Evolut R . . . 158

# LIST OF TABLES

1.1 Classification of AS severity. . . . . . . . . . . . . . . . . . . . . . 9

2.1 Chart currently used to size the CoreValve Evolut R device. . . . 24
2.2 TAVR common complications derived from available clinical trials and clinical studies . . . . . . . . . . . . . . . . . . . . . . . . 30
2.3 Unifying 5-class grading scheme proposed by Pibarot et al. Only the parameters that are most frequently used to grade the severity of paravalvular AR are reported. Adapted from [150]. . . . . . . . 46

3.1 Overview of patient-specific numerical simulation of TAVR performed from 2011 to 2018. . . . . . . . . . . . . . . . . . . . . . . . 49
3.2 Summary of the software adopted in each study: from patient-specific geometry reconstruction to simulation. Some relevant modeling aspects are also reported. Information that was not applicable or clearly reported in the manuscript, is here indicated with a dash ('-'). . . . . . . . . . . . . . . . . . . . . . . . . . . . 53
3.3 Summary of the material models adopted in each patient-specific study. A dash ('-') indicates that the native calcified leaflets were not included in the model. . . . . . . . . . . . . . . . . . . . . . . 54

4.1 Mesh sensitivity analysis of the aortic wall model. The selected mesh is highlighted in bold. . . . . . . . . . . . . . . . . . . . . . 80
4.2 Impact of the aortic wall mesh size on the predicted frame morphology at four predefined levels of the frame. In the second column the maximum relative difference respect to the finest mesh is reported. . . . . . . . . . . . . . . . . . . . . . . . . . . . 81
4.3 Characteristics of the study population . . . . . . . . . . . . . . . 82
4.4 Simulation results . . . . . . . . . . . . . . . . . . . . . . . . . . . 84
4.5 Results of the logistic regression for association with post-TAVR conduction abnormalities . . . . . . . . . . . . . . . . . . . . . . . 85

5.1 Baseline characteristics . . . . . . . . . . . . . . . . . . . . . . . . 95
5.2 Procedural characteristics . . . . . . . . . . . . . . . . . . . . . . . 97

5.3 Predicted AR [ml/s] in patients with AR grade 0-1 and 2-3 (angiography, echo) . . . . . . . . . . . . . . . . . . . . . . . . . . . . 97

6.1 Sensitivity, specificity, positive and negative predicted values and accuracy for computer simulations predicted outcomes. . . . . . 107

7.1 Frame reference adopted geometrical parameters. . . . . . . . . . 120
7.2 Nitinol material parameters for modeling the frame behavior [174]. 121
7.3 Patients selected for the study. The 'received device' column refers to the device that was implanted in each patient during TAVR. The last two columns report clinical outcomes in form of paravalvular AR and conduction abnormalities. '-' indicates that no conduction abnormalities occurred after TAVR. . . . . . . . . 122
7.4 Tested levels of experimental variables $X_1$ and $X_2$in the initial design space. . . . . . . . . . . . . . . . . . . . . . . . . . . . . 124
7.5 Tested levels of experimental variables $X_1$ and $X_2$in the refined design space. . . . . . . . . . . . . . . . . . . . . . . . . . . . . 125
7.6 Mesh sensitivity analysis of the device model. The selected mesh is highlighted in bold. . . . . . . . . . . . . . . . . . . . . . . . . 129
7.7 Quality of the RSM models. . . . . . . . . . . . . . . . . . . . . . . 129

A.1 Optimal material parameters from the calibration analysis. . . . 153

# Abbreviations and symbols

The following list summarizes the most commonly used abbreviations and symbols in this thesis.

## Abbreviations

| | |
|---|---|
| AKI | Acute kidney injury |
| AoV | Aortic valve |
| AP | Anteroposterior |
| AR | Aortic regurgitation |
| AS | Aortic stenosis |
| AUC | Area under the receiver-operator characteristics curve |
| AV | Atrioventricular |
| AVB | Atrioventricular block |
| AVR | Aortic valve replacement |
| BAV | Bicuspid aortic valve |
| BSA | Body surface area |
| CAGR | Compounded average growth rate |
| CCD | Central composite design |
| CE | Conformité europé en |
| CFD | Computational fluid dynamics |
| CI | Confidence interval |
| CS | Coronary sinus |
| DBP | Diastolic blood pressure |
| ECG | Echocardiogram |
| FDA | Food and drug administration |
| FEA | Finite element analysis |
| FO | Fossa ovalis |
| FSI | Fluid-structure interactions |
| IBMS | Inferior border of the membranous septum |
| IQR | Interquartile range |
| LAT | Lateral |
| LBB | Left bundle branch |

| | |
|---|---|
| LBBB | Left bundle branch block |
| LCC | Left- coronary cusp |
| LV | Left ventricle |
| LVEDP | Left ventricular end-diastolic pressure |
| LVOT | Left ventricular outflow tract |
| MDCT | Multidetector computer tomography |
| MRI | Magnetic resonance imaging |
| NCC | Non- coronary cusp |
| NPV | Negative predictive value |
| PPM | Permanent pacemaker |
| PPV | Positive predictive value |
| RBB | Right bundle branch |
| RCC | Right- coronary cusp |
| RF | Regurgitant fraction |
| ROC | Receiver-operating characteristics |
| RSM | Response surface model |
| SA | Sinoatrial |
| SAVR | Surgical aortic valve replacement |
| SBP | Systolic blood pressure |
| SD | Standard deviation |
| SL | Septal leaflet of the tricuspid valve |
| TAV | Transcatheter aortic valve |
| TAVR | Transcatheter aortic valve replacement |
| TEE | Transesophageal echocardiography |
| TTE | Transthoracic echocardiography |
| VARC | Valve Academic Research Consortium |

## Symbols

| | | |
|---|---|---|
| $\alpha$ | Angle between the inferior border of the membranous septum and the annular plane | [$^o$] |
| $\lambda$ | Distance from the center of the design space to the fractional factorial points | [-] |
| $\mu$ | Viscosity of the fluid | [Pa s] |
| $\nu$ | Poissons's ratio | [-] |
| $\rho$ | Density of the fluid | [kg/$m^3$] |
| $\sigma_L^E$ | End of transformation loading | [Pa] |
| $\sigma_L^S$ | Start of transformation loading | [Pa] |
| $\sigma_U^E$ | End of transformation unloading | [Pa] |
| $\sigma_U^S$ | Start of transformation unloading | [Pa] |
| $\varepsilon^L$ | Maximum transformation strain | [%] |

|  |  |  |
|---|---|---|
| $\varepsilon_r$ | Interpolation error | [-] |
| $\varepsilon_V^L$ | Maximum volumetric transformation strain | [%] |
| $E$ | Young's modulus | [Pa] |
| $E^A$ | Austenite elastic modulus | [Pa] |
| $E^M$ | Martensite elastic modulus | [Pa] |
| $R$ | Spearman coefficient of correlation | [-] |
| $R^2$ | Coefficient of determination | [-] |
| $w$ | Weight factor | [-] |

# PREFACE

*Non mi giudicate per i miei successi ma*
*per tutte quelle volte che sono caduto e*
*sono riuscito a rialzarmi.*
*Do not judge me by my successes, judge*
*me by how many times I fell down and got*
*back up again.*
*Nelson Mandela*

Time flies, how true is that! About 5 years ago I came to Gent to work on my master thesis and, at that moment, I had never thought that this would have been just the starting of a long, fantastic, prosperous and rewarding life experience. Fortunately, this journey is not over yet, I am still in Gent and now close to another big achievement: the PhD degree! When I turn to look back at those last years, there are many people I would like to thank.

First of all I have to thank my supervisor Patrick, the first person that I met in Gent, for giving me this opportunity (twice) and being always very fast in providing feedbacks to manuscripts, abstracts, presentations and much more. Many thanks to Peter and Matthieu to believe in me since the first moment and finally welcome me in their team. Especially to Peter, he has always been very positive about what I was doing and he always had few minutes to listen to me and to advise me.

Thanks to the jury members of this PhD committee for their time, interest in this research and the valuable comments and revision of my PhD thesis.

Many thanks to all my colleagues at bioMMeda and at FEops for the coffee breaks, the endless chats, for listening to all my complains and sharing my (dis-)adventures. Among them, thanks to Alessio for being my 'twin brother' in the first years in Gent. Federico and Viviana, for the chats in the corridor and for all the coffee pads you generously shared with me =) Daniela, the atmosphere at the office would not have been so nice without you and your humor. Thanks for taking care of me during our trip in Creta, I am looking forward the next trip! Annette, many thanks for all the help and support in the last stressful period. Nic, Sander, Alessandra, Gianluca, Elisa,

you made sure that my blood sugar level was never too low. Oreos, cakes and ice-creams have been very much appreciated! Many thanks to Fady for your support 24/7. Even though I hard tested you, you have always found a solution to all my tricky issues with smile and very much patience.

Many thanks to all my friends, it is because of all of you that I enjoy my time in Belgium.

In particolare, un ringraziamento alla big Italian community di Gent. Raffa, Alessio, Francesco, Domenico, Michela, Chiara, Anna, Vincenzo….. incontrare voi e' stato come sentirsi a casa. Grazie per tutto il tempo trascorso assieme, i cotechini, il limoncello, le cene, le feste, il beach volley, le serate…. E soprattutto per tutte le risate!!! Francesco: un collega, un amico e spesso un secondo fratello maggiore. Mi hai insegnato molto, forse troppo!

Muchas gracias a Minerva, Amparo, Trompi, Gonzalo, los vagos, los rajadores y a todos los espanoles que siguen en Gante y que ya se han ido, por haberme adoptada.

Thanks to my volleyball teammates for the warm welcome and their endorsement of my freak-out moments.

Un speciale ringraziamento va alla mia famiglia che ha vissuto con me le 'montagne russe' di questi anni e mi ha sempre supportata nelle mie scelte soffrendo in silenzio per la distanza. Mamma, papa', Mauri, grazie per i valori che mi avete trasmesso, per aver sempre creduto in me e per esserci sempre. Siete per me un grande esempio e spero di rendervi orgorgliosi!

Grazie ai miei amici rodigini, e in particolare all'Antonellina che 'se Maometto non va alla montagna, la montagna va da Maometto' fa sempre in modo che non passino troppi mesi tra una visita e l'altra, dimostrandomi che l'amicizia vera abbatte qualsiasi confine, anche 1200 km di distanza!

Infine grazie a Pepe, il mio compagno di viaggio. Sei per me un esempio di perserveranza, motivo di confronto e crescita continua. Quest'ultimo periodo non dev'essere stato semplice starmi vicino, ma tu ci sei stato sempre. Sei stato la mia spalla quotidiana, il mio porto sicuro, supportandomi e sopportandomi ogni giorno. Incontrarti e' stata forse la cosa piu' bella che questa esperienza in Belgio mi abbia regalato.

# SAMENVATTING

## INLEIDING

Aortaklepstenose is één van de meest voorkomende kleppathologiein in westerse landen. De vernauwing belemmert de bloedstroom vanuit het linkerventrikel en leidt tot een verhoogde ventriculaire bloeddruk, linkerventrikelhypertrofie en kan uiteindelijk resulteren in hartfalen. De progressie van deze afwijking kan niet worden afgeremd en een hartklepvervanging is daarom noodzakelijk bij ernstige aortaklepstenose. De traditionele chirurgische klepvervanging is een zware ingreep die voor zwakke patiënten hoge risico's meebrengt. Voor deze patiënten is de minimaal invasieve aortaklepvervanging (TAVR) een beter alternatief. Ook bij TAVR zijn er nog enkele veel voorkomende complicaties zoals aorta regurgitatie (AR) en geleidingsstoornissen, die gelinkt zijn met een verhoogde mortaliteit.

Medische beeldvorming zoals MDCT en echocardiografie zijn cruciaal tijdens het plannen van TAVR. Deze beeldvormingstechnieken leveren kwantitatieve informatie over de anatomie, die noodzakelijk is om de nieuwe klepmaat te bepalen. Het risico op complicaties is echter moeilijk in te schatten op basis van enkel medische beelden, aangezien deze complicaties afhangen van de mechanische interactie tussen het implantaat en de omliggende weefsels. Door de medische beelden te combineren met geavanceerde computer simulaties is het wel mogelijk om beter te begrijpen hoe het implantaat zich zal gedragen in een specifieke patiënt, en zo kan het risico op complicaties beter worden ingeschat. Dergelijke informatie heeft een belangrijke klinische waarde, aangezien dit gebruikt kan worden om de best passende klepmaat te selecteren en de procedure dus beter te plannen. Via computersimulatie kan men ook virtueel implantaten gaan optimaliseren, en dus de tijd en kosten die geassocieerd zijn met experimentele testen reduceren.

De focus van dit doctoraatsonderzoek was de ontwikkeling en validatie van computationeel simulatie platform gericht op het beter begrijpen van de biomechanische impact van de minimaal invasieve kunstklep op het omliggende cardiovasculaire weefsel, dat toelaat om het risico op complicaties in te schatten en betere implantaten te ontwikkelen. Dit onderzoek was deel van het MUSICARE PhD trainingsprogramma ondersteund door het Europese Horizon 2020 programma.

Deze dissertatie bestaat uit drie onderdelen. Deel I bevat een algemene introductie omtrent aortaklepstenose en TAVR en licht enkele belangrijke complicaties van deze interventie toe. In dit onderdeel wordt er ook een overzicht gegeven van computationele simulatiestudies die beschreven zijn in de wetenschappelijke lilteratuur in verband met TAVR. Deel II beschrijft de verdere ontwikkeling, validatie en toepassing van het TAVIguide simulatieplatform ontwikkeld door FEops (Gent, België) dat toelaat om TAVR gerelateerde complicaties te voorspellen. Dit onderdeel bevat ook een nieuwe methodiek om het ontwerp van TAVR implantaten te optimaliseren. Het laatste deel (III) beschrijft de belangrijkste bevindingen van dit onderzoek en blikt vooruit naar mogelijks verder onderzoek. Hieronder staat een korte samenvatting van de verschillende onderdelen en hoofdstukken.

## DEEL I: ACHTERGROND

### Hoofdstuk 1: Aortaklep: anatomie, pathologie en behandeling

Dit hoofdstuk bevat basisinformatie omtrent de anatomie en fysiologie van de menselijke aortaklep, wat noodzakelijk is om het hier beschreven onderzoek te begrijpen. Een beschrijving van aortaklepstenose en de behandeling ervan is ook opgenomen. De beschikbare klepimplantaten voor zowel chirurgische als minimaal invasieve operaties worden opgelijst. Daarnaast wordt een overzicht gegeven van de resultaten van klinische studies die chirurgische en minimaal invasieve aortaklepvervanging vergelijken, waaruit blijkt dat TAVR een veilige en doeltreffende behandeling is voor hoog risico patiënten. Het aantal patiënten dat in aanmerking komt voor TAVR zal zeer waarschijnlijk nog sterk toenemen doordat deze behandeling ook voor jongere patiënten zal worden toegepast, en door de veroudering van de bevolking. Tenslotte wordt er kort ingegaan op de TAVR marktgrootte en de verwachte groei van deze markt.

### Hoofdstuk 2: Inzicht in minimaal invasieve aortaklepvervanging: planning en complicaties

De focus van dit onderzoek zijn minimaal invasieve aortaklepvervangingen, en daarom wordt er in hoofdstuk 2 een gedetailleerde beschrijving gegeven van deze behandelingsoptie. Hierbij gaat de meeste aandacht naar de planning van deze procedures en de gerelateerde complicaties. Het eerste deel bevat een overzicht van de medische beeldvorming die gebruikt wordt om de procedure te plannen, maar ook om de procedure uit te voeren en achteraf te evalueren. Beeldvorming laat toe om voor de procedure de graad van aortaklepstenose vast te stellen, alsook om de dimensies van de aortawortel te meten om de optimale klepmaat te kunnen bepalen, en tot slot om de optimale toegangsroute te kiezen. Tijdens de procedure is beeldvorming cruciaal om de nieuwe klep goed te kunnen positioneren. Ook na de procedure is er een belangrijk rol voor medische beeldvorming, namelijk om eventuele complicaties te detecteren. Dit hoofdstuk bevat daarnaast ook een overzicht van de complicaties die na TAVR kunnen optreden. Hierbij wordt gefocust op geleidingsstoornissen en aorta regurgitatie omdat deze complicaties sterk aan bod komen in de rest van dit werk. De complexiteit van het menselijke elektrische geleidingssysteem wordt beschreven samen met de verschilllende types van geleidingsstoornissen die na TAVR kunnen optreden, en hoe deze vastgesteld, behandeld en voorspeld kunnen worden. Deze zelfde aspecten worden toegelicht voor aorta regurgitatie.

### Hoofdstuk 3: Numerieke simulaties voor TAVR

Het onderzoek is gebaseerd op patientspecifieke numerieke modellering. Daarom wordt er in hoofdstuk 3 een overzicht gegeven van de belangrijkste wetenschappelijke publicaties in dit domein die focussen op TAVR. Eén van de belangrijkste stappen bij dergelijke patiënt-specifieke simulaties is het opstellen van nauwkeurige modellen (zowel op vlak van geometrie en materiaaleigenschappen). Verschillende methodieken worden opgelijst die hierbij worden gebruikt, en ook op vlak van modelleringsstrategieën wordt een overzicht gegeven. Het hoofdstuk beschrijft ook de verschillende toepassingen gerelateerd aan TAVR die worden beoogd met numerieke simulaties. Patiënt-specifieke numerieke simulaties worden gebruikt om het mechanische gedrag van het implantaat te bestuderen, alsook de interactie met omliggende weefsels. Daarnaast worden simulaties ook gebruikt om de impact van implantaatpositie te evalueren, of de hemodynamica na klepontplooiing te bekijken. Ook de voorspelling van TAVR complicaties (bvb. risico op annulusruptuur, lekkage, thrombose) vormt de focus van bepaalde studies. De belangrijkste beperking van de beschikbare studies is het gebrek aan model validatie met in vitro of in vivo data. Deze literatuursstudie heeft niet als doel om allesomvattend te zijn, maar tracht om essentiële informatie aan te rijken die belangrijk is voor een goed begrip van deze thesis.

Het laatste onderdeel van dit hoofdstuk beschrijft TAVIguide, het computationele platform ontwikkeld door FEops NV (Gent, België) om TAVR te simuleren in patiënt-specifieke anatomische modellen met als doel TAVR complicaties te voorspellen.

## DEEL II: COMPUTER SIMULATIE: VOORSPELLING VAN TAVR COMPLICATIES

### Hoofdstuk 4: Patiënt-specifieke computer simulatie om geleidingsstoornissen na TAVR te voorspellen

Het mechanisme achter het optreden van geleidingsstoornissen na TAVR is niet helemaal duidelijk. Er zijn enkele patiënt en procedure gerelateerde factoren voorgesteld als voorspellers van nieuwe geleidingsstoornissen (bvb. calcificaties, bestaande rechterbundeltakblok, te grote klepmaat, implantatiediepte), maar geen enkele van deze factoren houdt rekening met de interactie tussen de geimplanteerde klep en de omliggende structuren. Om het risico op nieuwe geleidingsstoornissen beter te kunnen begrijpen hebben we TAVIguide gebruikt om in 112 patiënten de TAVR procedure te simuleren. Deze simulaties laten toe om de contactdruk in de buurt van atrioventriculaire (AV) geleidingssysteem te voorspellen. Hierbij wordt de anatomische locatie van het AV geleidingssysteem op basis van pre-operatieve MDCT beelden bepaald. De simulatieresultaten tonen een significant hogere contactdruk en een grotere contactregio in de buurt van het AV geleidingssysteem bij patiënten die in werkelijkheid nieuwe geleidingsstoornissen hadden na TAVR. Ook anatomische en procedurele parameters zoals de locatie van het membraneuze septum, de implantatiediepte en het kleptype dragen bij tot een hogere incidentie van nieuwe geleidingsstoornissen. Op basis van een statistische analyse blijkt echter dat enkel de maximum contactdruk en de omvang van de contactregio afgeleid uit de computersimulaties goede voorspellers zijn voor nieuwe geleidingsstoornissen.

### Hoofdstuk 5: Effect van het aligneren van de commissuren op aorta regurgitatie na TAVR

Tijdens chirurgische aortaklepvervanging worden de originele aortaklepblaadjes verwijderd bij het plaatsen van de nieuwe klep, maar dit is niet het geval bij TAVR waar het implantaat in de verkalke aortaklep wordt ontplooid. Daarnaast is het ook moeilijk om de exacte orientatie van de nieuwe klep ten opzichte van de originele klep te controleren. In dit hoofdstuk wordt het effect op aorta regurgitatie van het aligneren van de nieuwe (CoreValve) en de originele klepblaadjes onderzocht met TAVIguide. In een eerste stap wordt de voorspelling van aorta regurgitatie gevalideerd voor 63 patiënten door middel van post-operatieve beeldvorming (angiografie en echocardiografie) om zo de nauwkeurigheid van TAVIguide te evalueren. Daarna wordt in elke patiënt zowel een goede als een slechte alignering van de nieuwe en originele klepblaadjes gemodelleerd om het effect hiervan op aorta regurgitatie te onderzoeken. Onze resultaten tonen aan dat een goeie alignering leidt tot een beter aansluiting van het implantaat, en dus resulteert in minder lekkage. Lekkage kanalen blijken typisch voor te komen ter hoogte van de commissuren, vooral bij sterk verkalkte klepblaadjes. Verdeling en hoeveelheid kalk op de klepblaadjes blijkt ook de klepvervorming te beïnvloeden, maar een kwantificatie van eccentriciteit van de klep toont aan dat een ellipische vervorming niet de belangrijkste oorzaak is van aorta regurgitatie.

### Hoofdstuk 6: De impact van de maat en positie van een mechanisch expandeerbare minimaal invasieve aortaklep

In hoofdstuk 4 en 5 is TAVIguide gebruikt om zelf-expandeerbare implantaten te bestuderen. In dit hoofdstuk bekijken we het effect van klepmaat en positie op de voorspelde resultaten in het geval van de mechanisch expandeerbare Lotus klep. Deze klep kan zeer nauwkeurig worden gepositioneerd, maar de selectie van de optimale klepmaat is een uitdaging. In een eerste deel zullen we de nauwkeurigheid van TAVIguide voor de voorspelling van het risico op complicaties voor deze klep onderzoeken in een groep van 62 patiënten. Daarna wordt de keuze van klepmaat en de positie van het implantaat onderzocht in een subgroep van patiënten met twijfelachtige afmetingen van de aortawortel waarbij de instructies van de fabrikant niet geheel duidelijk zijn (i.e. patiënten waarvoor twee klepmaten in aanmerking komen). Onze numerieke resultaten tonen aan dat een grotere klepmaat de hoeveelheid aorta regurgitatie reduceert, terwijl een lagere implantatiepositie en een grotere klepmaat het risico op geleidingsstoornissen doet verhogen. Belangrijk is echter dat naast deze algemene bevindingen, de conclusie verschilt van patiënt tot patiënt.

### Hoofdstuk 7: Optimalisatie van een minimaal invasieve aortaklep door middel van patiënt-specifieke computer simulatie

TAVR schuift geleidelijk op naar jongere patiënten omwille van de zeer goede resultaten in termen van veiligheid en doeltreffendheid die behaald worden bij de hoog risico patiënten. Het voorkomen van complicaties na TAVR wordt bij deze jongere patiënten nog belangrijker. Naast verbeteringen aan de procedure, kunnen de huidige complicaties ook worden aangepakt door betere implantaten te ontwikkelen. In dit hoofdstuk stellen we een nieuwe methodiek voor om betere implantaten te ontwikkelen, die leiden tot minder geleidingsstoornissen en aorta regurgitatie. Deze methodiek is gebaseerd op het combineren van patiënt-specifieke computersimulaties met optimalisatietechnieken. In deze pilootstudie worden twee geometrische parameters van een implantaat geoptimaliseerd. De optimalisatie is gebaseerd op de voorspelde resultaten in 12 patiënten, die representatief zijn voor de typische TAVR populatie (bvb. patiënten met sterk verkalkte klepblaadjes, patiënten met een bicuspide klep...). Onze resultaten tonen aan dat de geoptimaliseerde klep het risico op zowel geleidingsstoornissen en aorta regurgitatie beperkt in alle patiënten. Deze pilootstudie toont duidelijk het potentieel aan van het combineren van patiënt-specifieke simulaties met optimalisatie algoritmes om in silico klinische studies uit te voeren vooraleer de werkelijke humane klinische studie. Op deze manier kunnen de risico's voor patiënten en fabrikanten sterk verminderd worden.

## DEEL III: CONCLUSIES

### Hoofdstuk 8: Conclusies en toekomstperspectieven

Het finale hoofdstuk vat de belangrijkste bevindingen van dit doctoraatsonderzoek samen. De TAVIguide technologie is gebruikt en uitgebreid met nieuwe strategieën om complicaties na TAVR te onderzoeken, te voorspellen en hopelijk te voorkomen. Dit hoofdstuk wordt afgesloten met enkele suggesties voor verder onderzoek om enkele huidige limitaties weg te werken, alsook om TAVIguide verder te ontwikkelen.

# SUMMARY

## INTRODUCTION

Aortic valve stenosis is one of the most prevalent valve pathology worldwide. The stenosis obstructs the ejection of the blood flow from the left ventricle and, when left untreated, it leads to high ventricular pressure, left ventricular hypertrophy and may ultimately lead to heart failure. As no medical therapy can halt the progress of the disease, patients with severe aortic stenosis need a valve replacement. However, the standard surgery is highly invasive and can be fatal for fragile patients. The minimally invasive transcatheter aortic valve replacement (TAVR) has shown to be effective in those patients; nonetheless, frequent complications arising after the intervention such as paravalvular aortic regurgitation (AR) and conduction abnormalities are crucial and have been associated with increased patient's morbidity and mortality. Medical imaging techniques such as multi-detector computed tomography (MDCT) and echocardiography are fundamental during the planning of the procedure as they provide quantitative information on the patient's anatomy that is useful for instance to size the bioprosthetic valve, anticipate complications and qualitatively evaluate possible implantation options. Though, they only provide limited insights about the risk of post-procedural complications. Complications, in fact, strongly depend on the mechanical interactions between the implanted device and the surrounding structures. Available imaging techniques used in conjunction with computer simulation can provide detailed information on the device performance in a patient-specific anatomy to better understand the risk of complications, as well as the underlying reason. Such information can be of clinical value to properly select the most appropriate device and plan the procedure. In addition, computer simulation allows for virtual testing and design optimization of a device, for instance reducing time and costs of experimental tests and manufacturing prototypes.

In this PhD thesis, we focused on the development and validation of a computational modeling and simulation framework to gain a deeper understanding in the biomechanical impact of the bioprosthetic valve on the surrounding cardiac structures, for the prediction of TAVR post-operative complications as well as for the development of more effective devices. This research was part of the MUSICARE PhD training programme and was supported by the European Horizon 2020 Framework.

The dissertation is composed of three main parts. Part I gives a general introduction about aortic stenosis and TAVR and explains the principles behind the postoperative complications under investigation. This part also gives an overview of the computational workflows used in literature to address clinical questions related to TAVR. Part II presents the further development, validation and application of the computational workflow developed at FEops (Gent, Belgium) to predict TAVR complications. This part also presents a framework to optimize the design of a TAVR device. The last part offers an overview of the main results and starting points for future research. Below, a summary of each part and chapter is provided.

## Part I: Background

### Chapter 1: Aortic valve: anatomy, pathology and treatments

This chapter provides the basis of the anatomy and physiology of the human aortic valve which is necessary to understand and follow the work described in this dissertation. Then, it continues explaining the pathologic condition of the aortic valve stenosis and its treatment. The available prosthetic valves for the surgical and transcatheter treatment are also described. An overview of the clinical trials comparing the outcome of surgical and transcatheter treatment shows the efficacy and safety of TAVR in high-surgical risk patients. The number of patients undergoing TAVR is expected to further increase in the future with the inclusion of younger patients as well with the ageing of the population. The chapter concludes with a concise note on the current market size of TAVR and its short-term forecast.

### Chapter 2: Insight into transcatheter aortic valve replacement: planning and complications

As TAVR is the main focus of this thesis, Chapter 2 provides a detailed description of this treatment option, focusing on the procedural planning and complications. The first section offers an overview of the medical imaging used during the procedural planning phase as well as peri-procedurally and post-procedurally. In the pre-procedural planning phase, imaging allows to assess the severity of the patient's aortic stenosis, the anatomic aortic root dimensions for prosthesis sizing, and to evaluate the sites of peripheral access. During the procedure, imaging provides guidance for precise placement of the prosthesis. After the procedure, imaging is a useful tool to detect complications. This chapter provides also a brief overview of the complications emerging after TAVR. A particular focus is given to conduction abnormalities and paravalvular AR which are the complications of interest of this investigation. The complexity of the human conduction system is highlighted together with the types of conduction abnormalities, their diagnosis, management and current predictors. Similarly, diagnosis, management and current predictors for AR are reported.

### Chapter 3: Numerical simulations in TAVR

Patient-specific numerical simulation is the main tool used in this research. Chapter 3 reviews the progress and the state of the art of patient-specific numerical simulation in the domain of TAVR in the last decade. The generation of accurate models (both in terms of geometry and material property) is one of the most important steps in the patient-specific modeling field. Modeling strategies and considerations are provided in the first section of this chapter. The chapter continues with an overview of the clinical applications of numerical simulation in TAVR. Patient-specific numerical simulation has been used to study the mechanical behavior of the implanted device and its interaction with the surrounding tissues, the effect of device positioning on the device performance, or the hemodynamics after the deployment. Simulations have also been adopted as a tool for assessment of treatment outcome (e.g. risk of annulus rupture, paravalvular AR, thrombosis). The main limitation of the available studies is the lack of model validation with in vitro or in vivo data. This review does not intend to be fully exhaustive, but it aims to provide the essential information regarding the state-of-the-art in this domain.

The last section of this chapter introduces TAVIguide, the computational framework that was developed at FEops NV (Gent, Belgium) to simulate TAVR in patient-specific anatomies and to assess the risk of TAVR complications.

## PART II: COMPUTER SIMULATION: PREDICTION OF TAVR COMPLICATIONS

### Chapter 4: Patient-specific computer simulation to predict new conduction abnormalities after TAVR

The mechanism behind the occurrence of new conduction abnormalities after TAVR is still unclear. Despite the fact that few patient- and procedure-related factors have been proposed as predictors of new conduction abnormalities (e.g. calcifications, existing right bundle branch block, valve oversizing, implantation depth), none of them accounts for the actual interactions between the bioprosthetic valve and the surrounding structures. In order to predict the risk of new conduction abnormalities, TAVIguide is used to simulate the TAVR procedure in 112 patient-specific aortic roots and to predict the contact pressure in the region of the atrioventricular (AV) conduction system. The anatomical location of the AV conduction system is identified from preoperative MDCT images. Simulations predict significantly higher contact pressure and an extended area of contact within the region of the AV conduction system in patients with new conduction abnormalities. Anatomical and procedural parameters such as the location of the membranous septum, implantation depth of the device and device type also contribute to the occurrence of new conduction abnormalities. Nevertheless, statistical analysis shows that only the maximum contact pressure value and the area of contact predicted with simulations are good predictors for new conduction abnormalities.

### Chapter 5: Effect of commissural alignment on paravalvular regurgitation after TAVR

Differently to the surgical aortic valve replacement where the native aortic leaflets are removed to free space for the bioposthetic valve, in TAVR the bioprosthesis is deployed within the native aortic leaflets. It is also difficult for clinicians to control the exact orientation of the device within the aortic root. In this chapter TAVIguide is used to investigate the effect of the alignment between the commissures of a self-expandable CoreValve and native leaflet commissures on the paravalvular AR. First, a validation of the prediction of paravalvular AR with postoperative angiography or echocardiography demonstrated the reliability of TAVIguide in 63 patients. Then, alignment and misalignment between the bioprosthetic and the native commissures was simulated in each patient to evaluate the effect of the device orientation on predicted AR. Our findings indicate that a good alignment between the prosthetic and native leaflets favors a better apposition of the device skirt to the aortic root, with consequent reduction of AR. Leakage paths are often observed near the native valve commissures, especially between severely calcified leaflets. Distribution and size of the calcifications on the leaflets seems to influence the frame deformation. However, the quantification of the frame eccentricity revealed that an elliptical frame is not the main responsible of paravalvular AR.

### Chapter 6: The impact of size and position of a mechanical expandable transcatheter aortic valve

In Chapter 4 and 5 TAVIguide has been used with self-expandable devices. In this chapter, it is adopted to investigate the effect of device size and positioning on predicted outcome with the mechanically-expandable Lotus device. The Lotus valve can be precisely deployed, but the selection of the appropriate sizing is still challenging. First, the reliability of TAVIguide as a tool for the assessment of procedural/post-procedural risks after implantation of a Lotus valve is verified in 62 patients. Then, sizing and positioning of the prosthesis have been evaluated in a subgroup of critical patients with equivocal aortic root dimensions (i.e. patients who would fit two different valve sizes), for which there is a lack in the procedural guidelines. Numerical results reveal that a larger device size limits paravalvular AR, while lower implantation depth and aggressive device oversizing increase the risk of conduction abnormalities. Nonetheless, our findings suggest that besides the general impact of device size and position on predicted outcomes, the optimal sizing and positioning differ from one patient to another.

### Chapter 7: Optimization of a transcatheter aortic valve frame using patient-specific computer simulation

Given the promising results in terms of safety and efficacy achieved in high-surgical risk patients as reported in clinical trials, TAVR is shifting towards younger patients. Prevention of procedural complications becomes even more important in these patients and needs to be addressed. Next to procedural improvements, complications can also be addressed by new optimized devices. In this chapter, we propose a novel framework for the development of more effective devices aiming to reduce conduction abnormalities and paravalvular regurgitation after TAVR. To this goal, TAVIguide is used in conjunction with optimization algorithms. Two geometrical parameters of a prosthetic device are optimized. The optimization is based on the predicted outcomes in 12 patients, representative of the TAVR population (e.g. patients with heavily calcified aortic valve, patients with bicuspid valve…). Numerical results reveal that the implantation of the optimized device reduces the risk of conduction abnormalities and paravalvular regurgitation in all patients. This is a proof-of-concept study that shows the potential of combining patient-specific simulation with an optimization algorithm to perform in-silico clinical trials that can be conducted prior to the actual first-in-human clinical study. In this way, risks for patients and manufacturers can be significantly reduced. The potential as well as the limitations of this framework are discussed in depth in this chapter.

## Part III: Conclusions

### Chapter 8: Conclusions and future perspectives

The final chapter summarizes and discusses the main achievements of this PhD research. The TAVIguide computational workflow has been extended with novel strategies to investigate, predict and hopefully avoid complications after TAVR. The chapter concludes with suggestions for further investigation to overcome some limitations of this research as well as to further develop TAVIguide as a tool to serve the clinicians towards optimal planning of the procedure.

# INTRODUCTION

## RATIONALE

Cardiovascular pathologies are the number one cause of death or permanent disability worldwide, affecting 20% of individuals in Europe. Some diseases can be congenital and affect newborns or young individuals, but most of the cardiovascular diseases are degenerative and affect mainly the elderly population. Among those pathologies, aortic valve stenosis is the most common one, with a prevalence reaching 12.4% worldwide [1].

Aortic valve stenosis is the result of the degenerative remodeling of the aortic valve leaflets due to fibrosis and calcification processes. Unfortunately, there is no medical therapy that can halt the progress of the disease, except for valve replacement.

Since 1950 prosthetic valves, either mechanical or biological, have been developed to replace the diseased valve. However, valve replacement is a highly invasive surgery and can be fatal for many fragile patients deemed at high surgical risk. More and more, minimally invasive techniques have been adopted to treat these patients. Transcatheter aortic valve replacement (TAVR) was performed the first time in 2002 [2]. With this procedure, the prosthetic valve is introduced into the body through a catheter and deployed within the native diseased aortic valve. Despite continuous advancements, further improvements are still required. Complications such as paravalvular aortic regurgitation and conduction abnormalities occur respectively in about the 10% and 20% of the cases after TAVR [3–5]. Aortic regurgitation has been associated with increased mortality [6–8], whereas conduction abnormalities leading to implantation of a permanent pacemaker are associated with increased costs, longer rehospitalization and increased patient morbidity. Considering the prospective of treating younger patients at low surgical risk, those complications are unacceptable and need to be addressed by new devices and/or improved procedures.

In the cardiovascular field, and in TAVR, the integration of computer simulations and clinical images has generated the opportunities to study, *in* *silico*, the behaviour of the implanted device in a specific anatomy and to better understand the source of complications. Patient-specific computational models can be clinically valuable for example in the virtual planning of a surgical procedure. It can offer support in the choice of the device and can be a tool in the assessment of the device performance, in the assessment of procedural/ post-procedural risk as well as in the screening of a specific patient to be treated. Computer simulation can also be applied in the virtual testing and design optimization of a device, providing a valuable insight into the device performance, reducing time and costs of the overall development process.

The focus of this dissertation is on the development and validation of a computational modeling and simulation framework to gain a deeper understanding of the biomechanical impact of the transcatheter aortic valve prosthesis on the surrounding cardiac structures, for the prediction of TAVR post-operative complications as well as for the development of more effective devices. This project was part of the MUSICARE Programme and was supported by the European Horizon 2020 Framework through the Marie Sklodowska-Curie Action International Training Network (MSCA-ITN) European training Networks (project number 642458) (`http://www.musicare2020.eu`).

## MUSICARE PhD training programme

The MUSICARE (MUltiSectorial Integrative approaches to CArdiac caRE) PhD training programme gathered medical professionals, academia and industry to prepare PhD students for a career in research or industry to deal with the main challenges in the cardiac field, for a more effective treatment of patients. The partnership consisted of four universities (Politecnico di Milano, Imperial College London, Technische Universiteit Eindhoven, Universiteit Gent) and six industrial partners (Philips, Sorin, Materialise, Bel, FEops, Lifetec).

The project focused on (i) computer studies to simulate the effects of percutaneous access and to quantify the biomechanical impact of new devices, (ii) on the development of image-processing tools to integrate different information from multi-modal imaging and for the real 3D reconstruction of the cardiac structures and (iii) on *in vitro* simulators to address issues related to maneuver precision of the catheter and device repositioning in minimally invasive heart surgery and percutaneous valve therapies. The project also included investigation on the tissue adaptation, growth and remodeling to better understand the progression of the diseases and to predict the long-term effects of implantable devices on the cardiac structures.

## RESEARCH GOALS

This PhD thesis was realized within the MUSICARE project, and resulted from a strong collaboration between Ghent University and FEops. The final goal was to further improve the computational framework developed at FEops that allows to accurately simulate TAVR procedures. In this respect, four main goals were defined:

***Goal 1.*** *To further improve the computational TAVIguide framework for prediction of conduction abnormalities after TAVR;*

***Goal 2.*** *To further validate the computational framework for prediction of paravalvular regurgitation after implantation of self-expandable valves;*

***Goal 3.*** *To extend this computational framework with mechanically-expandable devices to provide insight related to device sizing and positioning;*

***Goal 4.*** *To develop a strategy for design optimization of a transcatheter heart valve, adopting the developed computational framework.*

## DISSERTATION STRUCTURE OVERVIEW

This PhD thesis is divided in three main parts.

Part I provides the clinical and computational background which is fundamental to understand the rationale behind this work. Chapter 1 provides a summary on the anatomy, physiology and pathophysiology of the aortic valve, and briefly introduces the current treatments for aortic valve stenosis. Chapter 2 focuses on TAVR. It provides an exhaustive description of the planning phase of the procedure and the critical complications after the procedure, which are crucial for this study. Subsequently, Chapter 3 gives an overview of the computational workflows described in literature to address clinical questions related to TAVR.

Part II is the core of this dissertation. Chapter 4 presents the newly developed computational framework to predict the risk of developing conduction abnormalities after TAVR. Chapter 5, presents the validation of the framework to predict the risk of aortic regurgitation after TAVR. In Chapter 6, this computational framework is used to investigate the performance of a second-generation TAVR device and in Chapter 7 to develop a framework to optimize the design of a TAVR device.

Part III recapitulates the key findings and concludes with some future perspectives.

## LIST OF PUBLICATIONS

### First author peer-reviewed papers

- Rocatello G, El Faquir N, De Santis G, Iannaccone F, Bosmans J, De Backer O, Sondergaard L, Segers P, De Beule M, de Jaegere P, Mortier P. Patient-Specific Computer Simulation to Elucidate the Role of Contact Pressure in the Development of New Conduction Abnormalities After Catheter-Based Implantation of a Self-Expanding Aortic Valve. Circ Cardiovasc Interv. 2018 Feb;11(2):e005344. doi: 10.1161/CIRCINTERVENTIONS.117.005344.
- Collas V*, Rocatello G*, El Faquir N, Paelink B, De Santis G, Dezutter T, Segers P, De Beule M, Mortier P, de Jaegere P, Bosmans J. Effect of commissural alignment on paravalvular aortic regurgitation after TAVI. (submitted)

  *Collas V and Rocatello G contributed equally to this study.
- Rocatello G, El Faquir N, De Backer O, Swaans M.J, Latib A, Vicentini L, Segers P, De Beule M, de Jaegere P, Mortier P. The impact of size and position of a mechanical expandable transcatheter aortic valve: novel insights through computational modelling and simulation. (accepted)
- Rocatello G, De Bock S, De Beule M, Segers P, Mortier P. Optimization of a transcatheter heart valve frame using patient-specific computer simulation. (submitted)

### Conference contributions

- Rocatello G et al. Transcatheter heart valve frame optimization: a population-based approach. ATTICC 2018, Venice, Italy
- Rocatello G et al. Patient-specific computer simulation to elucidate the role of contact pressure in the development of new conduction abnormalities after catheter based implantation of a self-expanding aortic valve. World Biomechanics congress 2018, Dublin, Ireland
- Rocatello G et al. Optimization framework for transcatheter aortic valve design based on patient-specific computer simulations. World Biomechanics congress 2018, Dublin, Ireland
- Rocatello G et al. Low Implantation Depth During TAVR Increases the Pressure Exerted on the Atrioventricular Conduction System: a Biomechanical Analysis. In Journal of the American College of Cardiology, 70:B267–B268. New York: Elsevier Science Inc. TCT 2017, Denver (Colorado), US

- Rocatello G et al. Low implantation depth during TAVR increases the pressure exerted on the atrioventricular conduction system: a biomechanical analysis. Belgian National Day 2017, Brussels, Belgium

- Rocatello G et al. Patient-specific computer simulations to elucidate the role of contact pressure in the development of new conduction abnormalities after catheter-based implantation of a self-expanding aortic valve. In European Heart Journal. Vol. 38. EuroPCR 2017, Paris, France

- Rocatello G. et al. Computer simulations to predict paravalvular leakage after TAVI: a comparison between Medtronic CoreValve and Medtronic CoreValve Evolut R Systems. VPH 2016, Amsterdam, The Netherlands

- Rocatello G. et al. Novel predictors for conduction disturbances after Transcatheter Aortic Valve Implantation. VPH 2016, Amsterdam, The Netherlands

- Rocatello G. et al. Novel predictors for conduction disturbances after Transcatheter Aortic Valve Implantation. Belgian National Day 2016, Brussels, Belgium

# I

# Background

Chapters

1 **Aortic valve: anatomy, pathology and treatments** 3

2 **Insight into transcatheter aortic valve replacement: planning and complications** 23

3 **Numerical simulations in TAVR** 47

CHAPTER 1

# AORTIC VALVE: ANATOMY, PATHOLOGY AND TREATMENTS

This chapter provides the necessary aortic valve anatomical and (patho-) physiological background to follow and understand this work. First a general introduction into the anatomy and physiology of a healthy aortic valve is given, followed by the description of the diseased stenotic valve condition. Lastly, the available treatments are discussed.

## 1.1 ANATOMY AND PHYSIOLOGY OF THE AORTIC VALVE

The aortic valve (AoV) is one of the four valves in the mammalian heart and it is located between the left ventricle (LV) and the aorta (Fig. 1.1). The main function of the AoV is to guarantee the unidirectionality of the blood flow during the entire cardiac cycle: it allows the blood ejection into the systemic circulation during systole, while preventing regurgitation during diastole [9], hereby ensuring high blood pressure in the systemic circulation in diastole. It is a passive structure that does not require external energy for its motion because its kinematics is driven by pressure gradients.

The AoV is anchored into a complex structure known as the aortic root, which consists of the virtual basal ring, the sinuses of Valsalva and the sinotubular junction (Fig. 1.2a). The virtual basal ring is located at the ventricular portion of the aortic root and is defined by the three basal attachment points of the AoV cusps. At this location, the transition between the muscular ventricular wall and the fibro-elastic aortic tissue begins. The virtual basal

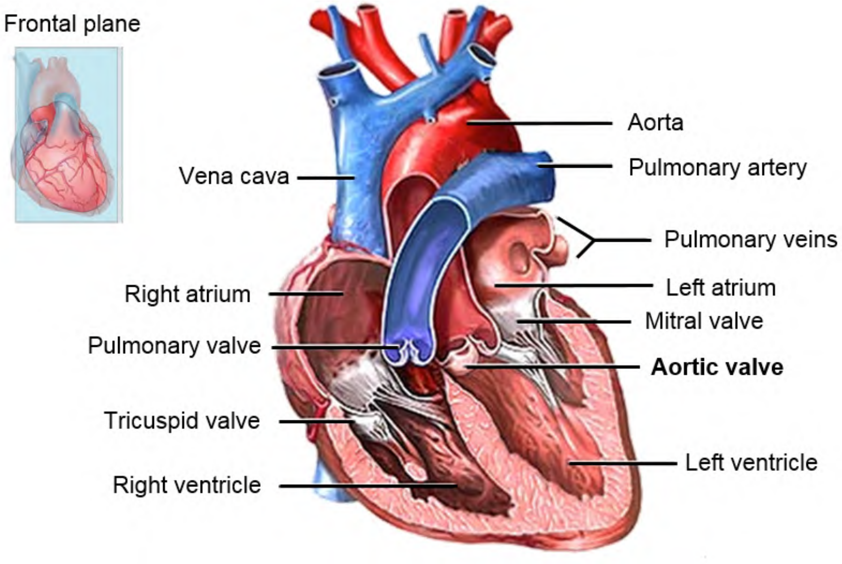

**Figure 1.1:** Schematic frontal view of the heart and its components (adapted from `https://www.khanacademy.org`).

ring is also called aortic annulus. However, although the word annulus implies a circular structure, it can have an elliptical or even non-homogeneous shape due to calcifications.

Right above the AoV, the aortic root shows three enlargements, named sinuses of Valsalva. Two of the three sinuses give rise to the coronary arteries, with the function of providing the cells of the *myocardium* with nutrients and oxygen. These two sinuses and the aortic valve leaflets are named after the coronary arteries: the left/right sinus of Valsalva hosts the left/right coronary *ostium*. The third sinus is named the non-coronary sinus. The sinuses provide some space between the aortic leaflets and the aortic wall, preventing the obstruction of the coronaries when the valve is open. Also, their shape facilitates the development of eddy currents behind the leaflets when they are in the open configuration, preventing the leaflets from striking against the aortic wall and promoting their closure during diastole [10].

The area bounded by the semi-lunar attachment of the leaflets to the aortic root wall is called interleaflet triangle (Fig. 1.2b). Although it is an extension of the left ventricular outflow tract (LVOT), it is made of the same fibrous tissue as the aortic wall. The points where the leaflet attachments run parallel, distally towards the ascending aorta, are called the commissures.

Finally, the sinotubular junction represents the transition between the sinuses of Valsalva and the ascending aorta. The aorta is a layered structure

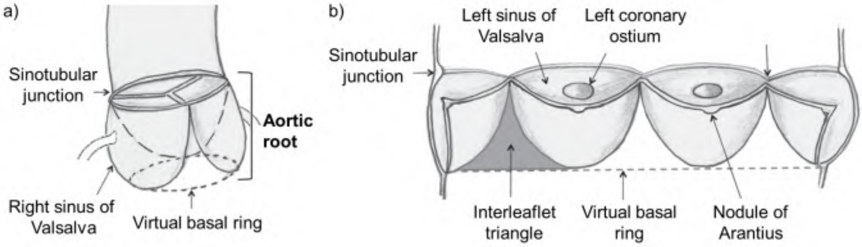

**Figure 1.2:** Fundamental component of the aortic root. (a) Schematic drawn of the aortic root, (b) cut-open view of the AoV (Adapted from [11]).

composed of connective tissue and muscle cells which guarantee the elastic behavior: the vessel extends and shrinks in response of the blood pressure and volume [11].

The AoV is normally composed of three semilunar leaflets, which are not perfectly equal in size [12, 13]. Each leaflet contains endothelial cells (at each side of the cusp) and valvular interstitial cells (fibroblasts, smooth muscle cells and myofibroblasts) which are responsible for maintaining the valve homeostasis and structural integrity. Each cusp has a three-layered structure which determines the biomechanical properties of the valve, guaranteeing high flexibility and elasticity (Fig. 1.3): the *fibrosa* layer facing the aorta, the *ventricularis* layer facing the left ventricular chamber and a middle layer called the *spongiosa*. The *fibrosa*, is the thickest of the three layers and it is predominantly composed of a highly organized network of collagen fibers. This layer is considered the stiffest and the strongest part of the leaflet, and it is responsible to absorb the diastolic and systolic stresses. The *ventricularis*, which is the thinnest of the three layers, is mainly composed of radially oriented elastin fibers which can extend in diastole and recoil in systole to minimize the leaflet area. The *spongiosa* is mainly composed of a very high concentration of proteoglycans which accommodate shear and compressive forces of the leaflets during the cardiac cycle [14, 15].

The thickness of the leaflets is not homogeneous, and it decreases towards the free edge. In the middle of the free edge, a small thickened and fibrous node is present. This structure is called the nodule of Arantius and its main function consists in giving additional mechanical support to the tip of the leaflets and in providing coaptation with the other leaflets in the closed configuration. The full closure of the valve is guaranteed as well by a partial overlapping of the leaflets during diastole, which avoids the retrograde flow from the ascending aorta into the left ventricle (i.e. leaflets coaptation).

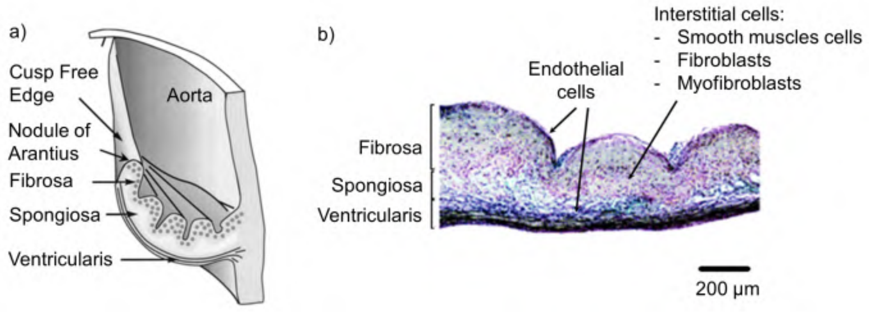

**Figure 1.3:** Fundamental composition of the aortic valve leaflets. (a) Schematic drawing of a leaflet section showing the internal layer subdivision. (b) Histological section of a normal porcine aortic valve leaflet (Adapted from [14] and [15]).

Even though normal AoV is trifoliate, due to congenital malformations, the AoV can also be composed of two leaflets or even of one leaflet only. In such cases, the valve is referred as bicuspid aortic valve (BAV) or unicuspid aortic valve respectively.

### 1.1.1 Bicuspid aortic valve

Bicuspid aortic valve is the most common congenital cardiovascular abnormality, affecting 1-2% of the general population, with a higher prevalence in males [16, 17]. BAV is typically made of two unequal-sized cusps with a prominent raphe (i.e. a ridge with many elastic fibers) that partially or completely fuses one commissure [18]. Fusion between the left- and right-coronary cusps (L-R) is the most common morphology reported in about 60-70% of BAV cases. Fusion between the right- and non-coronary cusps (R-N) occurs in about 15% of the cases, while fusion of the left- and non-coronary cusps (L-N) is quite rare, occurring in about 3-7% of the cases [19]. The interleaflet triangle between the fused cusps and the relative sinuses are usually much smaller than normal and can lead to reduced mobility of the cusps. Also, dilatation of the aortic root and sinotubular junction are common traits of BAVs and can lead to progressive deterioration of the valvular function [20].

BAV types are generally classified according to the number of raphe(s) present (e.g. 0, 1, or 2), spatial orientation of the cusps and location of the raphe(s) [21] (Fig. 1.4). For ‘type 0’ (‘pure’ BAV with no raphe), occurring in about 7% of the cases, the orientation of the cusps was found to be either anteroposterior (AP) or lateral (LAT). For ‘type 1’ (valve with one raphe) and ‘type 2’ (valve with two raphes), the orientation of the cusps depends on the position of the raphe. ‘Type 1’ is the most common variant seen in about 88% of the patients, while ‘type 2’ is rarely seen (about 5% of the cases).

At birth and during early life BAVs show normal functioning. However, later in life, BAVs normally induce abnormal turbulent flow pattern and increased stresses at the location of the raphe. These pathological conditions make BAV predisposed to progressive calcification. In fact, young adults with initially functioning BAV have a 24% risk of aortic valve replacement over the next 20 years, most often due to aortic stenosis [22].

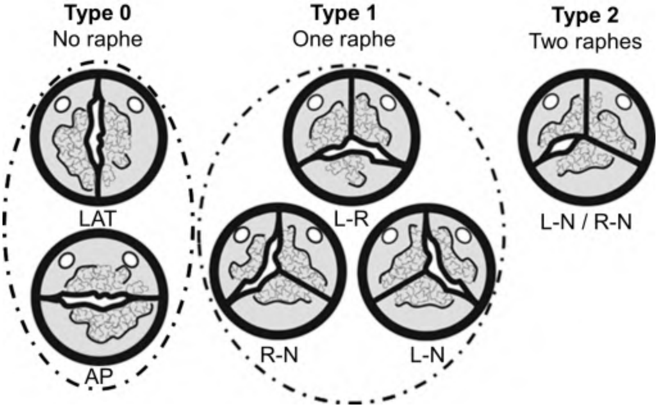

**Figure 1.4:** Sievers' classification of bicuspid aortic valves (adapted from [23]). AP=anteroposterior. L=left coronary cusp. LAT=lateral. N=non-coronary cusp. R=right coronary cusp.

## 1.2 Aortic stenosis: a silent killer

Aortic stenosis (AS) is a pathology that occurs when the AoV opening narrows, thereby obstructing the ejection of the blood flow from the heart into the aorta (Fig. 1.5a-b).

Worldwide, rheumatic fever is the main underlying cause of AS. However, in industrialized countries it is more commonly a consequence of degenerative remodeling of a normal trileaflet AoV or due to a congenital BAV. The prevalence of AS in the elderly population (>80 years) with an initially functioning trileaflet AoV is reported to range from 2.6% to 12.4% [1, 24–30].

AS is strongly associated with age, and it has been estimated to increase by 2.4 fold by the year 2040 and more than triple by the year 2060 [30].

Fibrosis and calcification processes are the main drivers of the degenerative remodeling of AoV leaflets during aging. In the initiation phase, lipid deposition, injuries and status of inflammation lead to the accelerated fibrosis. Accumulation of fibrous tissue and remodeling of the extracellular matrix

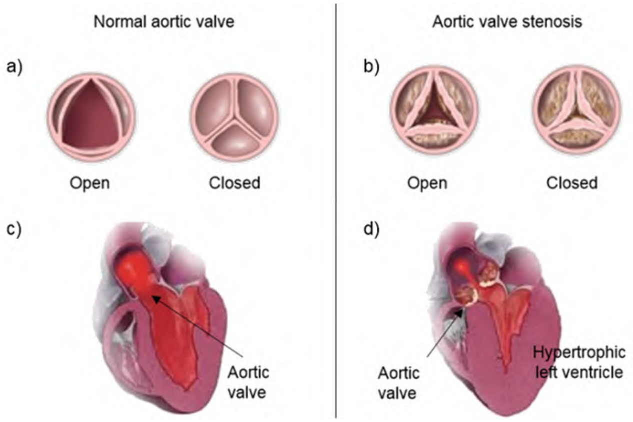

**Figure 1.5:** Schematic comparison between a healthy aortic valve anatomy and an AS condition. (a-b) representation of a normal aortic valve and a stenotic aortic valve in the open and closed configuration (adapted from `http://heartsurgeryinfo.com`), (c-d) representation of a healthy and hypertrophic left ventricle (Adapted from `http://www.heartupdate.com`).

generate an extensive thickening and stiffening of the leaflet [31–33]. Furthermore, scar tissue can roughen the leaflet surface, promoting the deposit of calcium, which is the leading factor in the further progression of the disease in a subsequent phase (propagation phase) causing impaired leaflet motion [34]. In addition to this process, aging is responsible for gradual loss of elastin fibers in the aortic wall, and therefore for a significant decrease of the compliant property of the aortic wall. In optimal condition, this compliance contributes to the pressure load distribution and to the proper opening/closing of the valve. Therefore, a reduction of the aortic wall compliance contributes to a significant stress overload on the leaflets [34].

When AS becomes significant, it results in an increased resistance forcing the left ventricle to work harder to guarantee a sufficient blood ejection into the aorta. The increased systolic pressure in the ventricular chamber leads to concentric hypertrophy as a compensatory adaptive mechanism to maintain normal wall stresses [35]. However, with the progress of the stenosis, the ventricular wall gets thicker and the ventricular chamber decreases the capacity to relax and fill. As a result, the risk of heart failure increases [36] (Fig. 1.5c-d).

Mild forms of AS can remain asymptomatic, therefore AS is mainly discovered during routine controls or during investigations for other pathologies. The progression of the disease is mainly checked with (Doppler) echocardiographic imaging techniques which provide detailed, non-invasive information about the anatomy of the valve (i.e. tricuspid or bicuspid), and the degree of AS severity. Standard measures of AS severity are the maximum velocity across the AoV, the mean transaortic pressure gradient calculated using the Bernoulli equation and the functional aortic valve area (also called effective orifice area) based on the continuity equation [37, 38] (Table 1.1).

**Table 1.1:** Classification of AS severity.

| | Aortic velocity (m/s) | Mean gradient (mmHg)* | Aortic valve area ($cm^2$) |
|---|---|---|---|
| Mild AS | 2.0-3.0 | <20 | 1.5-3.0 |
| Moderate AS | 3.0-4.0 | 20-40 | 1.0-1.5 |
| Severe AS | >4.0 | >40 | <1.0 |

* Mean gradient is calculated as $4(v_2^2\text{-}v_1^2)$ being $v_2$ the transaortic peak velocity (m/s) and $v_1$ the subaortic peak velocity (m/s). Adapted from [37, 38].

When AS becomes moderate or severe, typical clinical symptoms of AS appear, such as shortness of breath, fainting episodes (syncope), palpitations, chest pain/pressure (angina). The person might feel weaker, observe a decline in the activity level and hear heart murmur.

The onset of symptoms is an indicator of poor prognosis for patients with AS. When left untreated, more than half of the people would die within the next 2 years and 80% within 5 years after the onset of symptoms (Fig. 1.6). Unfortunately, there is no medical therapy that can halt the progress of the disease except for AoV replacement [39, 40].

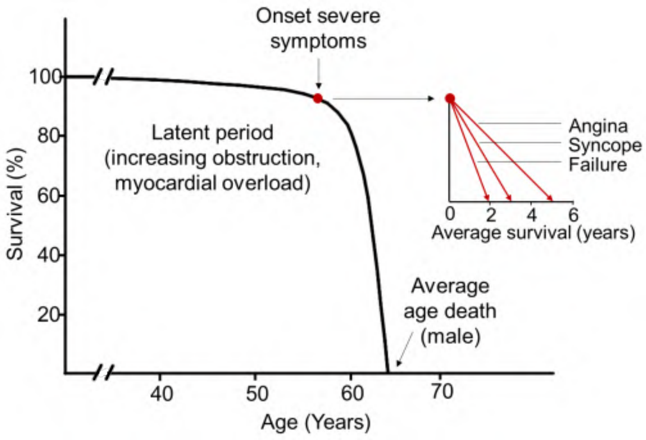

**Figure 1.6:** Prognosis of patients with aortic stenosis and who did not undergo valve replacement, a post-mortem study (Adapted from [39]).

## 1.3 TREATMENT OF AORTIC STENOSIS

For patients older than 40 years suffering of AS, in absence of serious comorbidities, the surgical aortic valve replacement (SAVR) is the treatment of choice. However, since the last decade an increasing number of patients at high surgical risk has been treated with the minimally invasive transcatheter aortic valve replacement (TAVR).

### 1.3.1 Surgical aortic valve replacement (SAVR)

On average 50000 SAVR are performed every year both in Europe and in the US. SAVR is a highly invasive open-heart treatment that allows the replacement of the stenotic aortic valve with a prosthetic valve. During the procedure the patient is brought under general anesthesia. A sternotomy (incision in the sternum) or thoracotomy (incision through the ribs) is performed to expose the heart and, once the pericardium has been opened, the patient is connected to a cardiopulmonary bypass machine which takes over the role of the heart and lungs during the operation (Fig. 1.7). After the aorta has been clamped, the heart is stopped to reduce the myocardial oxygen consumption (using a solution called cardioplegia) and drained to facilitate the access to the aortic valve. The diseased valve is then removed, the aortic annulus measured and the bioprosthetic valve brought in and sutured to the aortic annulus. This valve can be either mechanical or biological, further details are reported in paragraph 1.3.1.1. After the replacement is completed, the patient is taken off the bypass machine.

Normally, the patient is put under close surveillance in an intensive care unit for the 12-36 hours after the procedure. If complications do not arise, discharge is planned within one week after the procedure, while a longer period of 3-4 months is necessary for a full recovery.

#### *1.3.1.1 Prosthetic aortic valves*

Prosthetic aortic valves should mimic the characteristics of the native valves; therefore, they should have excellent hemodynamics, long durability, high thromboresistance and excellent implantability. A distinction can be made between mechanical and biological valves [41].

Mechanical valves are designed as a functional substitute of the natural AoV, though its shape is not analogous to the native anatomy. There are three types of mechanical valves: the cage-ball valve, the tilting disc valve and the bileaflet valve (Fig 1.8). The bileaflet valve is the most recent one. It consists of two semilunar metallic leaflets, covered by a biocompatible titanium layer, which ensure a more physiologic blood flow during systole

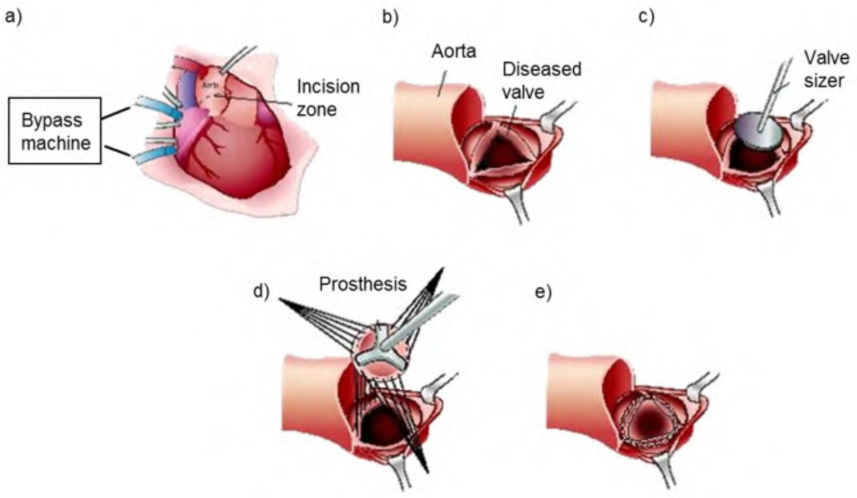

**Figure 1.7:** Procedure of the surgical aortic valve replacement. (a) the heart function is replaced by the cardiopulmonary bypass machine, (b) the aortic root is cut open and the aortic valve is exposed, (c) the aortic annulus size is measured, (d-e) the prosthesis is sutured in place (adapted from `http://www.surgeryencyclopedia.com`).

than monoleaflet (tilting disc) or cage ball valves. It has excellent durability with a life expectancy of about 30 years, but it is associated with risk of thromboembolism and thrombotic obstruction. As a consequence, it requires lifelong anticoagulation administration [42]. For this reason, this valve is preferred for patients who have a long-life expectancy and for those who are already taking anticoagulant drugs (patients with a mechanical valve already implanted in a different location or at high risk for thromboembolism).

The biological valves, instead, mimic the anatomy of the natural AoV. They are made of trileaflet porcine aortic valves or fabricated from sheets of bovine pericardium, fixed in glutaraldehyde, and chemically treated to enhance biocompatibility and durability [44, 45]. However, because of their biological origin, they undergo the same problems of a native valve, i.e. calcifications, deterioration, infections, prolapse, leading to their failure and with a possible need for re-intervention [46]. Due to their limited life-time (about 10-15 years), they are more often used in the elderly population.

Some of these valves are mounted on a polymer or metallic supporting stent, i.e. stented valves. Stentless aortic valves are intended to achieve a more physiological blood flow pattern than stented valves. Randomized clinical trials have shown that stentless aortic valves improve clinical outcomes as the effective orifice area, the mean gradient and the peak gradient over short and

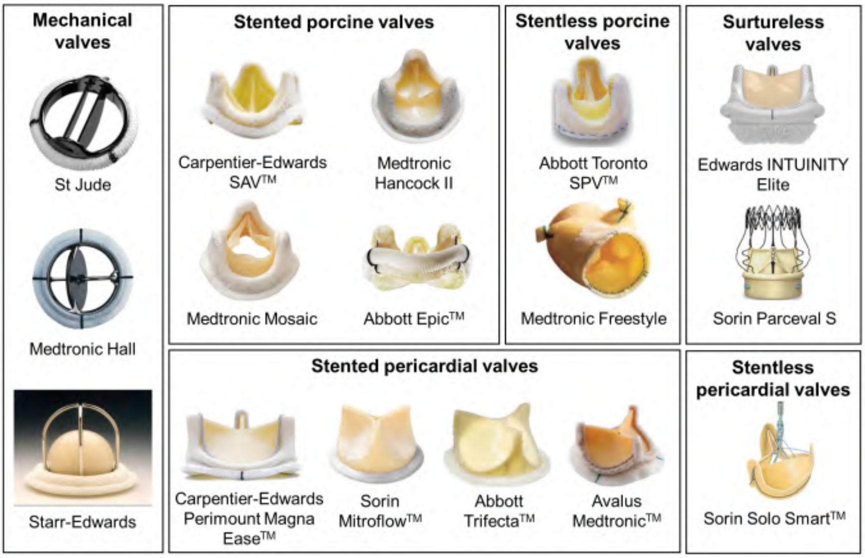
Mechanical valves
St Jude
Medtronic Hall
Starr-Edwards
Stented porcine valves
Carpentier-Edwards SAV™
Medtronic Hancock II
Medtronic Mosaic
Abbott Epic™
Stentless porcine valves
Abbott Toronto SPV™
Medtronic Freestyle
Surtureless valves
Edwards INTUINITY Elite
Sorin Parceval S
Stented pericardial valves
Carpentier-Edwards Perimount Magna Ease™
Sorin Mitroflow™
Abbott Trifecta™
Avalus Medtronic™
Stentless pericardial valves
Sorin Solo Smart™

**Figure 1.8:** Different types of prosthetic aortic valves (Adapted from [43]).

long term [47, 48]. However, the superior hemodynamics did not impact the patient's morbidity and mortality. Examples of stentless and stented valves are shown in Fig 1.8.

More recently, sutureless and rapid deployment valves have emerged as alternative bioprosthesis aortic valves, showing excellent hemodynamical results, excellent effective orifice area, low mean and peak systolic gradient [49]. Next to these promising results, their main advantage consists in a significantly reduction in procedural time, which in turn reduces cardiopulmonary bypass and facilitates minimally invasive approaches.

Other types of bioprosthetic valves are pulmonary autograft and aortic valve homograft. The former, also known as the Ross procedure [50], consists in the replacement of the diseased AoV with the pulmonary valve from the same patient. Then, a pulmonary allograft (from cadaver) is used to replace the patient's pulmonary valve. Given its growth potential, is mostly used in the pediatric population. It showed excellent hemodynamics and good durability and it is free from anticoagulation therapy. However, long-term pulmonary autograft dilatation remains a daunting issue as it results in reoperation and increased mortality [51]. Valve homograft is less used due to the lack of tissue donors but also because it is more difficult to implant compared to prosthetic devices [52].

Compared to mechanical valves, biological valves offer a more favorable blood flow and less cloth formation. Thus, anticoagulation treatment is not necessary.

### 1.3.2 Transcatheter aortic valve replacement (TAVR)

The first in man TAVR was performed by Cribier in 2002 [2]. In the last decade, about 400000 procedures have been performed worldwide, and an increase of 40% is expected annually. The procedure normally takes about 1-2 hours and is performed with the patient awake, under local anesthesia. Different types of valve are currently available in the market and will be presented further in paragraph 1.3.2.1. The bioprosthetic aortic valve is crimped onto a catheter. Subsequently, the catheter is introduced into the patient's body (Fig 1.9). The preferred access remains the transfemoral approach: the catheter is introduced through the femoral artery with a small incision in the groin. However, a heavily calcified artery with extreme tortuosity may not be amenable to access. In this case, the clinician could decide to insert the catheter through the apex of the heart (transapical approach), with a small incision under the left nipple. Typically, when TAVR cannot be performed using the transfemoral nor the transapical approach due to anatomical reasons, then the subclavian approach is a good alternative. In this case, the subclavian artery located beneath the collar bone serves as access route for the catheter. A last approach consists in the transaortic access. However, with this approach a partial sternotomy is required to access and introduce the catheter in the ascending aorta.

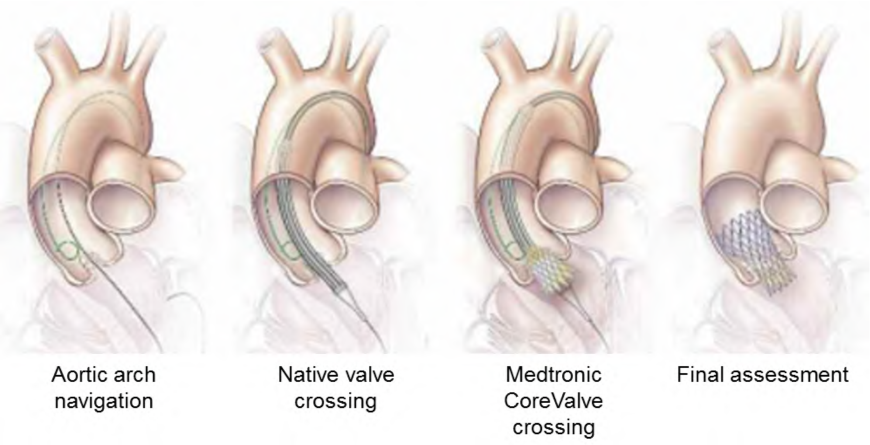

**Figure 1.9:** Procedural steps of the transcatheter aortic valve replacement (Adapted from `http://www.americannursetoday.com`).

The transcatheter aortic valve (TAV) is guided to the correct position with respect to the aortic annulus and is expanded (Fig 1.9). The expansion mechanism strongly depends on the TAV used. Of note, in TAVR, the native diseased valve is not removed, but it is simply crushed by the new one towards the aortic wall. In some cases, a balloon valvuloplasty is required to pre-dilatate the old valve (i.e. break some calcifications and create more space for the new valve) or to post-dilatate the new valve and guarantee the full expansion of the valve frame. After the TAV is deployed and expanded, the catheter and the guidewire are removed. Because TAVR is a minimally invasive technique, the recovery time is very short compared to SAVR (few days instead of few months).

#### *1.3.2.1 Prosthetic transcatheter aortic valves*

TAV devices can be subdivided according to the expansion mechanism into 3 categories: self-expandable, balloon-expandable or mechanically expandable devices (Fig 1.10). Only TAV that have received the CE (*Conformité Européenne*) approval will be described.

*Self-expandable devices*

Medtronic (Minneapolis, MN) is the current leader in the TAVR market for self-expandable devices. The **CoreValve** Revalving system contains a trileaflet porcine pericardial tissue valve fixed on a nitinol self-expanding frame. The proximal end of the CoreValve frame has a larger diameter than the distal end, to ensure fixation into the ascending aorta. The central portion of the stent is narrowed to prevent occlusion of the coronary ostia. The **Evolut R** frame, i.e. the second-generation CoreValve, has a slightly shorter profile, while preserves the height of the pericardial skirt (13 mm) with an extended skirt at the inflow portion to limit paravalvular aortic regurgitation. In addition, cell geometry has been redesigned to achieve optimized radial force. The **Evolut Pro**, i.e. the latest-generation CoreValve, has the same profile as the Evolut R but it has an external skirt at the ventricular inlet, which provides added tissue volume between the TAV and the native anatomy to reduce gaps and therefore to prevent paravalvular aortic regurgitation. The Evolut R was the first TAV approved by the FDA (*Food and Drug Administration*) for valve-in-valve replacement. Both Evolut devices can be delivered with a femoral or subclavian approach, and they can be recaptured and repositioned in case of suboptimal deployment. The Evolut R and Evolut Pro devices are available respectively in four and three sizes, to treat patients with aortic annulus diameters from 17-18 mm up to 30 mm, the broadest annulus range commercially available.

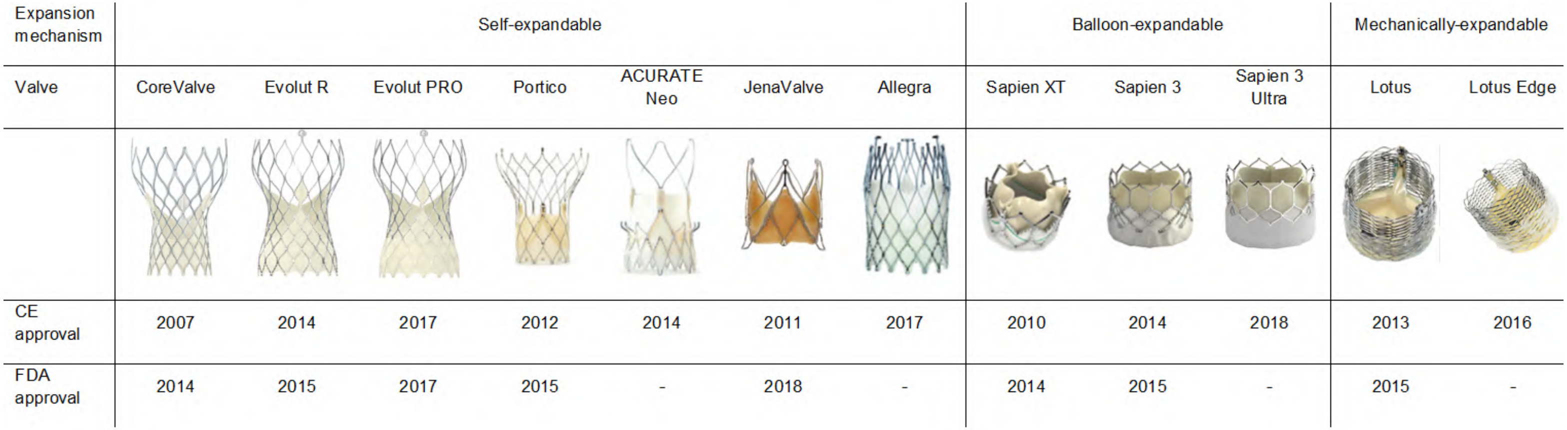

| Expansion mechanism | Self-expandable | | | | | | | Balloon-expandable | | | Mechanically-expandable | |
|---|---|---|---|---|---|---|---|---|---|---|---|---|
| Valve | CoreValve | Evolut R | Evolut PRO | Portico | ACURATE Neo | JenaValve | Allegra | Sapien XT | Sapien 3 | Sapien 3 Ultra | Lotus | Lotus Edge |
| CE approval | 2007 | 2014 | 2017 | 2012 | 2014 | 2011 | 2017 | 2010 | 2014 | 2018 | 2013 | 2016 |
| FDA approval | 2014 | 2015 | 2017 | 2015 | - | 2018 | - | 2014 | 2015 | - | 2015 | - |

**Figure 1.10:** Transcatheter aortic valves with CE mark approval.

The **Portico** valve (Abbott, Chicago, IL) consists of a bovine pericardial valve with a porcine pericardial sealing cuff attached to a nitinol self-expanding frame which can be delivered via a transfemoral access [53]. It can be fully retrieved and repositioned in situ and it allows the valve leaflets function during the deployment to maintain hemodynamic stability. The device is available in four sizes to treat patients with annulus diameters from 19 to 27 mm.

The self-expandable **ACURATE neo** (Boston Scientific, Marlborough, MA) is composed of a porcine pericardial tissue valve sewn into a self-expanding nitinol stent covered with a porcine pericardial skirt. It is designed for a transapical or transfemoral approach and it is available in three sizes to treat patient with aortic annulus diameters from 21 mm to 27 mm.

The **JenaValve** technology (JenaValve Technology, Irvine) comprises a porcine pericardial trileaflet valve mounted on a low-profile nitinol frame which can be delivered using both the transfemoral or transapical approaches. The unique characteristic of this prosthesis is that the implantation relies on active clip fixation of the native aortic leaflets, thus eliminating the radial forces on cardiac and aortic structures. This clip fixation mechanism of the JenaValve to the native aortic valve leaflets could provide secure anchorage even in the absence of calcifications. In fact, this is the only TAVR device to have obtained CE Mark approval for noncalcified aortic regurgitation. The JenaValve is available in three sizes, covering aortic valve annuli from 21 to 27 mm.

The **Allegra** valve (NVT AG) is a self-expandable device consisting of a nitinol frame and bovine pericardium leaflets and skirt. The frame consists of a variable cell size which guarantees higher radial force at the annular level for secure anchoring. The prosthesis can be implanted through a transfemoral route, and three valve sizes are commercially available in Europe covering an annulus diameter which ranges from 19 mm to 28 mm.

*Balloon-expandable devices*

The SAPIEN aortic valve (Edwards Lifesciences, Irvine, CA) is a balloon-expandable device made of a trileaflet bovine pericardial valve attached to a stainless-steel framework. The Edwards **Sapien XT**, i.e. the second generation of Edwards TAV, has a thinner cobalt-chromium stent with fewer struts and is approved also for valve-in-valve procedures. The **Sapien 3**, i.e. the later generation of Edwards TAV, has a lower profile and an additional polyethylene terephthalate outer skirt to reduce paravalvular aortic regurgitation. This outer skirt has been extended to cover the 40% of the frame in the **Sapien 3 Ultra**, i.e. the latest Edwards TAV generation. The SAPIEN valves can be delivered either through a transfemoral, subclavian or transapical approach, and they are available in three sizes allowing clinicians to treat patients with annular diameters from 16 to 28 mm.

*Mechanically expandable devices*

The **Lotus** valve (Boston Scientific, Marlborough, MA) is a mechanically expandable device consisting of leaflets and external skirt made of bovine pericardium and installed on a braided nitinol stent. During the controlled mechanical expansion, the Lotus device shortens in length from approximately 70 mm to 19 mm as it expands radially. Subsequently, it locks into its final configuration. The self-locking mechanism allows to fully retrieve and reposition the valve, by unlocking it. The Lotus Edge, i.e. latest generation of Lotus TAV, was designed to anchor earlier during deployment, minimizing the depth of the valve in the LVOT. However, the Lotus Edge valve was recalled in 2017 and it will remain off the market until 2019 due to problems in the locking mechanism. The Lotus system was designed to be delivered via a transfemoral approach and was available in three sizes covering a range of aortic annulus diameters from 19 to 27 mm. Furthermore, the valve leaflets were fully functional at 50% deployment, allowing a slower and more controlled deployment without hemodynamic instability.

### 1.3.3 TAVR versus SAVR: evidence of benefits in clinical trials

In the last decade TAVR has proven to be safe and effective in patients deemed at extreme-, high- and intermediate surgical risk. Randomized clinical trials have been conducted to compare TAVR with different devices to SAVR in patients with severe aortic stenosis at different surgical risk level. Below, an overview of the most relevant clinical trials and clinical studies available in literature is given.

#### *1.3.3.1 Randomized clinical trials*

*CoreValve US High-risk pivotal trial*

The CoreValve US High risk pivotal trial is a multicenter, randomized trial, initiated and funded by Medtronic, that compares the clinical outcomes after SAVR and TAVR performed with the self-expandable CoreValve. Nine-hundred ninety-five patients at high surgical risk were enrolled between February 2011 and September 2012 in the US. The trial showed that TAVR is noninferior compared to SAVR at 1-, 2-, 3- and 5-years follow up.

The rate of mortality was significantly lower in the TAVR group, compared to SAVR, after 1 and 2 years [3, 43, 54]. The incidence of stroke tended to be lower in the TAVR group at each follow up. Low rate of strokes was also reported in patients at extreme surgical risk [55]. However, mortality and stroke rates following TAVR or SAVR were comparable at 5-years follow up

[56]. Bleeding, acute kidney injury (AKI), atrial fibrillation and prosthesis mismatch were more common in the SAVR [57]. Prosthesis patient mismatch occurs when the normally functioning implanted valve prosthesis has a small effective orifice area in relation to the body surface area. On the other side, vascular complications, paravalvular aortic regurgitation (AR) and permanent pacemaker (PPM) implantation were more common in the TAVR group. Patients treated with TAVR had improved clinical outcomes compared with SAVR after 3 years, especially in terms of hemodynamics [3].

This trial showed that the CoreValve is safe and effective in patients at high- and extreme-risk for surgery, resulting also in a more rapid improvement in heart failure symptoms and functional status compared to SAVR [58].

*SURTAVI*

The SURTAVI (SURgical replacement and Transcatheter Aortic Valve Implantation) trial compared the safety and efficacy of TAVR performed with the self-expandable CoreValve or Evolut R with SAVR in patients at intermediate risk for surgery [59]. A total of 1746 patients underwent randomization in US, Europe and Canada from June 2012 to June 2016. This trial proved that TAVR is a noninferior alternative to surgery in patients at intermediate surgical risk. Slightly higher rate of mortality was observed in the SAVR group (14.0% vs 12.6%). SAVR was associated with higher AKI, atrial fibrillation, and transfusions, whereas TAVR had higher residual AR and PPM.

*NOTION*

The NOTION (NOrdic aortic valve intervenTION) trial is a multicenter, randomized, nonblinded superiority trial conducted in Denmark and Sweden that compared TAVR versus SAVR in patients at low-risk. A total of 280 patients were randomly assigned to TAVR using a self-expandable CoreValve versus SAVR and followed up for 5 years. The study started in December 2009.

No significant difference between TAVR and SAVR was found for the rate of death, stroke, and myocardial infarction at 1 year follow up [60]. Rate of death remained not significant at 5-years follow up [61]. The mortality rate of the NOTION (3.7%) was one of the lowest mortality rates compared with any previously reported series. AR was more prevalent in TAVR (15.7% vs 0.9% had moderate or severe regurgitation after 1 year), and it remained more prevalent after 5 years. However, it showed to improve over time [62]. PPM rate was higher in TAVR after 1 year (41.3% vs 4.2%) and only few new PPM implantations occurred after 5 years.

The NOTION trial did not demonstrate superiority of TAVR respect to SAVR. However, TAVR showed to be safe and effective in low- and intermediate- risk patients at 1, 2 and 5-years follow-up.

Prosthesis-patient mismatch was evaluated in a following study [63] and, as reported in the CoreValve US High-risk pivotal trial, was more common in SAVR. Furthermore, it has been associated to increased mortality and decreased LV mass regression.

*REPRISE III*

The REPRISE III (Repositionable Percutaneous Replacement of Stenotic Aortic Valve Through Implantation of Lotus Valve System Randomized Clinical Evaluation) [5] is a multicenter randomized clinical trial designed to prove the noninferiority of the mechanically expandable Lotus valve in comparison with the self-expandable CoreValve and Evolut R in patients at high or extreme risk. Patients enrollment was performed between September 2014 and December 2015. This study proved that the Lotus valve is noninferior to the Medtronic CoreValve or Evolut R at 30 days and 1 year after the procedure. Mortality rates were comparable (about 2.5% at 30 days and 11.9% at 1 year). At 1-year Lotus showed lower rates of moderate or severe AR, fewer disabling strokes, repeated procedures and less valve-in-valve deployments or malpositioning. In contrast Lotus had more new PPM implantations and valve thrombosis. The risk of overall stroke with Lotus was 7%, which is comparable to Medtronic devices. But the rate of disabling stroke at 30 days is lower with Lotus.

*PARTNER*

The PARTNER (Placement of AoRTic TraNscathetER Valve) trial showed that TAVR performed using a balloon-expandable valve is an alternative to SAVR for patients with aortic stenosis that are at high-risk or inoperable. This study was funded by Edwards Lifesciences. A total of 699 patients were randomized in Canada, Germany and USA from May 2007 to August 2009. The observed mortality rate at 1-, 2-, 3- and 5-years was very similar after TAVR or SAVR, but slightly higher in patients deemed inoperable [4, 7, 8, 64–68]. The findings from this study suggested a sustained benefit of TAVR as measured by mortality, repeat hospital admission and functional status, especially for patients deemed inoperable. Valves were durable, hemodynamics was preserved after 5 years and no worsening of AR was observed.

A subsequent trial (the PARTNER 3), which enrolled 1000 patients from March 2016 through October 2017, showed the superiority of TAVR respect to SAVR in low-risk patients [69]. Nevertheless, new bundle branch block and mild AR at 1-year follow up were more frequent after TAVR.

#### 1.3.3.2 *Other relevant clinical studies*

Randomized clinical trials of the later generation CoreValve devices (Evolut R and Evolut Pro) are ongoing at the time of writing. However, preliminary results proving the safety and efficacy of those devices have been evaluated in small non-randomized clinical studies. Such results, available on the Medtronic website (`https://www.medtronic.com`), are reported below.

*Evolut R US clinical study*

The Evolut R US clinical study evaluated one-year safety and efficacy of the Evolut R system in patients with aortic stenosis deemed at high- or extreme-risk for SAVR (http://www.medtronic.com). Two-hundred and forty-one patients were enrolled in the study. This study showed promising results: low mortality rate (8.6%) and disabling stroke (5.1%) at 1-year follow up, proving the safety of the device.

*Evolut PRO US clinical study*

The Evolut PRO US clinical study reported preliminary results (6 months follow up) on 60 patients who received an Evolut Pro valve. It is a prospective, multicenter, controlled, non-randomized single-arm study funded by Medtronic (http://www.medtronic.com). Although the enrolled population is very limited, preliminary results concerning postoperative AR are promising: the majority of the patients (88%) had no or trace AR at 6 months, showing the efficacy of the external wrap in preventing AR.

### 1.3.4 To operate now or to wait?

Current guidelines [37, 38, 70] recommend aortic valve replacement (AVR) for severe AS patients in the presence of either: (i) onset symptoms and/or (ii) left ventricular (LV) systolic dysfunction. However, while for symptomatic patients with severe AS the decision to treat is relatively simple, the timing for intervention in asymptomatic patients remains matter of continued debate [71, 72].

Patients with severe but asymptomatic AS have a higher risk of sudden death (1.4% per year) [73], and some patients, for example at higher risk for development of symptoms and/or LV dysfunction, might benefit from early AVR.

In the last decades, thanks to improvement in technologies and techniques, AVR operative mortality has drastically decreased to 2-3%, arguing in favor of earlier intervention. Furthermore, a prospective study found that early surgery in asymptomatic patients with severe AS is associated with an improved long-term survival compared to SAVR. Therefore, despite the lack of more solid evidence, early surgery might represent a therapeutic option to further improve clinical outcomes in asymptomatic patients with severe AS at low operative risk [74].

### 1.3.5 TAVR Market Share

About 400000 TAVR have been performed since 2002 in US and Europe and given the promising results in clinical trials showing that TAVR is non-inferior and possibly superior to SAVR, it is expected to further increase in the future.

Currently, the price of a TAV is about $30000, more than six times the price of the average prosthetic valve for surgical replacement. Nonetheless, according to the Cardiothoracic Surgery, TAVR devices are considered cost-effective in treating high-risk patients. In fact, there are some cost savings compared to surgery, such as the shorter length of stay in the hospital and in the intensive care unit. In America and Europe, TAVR devices are government funded. Japan is an exception of the Asian countries, where the Japanese government covers the treatment cost. In the rest of Asian countries, patients pay treatment costs out of their own pocket.

In 2017, the global market size of TAVR was valued at $1.8 billion in US, and $1.3 billion in Europe, and it is anticipated to rise at a 'compounded average growth rate' (CAGR) of 18.8% by the year 2022 (Fig 1.11). The key drivers of this growth are the increasing number of patients across the world suffering of cardiovascular diseases, the promising results in clinical trials that showed the safety and efficacy of TAVR and the continue advancement in the technology and in new TAVR devices. Geographically, North-America dominated the market in 2017, accounting for more than 40% of the TAVR market. This can be attributed to high adoption of technologically advanced products, acquisitions, and favorable reimbursement policies.

Key participants in the market to date are Medtronic plc; Boston Scientific Corp; Edwards Lifesciences Corporation; and Abbott (Fig 1.12).

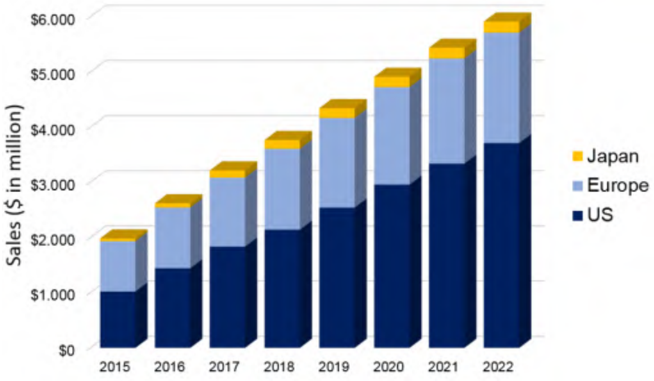

**Figure 1.11:** Transcatheter aortic valve replacement (TAVR) procedures market size: forecast to 2022.

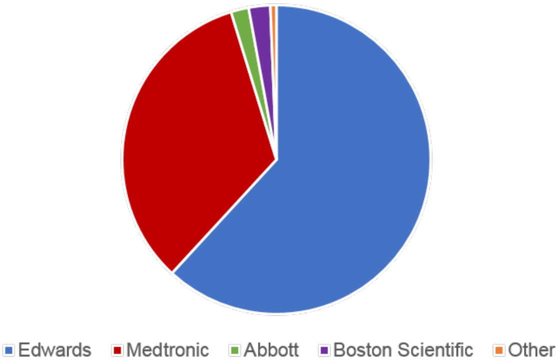

**Figure 1.12:** Transcatheter aortic valve replacement (TAVR) market share (%) in 2017.

Chapter 2

# INSIGHT INTO TRANSCATHETER AORTIC VALVE REPLACEMENT: PLANNING AND COMPLICATIONS

In this chapter, we will give a detailed insight into the transcatheter aortic valve replacement procedure. The first section discusses the role of the imaging tools. The next section gives a concise overview of the current complications associated with TAVR. Notable attention is paid to conduction abnormalities and paravalvular aortic regurgitation: how they develop, how they can be detected and treated.

## 2.1 THE CRUCIAL ROLE OF IMAGING TECHNIQUES DURING TAVR

Imaging plays a crucial role in TAVR. In the pre-procedural planning phase, imaging allows to assess the severity of the patient's AS, the anatomic aortic root dimensions for prosthesis sizing, and to evaluate the sites of peripheral access. During the procedure, imaging provides guidance for precise placement of the prosthesis.

### 2.1.1 Valve sizing

Correct sizing of the TAV is of paramount importance for a successful intervention. Inaccurate sizing bears the risk of severe complications, such as paravalvular aortic regurgitation (AR) or prosthesis dislocation in case of undersizing, annular rupture or conduction abnormalities in case of oversizing. Complications following TAVR will be further addressed in section 2.2.

It is important to state that accurate preoperative measurements of the aortic annulus are crucial to prevent complications.

The selection of the TAV size is determined according to the sizing chart provided by each specific manufacturer. Currently, such sizing charts are based on multidetector computed tomography (MDCT)-based annulus dimensions and may, therefore, not be appropriate when an alternative imaging modality is chosen. Table 2.1 shows a representative example of a sizing chart for the CoreValve Evolut R System. Strict cut-off values between two different sizes are usually provided for aortic root dimensions. However, sizing should be performed with caution as the annular dimension can vary in size at the different stages of the cardiac cycle: systole generally corresponds to larger annular dimensions and it should be utilized for annular sizing [75].

No additional recommendations are given for patients with aortic annular dimensions in between the manufacturer's recommendations for two TAV sizes (borderline measurements). In this case, other clinical factors need to be evaluated, such as body size, extent and location of calcifications [76].

**Table 2.1:** Chart currently used to size the CoreValve Evolut R device.

| Size | 23 mm | 26 mm | 29 mm | 34 mm |
|---|---|---|---|---|
| Annulus diameter | 18-20 mm | 20-23 mm | 23-26 mm | 26-29 mm |
| Annulus perimeter* | 56.5-62.8 mm | 62.8-72.3 mm | 72.3-81.7 mm | 81.7-91.1 mm |
| Sinus of Valsalva diameter (mean) | $\geqslant$25 mm | $\geqslant$27 mm | $\geqslant$29 mm | $\geqslant$29 mm |
| Sinus of Valsalva height (mean) | $\geqslant$15 mm | $\geqslant$15 mm | $\geqslant$15 mm | $\geqslant$15 mm |

*Annulus perimeter = Annulus diameter x $\pi$.

### 2.1.2 Pre-procedural imaging techniques

There are different pre-procedural imaging techniques available to perform aortic annular measurements: transthoracic and transoesophageal echocardiography (TTE and TEE respectively), magnetic resonance imaging (MRI) and MDCT. The latter is currently the gold standard imaging modality for TAVR planning.

**Two-dimensional TTE and TEE** B-mode images have been widely used in the past to derive aortic annular dimensions (Fig 2.1a). The main disadvantage of those techniques is that they can only provide one diameter, which is insufficient to properly describe a non-circular structure. Typically, the annular diameter is measured in the long-axis view (sagittal plane) leading to an underestimation of the actual annular dimensions [77–79]. Furthermore, the selected plane may not pass exactly through the center of the aortic annulus, contributing to the underestimation. Of note, given the narrow ranges that the manufacturer's sizing charts assign to a specific device size, even a small difference in the annular measurement may lead to a different size selection.

**Three-dimensional TEE** is a relatively safe procedure that is gaining interest especially for patients suffering of severe renal insufficiency (a contraindication for contrast-enhanced imaging). It overcomes the spatial recognition limitation of the 2D imaging techniques and it can provide multiple measurements such as minimum and maximum annular diameters, annular perimeter and area. However, 3D TEE has the tendency to detect a more circular annulus [77, 80]. Also, manual measurements are significantly smaller when compared to measurements obtained from MDCT [77, 80–83]. This leads to disagreement in prosthesis sizing in a large portion of the population [76, 84–87]. Underestimation increases when a significant amount of calcium is detected at the level of the aortic annulus. Though, studies that rely on automatic 3D TEE aortic annular measurements for valve sizing yielded an overall good correlation with MDCT measurements and excellent agreement in TAV size selection [77, 82].

**MRI** can provide three-dimensional images with high spatial resolution (in the order of about 1.25mm x 1.25mm x 1.3mm). Excellent correlation was found between MRI and MDCT for all aortic annulus measurements and TAV size selection [88]. Unfortunately, there are several disadvantages that limit the use of MRI in TAVR pre-procedural planning. Patients with metallic devices or with a permanent pacemaker (PPM) implanted cannot undergo MRI. Also, obese patients may not fit in the MRI machine. Finally, quantification of calcifications with MRI is more difficult: calcifications appear as darker areas in the MRI images and might be underestimated.

**MDCT** has emerged as the gold standard imaging modality for pre-procedural TAVR planning in the last years. MDCT provides comprehensive details about the peripheral vascular access, coronary arteries as well as the geometry of the aortic annulus. Assessment of the vessel tortuosity and vessel luminal diameters is important for the access route evaluation. Previously, two-dimensional aortic annular measurements (performed in the sagittal and coronal planes) were used to assess the annulus diameter and to select the TAV size (Fig 2.1b). However, underestimation was observed in aortic annulus dimensions [78]. Three-dimensional MDCT allows the double-oblique multiplanar view (Fig 2.1c). From this view, the three cusps and the aortic annulus are clearly visible, and the annular dimensions can be accurately assessed. In fact, TAV sizing based on MDCT-based measurements showed to significantly reduce the risk of paravalvular AR [77–79, 89]. Finally, thanks to the CT's high spatial resolution, a quantitative assessment of the calcifications and their location can be performed. The evaluation of the degree of calcium is indeed very important when planning TAVR, as it may affect the alignment and deployment of the TAV as well as TAVR outcomes [90, 91]. The main limitation of this modality is related to the use of contrast medium in patients with severe renal insufficiency, as it may have adverse effects. Also, given the old and frail population that represents the majority of the patients currently treated with TAVR, image quality is in many cases suboptimal and affected by motion artefacts.

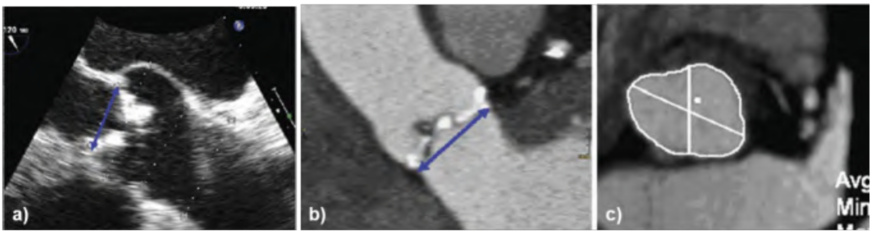

**Figure 2.1:** Assessment of the aortic annulus dimensions using transoesophageal echocardiography (a), MDCT from the coronal view (b), and using the double-oblique multiplanar view (c). (Adapted from [92]).

### 2.1.3 Peri-procedural imaging techniques

TAVR is always performed under real-time fluoroscopic guidance. Fig 2.2 shows the main steps of the implantation of a SAPIEN valve using real-time fluoroscopic guidance [93]. Next to it, TEE can help to visualize the valve deployment during the procedure. TEE can confirm the annulus measurements and can offer a precise and real-time assessment of complications as tamponade, coronary occlusion, aortic dissection and aortic and mitral regurgitation [94]. In addition, immediately after the procedure, it allows to assess the valve deployment and the leaflets mobility. Therefore, the fusion of these two imaging techniques (TEE and fluoroscopy) can guide the clinician to the most appropriate implantation position, with the main advantage that TAVR can be performed without contrast.

Compared to TEE, TTE offers lower quality images due to the supine positioning, and a suboptimal imaging of the aortic root and the aorta for early detection of complications. However, TTE is undertaken in many centers with the use of general anesthesia [95].

MDCT is normally not available in the Cath lab and is not adopted during the peri-procedural phase, mostly for timing and resolution reasons. A complete acquisition sequence might take up to 20 sec with loss of temporal resolution. Also, after the acquisition, the 3D reconstruction would be a time-consuming process during live TAVR [96]. Besides that, the patient would be exposed to additional radiation.

## 2.2 TAVR COMPLICATIONS

Clinical trials have demonstrated that TAVR reduces 30-day mortality (∼3%) with respect to the conventional surgical replacement (∼4.5%) and

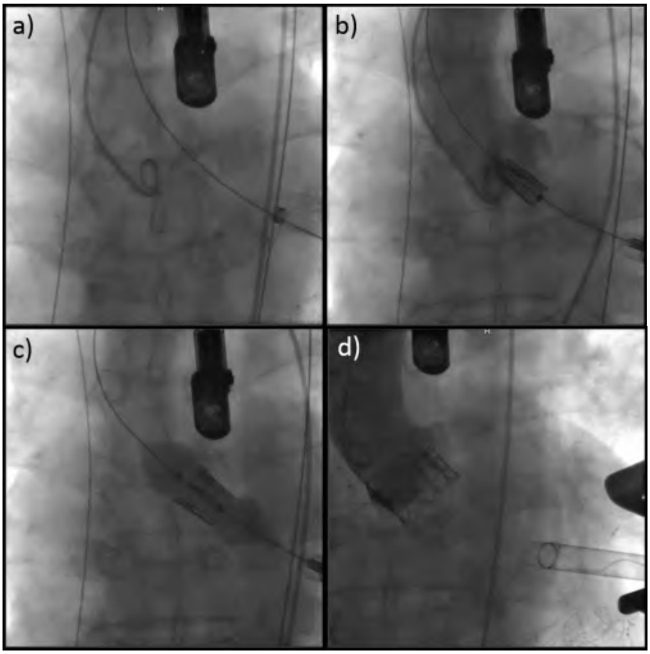

**Figure 2.2:** The main steps in the implantation of a SAPIEN valve using fluoroscopic images: a) placement of the guidewire; b) positioning of the SAPIEN device; c) inflation of the balloon; d) implanted valve (Adapted from [93]).

leads to a more rapid recovery for patients at extreme- high- or intermediate-risk [58]. However, there are several postoperative complications related to TAVR that should be addressed.

Complications can be categorized as early/procedural complications (occurring during or shortly after the procedure) or late/post-procedural complications (occurring several weeks later). Table 2.2 summarizes the rates of complications observed in clinical trials. The most common complications are briefly described below.

*Vascular complications* such as vascular injury, aortic dissection, aortic or annulus rupture and LV perforations occur in about 6-8% of the patients undergoing TAVR [55, 59, 60, 97]. Patients with calcified peripheral vessels or vessels with small minimal lumen diameter are more prone to develop vascular complications. Moreover, a higher rate of vascular complications has been reported for balloon-expandable devices (8.0%-17.4%), most probably because of the large sheath required for this TAVR system [66]. Although vascular complications are associated with increased mortality and major bleeding, they can be treated percutaneously with acceptable clinical outcomes.

*Coronary occlusion* occurs rarely after TAVR (0.2-0.6%), though it can be fatal [43, 59, 66, 97]. Usually, it results from valve calcifications that are pushed towards the sinuses of Valsalva during valve deployment, preventing the blood flow towards the coronary ostia. Adverse effects can normally be avoided with conversion to SAVR, where the native calcified valve is removed. Alternatively, percutaneous coronary interventions can be performed in concomitance with TAVR.

*Acute kidney injury (AKI)* after TAVR is more prevalent in extreme-risk patients (11.8% at 1-year) [98] compared to high-risk patients (about 6%) [43] or lower- and intermediate-risk patients (0.7%-1.7%) [59, 60]. Although its incidence after TAVR is much lower compared to SAVR (6.0% vs 15.1%), it is associated with high mortality [43]. AKI is the rapid loss of kidney function occurring over hours or days. This causes dysregulation of vascular volume and electrolyte homeostasis and accumulation of metabolic waste products. For this reason, pre-procedural and procedural imaging techniques that require contrast medium administration should be avoided especially in extreme-risk patients.

*Stroke* rates vary proportionally to the TAVR risk score. At 1-year after TAVR, stroke occurs in about 10% of the patients deemed inoperable [68], in 5.4%-8.0% of the patients at intermediate-risk [8, 59] and in about 2.9% of the patients at low-risk [60]. Usually, it occurs during or immediately after the procedure (0-3 days) [97]. However, a moderate increase in rate is observed over time [3, 43, 54]. The majority of strokes are caused by embolization of atherosclerotic material from the stenotic valve during TAVR. Patients with inadequate iliofemoral access for TAVR and patients who were treated with antiplatelet agents in addition to aspirin are more prone to neurologic events [99].

*(New onset or worsening) atrial fibrillation* incidence ranges from 4.2% to 19.5% [3, 5, 54, 55, 59, 60, 66]. Atrial fibrillation is a common arrhythmia in patients with AS, which can get worse during and/or after TAVR. It is associated with increased mortality, adverse ischaemic and haemorrhagic events. Therefore, it is very important to properly prevent it and treat it.

*Valve migration* is a rare (0.2-2.8%) but serious complication that may occur when the device is improperly anchored to the aortic root complex. The main causes of device migration are mis-sizing of the device or suboptimal position within the aortic root. It usually occurs during or shortly after the procedure, and it can be managed by implanting a second device while leaving the dislocated device in situ. Lately, valve migration is becoming less frequent with the advent of repositionable TAVs (e.g. Lotus, Evolut R) which, if not completely released, can be retrieved and correctly repositioned [5, 97].

*Permanent pacemaker* (PPM) implantation after TAVR rate varies from about 5% to more than 40%. Given the high occurrence, it is considered an Achille's heel of TAVR. PPM is usually implanted shortly after the procedure (3-7 days), and comparable rates are reported over time [3, 43, 54]. PPM implantation following new conduction abnormalities strongly depends on the implanted TAV type. The CoreValve US Pivotal study observed very high PPM rates especially in lower-risk patients (34.1% at 1- year) [60, 62]. The PARTNER trial reported much lower PPM incidence after TAVR with a balloon-expandable device (4.5-9.9% at 1-year) [4, 64]. PPM does not seem to influence late mortality [5, 100]. However, it is associated with increased costs, longer hospitality and perhaps patient's morbidity. Therefore, given that TAVR is moving towards younger patients, it is necessary to predict the risk of new conduction abnormalities upfront and avoid TAVR in patients with high risk of receiving a PPM. The mechanism behind the development of conduction abnormalities is still unclear and currently under investigation. A detailed insight on the current state of the art will be given in section 2.2.1.3.

*Paravalvular aortic regurgitation* (AR) incidence (at 1-year) ranges from 3.5% to 12.8% after implantation of a CoreValve System and it is comparable among intermediate-, high- and extreme-risk patients [5, 43, 55, 59, 98, 101]. Significantly higher incidence of AR (about 15%) has been reported by the NOTION clinical trial [60, 63] in lower-risk patients. However, during the NOTION clinical study, echocardiography was used to determine the annulus diameter, which may have led to prosthesis undersizing. The PARTNER trial reported low occurrence of moderate (or more severe) AR, especially in patients deemed inoperable. The REPRISE III trial reported a very low rate of AR at 1-year after Lotus valve implantation (0.9%) [5]. Paravalvular AR refers to blood flowing through a channel between the implanted TAVR device and the aortic root wall. Data about the progression of AR over time are discordant. Some clinical trials reported stable AR over time [3, 7, 54, 59, 66]. Others reported worsening of paravalvular AR at 5-years follow up [6]. Moderate and severe AR are associated with higher mortality [102]. Nevertheless, in patients at high surgical risk even mild AR was found to be associated with increased mortality [7, 56, 66]. Therefore, although improvements in TAVR devices and periprocedural techniques have reduced AR rate, mild or more AR should be eliminated, especially in the perspective of expanding indications to younger low-risk patients. Mechanisms that cause progression of paravalvular AR after TAVR remain to be clarified. A detailed insight on the current state of the art of paravalvular AR will be given in section 2.2.2.

Table 2.2: TAVR common complications derived from available clinical trials and clinical studies

| Study name | REPRISE III | | SURTAVI | | NOTION | | | CoreValve US High-risk pivotal trial | | | | | - |
|---|---|---|---|---|---|---|---|---|---|---|---|---|---|
| Device | Lotus | CoreValve/ Evolut R | CoreValve/ Evolut R | | CoreValve | | | CoreValve | | | | | CoreValve |
| Target population | High- or extreme-risk | | Intermediate-risk | | Lower-risk | | | Extreme-risk | High-risk | High-risk | High-risk | High-risk | Low-risk |
| Enrollment period | 09/2014-03/2015 | | Last enrollment 2016 | | 12/2009 - 12/2012 | 12/2009 - 04/2013 | 12/2009 - 04/2013 | 02/2011 – 09/2012 | | | | | 03/2016 – 11/2018 |
| Longest follow up | 1 year | | 1 year | 2 years | 1 year | 2 years | 5 years | 1 year | 1 year | 2 years | 3 years | 5 years | 1 years |
| **Mortality** | 11.9% | 13.5% | 6.7% | 11.4% | 4.9% | 8.0% | 27.6% | 24.3% | 14.2% | 22.2% | 32.9% | 55.4% | 2.4% |
| **Cardiovascular death** | 7.7% | 9.8% | 4.8% | 7.7% | 4.3% | 6.5% | 20.8% | 18.3% | 10.4% | 15.4% | 22.9% | 39.5% | 1.7% |
| **Vascular complications** | 7.7% | 6.1% | 6.0%* | - | 5.6%* | - | - | 8.4% | 6.2% | 7.1% | 7.1% | 7.1% | 3.8% |
| **Life-threatening or disabling bleeding** | 9.9% | 9.8% | 12.2%* | - | 11.3%* | - | - | 17.6 % | 16.6% | 18.1% | 19.1% | - | 3.2% |
| **Coronary occlusion** | - | - | 0.2%* | - | - | - | - | - | 0.6% | - | - | - | 0.9% |
| **Acute kidney injury** | 2.6% | 3.7% | 1.7%* | - | 0.7%* | - | - | 11.8% | 6.0% | 6.2% | 6.2% | - | 0.9% |
| **All stroke** | 7.0% | 9.4% | 5.4% | 6.2% | 2.9% | 3.6% | 9.0% | 7.0% | 8.8% | 10.9% | 12.6% | 17.5% | 4.1% |
| **New onset or worsening atrial fibrillation** | 6.6% | 4.7% | 12.9%* | - | 16.9% | 22.7% | 23.4% | - | 15.9% | 19.5% | - | - | 9.8% |
| **More than moderate PVL** | 0.9% | 6.9% | 5.3% | - | 15.7% | 15.4% | 8.2% | 4.2% | 6.1% | 6.1% | 7.1% | 3.6% | 3.5%* |
| **Permanent pacemaker** | 41.4% | 23.0% | 25.9%* | - | 34.1% | 41.3% | 41.7% | 26.2% | 22.3% | 25.8% | 28.0% | 22.3% | 19.4% |
| **Valve migration** | 0.0% | 2.7% | - | - | - | - | - | 0.2% | 6.4% | 0% | - | - | - |

| **Study name** | PARTNER | | | | | | | | | | |
|---|---|---|---|---|---|---|---|---|---|---|---|
| **Device** | Sapien | | | | | | | | | | |
| **Target population** | Low-risk | Intermediate-risk | High-risk | Inoperable | Intermediate-risk | High-risk | Inoperable | High-risk | Inoperable | High-risk | Inoperable |
| **Enrollment period** | 03/2016 – 10/2017 | 12/2011 – 11/2013 | 05/2007–08/2009 | 05/2007 – 03/2009 | 12/2011 – 11/2013 | 05/2007–08/2009 | 05/2007 – 03/2009 | 05/2007–08/2009 | 05/2007 – 03/2009 | 05/2007–08/2009 | 05/2007 – 03/2009 |
| **Longest follow up** | 1 year | | | | 2 years | | | 3 years | | 5 years | |
| **Mortality** | 8.5% | 12.3% | 24.2% | 30.7% | 16.7% | 33.9% | 43.3% | - | 54% | 67.8% | 71.8% |
| **Cardiovascular death** | 0.8% | 7.1% | 14.0% | 19.6% | 10.1% | 21.4% | 31.0% | - | 41.4% | 53.1% | 57.5% |
| **Vascular complications** | 2.8% | 8.4% | 11.3% | 16.8% | 8.6% | 11.6% | - | 12.5% | 17.4% | 11.9% | - |
| **Major bleeding** | 7.7% | 15.2% | 15.7% | 22.3% | 17.3% | 19.0% | 28.9% | 20.8% | 32.0% | 26.6% | - |
| **Coronary occlusion** | 0.2% | 0.4% | - | - | 0.4% | - | - | - | - | - | - |
| **Acute kidney injury** | 0.4%* | 3.4% | 5.4% | 1.7% | 3.8% | 6.2% | 3.2% | 7.2% | 3.2% | 8.6% | - |
| **All stroke** | 1.2% | 8.0% | 6.0% | 10.1% | 9.5% | 7.7% | 13.8% | 6.9% | 15.7% | 10.4% | 16% |
| **New onset or worsening atrial fibrillation** | 7.0% | 10.1% | - | 0.6% | 11.3% | - | - | - | - | - | - |
| **More than moderate AR** | 29.4%** | 2.6% | 7.0% | 11.8% | 2.0% | 6.9% | 4.5% | - | 4.5% | 14% | 14% |
| **Permanent pacemaker** | 7.5% | 9.9% | 6.4% | 4.5% | 11.8% | 7.2% | 6.4% | 8.1% | 7.6% | 9.7% | - |
| **Valve migration** | - | - | - | - | - | - | - | - | - | - | - |

**Complication occurrences evaluated at 30 days from the procedure.*
***More than mild paravalvular AR.*

### 2.2.1 Conduction abnormalities: the first TAVR Achille's heel

To understand the mechanism behind the development of conduction abnormalities, some anatomic and physiologic principles of the cardiac conduction system need to be considered in detail.

#### *2.2.1.1 Physiology of the conduction system of the heart*

The cardiac conduction system consists of cardiac muscle (pacemaker) cells and conduction fibers that are specialized to initiate and distribute impulses throughout the heart, so that its chambers contract in an orderly and sequential manner throughout the cardiac cycle. Fig 2.3 shows the sequence of the electrical excitation [9]. Briefly, (1) rhythmical electric signals arise in the sinoatrial (SA) node located in the right atrium, just inferior to the entrance of the superior vena cava. This sinus rhythm determines the intrinsic heart rate. (2) From the SA node, the electric signals travel to the AV node located in the inferior portion of the interatrial septum, immediately above the tricuspid valve. (3) After a small delay of about 0.1 s, the signaling impulse sweeps to the bundle of His (also called AV bundle) in the superior part of the interventricular septum. The bundle of His is the only electrical connection between atria and ventricles. (4) Then, the impulse diverges through the right and left bundle branches (RBB and LBB respectively), which run along the interventricular septum towards the apex of the heart. Finally (5), the signals run to the respective Purkinje fibers for each side of the heart. Because the LV is much larger than the right, the Purkinje network is more elaborate in that side of the heart.

#### *2.2.1.2 Relationship between the aortic valve and the atrioventricular conduction system*

The AV node, bundle of His and LBB and RBB constitute the so-called AV conduction system, which lies in close proximity to the aortic root (AoV and LVOT).

The AV node is located within the triangle of Koch (in the right atrium) which is formed by the tendon of Todaro, the tricuspid valve attachment and the orifice of the coronary sinus [103] (Fig. 2.4). However, it is difficult to use the triangle of Koch as a landmark for the position of the AV node because, in many cases, the tendon of Todaro is not macroscopically visible. Therefore, the location of the AV conduction system is usually identified using the inferior border of the interventricular membranous septum as anatomical landmark [104, 105]. The AV node continues as the bundle of His, piercing the membranous septum and penetrating to the left through the central fibrous body. On the left side, the bundle of His exits beneath the membranous septum and runs superficially along the crest of the interventricular muscular

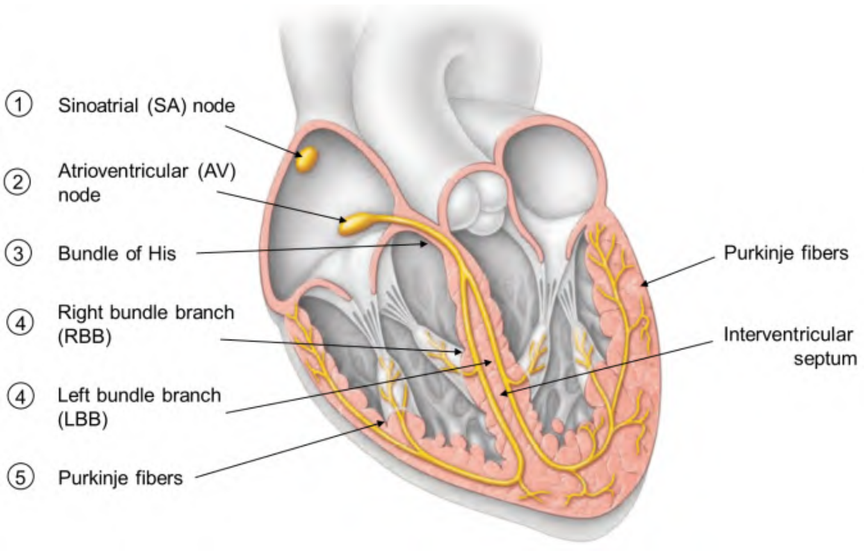
① Sinoatrial (SA) node
② Atrioventricular (AV) node
③ Bundle of His
④ Right bundle branch (RBB)
④ Left bundle branch (LBB)
⑤ Purkinje fibers
Purkinje fibers
Interventricular septum

**Figure 2.3:** Anatomy of the intrinsic cardiac conduction system showing the sequence of the electrical excitation (Adapted from [9]).

septum (Fig 2.5a). According to some measurements performed by Kristin (1949), the width of the bundle of His can vary from 0.7 to 3.5 mm and its length from 7.0 to 15.0 mm [106]. Of note, the depth of the bundle of His with respect to the inferior border of the membranous septum also varies among people: in 47% of the cases it runs along the border, in 32% within the muscular part and, in the remaining 21%, it runs onto the membranous part [104]. The crest of the interventricular muscular septum can be identified on high quality MSCT images. Further details can be found in Chapter 4. At the level of the crest of the interventricular septum, the bundle of His gives rise to the fascicles of the LBB. The LBB is intimately related to the aortic root. In fact, it exits approximately 2-3 mm below the base of the interleaflet triangle separating the NCC and RCC of the aortic valve [107], as clearly shown in the reconstruction made by Tawara in his monograph (Fig 2.5b).

Due to its proximity to the aortic root, the AV conduction system is particularly exposed and susceptible to injury during therapeutic procedures such as TAVR. An overview of the main conduction abnormalities following a TAVR procedure will be presented in the next paragraph (2.2.1.3).

#### 2.2.1.3 *Type of conduction abnormalities following TAVR*

The most prevalent conduction abnormalities after TAVR are LBB block (LBBB) and total AV block (AVB), most of the times leading to PPM implantation.

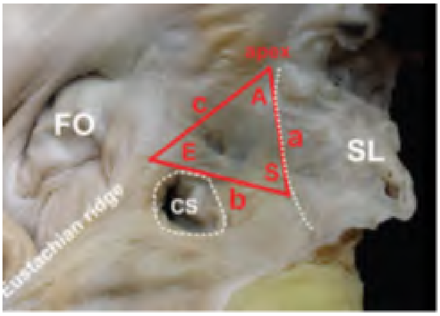
apex
A
c
a
FO
E
SL
S
b
CS
Eustachian ridge

**Figure 2.4:** Schematic view of the Koch's triangle (in red). a = anterior edge; A = apex angle; b = basal edge; c = posterior edge; CS = coronary sinus; E = Eustachian angle; FO = fossa ovalis; S = septal leaflet angle; SL = septal leaflet of the tricuspid valve (Adapted from [103]).

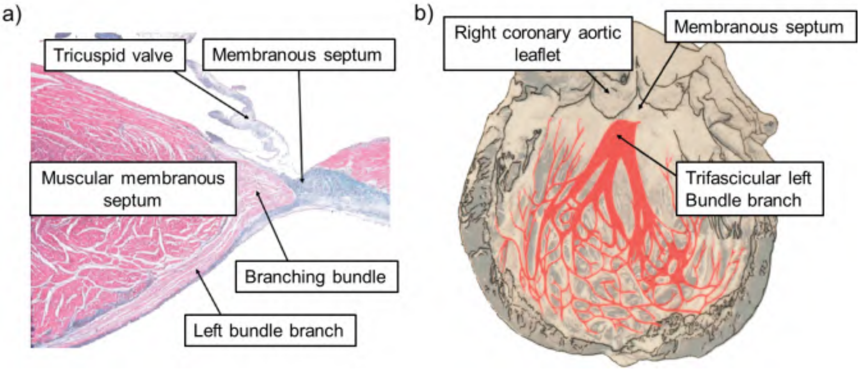
a)
Tricuspid valve
Membranous septum
Muscular membranous septum
Branching bundle
Left bundle branch
b)
Right coronary aortic leaflet
Membranous septum
Trifascicular left Bundle branch

**Figure 2.5:** a) Histological section which shows the atrioventricular bundle exiting superficially along the crest of the interventricular septum, and continuing to supply the left ventricle; b) Monograph of Tawara: how the left bundle branch exits below the base of the interleaflet triangle, separating the noncoronary and right coronary leaflets of the aortic valve and fanning along the ventricular septum to supply the left ventricle [107].

The LBBB is the most frequent cause of electromechanical asynchrony and it occurs because of damages to the fibers of the LBB. As a consequence, the ventricles contract sequentially (first right, then left) rather than simultaneously.

The AVB is a conduction defect affecting impulses from the atria to the ventricles and it is a direct consequence of damages to the AV node, to the bundle of His or the bundle branches. AVBs are subdivided according to the degree of block into: 1st, 2nd and 3rd degree or total AVB. First-degree AVB is just a delay in conduction of the atrial impulse, however all impulses are conducted to the ventricles (Fig 2.6a). It is rarely serious and in most of the cases it is left untreated. In second-degree AVB, some atrial impulses fail to reach the ventricles. It can be either nodal or infranodal. Nodal blocks occur within the AV node. Infranodal blocks occur within the bundle of His or the bundle branches. Second-degree AVB is additionally divided into Mobitz type I (commonly nodal) and Mobitz type II (commonly infranodal). Type I is also known as Wenckebach and it is described by a progressive delay between the atrial and the ventricular contraction that precedes a blocked impulse. Instead, in Mobitz type II no delay between the atrial and ventricular contraction is seen before the dropped impulse. Third-degree AVB occurs when the atrial and ventricular impulses are not synchronous and, normally, the atrial rate is faster than the independent ventricular rate. This block can be either nodal or infranodal. Also, total AVB can result from simultaneous block of the right and left bundle branches. In case of 2nd or 3rd degree (nodal) AVB, a focus of cells in the bundle of His that possess automaticity functions as pacemaker and discharge an 'ectopic' impulse (Fig 2.6b).

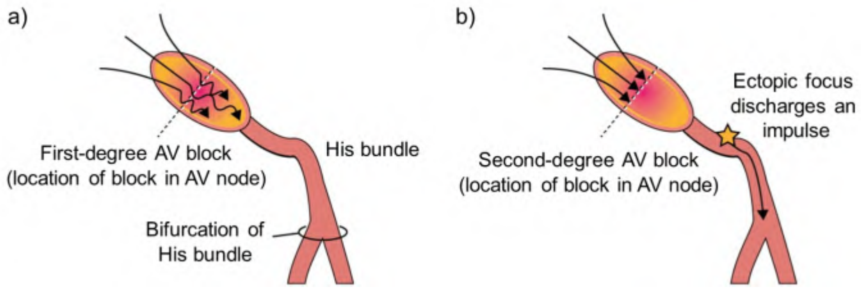

**Figure 2.6:** a) Schematic representation of the $1^{st}$ degree AVB. The impulse is delayed in the AV node but once it passes the subsequent conduction is normal. b) Schematic representation of a 2nd or 3rd degree (nodal) AVB. The impulse is blocked in the AV node, but the cells of the bundle of His possess automaticity and will discharge and impulse (Adapted from `https://ecgwaves.com/`).

#### 2.2.1.4 *Diagnosis of conduction abnormalities*

Conduction abnormalities can be detected by monitoring the electrical currents generated in and transmitted through the heart [9]. The graphic record of the heart activity is called electrocardiogram (ECG). A normal ECG is shown in Fig 2.7 and Fig 2.8a.

A typical ECG has 3 distinguishable waves. The first, P wave, lasts about 0.08 s and it results from the propagation of the depolarization wave from the SA node to the atria. Approximately 0.1 s after the P wave, the atria contract. The QRS complex results from the ventricular depolarization and precedes the ventricular contraction. Average duration of the QRS complex is 0.08 s. The T wave is caused by the ventricular repolarization and it lasts about 0.16 s. The P-Q interval (about 0.16 s) is the time from the beginning of the atria excitation and the beginning of the ventricular excitation. The P-R interval includes the atrial depolarization. During the S-T plateau the ventricles are depolarized. The Q-T interval (lasting about 0.38 s) is the period from the ventricular depolarization to the ventricular repolarization.

The size, duration and timing of the waves tend to be consistent. For this reason, changes in the pattern or timing of the ECG may reveal a diseased heart or problems to the cardiac conduction system. For example, the duration of the QRS complex may be used to differentiate between nodal and infranodal blocks. Nodal blocks that occur within the AV node usually results in a narrow QRS complex with a ventricular rate greater than 40 beats per minute (bpm). Infranodal blocks that originate within the bundle of His or the bundle branches often display a wide QRS complex with a ventricular rate of less than 40 bpm.

Some examples of abnormal ECGs are shown in Fig 2.8. The ECG of LBBB is characterized by a longer QRS complex (>0.12 s) with very small Q waves (Fig 2.8b) and can present a broad or notched ('M'-shaped) R wave. This reflects the sequential activation of the ventricles.

The ECG of $1^{st}$ degree AVB (Fig 2.8c) is characterized by a longer PR interval (>0.2 s). This pattern reflects the delayed impulse between atria and ventricles.

In the ECG of a $2^{nd}$ degree AVB not all P waves are followed by a QRS complex (Fig 2.8d). This represents impulses originated in the SA node but not always conducted through the AV node. Mobitz type I and type II can also be distinguished. Mobitz type I involves a progressive PR lengthening until the QRS "drops out", indicating that impulses take longer to travel through the AV node until one impulse is completely blocked. Whereas, Mobitz type II presents a repetitive pattern of conducted P waves followed by non-conducted P waves (PR interval is constant).

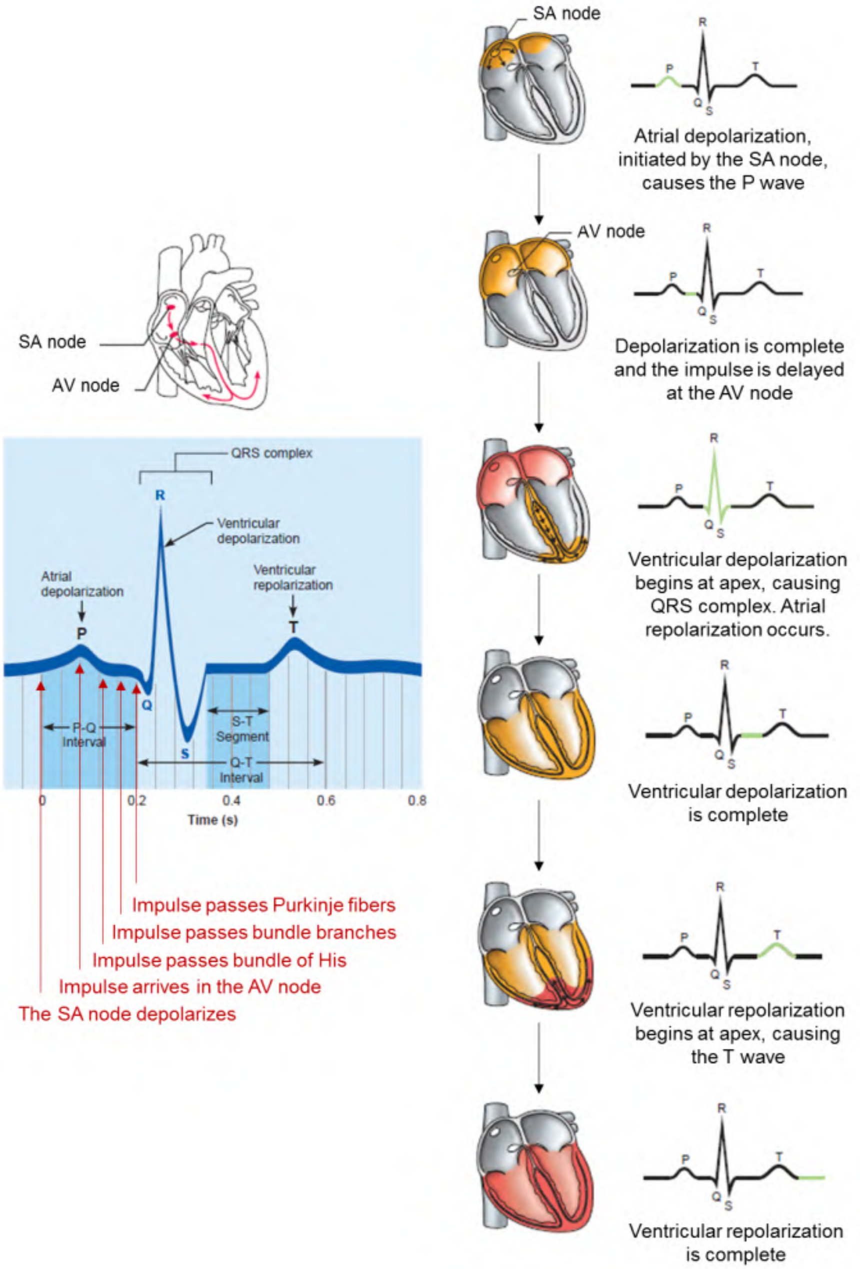
SA node
AV node
QRS complex
R
Ventricular depolarization
Atrial depolarization
Ventricular repolarization
P
T
Q
S
P-Q Interval
S-T Segment
Q-T Interval
0
0.2
0.4
0.6
0.8
Time (s)
Impulse passes Purkinje fibers
Impulse passes bundle branches
Impulse passes bundle of His
Impulse arrives in the AV node
The SA node depolarizes
SA node
Atrial depolarization, initiated by the SA node, causes the P wave
AV node
Depolarization is complete and the impulse is delayed at the AV node
Ventricular depolarization begins at apex, causing QRS complex. Atrial repolarization occurs.
Ventricular depolarization is complete
Ventricular repolarization begins at apex, causing the T wave
Ventricular repolarization is complete

**Figure 2.7:** Normal echocardiogram tracing (Adapted from [9]).

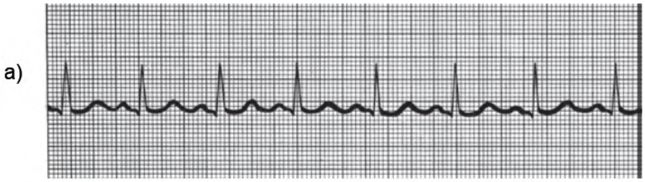

**Normal sinus rhythm**

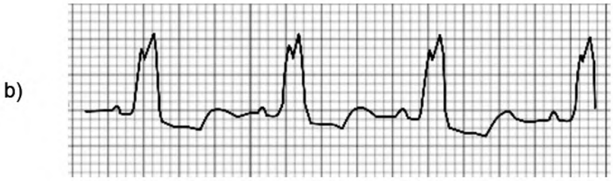

**LBBB.** The right ventricle is activated before the left and this produces a broad, notched ('M'-shaped) R wave.

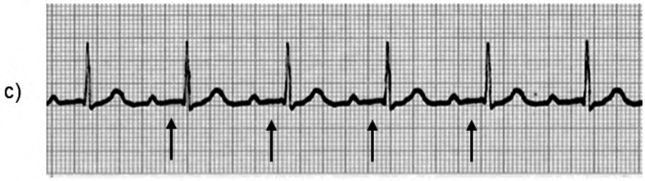

**First-degree AVB.** PR interval is longer than normal (>0.2 s).

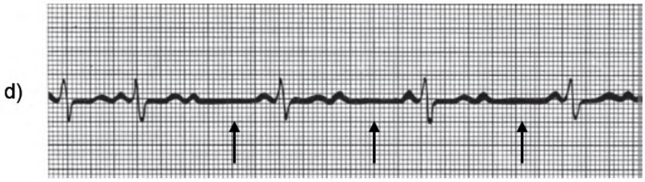

**Second-degree AVB.** Some P waves are not conducted through the AVN; hence more P than QRS waves are seen. In this tracing, the ratio of P waves to QRS waves is mostly 2:1.

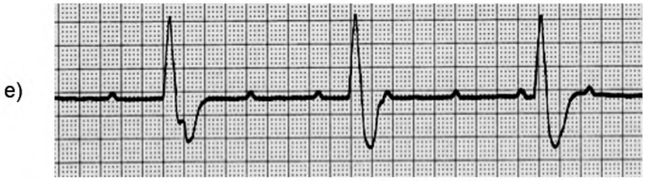

**Third-degree AVB.** No relationship between P waves and QRS complexes. The atrial rate is faster, hence more P than QRS waves are seen.

**Figure 2.8:** Normal and abnormal ECG tracing.

The ECG of $3^{rd}$ degree AVB shows no relationship between P waves and QRS complexes (Fig 2.8e). This reflects the asynchrony between atria and ventricles. Normally there will be more P waves than QRS complexes. Also, as the PR interval will be totally inconsistent, P waves might be superimposed to the QRS complexes.

#### *2.2.1.5 Management of conduction abnormalities: permanent pacemaker implantation*

The American Heart Association, the Heart Rhythm Society (ACC/AHA/HRS), and the European Society of Cardiology (ESC) strongly recommend the implantation of PPM in case of sinus node dysfunction and high-degree or symptomatic AVB [108, 109]. However, guidelines on timing for PPM do not exist.

Most AV conduction abnormalities appear within the first week after the procedure. Therefore, a 7-day ECG monitoring is recommended. If total AVB appears earlier, then PPM can be implanted earlier. However, as AVB after TAVR exhibits a dynamic nature, it might recover in some patients. Therefore, there is a lack of consensus in case of occurrence of 2nd degree AVB, bundle branch block or combination of AVB and bundle blocks.

#### *2.2.1.6 Predictors for conduction abnormalities*

A number of studies indicate that both patient- and procedure-related factors play a role in the occurrence of new conduction abnormalities after TAVR.

Among patient-related factors, the presence of existing conduction abnormalities, in particular RBB block, is the strongest predictor for new-onset of total AVB after TAVR [110–125]. The duration of QRS complex at baseline and high transaortic pressure gradients (>50 mmHg) have also been identified as predictors of persistent conduction abnormalities and the need of PPM [121, 126, 127].

In addition, many studies have identified anatomical features as the length of the membranous septum, the distance of the annulus to the left coronary ostium, the LVOT dimensions and presence of calcification in the LVOT, NCC or LCC, as predictive factors for new-onset LBBB and the need of PPM implantation [113, 122, 128–130].

Because of the spatial proximity between the AV conduction system and the aortic root, damages predominantly occur during the procedure (positioning and deployment of the valve). Irrespective of the valve type, the depth of implantation is one of the most frequently identified procedural factors, with deeper implantation associated with higher risk of new conduction abnormalities [116–118, 120, 125, 131]. The size of the balloon used during pre- or post-dilatation [114, 126] and the oversizing of the chosen valve have also been associated to the risk of new conduction abnormalities. They might result in overstretching of the LVOT tissues in the region of the membranous septum [111, 127, 131].

Finally, TAVR-related AV conduction abnormalities seem to be device specific. Several studies have reported higher incidence of conduction abnormalities and PPM implantation with the Lotus valve and CoreValve System, compared to the Sapien valves [121, 123, 126, 132], with the Lotus valve more prone to cause AV block than self-expandable devices (41.4% vs 23.0% respectively) [5, 132]. This indicates that valve design and deployment technique matter.

### 2.2.2 Aortic regurgitation: the second TAVR Achille's heel

The second major complication after TAVR is residual aortic regurgitation. To date, new TAV generations have partially addressed this complication and several improvements in imaging and treatment have been done. However, residual AR remains a strong and independent predictor for 1-year mortality [102]. This section will describe causes and predictors as well as diagnosis and treatment of residual AR.

#### 2.2.2.1 *Types of aortic regurgitation and main causes*

Traditionally aortic regurgitation is categorized as transvalvular, paravalvular or supra-skirtal (Fig 2.9). Transvalvular AR is located within the prosthetic valve (Fig 2.9a). It can result from limited motion of the TAV leaflets or elliptical TAV shape at the commissure level. TAV leaflets that are damaged during the crimping or the implantation phase might also cause transvalvular AR [133]. Furthermore, extensive post-dilatation may cause suboptimal leaflet coaptation [134].

Paravalvular AR occurs between the TAV and the native aortic annulus because of incomplete apposition of the TAV with the surrounding aortic tissues (Fig 2.9b). In fact, during TAVR the native calcified aortic valve is not removed, and, during the prosthetic valve deployment, the native leaflets are pushed against the aortic wall and into the sinuses of Valsalva. Therefore, the native leaflets, calcifications and the presence of subannular calcifications interfere between the TAVR device and the aortic wall, preventing a good apposition of the device with the aortic wall. As a consequence, paravalvular gaps originate between the TAV and the aortic root, leading to regurgitation jets. Besides extensive calcifications, prosthesis undersizing is a major cause of paravalvular AR. For instance, many studies reported that echocardiographic imaging underestimates the aortic annulus dimensions as compared to MDCT, and that is related to significantly more residual AR [78, 79].

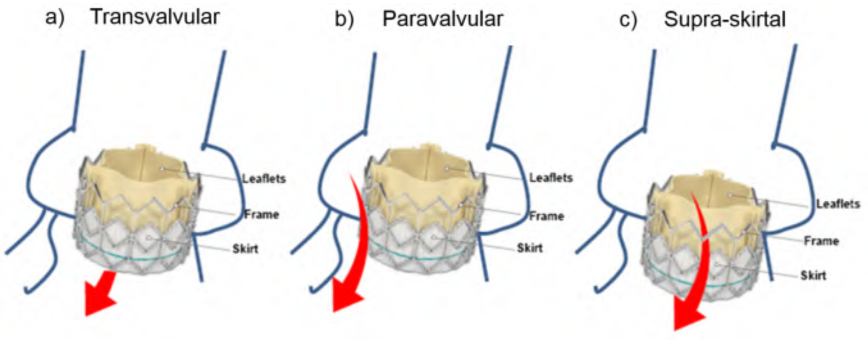

**Figure 2.9:** Different types of aortic regurgitation after implantation of the Sapien XT valve. a) transvalvular regurgitation, b) paravalvular regurgitation, c) supra-skirtal regurgitation. Regurgitation is represented by the red arrow. (Adapted from `www.edwards.com`).

Supra-skirtal AR is similar to paravalvular AR and it occurs when the device is implanted in an extremely low position (Fig 2.9c). The lower part of the TAV frames is covered by a skirt with the aim to seal the gap between the native leaflets and the TAV. Hence, if the TAV is implanted in a too low position, leakage through the uncovered part of the TAV, above the skirt, can occur.

Given the fact that the majority (about 95%) of significant AR after TAVR is paravalvular, not transvalvular [135], this PhD project focused on paravalvular AR only.

#### 2.2.2.2 *Diagnosis of residual paravalvular aortic regurgitation*

Several imaging techniques can be used to evaluate the grade of residual AR.

**Cardiac MRI** is considered the gold standard as it is the most reproducible, accurate and reliable method [136]. It is a non-invasive technique that allows a direct quantitative assessment of the regurgitation volume and fraction. Cardiac MRI grades of AR are defined according to the regurgitant fraction (RF), calculated as $\frac{\textit{Regurgitant volume}}{\textit{Stroke volume}} \cdot 100$ (Fig 2.10a). AR is then classified as none/trace (RF<15%), mild (16%-29%) or moderate/severe (⩾30%) [137]. Evaluation based on cardiac MRI showed to be strongly associated with adverse events [138, 139]. Furthermore, very low inter- and intra-observer variability has been reported. Unfortunately, MRI is expensive and limited availability. Also, it cannot be used in many patients (i.e. patients with PPM implanted).

**Contrast angiography** is also an important instrument to grade residual AR based on the visual grading of the severity of the backflow contrast agent from the aorta to the LV (Fig 2.10b). The Sellers classification subdivides residual AR in 5 grades: grade 0 = absence of AR; grade 1 = small amount of contrast entering the LV; grade 2 = contrast filling the entire LV in diastole but with less density as compared to contrast in the aorta; grade 3 = contrast filling the entire LV in diastole with same density as compared to contrast in the aorta; grade 4 = contrast filling the entire LV in diastole with greater density as compared to contrast in the aorta [140]. AR grades based on Sellers criteria correlate well with AR assessment based on MRI [141, 142]. However, angiography only provides a qualitative assessment of regurgitation and, therefore, it is strongly subjective. Furthermore, owing to the three-dimensional nature of the regurgitation jets, in some cases the qualitative assessment based on only one 2D view, can be very difficult. Finally, for many patients undergoing TAVR who suffer of renal insufficiency, the use of contrast agent should be limited.

**Color Doppler 2D and 3D TTE** is the current gold standard to evaluate AR severity. The assessment of AR is performed through the cross-sectional area of the regurgitant jet evaluation (also called *vena contracta*). Using 2D TTE, qualitative assessment of the width and area of the color Doppler jet is performed in the short and long parasternal axis (Fig 2.10c). The circumferential extent of the jet estimated in the short-axis view is the main parameter that has been proposed in the guidelines for semiquantitative assessment of paravalvular AR severity, and it is expressed as a percentage. According to the American Society of Echocardiography and the Valve Academic Research Consortium (VARC-2) guidelines, AR is graded as: none (no regurgitation), mild (jet width <25% of the LVOT width and circumferential extent <10%), moderate (jet width from 25 to 65% of the LVOT width and circumferential extent from 10 to 30%), and severe (jet width >65% of the LVOT width and circumferential extent >30%) [137, 143, 144]. Significant underestimation of AR severity using 2D TTE has been reported [138, 139, 145–147]. Underestimation is probably due to shadowing of calcification at annular level or in the LVOT and Doppler attenuation from the implanted TAV.

However, Doppler 3D echocardiography may overcome limitations of the 2D TTE. Three-dimensional TTE allows to generate a planimetry of the vena contracta (Fig 2.10d). This planimetry improves the evaluation of regurgitant jets and results correlate much better with MRI grading assessment than based on 2D echocardiography [136].

Quantitative **hemodynamic measurements** can provide complementary info for the assessment of AR degree. Hemodynamic measurements are based on the AR index, which is defined as $\frac{DBP - LVEDP}{SBP} \cdot 100$, where DBP is the (systemic) diastolic blood pressure, LVEDP is the LV end-diastolic pressure and SBP is the (systemic) systolic blood pressure (Fig 2.10e). AR index <25 has been reported to be an independent factor of increased mortality at 1-year for TAVR [148]. However, this method is very sensitive to the heart rate, aortic pressure, degree of mitral regurgitation and other factors. To overcome some of these limitations, Sinning et al recently proposed to use the dimensionless AR index, which expresses the ratio between AR index pre and post TAVR (cutoff of 0.60) [149]. The combination of the two parameters improves the discriminatory accuracy, and can help to identify patients with 'acute' hemodynamic deterioration independent of the degree of AR. As these indexes depend on the heart rate and aortic pressure, the average of these parameters over several cardiac cycles should be calculated and recorded at least 5 to 10 min after the deployment of the prosthesis. This would allow to exclude procedural bias as increased LVEDP due to balloon dilatation. Finally, another pitfall of the AR index is that it is an invasive technique and it cannot distinguish between paravalvular and central jets.

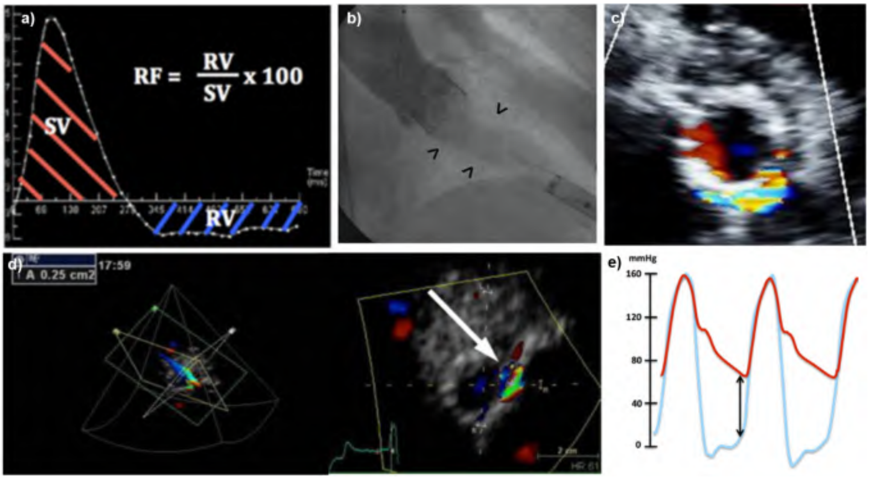

**Figure 2.10:** Determination of the severity of residual AR using different techniques. a) Aortic flow during one cardiac cycle and calculation of the RF using **cardiac MRI** (stroke volume in red, regurgitant volume in blue) [147]; b) **angiographic** image (arrows indicate agent backflow from the aorta into the LV) [141]; c) color **Doppler 2D TTE** image of the regurgitation jet in the short axis [145]; d) **Doppler 3D TTE** (jet planimetry on the left, *vena contracta* area indicated with a white arrow on the right) [136]; e) calculation of the AR index for **hemodynamic** evaluation (left ventricular end-diastolic pressure in blue and diastolic blood pressure in red) [148]. AR = Aortic regurgitation. LV = Left ventricle. MRI = Magnetic resonance image. TTE = transthoracic echocardiography.

Due to the advantages/disadvantages of each technique and the high subjective evaluation of residual AR, a multiparametric approach that combines the results from more techniques is needed. Also, different grading schemes that are adopted in different studies make the comparison between techniques and results between studies very challenging.

For instance, clinical trials reported that moderate/severe AR is associated with increased mortality at 30-days and 1-year after TAVR. However, results related to mild AR are conflicting. As a possible solution, Pibarot et al. proposed a unifying scheme for grading paravalvular AR based on 5-classes: trace, mild, mild-to-moderate, moderate, moderate-to-severe, severe [150] (Table 2.3).

Given the correlation between paravalvular AR and increased mortality, it is of paramount importance to limit it as much as possible. Some corrective actions that can be taken to improve the clinical outcomes during or after the procedure are listed below.

#### 2.2.2.3 *Management of paravalvular aortic regurgitation*

Periprocedural actions include post-dilatation, valve-in-valve procedure and repositioning of the TAV. Post-dilatation can reduce the severity of paravalvular AR by at least 1 grade. However, it is often associated with increased risk of cerebrovascular events, annulus rupture and incidence of transvalvular AR [151]. Valve-in-valve procedure is mostly used to correct transvalvular AR but can also be considered for paravalvular AR resulting from malpositioning of the TAV. However, severely inadequate positioning is becoming less frequent with the advent of retrievable and repositionable devices (Evolut R, Lotus, Portico). Therefore, the use of valve-in-valve procedure to correct inadequate positioning is less common. Finally, if those actions are not sufficient to reduce paravalvular AR, percutaneous paravalvular leak closure can be adopted [152]. During this procedure, the doctor places a closure device (i.e. a ring that acts as occluder) in the leak.

#### 2.2.2.4 *Predictors for paravalvular aortic regurgitation*

Anatomical and procedural factors have been identified as predictors for paravalvular AR after TAVR.

Among the anatomical factors, a baseline large mean aortic annulus diameter, derived from preoperative MDCT images, showed significant correlation with AR grade $\geqslant 3$ [153]. A large number of studies reported extended native aortic annulus calcifications or calcifications protruding in the LVOT (>4 mm) as the main predictive factors for paravalvular AR after implantation of a self-expandable or balloon-expandable TAV [153–161]. However, with respect to balloon-expandable TAV, results are conflicting. Bekeredian et al did not find aortic valve calcifications to be predictive for AR after balloon-expandable TAV implantation [156]. Van Belle et al reported the type of TAV as an important procedural factor with self-expandable TAV, not balloon-expandable, predictive for postoperative AR grade $\geqslant 2$ [162]. Among procedural factors, undersizing seems to be the major responsible of AR after implantation of balloon-expandable valves [160]. Whereas, implantation depth seems to play the biggest role after implantation of a self-expandable device [153, 163]. In fact, too deep or too shallow implantation depth of the valve might prevent adequate sealing of the skirt around the annulus with consequent increase of the risk of paravalvular AR.

**Table 2.3:** Unifying 5-class grading scheme proposed by Pibarot et al. Only the parameters that are most frequently used to grade the severity of paravalvular AR are reported. Adapted from [150].

| **3-Class grading scheme** | **Trace** | **Mild** | **Mild** | **Moderate** | **Moderate** | **Severe** |
|---|---|---|---|---|---|---|
| **4-Class grading scheme** | **1** | **1** | **2** | **2** | **3** | **4** |
| **Unifying 5-Class grading scheme** | **Trace** | **Mild** | **Mild-to-Moderate** | **Moderate** | **Moderate-to-Severe** | **Severe** |
| **Cineangiography** | Grade 1 | Grade 1 | Grade 1 | Grade 2 | Grade 3 | Grade 4 |
| **Hemodynamics** | | | | | | |
| Aortic regurgitation index | >25 | >25 | >25 | 10-25 | 10-25 | <10 |
| **Doppler echocardiography** | | | | | | |
| Multiple jets | Possible | Possible | Often present | Often present | Usually present | Usually present |
| Jet path visible along the stent | Absent | Absent | Possible | Often present | Usually present | Present |
| Vena *contracta* width (2D color Doppler) | <2 | <2 | 2-4 | 4-5 | 5-6 | >6 |
| Vena *contracta* area (2D/3D color Doppler) | <5 | 5-10 | 10-20 | 20-30 | 30-40 | >40 |
| Jet width (% LVOT) | <5 | 5-15 | 15-30 | 30-45 | 45-60 | >60 |
| Circumferential extent of AR (%) | <10 | <10 | 10-20 | 20-30 | >30 | >30 |
| **Cardiac magnetic resonance imaging** | | | | | | |
| Regurgitant fraction* | <10 | <10 | 10-20 | 20-30 | 20-30 | >30 |

*There isimportant variability in the cut point values of regurgitant fraction and volume reported in the published studies to grade AR by cardiac magnetic resonance imaging.

CHAPTER 3

# NUMERICAL SIMULATIONS IN TAVR

This chapter provides an extensive overview of the state of the art of computer modeling and simulation in TAVR. First, the role of patient-specific computer simulation and modeling strategies in numerical simulation are introduced. The review (2011-2018) is organized based on the clinical application. Finally, the computational framework developed at FEops NV (Ghent, Belgium) that allows to accurately simulate TAVR procedures will be described.

## 3.1 THE ROLE OF NUMERICAL SIMULATIONS

Although TAVR is an effective (and sometimes the only possible) treatment for patients at high- or extreme- surgical risk for aortic valve replacement, it is not free of complications such as annulus rupture, conduction abnormalities and paravalvular AR. These strongly depend on the specific patient anatomy as well as on device type and position. In that regard, the integration of clinical images and numerical simulations generates opportunities to assess the device performance in a realistic anatomy and to better understand the source of complications. More and more, the potential benefit of these numerical simulations as a tool to assess the risk of complications is recognized.

Numerical simulations can be classified into three main categories:

- Structural finite element analysis (FEA) to study the mechanical aspects related to the device implantation in the aortic root anatomy (e.g.

evaluation of the stresses on the aortic root wall as well as on the device leaflets and frame, frame deformation...),

- Computational fluid dynamics (CFD) to study the fluid domain and the impact of the device on the blood flow,
- Fluid-structure interactions (FSI) simulation, that couples FEA and CFD, to account for the relative effects of both the structural and fluid domain and in general obtain a more realistic solution.

Table 3.1 offers an overview of literature on patient-specific numerical simulations of TAVR, from 2011 to 2018, in a chronological order. The category of numerical simulation is also specified.

The next paragraph offers an overview of the modeling strategies and considerations adopted to build a patient-specific computer simulation of TAVR.

**Table 3.1:** Overview of patient-specific numerical simulation of TAVR performed from 2011 to 2018.

| Study | Study type | Application | N patients | Device type | Validation (y/n) |
|---|---|---|---|---|---|
| Sirois, 2011 [164] | CFD | Hemodynamics before and after TAVR | 1 | Similar to SAPIEN | No |
| Wang, 2012 [165] | FEA | Evaluation of aortic root geometry for TAV simulation | 1 | SAPIEN | No |
| Capelli, 2012 [166] | FEA | TAV in valve-in-valve procedure | 5 | SAPIEN | No |
| Russ, 2013 [167] | FEA | Material sensitivity analysis | 1 | CoreValve | Yes |
| Auricchio, 2014 [168] | FEA | TAV positioning | 1 | SAPIEN | No |
| Morganti, 2014 [169] | FEA | TAV positioning | 2 | SAPIEN | Yes |
| Gunning, 2014 [170] | FEA | TAV leaflets analysis | 1 | Self-expanding | No |
| Wang, 2015 [171] | FEA | Annular rupture | 3 | SAPIEN | Yes |
| Bailey, 2015 [172] | FEA | TAV leaflets analysis | 1 | SAPIEN XT | No |
| Bianchi, 2015 [173] | CFD | TAV positioning | 2 | SAPIEN, Polynova | No |
| Morganti, 2015 [174] | FEA | TAV positioning | 1 | CoreValve | No |
| Schultz, 2016 [175] | FEA | TAV deployment prediction | 39 | CoreValve, SAPIEN | Yes |
| de Jaegere, 2016 [176] | CFD | Paravalvular AR prediction | 60 | CoreValve | Yes |
| Sturla, 2016 [177] | FEA | Impact of calcifications on TAV deployment | 1 | SAPIEN | No |
| Bianchi, 2016 [178] | FEA | TAV positioning | 1 | SAPIEN | No |
| Bosmans, 2016 [179] | FEA | Paravalvular AR prediction | 10 | CoreValve | Yes |
| Ovcharenko, 2016 [180] | FEA | Geometry sensitivity analysis | 1 | CoreValve | Yes |
| Wu, 2016 [181] | FSI | Comparison between numerical simulation and *in vitro* testing | 1 | Self-expandable | No |
| Finotello, 2017 [182] | FEA | Material and mesh sensitivity analysis | 1 | CoreValve | Yes |
| Vahidkhah, 2017 [183–185] | FSI | TAV thrombosis | 1 | - | Yes |
| Bosi, 2018 [186] | FEA | Material property tuning | 14 | SAPIEN XT | Yes |
| McGee, 2018 [187] | FEA | TAV positioning | 1 | Lotus | No |
| Bianchi, 2018 [188] | CFD | TAV positioning and paravalvular AR | 3 | SAPIEN, CoreValve | Yes |
| Mao, 2018 [189] | CFD | Post-operative hemodynamics | 1 | CoreValve | Yes |
| Kandail, 2018 [190] | FSI | TAV positioning and hemodynamics | 1 | CoreValve | No |

## 3.2 Building a patient-specific numerical simulation of TAVR

Accurate models, both in terms of geometry and material properties, are needed to obtain a realistic simulation and achieve reliable results. In the following subsections it will be addressed in more detail how to reconstruct a patient-specific geometry of the anatomy, modeling the behavior of anatomical tissues as well as modeling a TAV device and its deployment.

### 3.2.1 Geometry of the anatomy

A detailed anatomical model of the aortic root can be extracted from high quality preoperative MDCT images, using dedicated commercial software such as Mimics (Materialise, Leuven, Belgium), Avizo (VSG, Burlington, MA), or open source software such as ITKsnap. The MDCT scan can be synchronized with the ECG activity of the patient (i.e. ECG-gated cardiac CT), which allows to select and model a specific phase of the cardiac cycle (e.g. end-diastole, peak-diastole, mid-systole, end-systole). An overview of the software adopted in each study is provided in Table 3.2.

Geometries that are reconstructed from *in vivo* images are physiologically loaded due to the systemic arterial pressure. This pre-stress condition should be taken into account to perform accurate patient-specific simulations. Wang et al. [165] proposed a method to determine the 'unloaded' state of the aortic root based on the relationship between the aorta diameter and the blood pressure estimated using experimental tests. The authors simulated the deployment of a SAPIEN valve in the aortic root reconstructed directly from MDCT images and in the 'unloaded' aortic root and observed significant differences in terms of stress, strain and contact forces on the aortic root. In addition, they suggested to include the myocardium in the simulation, as it showed to increase the mechanical response (i.e. stress and contact force) of the aortic root during deployment. However, no subsequent studies followed this recommendation.

Besides the aortic root geometry, structures as native leaflets and calcifications should be included in the model. Even though the quality of MDCT images can be very good, it is not instantaneous, and it fails to capture the quick movement of the aortic leaflets. Wang et al. [165] and Capelli et al. [166] were able to extract the aortic leaflets directly from MDCT images, however, it required expertise from the operator. Morganti et al. in 2014 [169] proposed a new strategy to reconstruct the leaflets in the fully open configuration based on 9 manual landmarks extracted from the aortic root reconstruction (Fig 3.1). The free margin was defined by a circular arc.

The thickness of the leaflets is not homogeneous, and it decreases towards the free edge. However, only Bianchi et al. [173, 178, 188] modeled leaflets

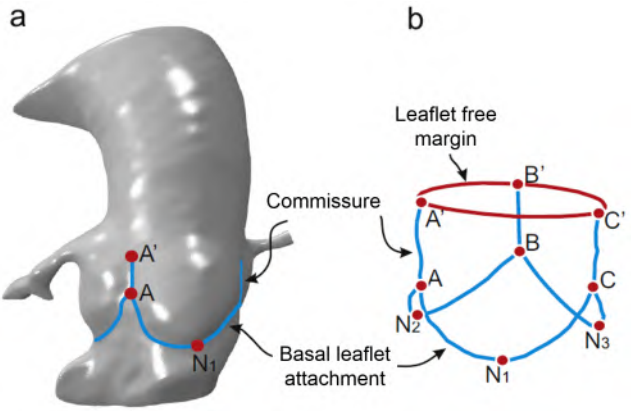

**Figure 3.1:** Reference points for modeling the native valve leaflets: a) the commissures and basal leaflet attachment lines are highlighted on a rendering of the aortic root; b) reference points extracted from the aortic root reconstruction [169].

with variable thickness. This was implemented by prescribing extrusion length proportional to the radial location of each node, resulting in thinner leaflets towards the free edge and thicker leaflets in the connection to the sinus. Whereas, the majority of the patients-specific studies available in literature assumed the thickness of the leaflets to be constant (typically in the range between 0.3 mm and 0.7 mm), and modeled them either as thin shell structures [169, 174, 177, 179, 187] or as 3D structures [167, 172].

Besides the native leaflets, calcifications are a characteristic feature of stenotic valves and should be included in the simulation. Various modeling strategies for leaflet calcifications can be found in literature. Some authors embedded the calcifications in the leaflet models [165, 166, 169, 173]. This resulted in leaflet zones with increased thickness and stiffness. In other studies, calcification volumes were extracted directly from MDCT and tied to the surface of the leaflets [167, 171, 179, 187]. Lastly, Sturla et al. [177] identified the calcific spots on the leaflets and modeled them by extrusion of the leaflet elements.

### 3.2.2 Constitutive laws for the soft tissues

Few studies investigated how the material properties may affect the post-deployment deformation of a TAV in a patient-specific geometry [167, 182]. Rigid, linear elastic and hyperelastic aortic roots were compared, with the rigid geometry leading to unrealistic results. Russ et al. [167] and Finotello et al. [182] agreed that hyperelastic aortic root models were the most accurate. In addition, Ovcharenko et al. [180] reported that a separate description of the fibrous ring might further improve the results. However, the difference found between the hyperelastic and the linear elastic models on the TAV post-deployment deformation were negligible [167, 182]. For this reason, linearization of the aortic material model can be reasonably adopted. Furthermore, when choosing the hyperelastic model, the mechanical response of the tissue is susceptible to the level of strain, and the assumption of an initially ‘unloaded’ geometry may lead to inaccurate result if not carefully checked. Therefore, going to a very complex model does not always lead to more accurate results [182]. The material models adopted in literature are reported in Table 3.3. The majority of the works adopted hyperelastic material models, both for the aortic and native leaflets tissue, to better represent the behavior of biological tissues. However, only Wang et al. [165] explicitly computed the ‘unloaded’ aortic root geometry.

Recently, Bosi et al. [186] combined patient-specific numerical simulation with optimization techniques to find the best combination of material properties and geometrical parameters to improve the accuracy of the model. The model was validated against clinical images (fluoroscopic angiography and postoperative echocardiography). They observed that geometrical and mechanical parameters tuned on 14 patients can significantly improve the accuracy of prediction of the SAPIEN XT frame deformation as well as the location of paravalvular AR gaps. Also, they observed that the thickness of the leaflets had the most significant impact on the accuracy of the predicted configuration, followed by the leaflets stiffness and the aortic root thickness.

The shape of the deployed stent depends not only on the aortic root model but also on the distribution of calcifications [177, 180, 182]. Also, Finotello et al. showed that a very stiff material for calcifications induces a great mismatch of the deployed TAV configuration from the real solution. Therefore, calcifications should be properly modelled to guarantee the accuracy of the simulation. Most of the published works modeled calcifications with linear elastic material [182] Table 3.2 and 3.3.

**Table 3.2:** Summary of the software adopted in each study: from patient-specific geometry reconstruction to simulation. Some relevant modeling aspects are also reported. Information that was not applicable or clearly reported in the manuscript, is here indicated with a dash (‘-‘).

| Study | Imaging software | Meshing software | FEA software | CFD software | Cardiac phase | Native leaflets | Calcifications | TAV leaflets (y/n) |
|---|---|---|---|---|---|---|---|---|
| Sirois, 2011 [164] | VTKPointPicker | HyperMesh | Abaqus | Star-CCM+ | - | Yes | No | Yes |
| Wang, 2012 [165] | Avizo | HyperMesh | Abaqus | - | Systole | Yes | Yes | No |
| Capelli, 2012 [166] | Mimics | - | Abaqus/E | - | Mid-systole | Yes | Yes | No |
| Russ, 2013 [167] | Philips Heart Navigator | ICEM CFD | Abaqus/E | - | Systole | Yes | Yes | No |
| Auricchio, 2014 [168] | Osirix | Matlab | Abaqus/E | - | End-diastole | No | No | Yes |
| Morganti, 2014 [169] | ITKsnap | Matlab | Abaqus/E | - | - | Yes | Yes | Yes |
| Gunning, 2014 [170] | Mimics | Abaqus | Abaqus/E | - | Peak-diastole | No | No | Yes |
| Wang, 2015 [171] | Avizo | HyperMesh | Abaqus/E | - | Diastole | Yes | Yes | No |
| Bailey, 2015 [172] | ScanIP | ScanIP | Abaqus/E | - | - | Yes | No | Yes |
| Bianchi, 2015 [173] | ITKsnap | - | - | - | - | Yes | Yes | No |
| Morganti, 2015 [174] | ITKsnap | VMTK | Abaqus/E | - | Diastole | Yes | Yes | Yes |
| Schultz, 2016 [175] | Mimics | pyFormex | Abaqus/E | - | End-diastole | Yes | Yes | No |
| de Jaegere, 2016 [176] | Mimics | pyFormex | Abaqus/E | Fluent | End-diastole | Yes | Yes | No |
| Sturla, 2016 [177] | - | - | LS-DYNA | - | - | Yes | Yes | Yes |
| Bianchi, 2016 [178] | ITKsnap | Ansis Fluent Meshing | Abaqus/E | - | End-systole | Yes | Yes | Yes/No |
| Bosmans, 2016 [179] | Mimics | 3-matic | Abaqus/E | - | End diastole | Yes | Yes | No |
| Ovcharenko, 2016 [180] | Amira | Abaqus | Abaqus | - | - | Yes | Yes | No |
| Wu, 2016 [181] | Mimics | - | ANSYS LS-DYNA | ANSYS LS-DYNA | - | No | No | Yes |
| Finotello, 2017 [182] | ITKsnap | Matlab | Abaqus/E | - | Diastolic | Yes | Yes | No |
| Vahidkhah, 2017 [183–185] | ScanIP | HyperMesh? | Abaqus/E? | Fluent | - | No | No | Yes |
| Bosi, 2018 [186] | Mimics | - | Abaqus/E | - | - | Yes | Yes | No |
| McGee, 2018 [187] | Mimics | - | Abaqus/E | - | End-systole | Yes | Yes | No |
| Bianchi, 2018 [188] | ITKsnap | Ansis Fluent Meshing | Abaqus/E | Fluent | End-diastole | Yes | Yes | Yes |
| Mao, 2018 [189] | Avizo | HyperMesh | Abaqus/E | Star-CCM+ | - | Yes | Yes | No |
| Kandail, 2018 [190] | CRIMSON | - | Abaqus/E | FlowVision | Post-implantation | No | No | Yes |

**Table 3.3:** Summary of the material models adopted in each patient-specific study. A dash ('-') indicates that the native calcified leaflets were not included in the model.

| Study | Aortic tissue | Leaflets | Calcification |
|---|---|---|---|
| Sirois, 2011 [164] | Hyperelastic (Fung) | Hyperelastic (Fung) | - |
| Wang, 2012 [165] | Hyprelastic (Holzapfel) | Anisotropic hyprelastic (Holzapfel) | Linear elastic |
| Capelli, 2012 [166] | Hyperelastic (Mooney-Rivlin) | Hyperelastic (Mooney-Rivlin) | Linear elastic |
| Russ, 2013 [167] | Rigid/Linear Elastic/Hyperelastic (Neo-Hooke) | Linear elastic/Hyperelastic | Linear elastic |
| Auricchio, 2014 [168] | Hyperelastic (Holzapfel) | - | - |
| Morganti, 2014 [169] | Hyperelastic (Mooney-Rivlin) | Hyperelastic (Mooney-Rivlin) | Linear elastic |
| Gunning, 2014 [170] | Hyperelastic (Mooney-Rivlin) | - | - |
| Wang, 2015 [171] | Hyperelastic (Holzapfel-Gasser-Odgen) | Hyperelastic (Holzapfel-Gasser-Odgen) | Linear elastic |
| Bailey, 2015 [172] | Linear elastic | Linear elastic | - |
| Bianchi, 2015 [173] | Hyperelastic (Odgen) | Hyperelastic (Odgen) | Linear elastic |
| Morganti, 2015 [174] | Linear elastic | Linear elastic | Linear elastic |
| Schultz, 2016 [175] | Linear elastic | Linear elastic | Linear elasto-plastic |
| de Jaegere, 2016 [176] | Linear elastic | Linear elastic | Linear elasto-plastic |
| Sturla, 2016 [177] | Linear elastic | Hyperelastic | Hyperelastic (Ogden) |
| Bianchi, 2016 [178] | Hyperelastic (Odgen) | Hyperelastic (Odgen) | Linear elastic |
| Bosmans, 2016 [179] | Hyperelastic (Neo-Hookean) | Hyperelastic (Neo-Hookean) | Linear elastic |
| Ovcharenko, 2016 [180] | Non-linear | Linear elastic | Linear elastic |
| Wu, 2016 [181] | Linear elastic | Linear elastic | - |
| Finotello, 2017 [182] | Rigid/Linear elastic/Hyperelastic isotropic/ Hyperelastic (Holzapfel-Gasser-Odgen) | Rigid/Linear elastic/Hyperelastic isotropic/ Hyperelastic (Holzapfel-Gasser-Odgen) | Linear elastic |
| Vahidkhah, 2017 [183–185] | - | - | - |
| Bosi, 2018 [186] | Linear elastic | Linear elastic | Elasto-plastic with perfect plasticity |
| McGee, 2018 [187] | Hyperelastic (Ogden) | Linear elastic | Hyperelastic (Mooney-Rivlin) |
| Bianchi, 2018 [188] | Hyperelastic | Hyperelastic | Linear elastic |
| Mao, 2018 [189] | Hyperelastic (Holzapfel-Gasser-Odgen) | Hyperelastic (Holzapfel-Gasser-Odgen) | Linear elastic |
| Kandail, 2018 [190] | Rigid | - | - |

### 3.2.3 TAV devices

The more commonly modeled devices are the balloon-expandable SAPIEN valve and the self-expandable CoreValve device. So far, only McGee et al. very recently (2018) modeled a Lotus device [187]. The overview of the device modeled in each study is reported in Table 3.1. Authors who had not access to a real TAV or could not perform a micro-CT scan, reconstructed the device model either based on data and pictures available online [168, 171, 189] or on measurements on the real device [177]. In some cases, the model of the device was reconstructed from high-resolution micro-CT images [169, 174, 179, 180, 182, 186]. However, this image modality does not allow to reconstruct biological tissues such as leaflets and skirt. Auricchio et al. (2014) [168], developed for the first time a strategy to include the TAV leaflets in the simulation. The TAV leaflets were created by means of a lofting procedure in the open configuration and mapped onto the frame after the device was deployed within the aortic root (Fig 3.2). However, using a post-deployment mapping technique they failed to recognize the effect that the leaflets have on the frame post-deployment. Successively, Bailey et al. (2015) [172] proposed a novel strategy to model the TAV leaflets from the initial step of the deployment. The leaflets were reconstructed in a planar configuration and then manipulated into the functional shape through geometric operations (Fig 3.3). However, they observed that the inclusion of the TAV leaflets had a minimal effect on the post-deployment deformation of the frame. This observation was later confirmed by Bianchi et al. [178]. Furthermore, Bailey et al. mentioned that a realistic crimping was not possible if the TAV leaflets were included in the model, because of severe leaflet distortion. Recently, Mao et al. [189] created the TAV leaflets by virtually reproducing the closed shape of the leaflets attached to the stent. However, they observed that a detailed closing shape of the TAV leaflets has a negligible effect on the paravalvular AR.

Ideally, material properties of TAV stents are derived from mechanical tests (e.g. crush test with parallel plates [170, 177, 191], tensile tests [181]). However, this is not always possible and most of the authors used constitutive models available in literature.

The self-expandable CoreValve device consists of a Nitinol frame. This has been described either with a simplified linear elastic-plastic [167] or more complex super-elastic behavior [174]. On the other hand, the frame of the balloon-expandable SAPIEN device is made of cobalt chromium. The constitutive model to accurately describe the cobalt chromium alloy has been reported by Morganti et al. [169].

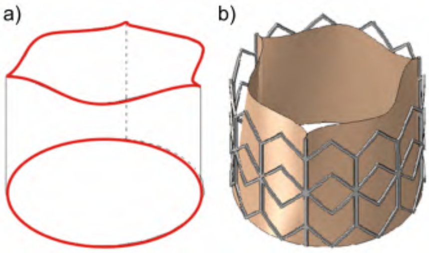

**Figure 3.2:** Modelling strategy of the leaflets of the SAPIEN valve: a) the valve is created by means of a lofting procedure carried out between the bottom and the top curves highlighted in red; b) the whole device model made of the frame and the leaflets [168].

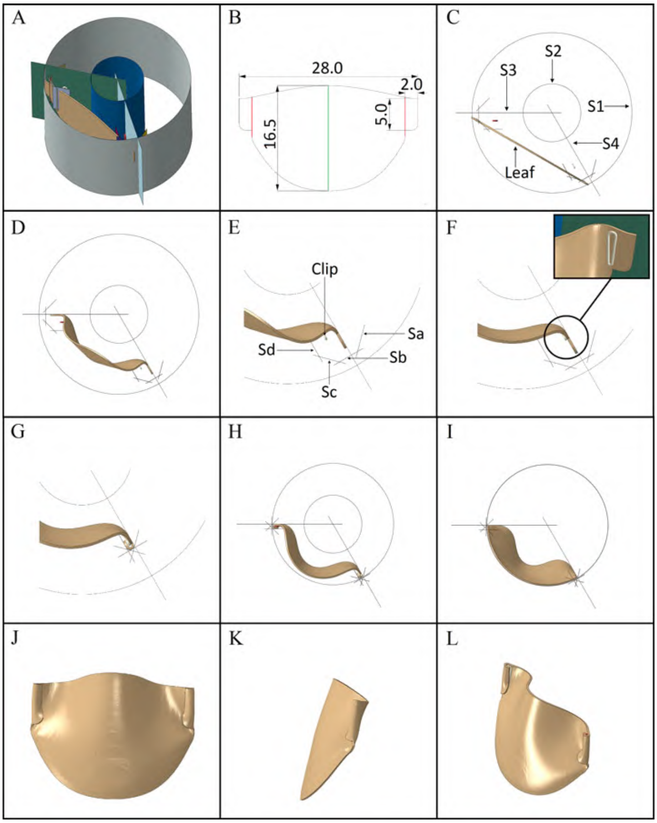
A
B
28.0
2.0
5.0
16.5
C
S2
S3
S1
S4
Leaf
D
E
Clip
Sa
Sd
Sb
Sc
F
G
H
I
J
K
L

**Figure 3.3:** Step-by-step modelling strategy of the leaflets of the SAPIEN valve as proposed by Bailey et al. [172]: A-I) geometrical manipulation of one leaflet; J) final geometry rear view; K) final geometry side view; L) final geometry isometric view.

### 3.2.4 TAV deployment strategy

The deployment of a TAV consists of 2 steps: the crimping onto the catheter and the expansion within the patient-specific aortic root model. Most of the studies modeled the crimping through radial displacement imposed on an outer cylinder (positioned coaxially the frame) to reduce the TAV diameter. Alternatively, Russ et al. [167] obtained the crimped configuration of a self-expandable CoreValve device by constraining the ventricular end of the frame while stretching the aortic end of the frame into the ascending aorta. Bosmans et al. [179] simulated the crimping phase by pulling the self-expandable CoreValve device through a funnel-shaped structure.

Expansion strategies depend on the modeled device. In clinical practice, the expansion of a self-expandable device happens in concomitant with the removal of the catheter. Accordingly, this is usually simulated by gradually moving the catheter upwards along its longitudinal axis [174, 180, 182, 189]. However, different strategies have been adopted in literature. Russ et al. [167] and Bosmans et al. [179] simulated the frame expansion by controlling the axial displacement of the nodes at the aortic end of the frame (i.e. moving those nodes towards the LVOT until the contact with the aortic root tissue is established). Kandail et al. [190] imposed radial expansion to the (outer) cylinder, until the contact between the frame and the aortic root was reached.

The mechanically-expandable Lotus valve not only expands radially but also shortens to guarantee the locking of the device. McGee et al. [187] simulated the locking phase by applying axial displacement (inward) to three connectors and lock the frame to a height of 19 mm.

On the other hand, to expand a balloon-expandable device the operators inject a definite volume inside the inner balloon. In the past, a rigid cylinder was used to represent the balloon, and the expansion was simulated by imposing radial displacement to the cylinder [165, 169]. Subsequently a more realistic balloon was integrated in the simulation, and the most adopted expandable strategy was to apply constant pressure to the balloon [166, 168, 172, 173, 177, 186]. However, a realistic modeling strategy was adopted only by Wang et al. in 2015 [171], who simulated balloon-expansion by inflating the balloon with a volume variable method.

### 3.2.5 The fluid domain

Besides the structural components, CFD and FSI numerical simulations need to accurately include the blood domain. It is well known that the blood is a concentrate suspension of cellular elements (i.e. red blood cells, white blood cells and platelets) in an aqueous solution called plasma. However, in large vessels the blood can be assumed Newtonian, whereas blood particles become particularly significant when the particle size is comparable to the lumen size (e.g. capillaries). Accordingly, some of the TAVR patient-specific simulation in literature have modeled the blood as an incompressible Newtonian fluid [181, 189, 190]. However, Sirois et al. assumed the blood as non-Newtonian [164] and Bianchi et al. as two-phase Newtonian [188].

Both laminar [164, 173, 181, 188, 190] and turbulent flow models have been adopted in literature. A turbulent flow model has been used by Vahidkhah to investigate valve thrombosis after TAVR [183–185]. Also, Mao et al. [189] implemented turbulent blood flow to describe the transitional flow regime in correspondence of the paravalvular AR jets where they estimated a Reynolds number above 3000. However, Bianchi et al. [188] evaluated the impact of using a laminar or turbulent blood flow on the paravalvular AR jets and observed small differences in AR volume (~3%). Therefore, they adopted a laminar flow in their simulation.

Finally, the boundary conditions applied to the fluid domain vary from one study to another. This is mainly because data on post-TAVR hemodynamics is not presented in literature yet. Sirois et al. [164] started from physiologic flow velocity available in literature and scaled it in accordance of the aortic annulus dimension after TAV implantation. Flow velocity was imposed at the LVOT (inlet), whereas a three elements Windkessel model was used to impose the pressure as function of the flow at the ascending aorta and coronary arteries (outlets). Patient-specific flow condition was instead used by Bianchi et al. [173], who obtained flow velocity and transvalvular pressure gradient from intra-procedural echo-Doppler measurements. Wu et al. [181] imposed physiological pressure waveforms from literature at the ventricular inlet and aortic outlet. They did not take into account coronary arteries in their model. Similarly, Bianchi et al. [188] applied a pressure gradient at the aortic inlet. However, they included the coronary arteries (outlet) in the model at which they applied flow boundary conditions. Pressure gradient and blood flow were found in literature. Vahidkhah et al. [183–185] imposed transvalvular pressure and flow magnitude that were previously measured in vitro using a pulse duplicator system. Also, they prescribed normal phasic coronary blood flow at the coronary artery outlets. Mao et al. [189] imposed physiological pressure waveform at the ascending aorta (inlet) and LVOT (outlet). A lumped parameter model was implemented at the coronary arteries to couple the local pressure with the flow rate. Finally, Kaindail et al. [190] imposed flow waveforms at the LVOT and coronary arteries (inlet) and pressure waveforms at the aortic outlet. Physiological waveforms were obtained from literature.

## 3.3 TAVR COMPUTER MODELLING AND CLINICAL CONSIDERATION

Computational models have been employed to study the interaction between the implanted TAV and the native aortic tissues, to evaluate the device performance from a structural and fluid perspective and to predict risk of complications related to TAVR. Patient-specific computer modeling and simulation relevant for this project have been listed below grouped according to their application. Table 3.1 gives an overview of those studies and their main application.

The first study adopting patient-specific geometries was proposed by Sirois et al. in 2011 to investigate the **hemodynamics** before and after TAV deployment [164]. They observed improvements in the hemodynamics after the procedure: reduced blood jet velocity in systole because of a larger effective orifice area, which resulted in lower wall shear stress (WSS) on the ascending aorta. Due to the lack of post-TAV hemodynamics data reported in literature at the time of this study, they could only partially compare their results with benchmark testing available in literature.

In 2012, Capelli et al. [166] for the first time adopted patient-specific computer simulation to evaluate the feasibility of a TAVR in **valve-in-valve** procedures (i.e. 4 patients with a failed percutaneous valve) and in a patient with incompetent aortic valve. In all patients a SAPIEN valve implantation was simulated. The authors reported that in all patients with a previous surgical valve, TAV deployed symmetrically against the sewing ring and valve leaflets. The maximum stress value was observed in the ascending aorta. Instead, in the patient without previous prosthesis, the maximum stress was observed in the LVOT. This result indicated that in valve-in-valve procedures the implanted bioprosthesis acts as a scaffold for the new implanted TAV. However, no validation was performed in this work.

In 2014, Gunning et al. [170] investigated the effects of the deployment on **TAV leaflets** in terms of deformation and stress distribution. The frame deformation was modeled by implanting the TAV in a patient-specific geometry reconstructed from MDCT, and in 2 idealized aortic root geometries (i.e. with circular and elliptical annulus). They observed that the distortion of the TAV frame is reflected in the stress distribution on the leaflets. Homogeneous stress distribution was observed on the leaflets of the circular TAV geometry, whereas high stress values were located at the commissural level in the distorted eccentric TAV geometry. Also, the authors reported lower stress values in case of alignment between the TAV and native valve commissure. Despite the interesting findings reported in this work, it has to be highlighted that native calcified leaflets were not accounted for in the simulation, while it is known that calcifications might significantly influence frame deformation after deployment. Of note, the self-expandable TAV modeled in this study did not resemble any commercially available device.

Few studies focused on the effect of **TAV positioning** on the device performance from a structural [166, 168, 174, 178, 187] perspective. They have been summarized in the following paragraph.

Capelli et al. (2012) [166] investigated the influence of the TAV landing zone in terms of mechanical response of the aortic root (e.g. stress distribution) and potential occlusion of the coronary arteries. A SAPIEN valve was implanted in a patient-specific aortic root at 3 different positions: aligned with the leaflet commissures, 4.2 mm lower (i.e. towards the LV) and 4.2 mm higher (i.e. towards the ascending aorta). Results showed that the stent implanted in the highest position caused the highest stresses on the aortic root in the leaflet region where it might induce damage or stimulate remodeling. On the other hand, no risk of coronary ostia occlusion was observed for this specific patient. However, those results were not validated with *in vitro* or *in vivo* data.

In 2014, Auricchio et al. [168] investigated the effect of positioning on the TAV leaflet performance in terms of coaptation area and stress distribution. They simulated the implantation of a SAPIEN valve in high position (i.e. immediately below the coronary ostia) and in low position (7 mm below the distal one). Results suggested that there was no significant difference in valve performance when placing the device low or high, even though slightly larger coaptation area and higher average Von Mises stress were observed in the low position. Furthermore, the low valve position resulted in higher stresses on the aortic root (Fig 3.4). However, they did not include the calcific aortic leaflets, despite the fact that calcifications may have a relevant effect on the deployment outcome. Also, the model lacked validation with respect to *in vitro* or *in vivo* data.

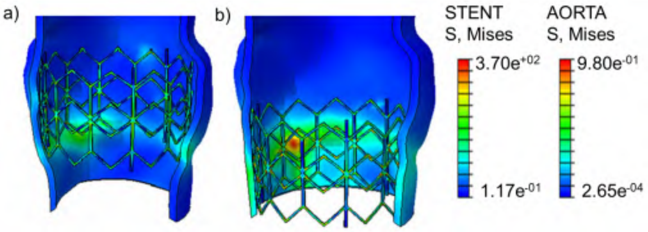

**Figure 3.4:** Von Mises stresses on the aortic root and on the stent after implantation of the valve in high (a) and low (b) position (adapted from [168].

Successively, Morganti et al. (2015) [174] for the first time investigated the impact of device position and implantation angle on the device performance, using a self-expandable CoreValve. Furthermore, they included the calcific native leaflets in their model. Similarly to Auricchio et al. [168], they mapped the TAV leaflets onto the deployed frame. They evaluated the stent deformation, grade of apposition to the aortic root and valve performance in terms of coaptation area at 3 different implantation depths and angles (Fig 3.5). Rotations were modeled in the plane corresponding to the one whose projection is used by the intraoperative angiography. Results showed that both implantation depth and angle affect the post-deployment device configuration, with the lowest implantation depth and the device rotated towards the outer aortic arch (negative implantation angle) causing the most asymmetrical frame. On the other side, symmetric stent configurations were obtained with the device rotated towards the inner aortic arch (positive angle). High distortion of the stent also showed to reduce the coaptation area between the TAV leaflets, therefore affecting the valve performance. Finally, the medium position favored the best apposition of the device to the aortic root, therefore reducing the risk of valve migration and paravalvular AR.

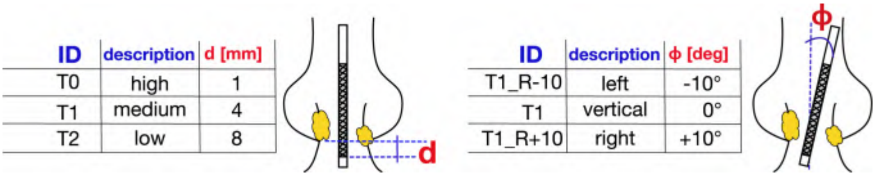

| ID | description | d [mm] |
|---|---|---|
| T0 | high | 1 |
| T1 | medium | 4 |
| T2 | low | 8 |

| ID | description | ϕ [deg] |
|---|---|---|
| T1_R-10 | left | -10° |
| T1 | vertical | 0° |
| T1_R+10 | right | +10° |

**Figure 3.5:** Summary of the simulated device configurations within the patient's aortic valve model: implantation depth was 1-, 4-, 8-mm below the annular plane (T0, T1, T2 respectively); the axis of the crimped device was parallel to the aorta centerline (T1_vertical) and tilted of ±10° (T1_right towards the inner aortic arch and T1_left towards the outer aortic arch) [174].

In 2016, Bianchi et al. (2016) [178] aimed for the first time to evaluate the effect of a SAPIEN valve position on the risk of valve migration in 1 patient, before and after the recoil phase. Valve migration was evaluated in terms of contact force. The device was implanted at the annular level, in a lower position (30% of the stent length towards the ascending LVOT) and in a higher position (30% of the stent length towards the ascending aorta). The highest position was associated with lower contact force between the device and the aortic root and therefore with higher risk of valve migration. Furthermore, results showed that the contact force between the frame and the aortic root dropped down after recoil, suggesting that recoil can play a big role in the valve migration. However, Bianchi et al. did not model the LVOT which might have provided additional constraints to the model.

Recently, McGee et al. (2018) [187] investigated for the first time the impact of positioning of a Lotus valve on the stent performance (i.e. eccentricity of the frame) and on the stress distribution in the aortic region close to the conduction system. The authors assumed the conduction system to be located in the interleaflet triangle between the RCC and NCC. They evaluated 3 different device positions in 1 patient-specific aortic root: at the annular level, 5 mm above (higher position) and 5 mm below (lower position) the annulus. Results showed that the Lotus valve frame retains its circular geometry even in an eccentric aortic root. However, the annular implantation was associated with the lowest eccentricity. Furthermore, the amount of stress in the interleaflet triangle between the RCC and NCC was found to be inversely proportional to the implantation depth (Fig 3.6). The authors claimed that high stresses in this region might increase the risk of postoperative conduction abnormalities. However, no validation with clinical data was performed.

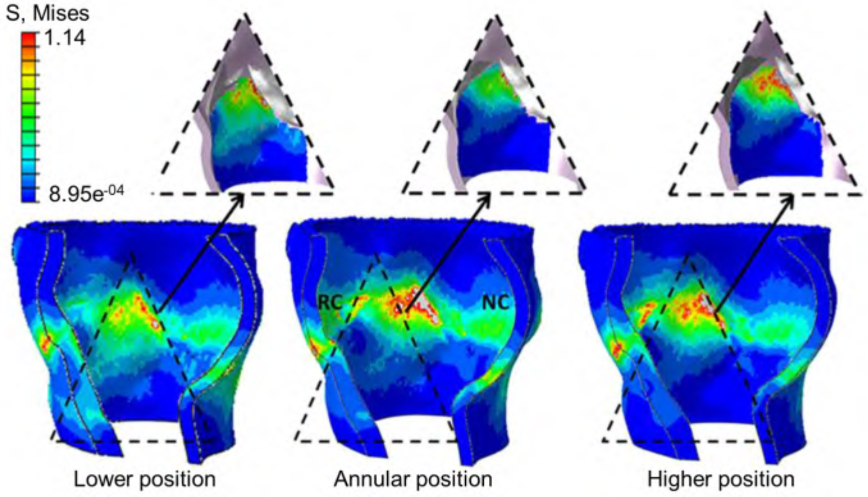

**Figure 3.6:** Von Mises stress distribution on the aortic root at different valve positions (adapted from [187]).

In the next paragraphs we report few studies which investigated the **risk of paravalvular AR** after TAVR. The evolution of the modeling strategy will become clear: from the structural approach [169] to fluid dynamics [179, 188, 189]. Some of those works did not focus only on prediction of AR but also evaluated the impact of **TAV positioning on paravalvular AR** [188, 189].

In 2014, Morganti et al. [169] quantified the risk of paravalvular AR after implantation of a SAPIEN device by measuring the paravalvular gaps between the stent and the native tissue in patient-specific geometries. Prediction of paravalvular AR in 2 patients was validated against postoperative Doppler echocardiographic and angiographic evaluation. Results showed good agreement with postoperative medical data. Greater gaps were associated with significantly higher regurgitant flow and with higher maximum retrograde jet velocity (Fig 3.7). Even though this was the first study comparing the results with clinical data, a comparison of the implantation depth and the TAV deployed configuration with postoperative data (i.e. postoperative MDCT) to verify the accuracy of the simulation strategy is missing.

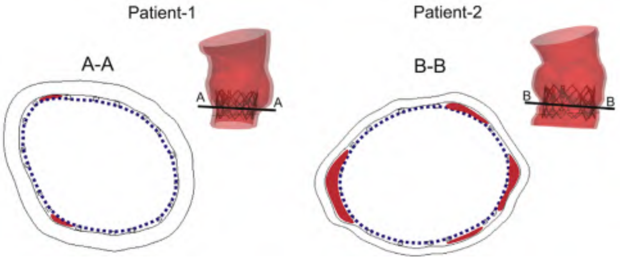

**Figure 3.7:** Paravalvular gaps (in red) between the stent and the patient-specific aortic root anatomy, responsible of paravalvular AR [169]).

Similarly, Bosmans et al. (2016) [179] proposed a max-flow algorithm to quantify paravalvular AR after implantation of a CoreValve device in 10 patients. The deployed frame geometry, its implantation depth and the displacement of calcifications were compared with postoperative MDCT data. The proposed max-flow algorithm creates a one-dimensional connected graph to represent the flow network based on the size of the gap between the device skirt and the aortic root. The predicted severity of paravalvular AR was validated against AR graded immediately after the implantation and at hospital discharge using echocardiographic evaluation. Results showed good correlation when no regurgitation was observed. However, the model suffered of inaccuracy in patients with clinically assessed AR.

More recently, Mao et al. (2018) [189] adopted CFD simulation to investigate the effect of CoreValve orientation (i.e. alignment/misalignment between the native and the TAV commissures), skirt height, frame thickness and implantation depth on post-deployment paravalvular AR in 1 patient. Results showed that paravalvular AR is strongly affected by all those parameters. Larger regurgitation was observed in case of a device with shorter skirt and in case of alignment between the native and the TAV commissures. The device implanted at annular level (the highest simulated position) exhibited much larger regurgitant jets than lower implantations. Furthermore, the majority of AR jets were observed at the commissural level. Finally, underestimation of paravalvular AR was observed when modeling the stent as a surface with zero strut thickness, whereas modeling the frame with real strut thickness led to results in good agreement with clinical data. This study provided a detailed analysis on the impact of TAV shape, deployment and modelling strategy on paravalvular AR. However, this computational model was constructed and validated for 1 patient only.

Bianchi et al. (2018) [188] proposed a FEA+CFD strategy to assess the effects of implantation depth on post-deployment paravalvular AR in 3 patients who experienced mild-to-moderate regurgitation based on echocardiographic evaluation. Two positions were investigated in 2 patients who received a SAPIEN valve (50% and 30% of the frame in the LVOT), and 3 positions in 1 patient who received a CoreValve (3-, 5- and 7- mm below the annular plane). The blood was modeled as a two-phase Newtonian fluid. Spherical platelets were seeded close to the aortic root wall in an injection plane on the aortic side with respect to the TAV. Results showed good agreement between the predicted regurgitant jet location and overall degree and the corresponding echocardiographic data. Simulation of SAPIEN deployment revealed that a lower valve position and balloon over-inflation led to higher anchorage forces, largest contact area between the TAV and the aortic root and reduced regurgitation jets. On the contrary, higher implantation of the CoreValve favored paravalvular AR reduction. However, the CFD analysis revealed that paravalvular AR is highly dependent on the patient-specific anatomy and calcification distribution more than on the depth of implantation.

Kandail et al. (2018) [190] adopted an FSI algorithm to investigate the impact of **TAV positioning** (annular position and 8 mm higher) of a CoreValve device on the aortic and coronary artery **hemodynamics** in terms of flow and WSS. The blood was modeled as a Newtonian fluid and physiological pressure waves were imposed at the aortic and ventricular inlets. Results indicated that the CoreValve position considerably impact the hemodynamics in the ascending aorta and coronary arteries. A jet-like flow was observed at peak systole, which disappeared at mid-systole because of the asymmetrical closure of the TAV leaflets (Fig 3.8). This result was comparable for both positions. However, WSS occurring where the jet-flow impinged the aortic wall were noticeably lower with the TAV in supra-annular position. Also, the higher implantation allowed to redirect slightly more flow to the coronaries during peak- and mid-systole. However, a larger quantity of flow was redirect to the coronary arteries during diastole through low-velocity recirculation zones in the aortic root, independent from the TAV positioning. Even though results from this study seems to recommend a higher implantation of a CoreValve device, it has to be highlighted that Kandail et al. reconstructed the aortic geometry from post-operative MDCT images rather than from pre-operative MDCT images. Furthermore, they assumed a rigid aortic wall. This assumption might have significant influence on the obtained results.

Wang et al. (2015) [171] developed a finite-element analysis to predict the **risk of annular rupture** in 3 patients undergoing TAVR with a SAPIEN valve. The patient-specific aortic root models and the surrounding myocardium

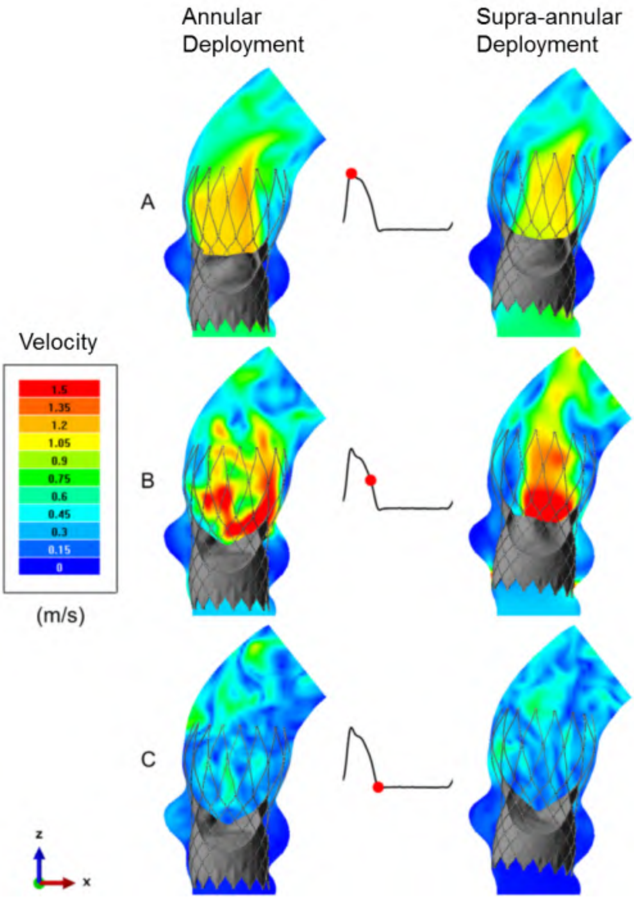

**Figure 3.8:** Flow velocity after valve implantaiton, during the cardiac cycle [190].

were reconstructed from preoperative MDCT. The aortic tissue was modeled as hyperelastic material and material failure was defined by the maximum principal stress limit of 2.5 MPa. The model showed to accurately predict the location of the aortic rupture in one retrospective case used for validation. The model was then used prospectively to predict the risk of annular rupture in the other 2 patients. In one of the two patients, the model predicted annular rupture and accordingly, the patient was not treated with TAVR. Although the validation was based on 1 patient only, this was the first study that was prospectively adopted in clinical practice, showing the potential of patient-specific simulation to serve clinicians with useful information during the pre-operative evaluation.

Computer modeling has been adopted to investigate TAV **leaflet thrombosis** [183–185]. Vahidkhah et al. (2017) for the first time adopted the FSI modeling approach on a patient-specific geometry to investigate the blood stasis on the TAV leaflets, which is a known precursor of valve thrombosis. In a first work they investigated the relation between the cardiac output and the blood stasis on the TAV leaflets [183]. Subsequently, they compared the blood stasis between a surgical and transcatheter aortic valve device [185]. And, in a final study, they quantified the impact of TAV positioning on leaflets blood stasis [184]. To do so, they adopted a turbulent flow model. Blood particles were seeded in the volume confined by the deployed TAV and tracked throughout one cardiac cycle. These studies showed that during the cardiac cycle (both in diastole as in systole) particles are still residing on the TAV leaflets. Furthermore, it was observed that the cardiac output and the TAV positioning affect the blood residence time on the leaflets, with higher blood residence time at lower cardiac output and intra-annular positioning during diastole [183, 184]. Therefore, the supra-annular positioning seems associated with a lower likelihood of leaflet thrombosis. When comparing a SAV with a TAV, a similar flow field and central jets were observed. However, particles were almost completely washed out from the leaflets of the SAV model during the final stage of the forward flow, whereas a significant amount of particles still resided on the leaflets in the TAV model. The innovative aspect of this study lies in the adoption of a complex FSI algorithm which accounts for the intricated interactions between the structural and the fluidic domain to investigate thrombosis after TAVR. However, they used an idealized TAV device without frame.

Other studies adopted computer modelling to **compare** the performance between **two devices** [173] or **against *in vitro* tests** [181] rather than as predictive tool for risk of complications.

In 2015, Bianchi et al. [173] evaluated and compared the crimping mechanism of the SAPIEN valve with the polymeric Polynova valve prosthesis by means of computer modeling. FEA was adopted to evaluate frame deformation and stress distribution on the frame after crimping and deployment in 2 patients who experienced valve migration. Subsequent CFD analysis was carried out to evaluate occurrence of paravalvular AR. Volumetric flow magnitude and transvalvular pressure were obtained from intra-procedural echo-Doppler measurements of the same patients. The flow measurements were imposed as boundary condition while the pressure gradient was used for verification purposes. FEA analysis revealed much higher stress values on the SAPIEN frame and on its leaflets in full crimped configuration, than the Polynova. Therefore, the Polynova performed better than the SAPIEN in terms of stress withstanding during crimping. However, incomplete expansion of both valves occurred because of calcium nodules. As a result, diastolic CFD analysis showed occurrence of paravalvular AR at the location of those gaps. On the other hand, systolic CFD showed significant hemodynamics improvement after TAVR in terms of transvalvular gradient.

In 2016, Wu et al. [181] for the first time proposed a framework to evaluate the performance of a self-expandable percutaneous valve using a FSI approach. The accuracy of the simulation was assessed with *in vitro* tests. Subsequently, they evaluated the performance of the same valve in a patient-specific case. The authors observed a different strain distribution of the frame between the *in vitro* and the patient-specific case. Also, they identified few elements prone to fatigue fracture in the frame implanted in the patient-specific geometry. Therefore, some differences in the valve behavior were observed between the *in vitro* and the patient-specific models, suggesting that the *in vitro* test might not be representative of the real behavior of the percutaneous valve.

## 3.4 TAVIGUIDE

TAVIguide is the computational framework developed at FEops NV (Ghent, Belgium) that was used in this project to simulate TAVR procedures and to assess possible related complications. Below, the main steps of the modeling strategy will be briefly described. Further details will be reported in the 'Materials and methods' section of each publication, listed in Part II of the dissertation as well as in Appendix A.

### 3.4.1 The patient-specific anatomy

Patient-specific aortic root models are segmented from anonymized pre-operative MDCT images using the dedicated software Mimics version 18.0 (Materialise, Leuven). Aortic root models include the ascending aorta, sino-tubular junction, LVOT and when visible also coronary arteries. Native leaflets and calcifications volumes, extracted from MDCT images, are reconstructed in a subsequent step using an in-house python-based algorithm.

The mechanical properties of the different tissues were calibrated in a previous work by an iterative back-calculation method using both pre- and post-operative MDCT images [175]. In summary, the biological tissues (aorta and native leaflets) are modeled with elastic material properties and uniform thickness, whereas calcifications were modeled using a stiffer elastic material with perfect plasticity.

### 3.4.2 Available TAVR devices

At the moment of this project, few devices were integrated in the software: the self-expandable Medtronic CoreValve and Evolut R, the balloon-expandable Edwards Sapien XT and the mechanically-expandable Lotus valve, in all their sizes. Successively, the Evolut PRO, i.e. the latest generation of CoreValves, has been added.

Medtronic frames were reconstructed from optical microscopy measurements and micro-CT images, while the mechanical characteristics of the Nitinol frame were derived from in vitro radial compression tests at body temperature. Accurate device models of the SAPIEN XT and all Lotus valves were generated based on information provided by the device manufacturer.

### 3.4.3 FEA computer simulation and output variables

FEA computer simulation to virtually implant the device in the patient-specific aortic root models are performed in Abaqus/Explicit (v6.12, Dassault Systemes Simulia Corp, Johnson, RI). In TAVIguide, all steps of a clinical implantation can be simulated (i.e. balloon pre-dilatation, device deployment, balloon post-dilatation).

From the FEA simulation, the deployed TAV frame geometry and the displacement of the native calcified leaflets can be predicted [175]. Several output variables are extracted to evaluate the post-deployment frame deformation, the grade of apposition of the device to the aortic root and the risk of coronary occlusion. The frame deformation is evaluated at 4 levels through geometrical measurements (i.e. diameters, perimeter, area, eccentricity and degree of under-expansion). The grade of device apposition is given by the distance between the TAV skirt and the aortic root wall. The distance between the coronary ostium and the nodule of calcium closest to the coronary ostium after TAV deployment is also computed.

### 3.4.4 CFD computer simulation and output variables

In a subsequent step, the post-deployment geometries are extracted from Abaqus and used to set up a CFD simulation in OpenFOAM (v2.1.1, OpenCFD Ltd., Bracknell, UK). The CFD simulation is performed to evaluate the risk of paravalvular AR. To this aim, the TAV leaflets are assumed in the closed configuration and simulated as a planar seal. The blood is assumed Newtonian and an end-diastolic transvalvular pressure gradient of 32 mmHg is applied as boundary condition. The imposed pressure difference is the average of the postoperative diastolic transaortic pressure difference retrospectively observed in a sample of 20 patients in a previous study [176].

From the CFD simulation, the location of the paravalvular jets and velocity can be extracted. The paravalvular flow is then computed from the velocity.

### 3.4.5 TAVIguide studies outside the PhD thesis

Previous studies have demonstrated the accuracy of patient-specific structural [175] and fluid simulation [176] performed using TAVIguide.

In 2016, Schultz et al. [175] performed an extensive study, simulating the implantation of a CoreValve device in 33 patients and a SAPIEN valve in 6 patients to validate the biomechanical properties of the aortic root model for the prediction of the post-deployment TAV geometry. The frame morphology at ventricular inflow (for both CoreValve and SAPIEN valves), nadir, coaptation and commissures (only for the CoreValve device) was compared with postoperative MDCT (Fig 3.9). Also, the displacement of the calcifications of the aortic leaflets was quantified by measuring the distance between the coronary ostia and the closest calcium nodule. Results revealed a strong correlation between the observed and predicted frame dimensions. High accuracy was found as well for the prediction of calcium displacement.

Successively, de Jaegere et al. [176] started from these simulations to model the blood flow during diastole and assess the paravalvular AR jets in 60 patients. Results were compared with postoperative AR evaluation based on echocardiography and/or angiography. They found good correlation between the predicted and observed AR (Fig 3.10). Also, they found a cut-off value (16.0 ml/s) that best differentiates between patients with none-to-mild and moderate-to-severe AR.

More recently (2018), Brouwer et al. [192] used TAVIguide to predict the feasibility of TAVR (with Evolut R or Lotus valve) for 7 critical patients with bicuspid aortic valve. Postoperative echocardiography and fluoroscopy were used to verify the accuracy of valve morphology and paravalvular AR prediction. Good correlation was found between the predicted and observed valve morphology and regurgitation. Also, the computational model correctly predicted unsuccessful TAVR procedure in one patient.

Those promising results clearly show the potential of this computational workflow to provide useful outcome prediction that can improve the preprocedural planning of TAVR. However, paravalvular AR prediction was validated only after implantation of the self-expandable CoreValve device. Therefore, further validation that proves the accuracy of computer simulation for other devices currently in the market is needed.

### 3.4.6 Studies performed within the PhD thesis

In line with the consideration stated above, one goal of this project was to further validate the TAVIguide workflow for prediction of postoperative AR and extend it to other devices (e.g. mechanically expandable Lotus valve).

Next to this, we aimed to further improve TAVIguide for prediction of other critical complications such as conduction abnormalities. TAVIguide was then adopted as a tool to provide insight into the device sizing and positioning and assess the impact of those variables on postoperative AR and conduction abnormalities. Also, it was combined with device optimization techniques to investigate the benefits it can bring in the design and develop-

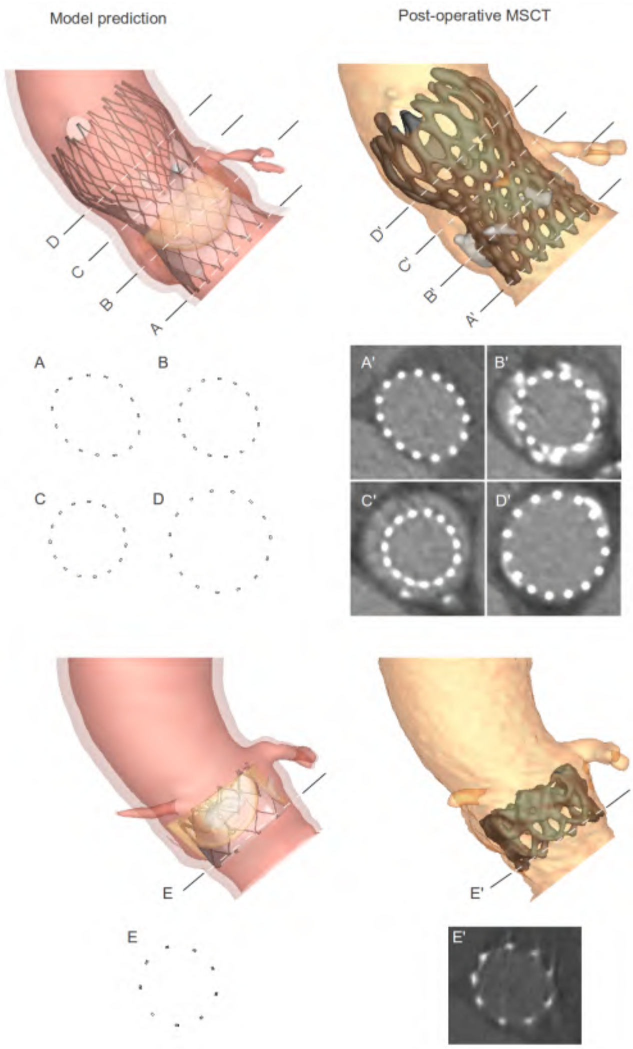
Model prediction
Post-operative MSCT
D
C
B
A
D'
C'
B'
A'
A
B
C
D
A'
B'
C'
D'
E
E'
E
E'

**Figure 3.9:** Levels of measurement on the CoreValve and SAPIEN valves. The geometry of predicted (model - left) and observed (MSCT - right) MCS (top) frame was quantified at the ventricular inflow (A and A'), nadir (B and B'), central coaptation (C and C') and commissures (D and D'). For the SAPIEN (bottom), only the ventricular end (E and E') was evaluated [175].

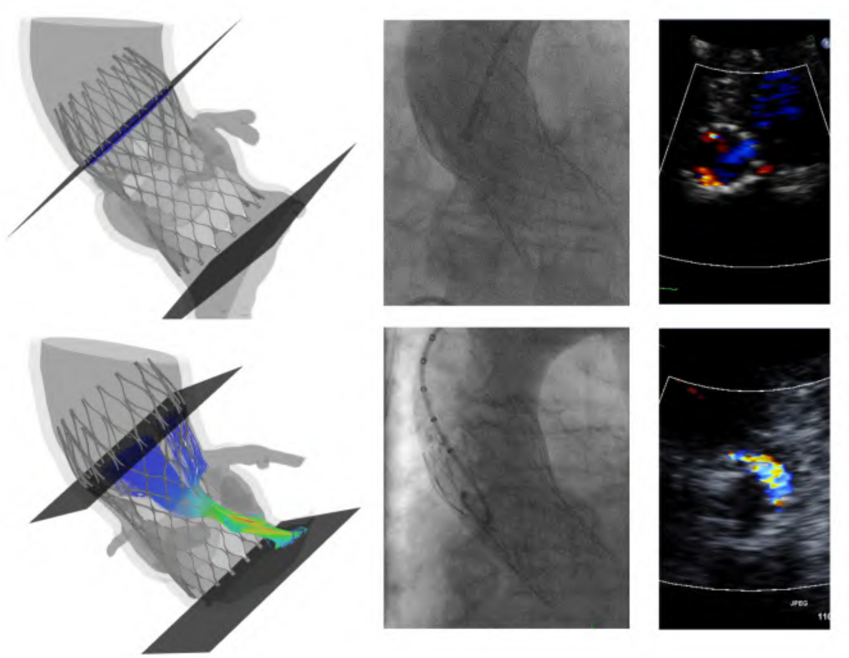

**Figure 3.10:** Comparison between the predicted AR (left) and the clinically assessed AR (right) in 2 patients [176].

ment phase of a new device. The obtained results will be presented in the next sections.

# II

# Computer simulation: prediction of TAVR complication

CHAPTERS

4 **Patient-specific computer simulation to predict new conduction abnormalities after TAVR** 75

5 **Effect of commissural alignment on paravalvular regurgitation after TAVR** 91

6 **The impact of size and position of a mechanical expandable transcatheter aortic valve** 101

7 **Optimization of a TAV frame using patient-specific computer simulations** **117**

# CHAPTER 4

# PATIENT-SPECIFIC COMPUTER SIMULATION TO PREDICT NEW CONDUCTION ABNORMALITIES AFTER TAVR

This chapter presents a patient-specific numerical simulation strategy developed to quantify the contact pressure exerted by the implanted TAV on the AV conduction system and to predict the risk of new conduction abnormalities after TAVR. The results of this study have been published [193]. With respect to the published version, the manuscript has been extended with results regarding the mesh sensitivity analysis of the aortic root model. In addition, some considerations about the correlation between parameters identified as possible predictors of new conduction abnormalities are reported.

## 4.1 INTRODUCTION

TAVR is increasingly used to treat patients with severe AS that are deemed inoperable or at high risk for SAVR [194]. Recent clinical data demonstrate that TAVR is also a good alternative for SAVR in intermediate risk patients [8], resulting in a further expansion of the indication for TAVR [195]. At variance with SAVR, conduction abnormalities (LBBB, high degree AVB) frequently occur after TAVR and remain a major clinical limitation as it may lead to PPM implantation [196].

Despite the fact that patient-, procedure- and device-related variables have been shown to be associated with an increase of conduction abnormalities after TAVR, the underlying mechanism is not completely clear [196]. Some authors have mentioned that pressure generated by the prosthetic valve frame on the atrioventricular conduction pathway may be an important driver of new conduction abnormalities although other mechanisms may play a role as well [197–200].

Therefore, the aim of this study was to investigate to what extent mechanical pressure, assessed by patient-specific computer simulations, affects the conduction system after TAVR.

## 4.2 MATERIALS AND METHODS

### 4.2.1 Study population

The study population consists of 112 patients who underwent TAVR on native valves (i.e. no valve-in-valve) using either the self-expanding CoreValve or an Evolut R transcatheter heart valve (Medtronic, MN, USA) because of severe AS (Table 4.3). All patients had undergone preoperative MDCT for sizing and that was of sufficient quality to allow computer simulation as previously described [175, 176]. MDCT in-plane and through-plane resolution ranged from 0.32-0.97 mm/pixel, slice increment from 0.25-0.8 mm and slice thickness from 0.5-1.5 mm.

Patients were selected for TAVR by the multidisciplinary Heart Team at the participating hospital. All patients were informed about the procedure and provided with informed written consent for the procedure and data collection.

### 4.2.2 Computer simulations

Pre-operative MDCT was used to generate patient-specific three-dimensional models of the native aortic root anatomy that included the LVOT, the calcified native leaflets and the ascending aorta, using image segmentation techniques (Mimics v18.0, Materialise, Leuven, Belgium). The aortic wall and the leaflets were assumed to have a constant thickness of 2 mm and 1.5 mm respectively [175]. Subsequently, virtual implantation of Medtronic CoreValve and CoreValve Evolut R systems in these aortic models was retrospectively performed using finite-element computer modelling (Abaqus/Explicit v6.12, Dassault Systèmes, Paris, France) as previously described [175]. Briefly, CoreValve and CoreValve Evolut R frames were reconstructed from optical microscopy measurements and micro-CT images, while the mechanical characteristics of the Nitinol frame were derived from *in-vitro* radial compression tests at body temperature. The mechanical properties of the different tissues in the computer model were calibrated by an iterative back-calculation method using both pre- and post-operative MDCT images [175]. The aortic tissue was modeled with elastic material properties (E = 2 MPa, $\nu$ = 0.45) and spring elements were added to incorporate the impact of surrounding structures in the model. The leaflets were assumed to be linear elastic (E = 0.6 MPa, $\nu$ = 0.3), while calcifications were modeled using a stiffer elastic material with perfect plasticity (E = 4 MPa, $\nu$ = 0.3, Yield stress = 0.6 MPa). General contact with finite sliding between all the surfaces was applied with hard contact properties to prevent penetrations along the normal direction. A friction coefficient of 0.7 was used to model the interaction between the frame and the aortic model.

These computer simulations allow to assess device-host interaction and, thus, device and aortic wall deformation as well as the resulting contact pressure exerted by the frame on the surrounding anatomy. A mesh sensitivity analysis on the aortic root wall was performed to ensure accurate numerical results in terms of predicted frame deformation and contact pressure. Results of the mesh sensitivity analysis are reported in paragraph 4.3.1. During the computer simulations, all steps of the clinical implantation consisting of pre-dilatation (i.e. balloon size), valve size, depth of implantation and post-dilatation (i.e. balloon size) if applied, were respected, as previously described in two studies in which the software was validated for the assessment of frame geometry and expansion, calcium displacement and paravalvular leakage [175, 176]. Device repositioning of the Evolut R was not integrated in the model, but the final depth of implantation at the NCC and LCC was matched with the actual depth of implantation derived from contrast angiography performed immediately after TAVR, using the same projection angle.

### 4.2.3 Pressure analysis

From each finite element simulation, the force exerted on the recipient anatomy was extracted. For the purpose of this study (i.e. relationship between contact pressure and new conduction abnormalities after TAVR) the region of the LVOT that contains the atrioventricular conduction system was defined as the region of interest. At that region, (i) maximum contact pressure and (ii) contact pressure index (i.e. the percentage of this region of interest subjected to contact pressure) were calculated (Fig 5.1,4.2,4.4).

The region of interest for the contact pressure analysis was selected on each three-dimensional aortic root model, starting from the inferior border of the membranous septum (IBMS), as this represents an anatomical surrogate for the surfacing of the His bundle and the transition to the left bundle branch [105, 201, 202]. To identify the IBMS, three dedicated landmarks were determined on the pre-operative MDCT images at the transition between the interventricular membranous and muscular septum [128] in the resliced view perpendicular to the annular plane (Fig 5.1). Two of these landmarks were selected at the beginning and at the end of the IBMS, namely $p_1$ and $p_3$, with $p_1$ closer to the non-coronary cusp and $p_3$ closer to the RCC. An additional point ($p_2$) was selected in between to better track the course of the IBMS as this is often not a straight line (Fig 5.1a). If an abrupt change in the IBMS was seen when scrolling through the MDCT images between $p_1$ and $p_3$, $p_2$ was chosen at that location. Based on anatomical findings [201, 203], the region of interest for the contact pressure analysis was defined by the area between the IBMS (extended towards the RCC by a 25° angle) and the plane 15 mm below the annulus (Fig 5.1b-c), to ensure the inclusion of the proximal part of the left bundle branch.

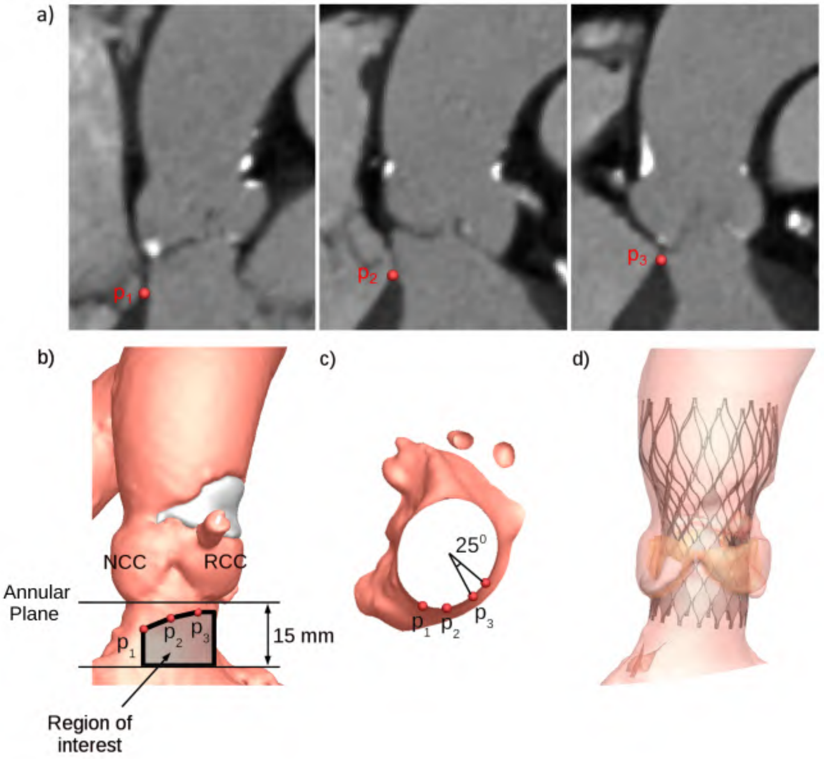

**Figure 4.1:** Identification of anatomical landmarks and computer modelling workflow - a) identification of IBMS in the preoperative MDCT images through three consecutive landmarks ($p_1$, $p_2$, $p_3$, in red); b-c) patient-specific 3D aortic model with, in black, the selected region of interest in vicinity of the atrioventricular conduction system from a frontal view (b) and from a top view (c); d) virtual implantation of the Medtronic CoreValve device at the same implantation depth as done in the real procedure. IBMS = inferior border of the membranous septum.

The effect of frame rotation on contact pressure and contact pressure index was taken into account by simulating for each patient 3 different rotations of the frame: starting from a reference position the frame was rotated with 6 and 12 degrees. The resulting maximum contact pressure and contact pressure index for these different rotations were then averaged per patient.

Besides the contact pressure analysis, the anatomical variability of the length, location and orientation of the IBMS was investigated (Fig 4.2a). The length of the IBMS (l) was defined as the distance between the first ($p_1$) and the last ($p_3$) selected landmarks, the location of the IBMS was defined as the relative distance of points $p_1$ ($d_1$) and $p_3$ ($d_3$) to the aortic annular plane, and the orientation of the IBMS was described by the angle α between the segment connecting $p_1$ and $p_3$, and the aortic annular plane.

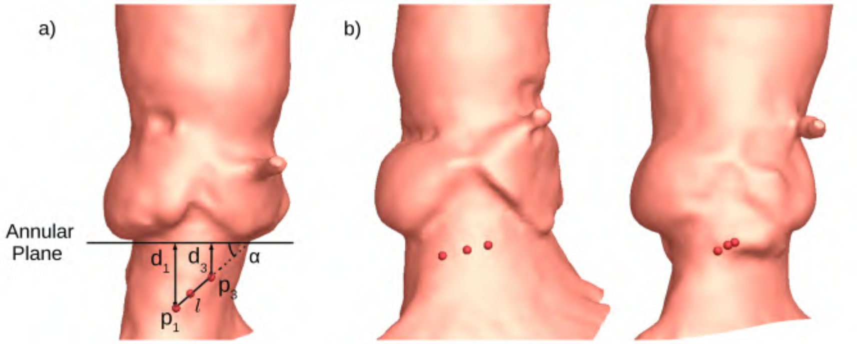

**Figure 4.2:** Anatomical variability - IBMS is represented by three red landmarks. a) illustration of the IBMS-related anatomical measurements: IBMS length (l) – distance between landmarks $p_1$ and $p_3$, IBMS location ($d_1$ and $d_3$) – distance of landmarks $p_1$ and $p_3$ from the annular plane, IBMS orientation ($\alpha$) – angle between the segment connecting $p_1$ and $p_3$ and the annular plane. b) Representative illustration of IBMS identification in two patients. IBMS = inferior border of the membranous septum.

### 4.2.4 Statistical analysis

Continuous variables are expressed as mean±standard deviation (SD) or median [interquartile range], stratified by the occurrence of new TAVR related conduction abnormalities, and compared using the Student's t-test or Mann-Whitney-Wilcoxon test depending on the variable distribution. Discrete variables are expressed as percentage and compared using the chi-squared or the Fisher's exact test where appropriate. The non-parametric Friedman test was used to analyze differences in maximum contact pressure and contact pressure index between three different rotations of the device. Anatomical baseline characteristics and procedural parameters that were considered relevant for the development of conduction abnormalities were analyzed as well as the maximum contact pressure and contact pressure index. Only variables yielding a p value <0.1 in the univariable analysis were included in the stepwise logistic regression (backward likelihood ratio) analysis. Only for significant results (p<0.05) receiver-operating characteristics (ROC) curves were generated to find optimal cut-off values (Youden index criterion [204]), and sensitivity, specificity, positive predictive value (PPV), negative predicted value (NPV) and accuracy were calculated. In addition, a correlation analysis was conducted on those parameters using the Spearman's rank correlation coefficient. Statistical analysis was performed with the statistical software package SPSS version 22.0 (IBM Corporation, New York, USA).

## 4.3 RESULTS

### 4.3.1 Mesh sensitivity analysis of the aortic root model

A selection of 8 different mesh sizes was used to perform the mesh sensitivity analysis on the aortic wall model. The mesh sensitivity analysis evaluated the influence of the mesh size on the maximum nodal force within the region of the AV conduction system. Computational time was also evaluated. Results are reported in Table 4.1 and Fig 4.3.

**Table 4.1:** Mesh sensitivity analysis of the aortic wall model. The selected mesh is highlighted in bold.

| **Mesh** | Mesh_1 | Mesh_2 | Mesh_3 | Mesh_4 | **Mesh_5** | Mesh_6 | Mesh_7 | Mesh_8 |
|---|---|---|---|---|---|---|---|---|
| **Element area [mm$^2$]** | 3.0 | 2.5 | 2.0 | 1.8 | **1.5** | 1.3 | 1.0 | 0.8 |
| **N elements** | 5292 | 6367 | 7688 | 8673 | **10808** | 12081 | 14991 | 19938 |
| **Max nodal force [N]** | 0.97 | 0.90 | 0.67 | 0.66 | **0.66** | 0.66 | 0.59 | 0.66 |
| **Simulation time [min]** | 60 | 60 | 62 | 66 | **65** | 67 | 71 | 78 |

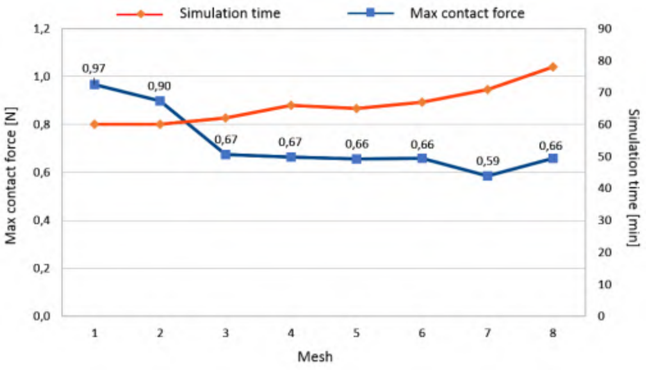

**Figure 4.3:** Maximum contact force obtained within the region of the atrioventricular conduction system by refining the aortic wall mesh (in blue) and the needed computational time.

Maximum contact force and simulation time were comparable from Mesh_3 to Mesh_8.

The impact of the aortic wall mesh density on the predicted frame morphology was also evaluated. Diameters (minimum, maximum), perimeter and area of the deformed frame were quantified at four predefined levels of the device: 1) commissure level, 2) central coaptation of the device leaflets, 3) nadir and 4) ventricular end (Table 4.2). Those parameters were compared after implantation in patient-specific aortic root having different mesh density. The maximum relative differences in frame morphology with respect to the finest aortic mesh were calculated. Results are reported in Table 4.2. The small differences between the frame morphology after implantation, suggests that aortic wall mesh density had low impact on the frame deformation.

**Table 4.2:** Impact of the aortic wall mesh size on the predicted frame morphology at four predefined levels of the frame. In the second column the maximum relative difference respect to the finest mesh is reported.

| **Frame morphology** | **Maximum relative difference** [%] |
|---|---|
| Commissure level | |
| D_min | 0.16 |
| D_max | 0.08 |
| Perimeter | 0.02 |
| Area | 0.06 |
| Central coaptation | |
| D_min | 0.06 |
| D_max | 0.13 |
| Perimeter | 0.09 |
| Area | 0.18 |
| Nadir | |
| D_min | 0.09 |
| D_max | 0.50 |
| Perimeter | 0.44 |
| Area | 0.87 |
| Ventricular end | |
| D_min | 1.00 |
| D_max | 0.99 |
| Perimeter | 0.88 |
| Area | 1.78 |

After evaluation of the impact of aortic wall mesh size on maximum contact force, computational time and frame deformation, Mesh_5 was chosen for the aortic wall model.

### 4.3.2 Clinical outcome

Baseline patient- and procedure-related characteristics are summarized in Table 4.3. Sixty-two patients (55%) developed new conduction abnormalities after TAVR: LBBB or high degree AVB (second degree AVB Mobitz 2 or third degree AVB). A higher number of patients developed new conduction abnormalities after implantation of a CoreValve compared to those who received a Evolut R (59% vs 35%). There were no other differences between patients with and without a new conduction abnormality, except for a deeper implantation of the valve in the LVOT (8.4 vs 5.8 mm, p<0.001) and a shallower position of the IBMS at $p_3$ (1.7 vs 2.8 mm) in the group with conduction abnormalities. An example of the variations in anatomy of the IBMS is illustrated in Fig 4.2.

**Table 4.3:** Characteristics of the study population

| | | **Conduction Abnormalities** | | |
|---|---|---|---|---|
| **Parameters** | **All patients(n=112)** | **Yes(n=62)** | **No(n=50)** | **p value** |
| *Baseline characteristics* | | | | |
| Female sex | 56 (50) | 31 (50) | 25 (50) | >0.99 |
| Age | 82 [77-85] | 83 [78.5-85] | 80 [75.8-84] | 0.12 |
| EUROscore | 12.2 [9.5-19.5] | 12.6 [9.5-18.5] | 11.7 [8.8-22.2] | 0.94 |
| Annular diameter [mm]* | 23.9±1.8 | 24.1±1.9 | 23.7±1.7 | 0.19 |
| Height [cm] | 164.2±8.1 | 163.9±8.4 | 164.7±7.8 | 0.64 |
| Weight [Kg] | 71.9±12.1 | 72.0±12.5 | 71.7±11.8 | 0.92 |
| BSA [$m^2$] | 1.8±0.2 | 1.8±0.2 | 1.8±0.2 | 0.73 |
| Pre RBBB | 5 (4) | 3 (5) | 2 (4) | 0.83 |
| IVS calcifications† | 12 (11) | 5 (8) | 7 (14) | 0.31 |
| *IBMS characteristics* | | | | |
| IBMS length [mm] | 10.2±3.7 | 10.5±3.9 | 9.8±3.3 | 0.29 |
| IBMS angle [deg] | 18.8±15.2 | 19.6±14.7 | 17.7±15.9 | 0.52 |
| $p_1$depth [mm] | 5.5±3.2 | 5.2±3.5 | 5.8±2.9 | 0.32 |
| $p_3$depth [mm] | 2.2±2.4 | 1.7±2.2 | 2.8±2.5 | 0.02 |
| *Procedural characteristics* | | | | |
| Implantation depth [mm]‡ | 7.2±3.5 | 8.4±3.2 | 5.8±3.2 | <0.001 |
| *Device type* | | | | 0.07 |
| CoreValve (CV) | 95 (85) | 56 (90) | 39 (78) | |
| Evolut R (CVER) | 17 (15) | 6 (10) | 11 (22) | |
| *Device size* | | | | 0.37 |
| CV26 | 30 (27) | 17 (28) | 13 (26) | |
| CV29 | 60 (54) | 35 (57) | 25 (50) | |
| CV31 | 5 (4) | 4 (6) | 1 (2) | |
| CVER26 | 6 (5) | 2 (3) | 4 (8) | |
| CVER29 | 11 (10) | 4 (6) | 7 (14) | |
| Sizing index◇ | 1.18±0.1 | 1.17±0.1 | 1.19±0.1 | 0.29 |

Values are mean±SD, median [IQR] or n (%).

*Perimeter-based diameter = annular perimeter/Π.

†Presence of calcifications in the IVS (plane perpendicular to the annulus).

‡Implantation depth assessed in post-operative angiograms: distance from the aortic annular plane on the NCC side to the deepest level of the most proximal edge of the device frame.

◇Sizing index = (device size)/(perimeter-based diameter).

BSA = body surface area. CV = CoreValve. CVER = CoreValve Evolut R. IBMS = inferior border of the membranous septum. IVS = interventricular septum. NCC = non-coronary cusp. RBBB = right bundle branch block.

#### *4.3.2.1 Contact pressure on the LVOT in the region of interest*

The non-parametric Friedman test showed no statistical difference in maximum contact pressure and contact pressure index between the three device rotations ($p = 0.073$ and $p = 0.698$, respectively). Maximum pressure and contact pressure index were both significantly higher in patients with a new conduction abnormality after TAVR ($p<0.001$, Table 4.4). The median value of maximum contact pressure (0.51 MPa [0.43-0.70] MPa) and contact pressure index (33% [22-44]%) was 2 to 3 fold higher in patients with a new conduction abnormality compared to patients without a new conduction abnormality (0.29 MPa [0.06-0.50] MPa and 12% [1-28]%, Fig 4.4). In the majority of patients (89%), the maximum contact pressure was observed in the upper half of the region of interest.

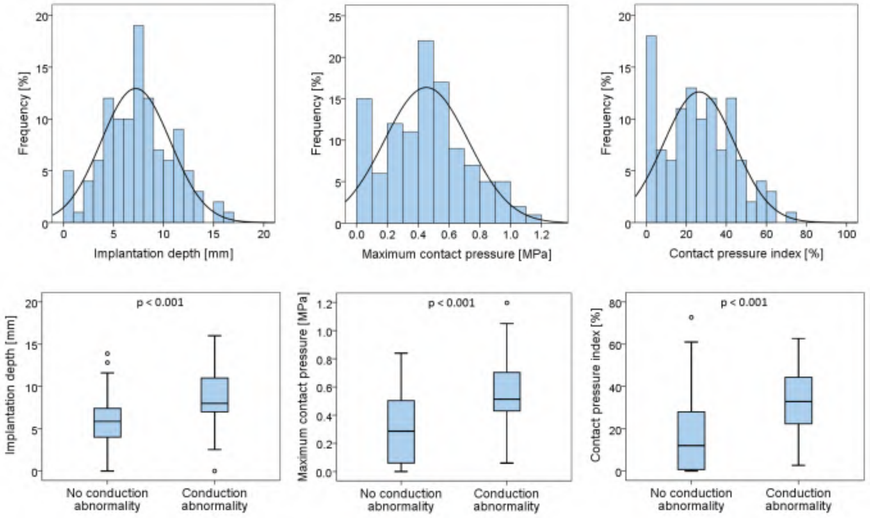

**Figure 4.4:** Histograms and box plot diagrams of valve implantation depth, maximum contact pressure and contact pressure index – (Upper panel) Distribution of valve implantation depth (left), maximum contact pressure (middle) and contact pressure index (right) in comparison to a normal probability curve (black curve). (Lower panel) Box plot diagrams of valve implantation depth ($p<0.001$, left), maximum contact pressure ($p<0.001$, middle) and contact pressure index ($p<0.001$, right) in patients with and without conduction abnormalities. Extreme values are presented as small circles (o).

Computer simulation results in a patient without and with a new conduction abnormality with comparable depth of implantation of the device, are shown in Fig 4.5. In the patient without a new conduction abnormality a low maximum contact pressure (≤ 0.11 MPa) in the vicinity of the conduction system (region of interest delimited by the black border) was observed. Conversely, the patient who developed a new AVB, experienced high contact

**Table 4.4:** Simulation results

| | | Conduction Abnormalities | | |
|---|---|---|---|---|
| **Parameters** | **All patients(n=112)** | **Yes(n=62)** | **No(n=50)** | **p value** |
| Maximum pressure [MPa] | 0.46 [0.26-0.62] | 0.51 [0.43-0.70] | 0.29 [0.06-0.50] | <0.001 |
| Contact pressure index [%] | 26 [13-40] | 33 [22-44] | 12 [1-28] | <0.001 |

Values are expressed as median [IQR].

pressure within the region of interest (up to 0.85 MPa) and an extended area of contact (contact pressure index of 29%).

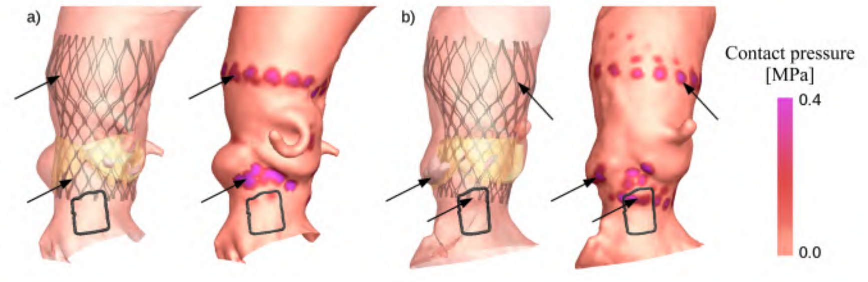

**Figure 4.5:** Contact pressure: representative examples - Representative example of contact pressure observed on the aortic root areas where the aortic root is in contact and interacts with calcifications and device frame (indicated by black arrows). The region of interest is delimited by the black line. a) case without a new TAVR-induced conduction abnormality: maximum contact pressure = 0.11 MPa and contact pressure index = 20%. b) case with new TAVR-induced high degree AVB: maximum contact pressure = 0.85 MPa, and contact pressure index = 29%. AVB = atrioventricular block. TAVR = transcatheter aortic valve implantation.

The Spearman test revealed a moderate correlation either between the valve implantation depth and the maximum contact pressure (R = 0.40), and valve implantation depth and contact pressure index (R=0.62). The scatterplots in Fig 4.6 show the relationship between depth of implantation and the two contact pressure parameters.

Interestingly, not all the models showed contact between the valve frame and the region of interest. Fig 4.7 illustrates 3 patients where no contact was observed in the region of interest because of a large calcium nodule precluding apposition of the frame (Fig 4.7a), of an anatomic low position of the IBMS (Fig 4.7b), and of a large LVOT resulting in mal-apposition of the frame (Fig 4.7c).

The multivariable regression analysis identified maximum contact pressure (odds ratio (OR): 1.35, confidence interval (CI): 1.1-1.7, p=0.01) and contact pressure index (OR: 1.52, CI: 1.1-2.1, p=0.01) as the only independent predictors of conduction abnormalities (Table 4.5).

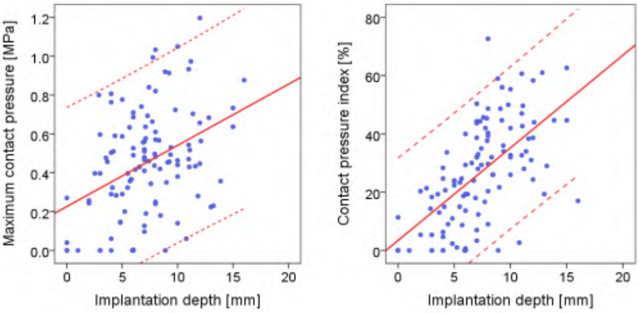

**Figure 4.6:** Scatterplots of implantation depth against maximum contact pressure (left) and implantation depth against contact pressure index (right). Approximation line is presented in red. Confidence interval (5% and 95%) is shown by red dotted lines.

**Table 4.5:** Results of the logistic regression for association with post-TAVR conduction abnormalities

| | **Univariable** | **Multivariable analysis** | | |
|---|---|---|---|---|
| **Parameters** | **p value** | **p value** | **Odds ratio** | **95% CI** |
| $p_3$ depth [mm] | 0.017 | - | - | - |
| Device type | 0.071 | - | - | - |
| Implantation depth [mm] | <0.001 | - | - | - |
| Maximum pressure [MPa] | <0.001 | 0.010 | 1.35 | 1.1-1.7 |
| Contact pressure index [%] | <0.001 | 0.013 | 1.52 | 1.1-2.1 |

CI = confidential interval

ROC curve analysis (Fig 4.8) revealed an area under the curve (AUC) of 0.76 and 0.79 for maximum contact pressure and contact pressure index respectively. A cut-off value of 0.39 MPa for the maximum contact pressure ensured a sensitivity, specificity, PPV, NPV and accuracy of 85%, 64%, 75%, 78% and 76%, respectively. This was 95%, 54%, 72%, 90% and 77%, respectively for a contact pressure index of 14%. The accuracy of prediction was further increased when combining both contact pressure parameters (Fig 4.9). Fifty-three patients (79%) with a maximum contact pressure >0.39 MPa and a contact pressure index >14% developed a new conduction abnormality. In case of a maximum contact pressure <0.39 MPa and a contact pressure index <14%, 23 patients (88%) did not experience new conduction abnormalities. Four patients with a maximum contact pressure >0.39 MPa and a contact pressure index <14% (i.e. small area of high contact pressure) did not develop conduction abnormalities, while 6 patients (40%) with a low maximum contact pressure and contact pressure index >14% developed new conduction abnormalities.

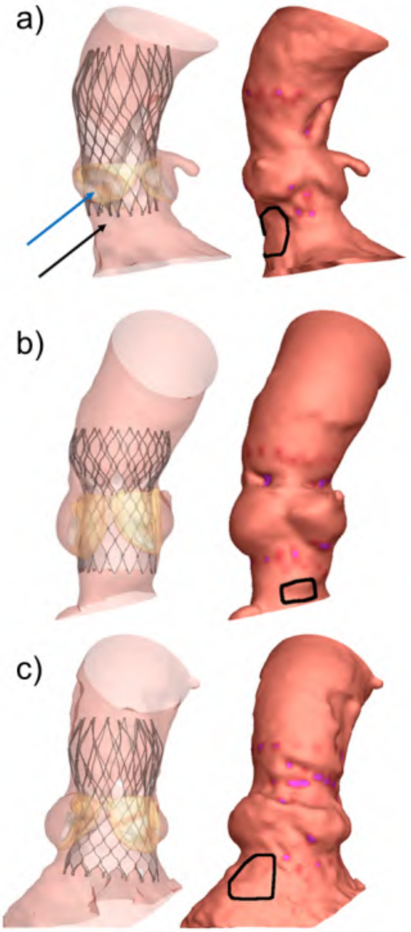

**Figure 4.7:** Representative cases with no contact within the region of interest - a) large valve calcification (blue arrow) that determines underexpansion of the frame (black arrow); b) anatomic low position of the IBMS; c) large LVOT and bad apposition of the valve frame with the aortic wall. LVOT = left ventricular outflow tract.

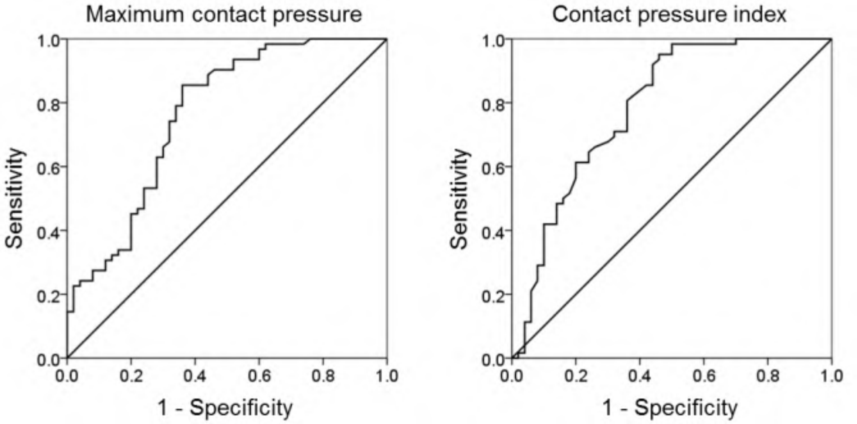

**Figure 4.8:** ROC curves of maximum contact pressure and contact pressure index - ROC curve analysis of maximum contact pressure (AUC = 0.76, left) and contact pressure index (AUC = 0.79, right). AUC = area under the receiver-operator characteristics curve. ROC = receiver-operator characteristics curve.

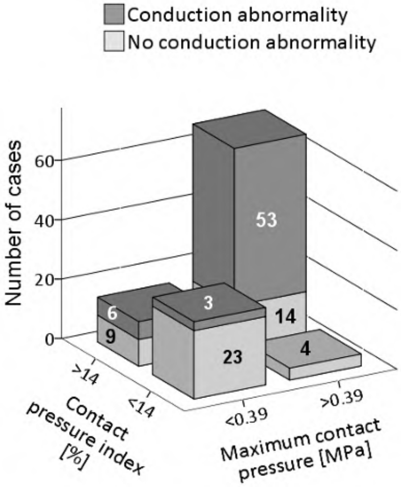

**Figure 4.9:** Prediction of conduction abnormalities according to the maximum contact pressure and contact pressure index - Prediction of conduction abnormalities according to the maximum contact pressure and contact pressure index based on the chosen cut-off values (0.39 MPa and 14% respectively).

## 4.4 DISCUSSION

The main goal of this study was to investigate the relation between the mechanical pressure generated by the prosthetic valve frame on the aortic root at the site of the atrioventricular conduction tissue and the development of new conduction abnormalities after TAVR. Using patient-specific computer simulations, maximum contact pressure and contact pressure index were both assessed. The impact of device rotation on the contact pressure within the region of interest was also evaluated, but no significant difference on the variations of both parameters due to the device rotations was observed. Both simulation-based parameters were associated with new conduction abnormalities (LBBB and high degree AVB) after implantation of a self-expanding valve. Of note, the multivariable analysis indicated that contact pressure, but not implantation depth is the driving force of the development of new conduction abnormalities. Yet, it remains difficult to elucidate whether pressure levels or relative area is the overriding factor. In addition, cut-off values were identified that could discern patients who did and did not develop new conduction abnormalities after TAVR.

Based on the pre-operative MDCT, anatomical landmarks were identified to define a patient-specific region on the LVOT in which the contact pressure was evaluated. The definition of this region is based on the consideration that the His bundle is located at (or slightly below) the transition between the interventricular membranous and muscular septum in at least 80% of the cases [105]. 3D measurements of the IBMS revealed large anatomical variability within the studied population in terms of location, orientation and length of the IBMS. In our analysis, the IBMS was located below the annular plane on the NCC side and extended towards the RCC. In about 13% of the cases the landmark $p_3$ was found to be superior to the annular plane, meaning that the distal part of the IBMS intersected the interleaflet triangle between NCC and RCC. A representative example is shown in Fig 4.10. These findings are in accordance with those of Kawashima et al. (2014) who also found the membranous septum (MS) to be located between the NCC and the RCC (frequently located on the RCC side), with reaching the annular plane in about 80% of the cases [203]. Irrespective to the inter-individual variability of the precise relationship between the membranous septum and the conduction tissue, this area is susceptible to injury during TAVR. In particular the position of the IBMS at the RCC side (depth of $p_3$) was found to be inversely associated with risk of new conduction abnormalities; however, the multivariable analysis did not show it to be an independent predictor of new conduction abnormalities.

Several studies consistently revealed the relation between a too deep implantation of the prosthesis and the occurrence of new onset LBBB and

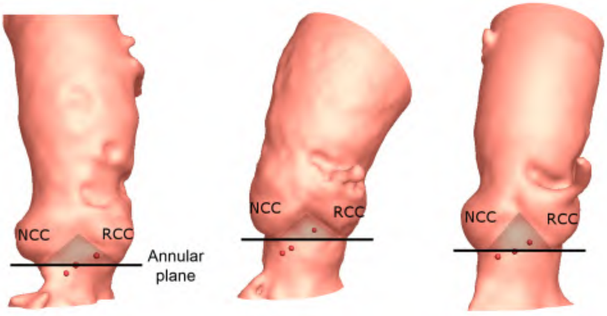

**Figure 4.10:** Representative examples of high IBMS - Three patients where the IBMS (red rots) was found to end superiorly to the annular plane (black line) and thus intersecting the interleaflet triangle between NCC and RCC (light grey zone). IBMS = inferior border of the membranous septum. NCC = non-coronary cusp. RCC = right-coronary cusp.

PPM implantation [117, 205–208]. In our study, such correlation emerged in the univariable analysis, but it did not show to be statistically significant in the subsequent multivariable analysis. The findings of this study are not in disagreement with those who focused on the role of depth of implantation since this study incorporated both depth of implantation and contact pressure and contact pressure area. Depth of implantation and area of contact pressure are intrinsically related to one another. This study merely indicates that the degree of pressure and area of contact pressure are more important than the depth of implantation by itself, which is from a pathophysiologic perspective a logic finding. Although a high implantation is nowadays recommended to avoid conduction abnormalities, the findings of this study indicate that the optimal implantation depth is patient-specific given the anatomic variability of the membranous septum. General implantation depth guidelines may not lead to the best clinical outcome for each individual. This is in agreement with the recent work of Hamdan et al. who identified the 2D MSCT-based distance from the IBMS to the annular plane and the difference between this parameter and the device implantation depth as predictors of high-degree AVB and PPM implantation [128]. The results of our anatomical analysis of the IBMS (e.g. the distance from the IBMS to the annular plane varies along the course of the IBMS), indicate however that a single 2D measurement may not fully describe this structure.

Given the above and in line with the demand from society and authorities to move to patient-specific treatment in order to enhance safety and efficacy of treatment, thereby, reducing costs, this and previous works on computer simulations indicate the role of patient-specific computer simulations in the planning of TAVR offering the physician to choose the valve size that best fits the individual patient in addition to the optimal depth of implantation [209, 210]]. The findings of this study indicate that patient-specific computer simulation pre-TAVR may identify which patient will develop a new conduction abnormality. Previous works indicated the reliability of specific computer simulation in the prediction of the presence and severity of paravalvular leakage [176]. Both outcome measures can currently be assessed and quantified during the same simulation and may, thus, help the physician to choose the valve that best fits the individual patient.

### Study limitations

The results of this study only relate to the self-expanding CoreValve and Evolut R valves. Its applicability to other transcatheter aortic valve systems currently in use should be confirmed. Also, the effect of device repositioning was not taken into account; however, it may be hypothesized that especially the final implantation depth is the most determining factor for inducing conduction abnormalities. Linear elastic material properties were used to model the aortic tissue. Although the hyperelastic model better reflects actual tissue behavior, the used material parameters accurately predict interactions between the aorta and the TAVR device, as previously demonstrated [167, 175]. Future studies should be performed to validate the cut-offs identified to discriminate between patients who did and did not develop a new conduction abnormality. Furthermore, it might be interesting to investigate the predictive power of maximum contact pressure and contact pressure index with respect to the type of disturbance (LBBB or AVB). Finally, a further quantitative analysis of the location of the maximum contact pressure within the region of interest during the entire cardiac cycle may offer a better insight in the mechanisms of the development of new conduction abnormalities after TAVR.

## 4.5 CONCLUSIONS

Patient-specific computer simulations revealed that maximum contact pressure and contact pressure index are associated with new conduction abnormalities after Corevalve/Evolut R implantation and can predict which patient will have a conduction abnormality after TAVR.

# CHAPTER 5

# EFFECT OF COMMISSURAL ALIGNMENT ON PARAVALVULAR REGURGITATION AFTER TAVR

This chapter will present the results of the validation of TAVIguide for prediction of paravalvular AR. Particular focus is given to the effect of the TAV orientation within the aortic root on paravalvular AR.

## 5.1 INTRODUCTION

TAVR is an accepted treatment for patients with AS at increased and intermediate surgical risk [8, 68, 70, 211]. Despite improvements in valve technology, paravalvular AR still may occur and may be associated with impaired survival, even when mild [8, 68].

AR may be caused by patient-, procedure-, and device-related factors such as calcium load of the aortic annulus, sizing, depth of implantation and valve type. With the availability of an increased number of valve technologies and sizes, the selection of the valve and size that best fits the individual patient is expected to further improve the outcomes (e.g. less AR post TAVR).

For that purpose, a patient-specific computer simulation technology (TAVIguide, FEops, Ghent, Belgium) has been developed to predict valve geometry and function and its ability to reliably discern patients with none-to-mild and moderate or severe AR was previously demonstrated [175, 176].

At variance with SAVR, the calcium is not removed during TAVR and the operator does not have the freedom to choose the valve orientation. Using patient-specific computer simulation, the clinical TAVR procedure can be repeated by incorporating all details of the procedure, but also to assess the effect of a different approach (e.g. different valve size or type, depth of implantation, bioprosthesis alignment) on outcome and valve performance. The purpose of this study was to assess the effect of the degree of alignment of the bioprosthetic commissures and native aortic leaflets on AR immediately post-TAVR.

## 5.2 MATERIAL AND METHODS

### 5.2.1 Study population

This study population consists of 63 patients who had received TAVR with the self-expandable first-generation CoreValve (Medtronic, MN, USA) after heart team consensus. Sizing was based upon end-diastolic preoperative cardiac MDCT using a 64-slice GE lightspeed (General Electric Company, Easton Turnpike, Fairfield, CT, USA) with a spatial resolution of 0.6 mm [212]. All patient- and procedural variables were prospectively collected and entered into a dedicated database (Table 5.1 and 5.2). All patients were informed about the procedure and provided written informed consent.

### 5.2.2 AR Assessment

*Observed AR*

AR post-TAVR was assessed by contrast angiography using the Sellers classification and transthoracic echocardiography using simple color Doppler flow mapping acquired in the parasternal long-axis and apical 3- and 5-chamber views [213]. In each view color gain was carefully set to demonstrate maximal jet by avoiding color Doppler speckles. The degree of AR was divided into "no AR" (grade 0) = no regurgitating jet; "mild AR" (grade 1) = total regurgitating jet area < 2.2 $cm^2$, "moderate AR" (grade 2) = total regurgitating jet area of 2.2-4.2 $cm^2$ and "severe AR" (grade 3) = total regurgitating jet area > 4.2 $cm^2$ [214].

*Predicted AR*

Patient-specific computer simulation was used to predict AR (ml/sec) in case of alignment and non-alignment of the native and bioprosthetic leaflets.

The computer simulation workflow (details described previously [175, 176]) starts from the patient's baseline MDCT of the heart to reconstruct the patient-specific anatomy followed by segmentation of the native aortic root including the left ventricular outflow tract, the calcified native leaflets and the ascending aorta (Mimics v17.0, Materialise, Leuven, Belgium). The clinical TAVR procedure was then simulated using finite element computer modelling (Abaqus/Explicit v6.12, Dassault Systèmes, Paris, France) respecting all steps (i.e. valve size, depth of implantation, and pre- and post-dilatation if applied). Depth of implantation at the non- and left-coronary cusp (NCC and LCC) was matched with the actual depth of implantation derived from contrast angiography performed immediately after TAVR. Skirt and prosthetic leaflets were added to the implanted frame aligning the prosthetic to the native leaflets. Non-alignment was then performed by rotating the prosthetic skirt and leaflets by 60 degrees. AR post simulation (i.e. predicted AR) was quantified for both alignment and non-alignment of the native and bioprosthetic leaflets by modelling blood flow during diastole using computational fluid-dynamics (OpenFOAM v2.1.1, OpenCFD Ltd., Bracknell, UK) with a fixed pressure difference of 32 mmHg. The imposed pressure is the average of the post-operative diastolic transaortic pressure difference retrospectively observed in a sample of 20 patients. The different steps of the computer simulation workflow are depicted in Fig 5.1, while Fig 5.2 illustrates the alignment and non-alignment of the native and bioprosthetic leaflets.

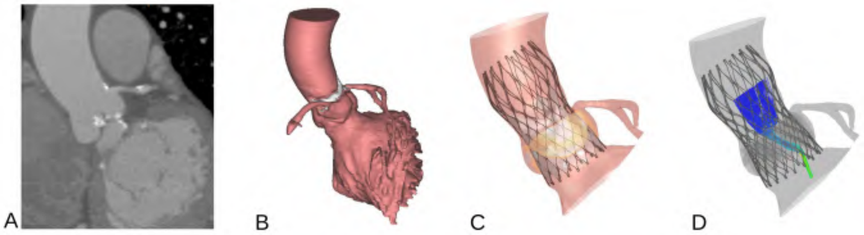

**Figure 5.1:** Description of the steps followed for prediction of AR: MDCT images (A) are used to create a reconstruction of the aortic 3D model (B), virtual implantation of the TAV (C – FEA simulation) and modelling of the blood flow with prediction of AR (D – CFD simulation). AR = Aortic regurgitation. CFD = Computational fluid-dynamics. FEA = Finite element analysis. MDCT = Multidetector computed tomography. TAV = Transcatheter aortic valve.

### 5.2.3 Analysis & Statistics

Predicted AR was compared with observed AR (contrast angiography, echocardiography) to assess the model accuracy. The mean of the predicted AR from the aligned and non-aligned simulation was used for this purpose as the actual alignment in the patient is unknown. Second, a comparison of the predicted AR in case of alignment and non-alignment of the bioprosthetic commissures with those of the patients' aortic valve was performed.

Data are presented as median [Q1-Q3] or mean±standard deviation (SD), depending on the distribution of the data evaluated with histograms, QQ-plots and Kolmogorov-Smirnov test. Categorical variables are presented as n

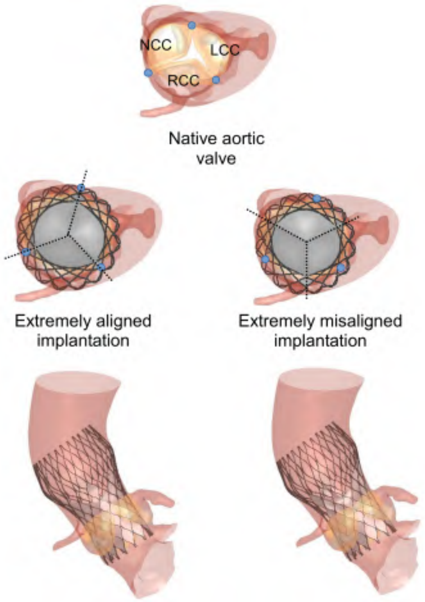
NCC
LCC
RCC
Native aortic valve
Extremely aligned implantation
Extremely misaligned implantation

**Figure 5.2:** Comparison between aligned (left panel) and misaligned (right panel) implantation for the prediction of AR: commissures of the native reconstructed valve are highlighted by blue dots, while commissures of the prosthetic valve are indicated by black dotted lines. In the three images at the top we are visualizing the aortic valve from the aorta towards the left ventricle. AR = Aortic regurgitation.

(%). Continuous variables were tested with Student t-test or Mann Whitney U-test, depending on the distribution. Aligned/non-aligned predicted AR were tested with Wilcoxon signed rank test for paired samples. SPSS Version 22.0 (IBM Corp., Armonk, NY, USA) was used. Statistical significance was defined as a two-tailed $p<0.05$.

## 5.3 RESULTS

### 5.3.1 AR prediction

Baseline and procedural characteristics are summarized in Table 5.1 and 5.2. Based on angiography, 15 patients (23.8%) had no AR post-TAVR, 25 (39.7%) had grade I, 20 (31.7%) had grade II and 3 (4.8%) had grade III. Based on echocardiography, 44 patients (80.0%) had "none-mild AR" post-TAVR, 9 (16.4%) had "moderate AR" and 2 (3.6%) had "severe AR". Only 1 patient received post-deployment balloon dilation, with a 25-mm balloon.

In all 63 patients, predicted AR was significantly higher in patients with AR grade 2-3 in comparison to patients with AR grade 0-1 based on angiography (16.5 [10.8-26.1] vs 10.8 [5.8-16.7] ml/s, p=0.049) and echocardiography (23.2 [15.2-45.6] vs 11.8 [5.4-16.4] ml/s, p=0.002) (Table 5.3, Fig 5.3).

**Table 5.1:** Baseline characteristics

| **Population** | n = 63 |
|---|---|
| Age (years) | 81 [77-85] |
| Gender (male) | 26 (46.0) |
| Height (cm) | 164±8 |
| Weight (kg) | 74±13 |
| Body surface area ($m^2$) | 1.8±0.2 |
| Body mass index ($kg/m^2$) | 27.4±4.3 |
| New York Heart Association classification III-IV – n (%) | 52 (74.6) |
| *Echocardiography* | |
| Peak gradient (mmHg) | 67±19 |
| Mean gradient (mmHg) | 44±13 |
| Aortic valve area ($cm^2$) | 0.65±0.20 |
| *Risk scores* | |
| Logistic EuroSCORE (%) 13.0 [9.5-21.5] EuroSCORE II (%) | 5.0 [2.8-8.8] |
| Society of Thoracic Surgeons score (%) | 4.3 [3.3-5.5] |
| *Medical history* | |
| Atrial fibrillation – n (%) | 26 (41.3) |
| Carotid disease – n (%) | 6 (9.5) |
| Coronary artery disease – n (%) | 28 (44.4) |
| Chronic obstructive pulmonary disease – n (%) | 11 (17.5) |
| Diabetes – n (%) | 14 (22.2) |
| Hypertension – n (%) | 38 (60.3) |
| Previous myocardial infarction – n (%) | 11 (17.5) |
| Peripheral artery disease – n (%) | 18 (28.6) |
| Previous stroke/transient ischemic attack – n (%) | 12 (19.0) |
| Pacemaker – n (%) | 6 (9.5) |
| Previous coronary artery bypass – n (%) | 22 (34.9) |
| Previous percutaneous coronary intervention – n (%) | 24 (38.1) |

### 5.3.2 Frame deformation

Computer simulations predicted an asymmetric profile (e.g. pear-shape, non-convex) of the valve frame in the 60% (15/25) of the patients with moderate or severe AR. This seems to be related to the distribution and size of calcium nodules on the aortic leaflets. Fig 5.4 shows four representative examples of the post-deployment morphology of the valve in those patients. From the top to the bottom the image presents: the morphology of the valve predicted with computer simulation (from the front view), the same models seen from the left ventricle chamber and the border of the valve frame at the ventricular inflow.

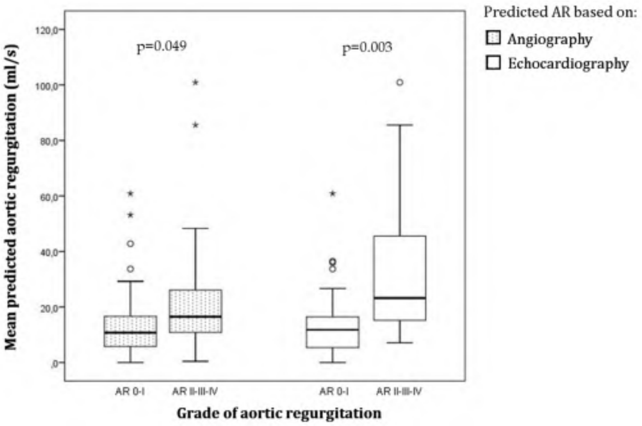

**Figure 5.3:** Difference between mean predicted AR (ml/s) and aortic regurgitation (AR) grade 0-I vs. grade II-III based on angiography (dotted boxplots; p=0.049) and echocardiography (white boxplots, p=0.003). Extreme values and outliers are presented by (○) and (*) respectively. AR = Aortic regurgitation.

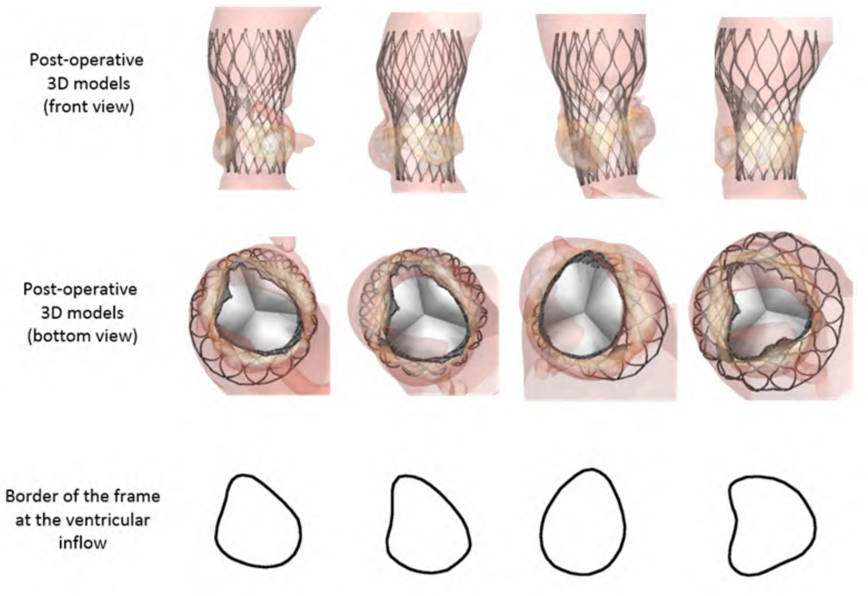
Post-operative
3D models
(front view)
Post-operative
3D models
(bottom view)
Border of the frame
at the ventricular
inflow

**Figure 5.4:** Representative examples of frame deformation in four patients with moderate or severe AR post-TAVR. The figure shows: the implantation of the device in the patient-specific 3D aortic model predicted by computer simulation seen from the front view (top row), the frame deformation seen from the left ventricular chamber (middle row) and the border of the frame at the ventricular inflow (left row).

**Table 5.2:** Procedural characteristics

| **Procedural characteristics** | |
|---|---|
| *Access* | |
| Transfemoral – n (%) | 50 (79.3) |
| Subclavian – n (%) | 2 (3.2) |
| Truncus brachiocephalicus – n (%) | 8 (12.7) |
| Direct aortic – n (%) | 3 (4.8) |
| *Valve size* | |
| 26 mm – n (%) | 14 (22.2) |
| 29 mm – n (%) | 40 (63.5) |
| 31 mm – n (%) | 9 (14.3) |
| Depth NCC – n (%) | 7.2±3.3 |
| Depth LCC – n (%) | 8.6±4.3 |

**Table 5.3:** Predicted AR [ml/s] in patients with AR grade 0-1 and 2-3 (angiography, echo)

| | **Grade AR 0-I** | **Grade AR II-III** | **p value** |
|---|---|---|---|
| *Angiography* | N = 40 | N = 23 | |
| | 10.8 [5.8-16.7] | 16.5 [10.8-26.1] | 0.049 |
| *Echocardiography* | N = 44 | N = 11 | |
| | 11.8 [5.4-16.4] | 23.2 [15.2-45.6] | 0.002 |

The eccentricity of the frame was also evaluated at 2 levels: at the ventricular inflow and at 12 mm above the ventricular inflow. The eccentricity at the two levels was comparable between the patients with AR grade 0-I and AR grade II-IIII-IV based on angiographic and echocardiographic evaluation (Fig 5.5a and Fig 5.5b respectively). This result indicates that a not perfectly circular valve (i.e. elliptical shape) is not the main responsible of paravalvular AR.

### 5.3.3 Frame alignment

When comparing alignment/non-alignment of the bioprosthetic leaflets with those of the native valve, predicted AR in case of non-alignment was higher (70% of the cases) (13.2 [6.9-21.5] vs 11.8 [6.7-19.0] ml/s, $p<0.001$). In 33 patients (62%) the difference between alignment/non-alignment was less than 1 ml/s. In 5 cases, the difference of the predicted AR between alignment/non-alignment was more than 5 ml/s (up to 32.4 ml/s). Leakage paths were often observed near the native valve commissures, especially between severely calcified leaflets.

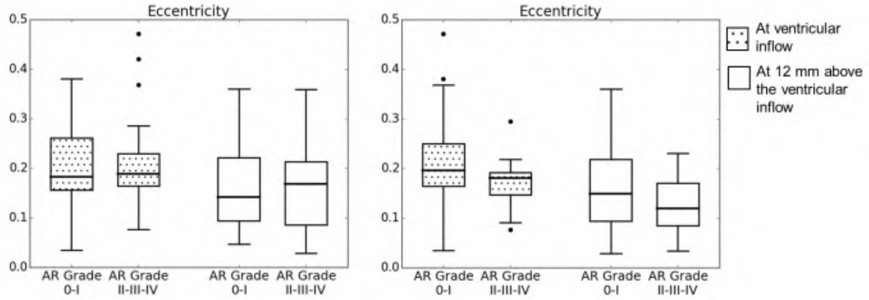

**Figure 5.5:** Boxplots distribution of the frame eccentricity in patients with (a) angiography- and (b) echocardiography-based AR grade 0-I and AR grade II-III-IV.

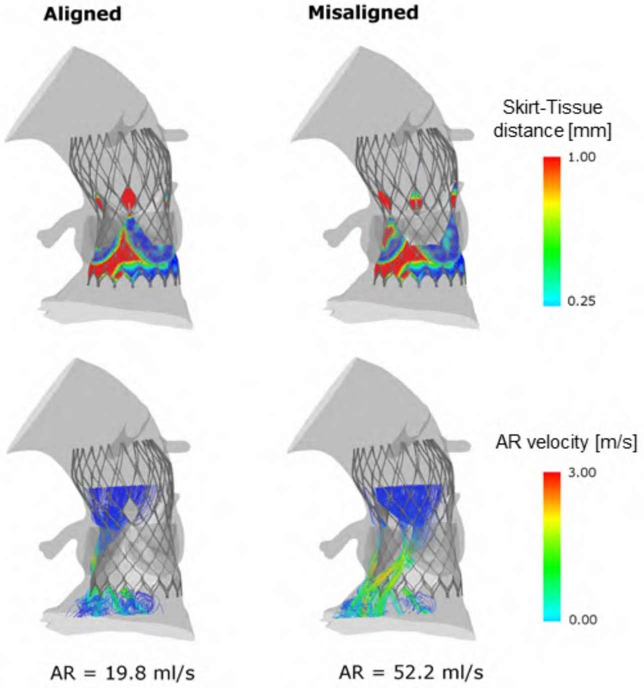
Aligned
Misaligned
Skirt-Tissue distance [mm]
1.00
0.25
AR velocity [m/s]
3.00
0.00
AR = 19.8 ml/s
AR = 52.2 ml/s

**Figure 5.6:** Case illustration: Difference between aligned (left panel) and misaligned (right panel) implantation for the prediction of AR (19.8 ml/s vs. 52.2 ml/s). AR = Aortic regurgitation.

Fig 5.6 shows that a good alignment between the bioprosthetic and the native aortic valve commissures resulted in a better apposition of the device skirt to the aortic wall, with the consequent reduction of AR.

## 5.4 Discussion

In the present study we found that the predicted AR was significantly higher in patients with moderate or severe AR post-TAVR based on echocardiography and angiography. This result confirms the findings of a previous study using another set of patients and a different pre-procedural MDCT phase to generate the 3D model of the patient's aortic root [176]. The novel finding is that alignment did affect the degree of AR in 70% of the patients albeit that its effect on severity of AR was variable between patients.

Asymmetric valve frame was observed in 60% of the patients with moderate or severe AR. The frame seems to assume a 'pear-shape' or a non-convex shape conform to the size and location of calcium nodules. Previous studies correlated the volume of calcium with the eccentricity of the deployed valve frame which, in turn, correlated with the severity of paravalvular AR [215]. However, our findings suggested that frame eccentricity was comparable among patients with different degree of paravalvular AR.

Predicted AR channels were observed at the commissures of the native aortic valve where, in most of the cases, calcium ridges prevented a good apposition of the valve frame to the aortic wall, creating paravalvular commissural space. This finding is in agreement with previous studies where calcifications nearby the commissures were predictive for the site of AR [216]. In this regard, TAVIguide simulations interestingly showed that in 70% of the patients, alignment of the bioprosthetic with native leaflets favored at the commissural region a better apposition of the valve to the aortic wall, resulting in lower AR. As mentioned above, despite statistical significance, the absolute difference of the predicted AR in case of the alignment/non-alignment between the bioprosthetic and native valve commissures was small (less than 1 ml/s), except for a few cases.

Alignment of the bioprosthesis with the native aortic valve implies that the natural position of the aortic valve and leaflets is respected. Although unproven, this may be desirable for valve function and durability. At variance with surgical aortic valve replacement, the operator cannot choose or determine the orientation of the bioprosthesis during TAVR, except for the recently introduced JenaValve (Munich, Germany) after which a low frequency of AR has been reported. It remains to be elucidated if and to what extent the control of valve orientation contributes to the elimination of paravalvular

AR as suggested by the herein reported findings and the frequency of AR after JenaValve implantation.

With respect to the issue of durability, alignment of the bioprosthesis may have an effect on the mechanics of the bioprosthetic leaflets. Recent computer simulation studies showed that the alignment of its commissures with the native ones minimizes the leaflet stress distribution [170, 217]. This finding may be taken into account for the design of future devices, i.e. bioprostheses that are either insensitive to the implantation alignment or which can be implanted with an optimal alignment. Last but not least, alignment of the bioprosthesis may also help to access coronary arteries for eventual future coronary interventions.

## 5.5 Conclusions

Patient-specific computer simulation accurately predicts the degree of AR post-TAVR. Alignment of the bioprosthesis affects the degree of AR albeit that the absolute difference is small and may, therefore, not play a clinical role.

# Chapter 6

# The impact of size and position of a mechanical expandable transcatheter aortic valve

In this chapter, the prediction of postoperative AR and conduction abnormalities using TAVIguide is validated for the mechanical-expandable Lotus device. Further to that, TAVIguide is adopted as a tool to provide insight into the device sizing and positioning and assess the impact of those variables on such complications. The results from this study have been accepted for publication in Journal of Cardiovascular translational research.

## 6.1 Introduction

TAVR is a widely accepted minimally invasive treatment for patients suffering from severe aortic stenosis [8, 68, 218]. Over the last decade, it has become clear that the selection of the appropriate transcatheter aortic valve (TAV) size is of critical importance for the success of the procedure. A too small device size might result in valve migration or paravalvular regurgitation, while oversizing can cause new conduction abnormalities [127, 131], annular rupture or coronary obstruction [219, 220]. Similarly, the final position of the TAV within the aortic root strongly influences procedural outcome. Too low/high positioning is in many cases associated with paravalvular AR [221], while several studies demonstrated that low TAV implantation increases the risk of TAVR-induced conduction abnormalities [196, 221].

The mechanically-expandable Lotus valve (Boston Scientific, MA, USA) is a repositionable second generation TAV which allows for great control over the deployment and precise positioning. On the other side, the selection of the appropriate device size remains challenging. According to the current recommendations, the selection of the Lotus valve size is based upon aortic root measurements (aortic annulus and LVOT), preferably assessed by MDCT [222]. Hence, in clinical practice, it often occurs that the sizing matrix offers the possibility to select two valve sizes for a specific patient. In those cases, industry guidelines do not provide detailed indications, and device size selection strongly relies on individual experience. Therefore, in patients with equivocal aortic root dimensions, a patient-specific computational model that allows virtual implantation of multiple device sizes at several implantation depths could provide useful additional insights facilitating decision-making.

Patient-specific computational modelling has previously been used to investigate the effect of the TAV positioning on the stress distribution on the aortic root [166, 187]. Others focused on the effect of TAV positioning on the TAV leaflet performance in terms of coaptation area and stress distribution [168, 174]. Bianchi et al. [178] explored whether TAV positioning influences device anchoring and therefore impacts the risk of device migration. However, these studies were based on a single patient-specific model and, as such, the specific results cannot be assumed to represent the entire population. A more extensive study, based on 112 patients, recently demonstrated that patient-specific computational modelling and simulation can accurately predict the occurrence of new conduction abnormalities [193]. This study quantified the pressure induced by the self-expandable CoreValve/Evolut R (Medtronic, Minneapolis, USA) frame on the aortic root, in the region of the atrioventricular conduction pathway. Furthermore, few patient-specific studies demonstrated that finite-element simulations can accurately predict the paravalvular AR after implantation of a self-expandable [176, 179, 189] or balloon-expandable device [188]. However, its accuracy for mechanically expandable devices remains unclear.

The aim of this paper is twofold. First, we verified the predictive power of computer simulations for post-TAVR complications in patients who received a mechanically-expandable Lotus device. Second, we evaluated to what extent different device sizes and different valve positions in patients with equivocal aortic root measurements influence the predicted pressure generated on the atrioventricular conduction pathway and the paravalvular regurgitation.

## 6.2 MATERIALS AND METHODS

### 6.2.1 Study population

The study population consists of 62 patients with severe aortic valve stenosis who underwent TAVR with a Lotus valve at four European centers (San Raffaele Hospital, Milan, Italy; Rigshospitalet, Copenhagen, Denmark; St Antonius, Nieuwegein and the Erasmus Medical Center, Rotterdam, The Netherlands). All patients had undergone preoperative MDCT for sizing and MDCT quality was sufficient to allow computer simulation as previously described [175, 176, 193]. The cardiac region of interest (i.e. aortic root) was fully visible in the MDCT set and filled with contrast. No motion artefacts or noise due to the presence of other implanted devices affected the cardiac region of interest. MDCT in-plane and through-plane resolution ranged from 0.31 to 0.93 mm/pixel, slice increment from 0.25 to 0.7 mm and slice thickness from 0.5 to 1.5 mm. Pre- and postoperative electrocardiogram was recorded for all patients. Postoperative echocardiography and angiography were available respectively for 42 and 58 patients. In 13 patients, postoperative MDCT was also available. At the participating hospital, all patients were informed about the procedure and provided written informed consent for the anonymous use of their data for scientific research.

### 6.2.2 Computer modelling

*Anatomical reconstruction* - Patient-specific 3D models of the native aortic root including the LVOT, the calcified native leaflets and the ascending aorta, were reconstructed from preoperative MDCT using image segmentation techniques (Mimics v18.0, Materialise, Leuven, Belgium)(Fig 6.1a). An in-house software (TAVIguide, FEops, Gent, Belgium) was used to generate high-quality meshes of the native leaflets, by fitting a template mesh to the output of the segmentation step.

The material properties assigned to each anatomical region were previously calibrated through an iterative back-calculation method using both pre- and postoperative MDCT [175]. The aortic tissue was modelled with elastic material properties ($E = 2$ MPa, $\nu = 0.45$) [172, 182] and spring elements were added at each node of the aortic wall to incorporate the impact of surrounding structures. The leaflets were assumed to be linear elastic ($E = 0.6$ MPa, $\nu = 0.3$), while calcifications were modelled using a stiffer elastic material with perfect plasticity ($E = 4$ MPa, $\nu = 0.3$, Yield stress = 0.6 MPa). A constant thickness of 2 mm and 1.5 mm was assumed for the aortic wall and the leaflets respectively [175]. Preoperative MDCT was also used to identify the inferior border of the membranous septum as landmark for the region (of interest) of the LVOT where the atrioventricular conduction system is located (Fig 6.1b). Starting from this inferior border of the membranous septum, the region of interest was extended towards the RCC and up to 15 mm below the annular plane, to ensure the inclusion of the left bundle branch [193].

*Finite-element computer simulations* – Implantation of the Lotus valve in each patient's aortic root model was retrospectively simulated using finite element computer modelling (Abaqus/Explicit v6.12, Dassault Systèmes, Paris, France). The aortic root wall was modelled with triangular elements, whereas prism elements were adopted for the native valve tissue and the calcifications.

Accurate device models of all Lotus valve sizes were generated based on information provided by the device manufacturer. Device models included the braided Nitinol stent and the external skirt. Device leaflets were not included in the model because they are assumed to fully coapt in the diastolic phase. Furthermore, previous studies have reported that detailed device leaflets have a negligible effect on the predicted paravalvular AR [189] as well as on the post-deployment deformation of the fame [172, 178]. General contact with finite sliding between all the surfaces was applied with hard contact properties to prevent penetrations along the normal direction. A friction coefficient of 0.7 was used to model the interaction between the frame and the aortic model. To validate the computer model, the implanted device size was respected. Device repositioning and retrieval attempts were not integrated in the model, but the final depth of implantation at the NCC and LCC was matched with the actual position derived from contrast angiography performed immediately after the final deployment ('matched' simulation). Alternatively, the simulated position was matched with the implanted device reconstructed from postoperative MDCT, when available.

For the purpose of this study (i.e. assessment of the impact of device size and position on AR and contact pressure in patients with equivocal aortic root dimensions), a smaller cohort of patients with annular and LVOT dimensions (diameters, perimeter, area) leading to equivocal TAV size was selected. The LVOT dimension was assessed at 4 mm below the annular plane. For each of those patients, four additional simulations were performed: two different Lotus valve sizes were implanted in a high and low position, respectively at 0-3 mm and 3-6 mm below the annular plane.

From each simulation (matched + four additional ones), the pressure exerted on the selected region of interest of the LVOT was extracted. In particular, the maximum contact pressure within that region and the contact pressure index (i.e. relative area of contact within the selected region) were evaluated (Fig 6.1b).

*Prediction of aortic regurgitation* – Subsequently, AR following each virtual Lotus implantation was quantified by modelling blood flow during diastole using computational fluid-dynamics (OpenFOAM v2.1.1, OpenCFD

Ltd., Bracknell, UK). The ico-FOAM solver available within OpenFOAM was adopted. The extended flow domain was discretized using hexahedral elements and refined within the region of interest (i.e. the lumen within the rigid aortic root wall). The blood was modelled as incompressible fluid with constant density of 1060 kg/$m^3$ and a viscosity of 0.0035 Pa s. The flow was assumed to be laminar. No slip condition was assumed at the aortic wall. A fixed pressure difference of 32 mmHg was applied over the valve (Fig 6.1c). The imposed pressure is the average of the postoperative diastolic transaortic pressure difference retrospectively observed in a sample of 20 patients in a previous study [176]. This value is in line with the end-diastolic gradient observed by Sinning et al. in a cohort of 146 patients [149].

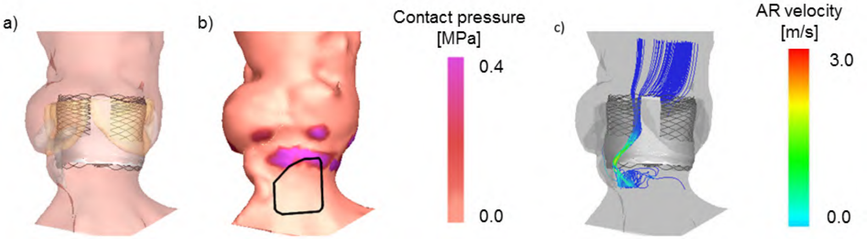

**Figure 6.1:** Computer modelling workflow. a) Lotus valve 25mm virtually implanted in a patient-specific aortic root 3D model reconstructed from preoperative MSCT images. b) Contact pressure exerted on the aortic root surface and selection of the region where the AV conduction system is located (selected region border in black) (maximum contact pressure = 0.47 MPa, contact pressure index = 9%). c) Predicted aortic regurgitation channel (predicted AR = 6.6 ml/s). AR = aortic regurgitation. MDCT = multidetector computed tomography.

### 6.2.3 Data analysis

*AR evaluation* – Post-TAVR AR was predicted by the 'matched' simulation for all patients (cohort A, Fig 6.2) and compared to the grade of clinically assessed postoperative AR based on echocardiography and angiography [140, 213]. The degree of AR was dichotomized in 'none or trace' and 'mild or more'.

*Predicted conduction abnormalities* – In 52 patients (cohort B, Fig 6.2) the contact pressure exerted on the region of the LVOT where the atrioventricular conduction system is located was measured and compared in patients with and without new conduction abnormalities (LBBB or high-degree AVB) that emerged after postoperative ECG evaluation. Patients with a previously implanted pacemaker (4 patients) and with the inferior border of the membranous septum not clearly visible on preoperative MDCT (6 patients) were excluded from this analysis.

*Device size and position in patients with equivocal aortic root dimensions* - Impact of implantation depth and device size on postoperative predicted AR and contact pressure was investigated in 12 patients with equivocal aortic root measurements (cohort C, Fig 6.2).

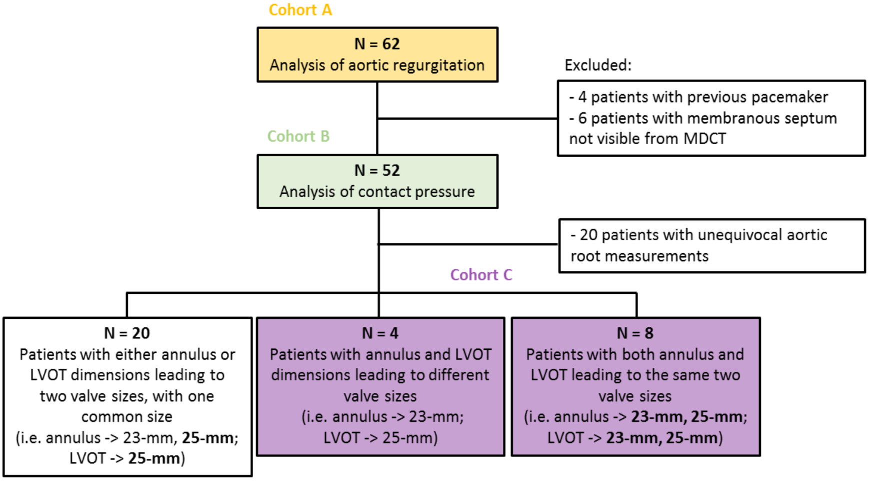
Cohort A
N = 62
Analysis of aortic regurgitation
Excluded:
- 4 patients with previous pacemaker
- 6 patients with membranous septum not visible from MDCT
Cohort B
N = 52
Analysis of contact pressure
- 20 patients with unequivocal aortic root measurements
Cohort C
N = 20
Patients with either annulus or LVOT dimensions leading to two valve sizes, with one common size
(i.e. annulus -> 23-mm, 25-mm; LVOT -> 25-mm)
N = 4
Patients with annulus and LVOT dimensions leading to different valve sizes
(i.e. annulus -> 23-mm; LVOT -> 25-mm)
N = 8
Patients with both annulus and LVOT leading to the same two valve sizes
(i.e. annulus -> 23-mm, 25-mm; LVOT -> 23-mm, 25-mm)

**Figure 6.2:** Diagram illustrating the study population: cohort A used for aortic regurgitation analysis (in orange), cohort B used for contact pressure analysis (in green), cohort C including patients with equivocal aortic root measurements (in purple). MDCT = multidetector computed tomography. LVOT = left ventricular outflow tract.

### 6.2.4 Statistical analysis

Data are presented as mean±standard deviation (SD) or median[Q1-Q3] and tested with Student t-test or Mann Whitney U-test, depending on the distribution. Effects of device size and position on predicted AR and conduction abnormalities were tested with the nonparametric Wilcoxon paired test. Statistical significance was set at $p<0.05$. Cut-off values to distinguish between patients with and without postoperative AR or new conduction abnormalities were identified using the Youden criterion [204]. The statistical analysis was performed in SPSS version 22.0 (IBM Corporation, New York, USA).

## 6.3 Results

Sixty-two patients (cohort A) were used to verify the predictive power of computer simulations for postoperative AR and 52 patients (cohort B) for postoperative conduction abnormalities. Twelve patients with equivocal aortic root dimensions (cohort C) were used to evaluate the impact of valve size and position on the predicted postoperative TAVR complications.

### 6.3.1 Postoperative AR

Angiography and/or echocardiography showed postoperative AR in 19 patients. Mean Lotus implantation depth was comparable in patients with and without postoperative AR (4.9±1.0 vs 4.9±1.9 mm). Patient-specific simulations predicted significantly higher AR in patients with postoperative 'mild or more AR' compared to patients with 'none or trace AR', respectively 9.6 [2.3-41.2] ml/s vs 3.7 [0.5-11.3] ml/s ($p<0.05$) (Fig 6.3a). Predicted AR of 13.5 ml/s was used as cut-off value to differentiate between patients with and without postoperative AR with an accuracy of 71%. Resulting sensitivity, specificity, positive predicted value (PPV) and negative predicted value (NPV) are reported in Table 6.1.

**Table 6.1:** Sensitivity, specificity, positive and negative predicted values and accuracy for computer simulations predicted outcomes.

| | **Predicted AR** | **Predicted maximum contact pressure** | **Predicted contact pressure index** |
|---|---|---|---|
| Sensitivity | 47% | 72% | 75% |
| Specificity | 81% | 81% | 63% |
| PPV | 53% | 90% | 82% |
| NPV | 78% | 57% | 52% |
| Accuracy | 71% | 75% | 71% |

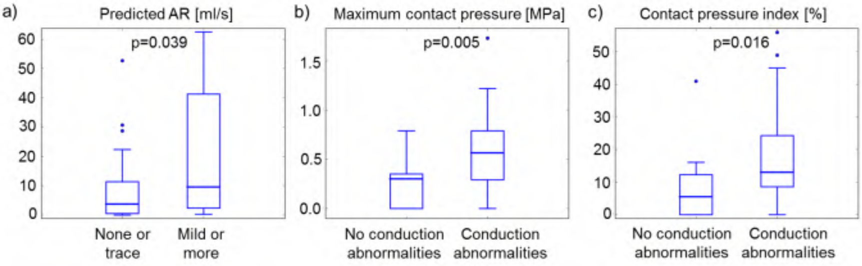

**Figure 6.3:** Box plot graphs of predicted AR, maximum contact pressure and contact pressure index. AR = aortic regurgitation.

### 6.3.2 Postoperative conduction abnormalities

Sixty-nine percent of the patients (36/52) experienced LBBB or total AVB block post-TAVR. Measured maximum contact pressure and contact pressure index in those patients were about twice the value observed in patients without new conduction abnormalities (Fig 6.3b-6.3c). Maximum contact pressure in patients with and without new conduction abnormalities was respectively 0.57 [0.29-0.80] MPa and 0.30 [0.00-0.36] MPa ($p=0.005$), while the contact pressure index was respectively 13 [8-25] % and 6 [0-13] % (p=0.016). The selected cut-off value was respectively 0.36 MPa for maximum contact pressure and 9% for contact pressure index, which respectively resulted in an accuracy of 75% and 71%. Obtained sensitivity, specificity, PPV and NPV are reported in Table 6.1. Moreover, the accuracy of the prediction further increases when combining the two contact pressure parameters (Fig 6.4).

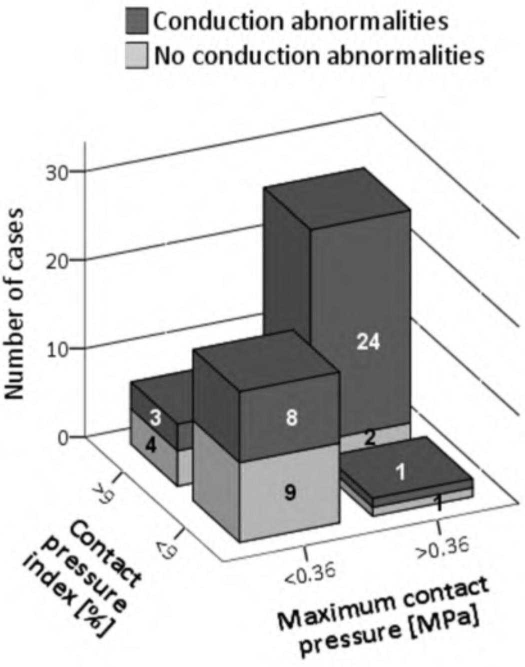

**Figure 6.4:** Prediction of conduction abnormalities according to the maximum contact pressure and contact pressure index based on the chosen cutoff values (0.36 MPa and 9%, respectively).

### 6.3.3 Analysis of patients with equivocal aortic root dimensions

Aortic annulus and LVOT dimensions led to unequivocal TAV size in 20 patients. In another group of 20 patients, equivocal annulus or LVOT dimensions led to the selection of two valve sizes, with one common size that was selected in clinical practice (i.e. annulus → 23-mm and 25-mm Lotus; LVOT → 25-mm Lotus). Twelve patients with equivocal aortic root measurements were considered suitable for two different device sizes (i.e. patients with annulus measurements suggesting a 23-mm Lotus and with LVOT measurements a 25-mm Lotus, or patients with annulus and LVOT measurements suggesting both a 23-mm and a 25-mm Lotus). In 3 patients simulations were performed with a 23- and 25-mm Lotus, and in 9 patients with a 25- and 27-mm Lotus.

Personalized simulations revealed an increase of maximum contact pressure and contact pressure index when a large TAV size is implanted or when the TAV position is deeper (p<0.001) (Fig 6.5, 6.6). Fig 6.5 shows the observed general trend of predicted contact pressure with respect to device size and position with a representative case.

With regard to the predicted AR, the device size plays a more crucial role as compared to depth of implantation. Modelling results showed a reduction of predicted AR in case the larger device was selected, regardless the valve position within the aortic root (p<0.001) (Fig 6.6).

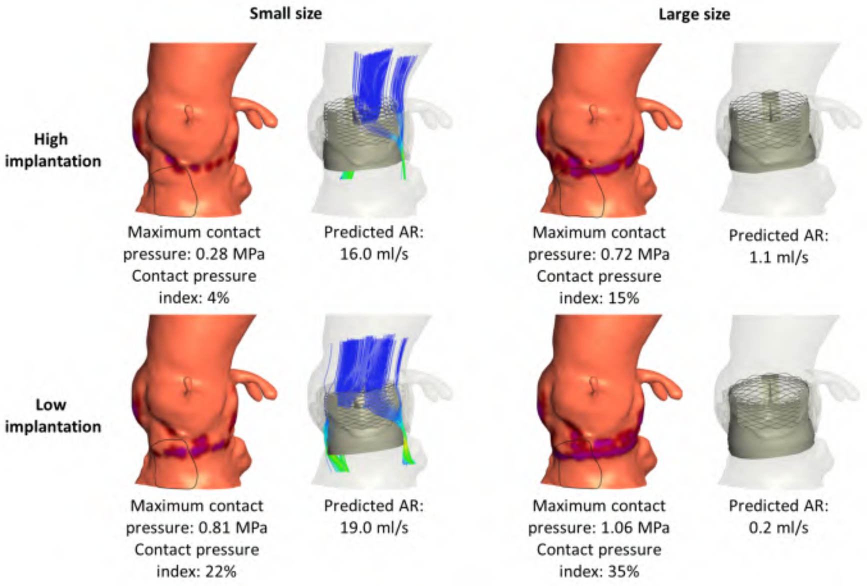
Small size
Large size
High implantation
Maximum contact pressure: 0.28 MPa Contact pressure index: 4%
Predicted AR: 16.0 ml/s
Maximum contact pressure: 0.72 MPa Contact pressure index: 15%
Predicted AR: 1.1 ml/s
Low implantation
Maximum contact pressure: 0.81 MPa Contact pressure index: 22%
Predicted AR: 19.0 ml/s
Maximum contact pressure: 1.06 MPa Contact pressure index: 35%
Predicted AR: 0.2 ml/s

**Figure 6.5:** Predicted AR and contact pressure-related parameters according to a different depth of implantation and device size. AR = aortic regurgitation.

Besides the general impact of device size and position on predicted outcomes, personalized simulations showed that optimal device size and position differ from one patient to another. In 25% of the cases, the smaller device showed to limit the contact pressure on the atrioventricular conduction system as well as postoperative AR (Fig 6.7, left panel). However, in some other cases (21%), the smaller device generated already significant contact pressure on the region of the atrioventricular conduction system, and was also associated with higher postoperative AR. Therefore, for those patients, the larger device would be the preferable choice to significantly reduce the postoperative AR while inducing comparable contact pressure on the atrioventricular conduction system (Fig 6.7, right panel).

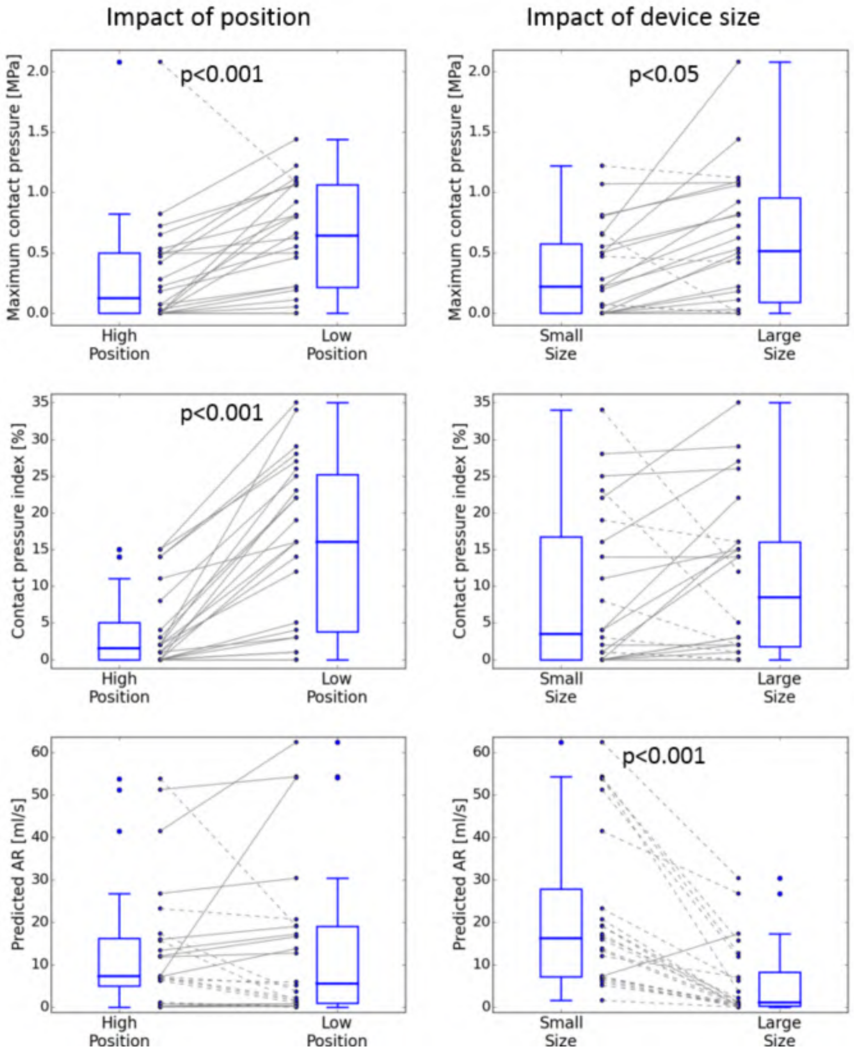

**Figure 6.6:** Predicted AR, maximum contact pressure and contact pressure index distribution in case of high/low implantation depth or large/small valve size. AR = aortic regurgitation.

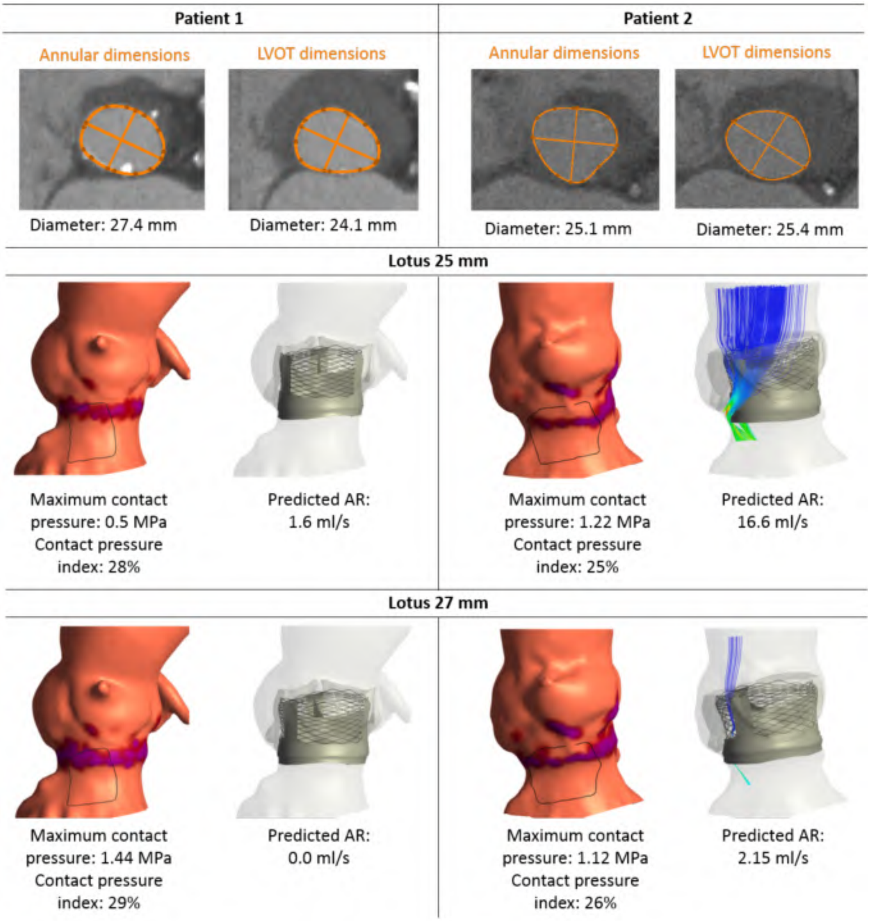
Patient 1
Patient 2
Annular dimensions
LVOT dimensions
Annular dimensions
LVOT dimensions
Diameter: 27.4 mm
Diameter: 24.1 mm
Diameter: 25.1 mm
Diameter: 25.4 mm
Lotus 25 mm
Maximum contact pressure: 0.5 MPa Contact pressure index: 28%
Predicted AR: 1.6 ml/s
Maximum contact pressure: 1.22 MPa Contact pressure index: 25%
Predicted AR: 16.6 ml/s
Lotus 27 mm
Maximum contact pressure: 1.44 MPa Contact pressure index: 29%
Predicted AR: 0.0 ml/s
Maximum contact pressure: 1.12 MPa Contact pressure index: 26%
Predicted AR: 2.15 ml/s

**Figure 6.7:** Predicted AR and contact pressure after implantation of the Lotus device (25 mm vs 27 mm). A representative example where the Lotus 25 mm (Patient 1) and Lotus 27 mm (Patient 2) represents the optimal choice. AR = aortic regurgitation.

## 6.4 DISCUSSION

This study showed that patient-specific computational modelling and simulation can accurately predict postoperative AR and conduction abnormalities in patients treated with a mechanically-expandable Lotus valve. Second, we used computational modelling and simulation to better understand the impact of device size and position in patients with equivocal aortic root dimensions. The obtained results show trends that are in line with previous clinical studies, but also reveal that optimal size and position are patient-specific.

Patient-specific computer simulation which integrates MDCT-derived patient-specific geometry and the mechanical properties of the valve accurately predicts the occurrence of AR after the implantation of a Lotus device: the selected cut-off value ensured to differentiate patients with 'none or trace' and 'mild or more' AR with good accuracy (71%). Using the same strategy, de Jaegere et al. reached an accuracy of 73% to predict the severity of AR following TAVR with a self-expandable valve ('none-to-mild' and 'moderate-to-severe') [176]. It has to be noted that the two studies adopted different dichotomization of the degree of postoperative AR.

Next to postoperative AR, we derived from the patient-specific computer simulations the contact pressure exerted by the device on the atrioventricular conduction system. In particular, we assessed the maximum contact pressure and contact pressure index parameters, which recently have been associated with new left bundle branch block or total atrioventricular block after TAVR [193]. The results of this study agreed with previous findings. The cut-off value for the maximum contact pressure that best identifies patients with new conduction abnormalities after implantation of Lotus valve (0.36 MPa) was comparable to what was found after implantation of the CoreValve System (0.39 MPa). Also, the accuracy of the prediction was comparable between the two studies (75% for the Lotus and 76% for the CoreValve). A slightly lower Lotus-related cut-off was identified for the contact pressure index (9% for the Lotus versus 14% for the CoreValve). As this parameter represents the area of contact within the selected atrioventricular conduction region, higher implantation depth of the Lotus device might explain the lower contact pressure index associated with that valve. In fact, in this study the Lotus valve was implanted on average at 4.8±1.7 mm below the annular plane, while Rocatello et al. reported the CoreValve System to be implanted at about 7.2±3.5 mm below the annular plane. The contact pressure index showed a slightly higher accuracy of prediction for new conduction abnormalities after CoreValve implantation (77% versus 71%). However, combining both maximum contact pressure and contact pressure index enhances the prediction of new conduction abnormalities after Lotus valve implantation. When both parameters are above the cut-off value, 24/26 patients (92.3%) with new conduction abnormalities were correctly identified (Fig 6.4).

Besides the verification of the model accuracy, we evaluated the influence of device size and position on the predicted outcomes in patients with equivocal aortic root dimensions. This revealed trends that are in line with previous clinical findings: selecting the larger device limits the predicted AR, while lower implantation and more aggressive device oversizing increase the contact pressure on the region of interest (and thus the risk on TAVR-induced conduction abnormalities).

Some studies have associated a high TAV position with increased rate of postoperative AR [189, 221, 223]. Using patient-specific computer simulation in a single patient, Mao et al. [189] observed that high implantation of a CoreValve device exhibits much larger regurgitant jets than lower positioning. This observation corresponds with the finding of Sherif et al. (2010) [221] who reported that a low implantation depth (about 10 mm below the aortic annulus) of a CoreValve device minimizes the AR degree. On the contrary, Bianchi et al. [188] observed that high implantation of the CoreValve (about 3mm below the annular plane) favored AR reduction in one patient. In the same study, the authors also observed that a Sapien valve implanted in high position increased regurgitation jets in two patients, suggesting that the effect of positioning on postoperative AR is device related.

Blackman et al. reported that patients with Lotus valve implanted less deep than 4.7 mm are more likely to develop postoperative AR [223]. However, this observation contrasts with our findings. In fact, among all patients enrolled in our study, no difference in implantation depth was observed between those with and without postoperative AR. Also, for patients with aortic root dimensions in the equivocal range, the device size seems to play a more relevant role, compared to the implantation depth, in preventing postoperative AR. Similarly, Bianchi et al. [188] observed that paravalvular AR is highly dependent on the patient-specific anatomy and calcification distribution more than depth of implantation.

Despite the general observation that a low implantation depth and larger TAV are associated with a higher maximum contact pressure and contact pressure index, analysis of the individual cases shows that this strongly depends on the patient-specific anatomy (i.e. location and amount of calcifications, location of the atrioventricular conduction system). We observed that in patients with a not very calcified aortic valve, the smaller TAV reached a good apposition preventing residual AR and maintaining the contact pressure on the atrioventricular conduction system low. However, bulky leaflets and subannular calcifications prevented the smaller TAV from an optimal sealing against AR. Also, in some patients, calcium nodules that accumulated mainly on the LCC or towards the commissure between the NCC and LCC, not only obstructed the good apposition of the valve, but also pushed the valve towards the opposite side (NCC/RCC), increasing the contact pressure on the atrioventricular conduction system, which is in line with previous findings [113]. In such cases, the larger TAV showed better performance: at comparable maximum contact pressure it reduced the postoperative AR. However, this was observed only in few patients, and therefore further investigation is required.

Our findings confirmed also that a deep valve implantation is generally associated with new conduction abnormalities, as reported in several clinical studies [196]. Similarly, McGee et al. observed that a deep TAV position increases the mechanical stresses on the bundle of His, under the assumption that the stress distribution in this region might contribute to new conduction abnormalities [187]. However, this observation is based on a single patient-specific model and, therefore, it cannot be assumed to represent the entire population. Furthermore, they limited the location of the bundle of His to the interleaflet triangle between the NCC and RCC. However, the atrioventricular conduction system is typically located near the inferior border of the membranous septum, which is subjected to inter-patients variability. Some patients have the membranous septum located in a high position (i.e. closer to the annular plane) [105, 193, 203]. Therefore, for those patients, a high valve implantation would not avoid the TAV to exert pressure on the atrioventricular conduction system, resulting in a quite high predicted contact pressure and a relatively extended region of contact (Fig 6.5). Therefore, a high TAV implantation seems not always advisable.

Another aspect that may influence device positioning is the coronary height and the sinotubular junction size. In a number of patients, the simulated high implantation showed that the deployed braid was adjacent to the coronary ostia and might therefore limit the access to the coronary for future percutaneous coronary intervention (see Fig 6.8). In such cases, very high valve implantation should probably be avoided.

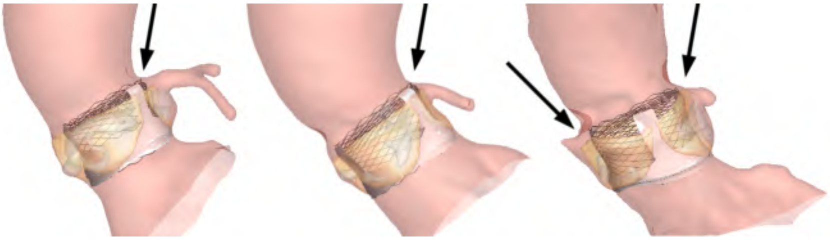

**Figure 6.8:** Three representative patients where a high valve position might lead to coronary obstruction or might obstruct the access to the coronary for future percutaneous coronary intervention.

These findings indicate that, despite certain general trends, optimal TAV size selection and positioning in patients with equivocal annulus dimension is complex. However, the selection of the valve size that best fits the individual patient, and its optimal position, is mandatory to ensure maximum safety and efficacy. Personalized computer simulation that can accurately predict post-TAVR AR and conduction abnormalities may offer additional support during decision making.

### Study limitations

The number of patients included in this study was not based on a power analysis, but on the amount of data received from the participating hospitals.

Also, the impact of device size and position on predicted AR and contact pressure in patients with equivocal aortic root dimensions was investigated in a limited cohort of patients. In future, a large sample size should be studied to confirm our findings.

Elastic material properties were used to model the aortic tissue. Although the hyperelastic model may better reflect the actual tissue mechanical behavior, previous studies have reported that the accuracy of the predicted frame deformation using a simple linear elastic material or a more complex hyperelastic material is comparable. Therefore, linearization of the material property seems viable [167, 182]. Similarly, there are many other modeling simplifications and assumptions and it is challenging to assess the impact of the modeling results for all simplifications and assumptions. However, based on the amount of validation that is available we believe that those are justified [175, 176, 193].

In this study, the contact pressure on the atrioventricular conduction system was evaluated after full device deployment. However, an analysis over the entire positioning and deployment phase might offer a more complete understanding in the mechanisms of the development of new conduction abnormalities, as high contact pressure might occur peri-procedurally.

Same boundary conditions were adopted to predict paravalvular AR in each patient although the postoperative end-diastolic pressure varies from patient to patient. However, a population averaged value needs to be employed when the aim is to develop a predictive model.

Finally, as we were interested in the paravalvular AR, only the diastolic phase was simulated and the valve was assumed to be fully closed (i.e. full leaflet coaptation). Therefore, the central regurgitation was not considered in this study.

## 6.5 CONCLUSIONS

Patient-specific computer simulations can accurately predict AR, maximum contact pressure and contact pressure index after implantation of the mechanically-expandable Lotus valve. Also, they offer insight on patients with equivocal aortic root dimensions and provide additional information related to optimal TAV size and position.

# CHAPTER 7

# OPTIMIZATION OF A TRANSCATHETER AORTIC VALVE FRAME USING PATIENT-SPECIFIC COMPUTER SIMULATIONS

In this chapter we will describe a new framework to optimize the design of a transcatheter aortic valve through patient-specific finite element and fluid dynamics simulation. The framework combines design of experiment (DOE) techniques and optimization algorithms available in Isight (Dassault Systemes Simulia Corp, Johnson, RI) to find the best combination of the frame geometrical parameters to minimize postoperative complications predicted with TAVIguide.

## 7.1 INTRODUCTION

To date, the design and development phase of new cardiovascular devices is mainly based on benchmark tests and animal experiments, leading to long iterative development cycles. However, in the end, it still remains unclear how the final device will perform in diseased human anatomies, resulting in significant risks for the first patients that undergo treatment with a new device, as well as for the manufacturers of these devices. Using patient-specific computational modelling and simulation during the design and development phase could help to address these challenges [224]. This approach allows to assess the interaction between devices and realistic human anatomies, opening the door towards *in-silico* clinical trials that could be conducted prior to the actual first-in-human clinical study. In this way, risks for patients and manufacturers can be significantly reduced. In addition, combining patient-specific computational modelling and simulation with device optimization techniques can help to develop better devices in a shorter time period.

Many computational modelling and simulation optimization studies have been performed to find optimal stent geometrical parameters based on mechanical or flow-related objectives: radial strength [225, 226], fatigue resistance [227–229], frame expansion [228, 229], flow disturbances and wall shear stress [230–232]. However, the majority of those studies evaluated solely unit stent models [227], thereby neglecting the interactions with the arterial tissues. Others have used three-dimensional models [230, 233, 234] and accounted for interactions with simplified vessel geometries [228, 232]. Very recently Bosi et al. [186] combined patient-specific modeling and optimization techniques to tune the material parameter of the aortic root in 14 patients, to improve simulation results (i.e. prediction of post-implantation device deformation and paravalvular gaps).

To the best of our knowledge, a device optimization study based on patient-specific modelling has not yet been performed. Such approach could be useful for a wide range of procedures and devices, but this study focuses on TAVR.

Clinical studies [3, 4, 64] have demonstrated the efficacy of TAVR to treat patients with aortic stenosis at extreme- and intermediate-risk. However, complications as paravalvular AR and conduction abnormalities are considered the Achille's heel of this treatment. AR has been associated with increased mortality [6, 8, 235], whereas conduction abnormalities leading to implantation of permanent pacemaker are associated with increased costs, longer hospital stays and increased patient's morbidity. Considering the prospective of treating younger patients at low surgical risk, those complications are inacceptable and need to be addressed by improved devices and procedures.

To be effective and prevent migration, TAVR devices need to anchor at or below the annulus of the aortic root. Furthermore, a good apposition between the device and the aortic wall plays a key role in avoiding paravalvular AR. On the other hand, the contact between the stent and the aortic root might generate high pressure on the atrioventricular conduction system which, in turn, might be responsible of conduction abnormalities.

Previous studies have reported that patient-specific computer simulation can be used to predict paravalvular AR and conduction abnormalities after implantation of a CoreValve Revalving System (Medtronic) [176, 179, 188, 189, 193].

In this proof-of-concept study, we propose a framework to improve geometric parameters of a representative TAVR device frame through patient-specific computer models able to predict post-operative outcomes.

## 7.2 MATERIAL AND METHODS

### Valve geometry and material properties

A parametric model of a 29-mm CoreValve-like transcatheter aortic valve was created. The base geometry of the frame was modeled starting from the planar 'unwrapped' configuration in pyFormex (`www.nongnu.org/pyformex`). The 'unwrapped' frame design can be seen as a repetition of 15 diamond-like cells along the circumferential axis and 4 diamond-like cells along the longitudinal axis (Fig 7.1a). Each cell was described with Cubic Bezier spline interpolation [236]. The profile of the frame of a CoreValve 29 mm was derived from pictures available online and interpolated using a cubic Bezier Spline function (Fig 7.1b). This function was then used to generate an offset of the 'planar' frame (i.e. varying radius) (Fig 7.1c). Finally, the planar frame was 'wrapped' to obtain a CoreValve-like shape, in the expanded configuration (Fig 7.1d), by converting the nodal coordinates from a Cartesian coordinate system to a cylindrical coordinate system. Geometric parameters of the reference frame design are summarized in Table 7.1. Briefly, the frame's height was 46.0 mm, the diameter at the ventricular inflow was 29.0 mm and the diameter at the aortic outflow was 38.0 mm. The strut width and thickness (0.25 mm, 0.45 mm) were in line with literature [170, 179]. The frame was modeled with Timoshenko beam elements (B31 in the Abaqus nomenclature) and WELD connectors were used at the interpolation points between adjacent cells (Fig 7.1e). A mesh sensitivity analysis was performed on the device radial force during the crimping and expansion phases. The final stent mesh counted 2670 elements. The material properties of the Nitinol alloy were taken from literature [174] (Table 7.2).

### 7.2.1 Patient-specific aortic root model

Three-dimensional aortic root models were retrospectively reconstructed from anonymized pre-operative MDCT images of 12 patients, who underwent TAVR in two European centers (Rigshospitalet in Copenhagen, Denmark; Erasmus medical Center in Rotterdam, The Netherlands). Selected patients (3 males, 9 females), between 74 and 89 years old, were considered representative of the TAVR population (e.g. patients with calcified tricuspid or bicuspid aortic valve, heavy calcified valve or sub-annular calcifications). All patients

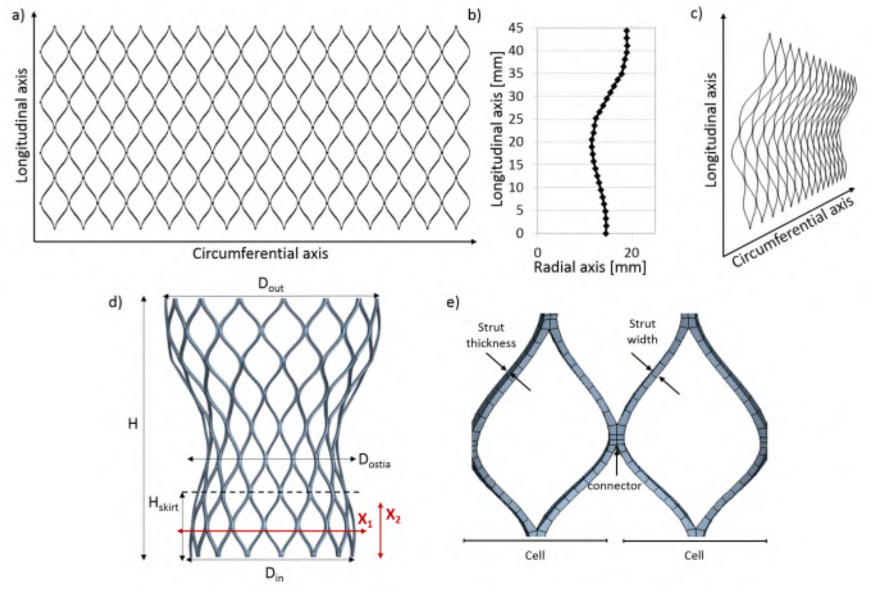
a)
Longitudinal axis
Circumferential axis
b)
Longitudinal axis [mm]
45
40
35
30
25
20
15
10
5
0
0
20
Radial axis [mm]
c)
Longitudinal axis
Circumferential axis
d)
$D_{out}$
H
$D_{ostia}$
$H_{skirt}$
$X_1$
$X_2$
$D_{in}$
e)
Strut thickness
Strut width
connector
Cell
Cell

**Figure 7.1:** Valve geometry. a) unwrapped configuration; b) profile of the frame of a CoreValve 29 mm derived from online pictures; c) unwrapped configuration with offset; d) expanded valve configuration e) detail of the valve strut. In red the geometrical frame parameters under investigation: $X_1$ is the diameter at 4 mm above the ventricular inflow, $X_2$ is the height of the first row of cells.

**Table 7.1:** Frame reference adopted geometrical parameters.

| Parameter | Description | Value |
|---|---|---|
| H | Height | 46.0 mm |
| $D_{in}$ | Diameter at ventricular inflow | 29.0 mm |
| $D_{out}$ | Diameter at aortic outflow | 38.0 mm |
| $D_{ostia}$ | Diameter at ostia level | 23.0 mm |
| $w_{st}$ | Strut width | 0.25 mm |
| $th_{st}$ | Strut thickness | 0.45 mm |
| $H_{skirt}$ | Skirt height | 13.0 mm |

had comparable annular diameters ranging from 23.0 mm to 26.0 mm. More details of the selected patients are reported in Table 7.3. Three-dimensional aortic root models consisted of the LVOT, the sinotubular junction and calcified aortic leaflets and ascending aorta (Fig 7.2a). Linear elastic models rather than a more realistic but complex hyperelastic anisotropic description were adopted to describe the aortic root tissues. Modelling parameters were derived in a previous study [175] with an iterative process of back-calculations using pre and postoperative MDCT of 39 patients. The aortic wall had an

**Table 7.2:** Nitinol material parameters for modeling the frame behavior [174].

| Parameter | Description | Value |
|---|---|---|
| $E^A$ | Austenite elastic modulus | 51.7 MPa |
| $E^M$ | Martensite elastic modulus | 47.8 MPa |
| $\nu$ | Poisson's ratio | 0.3 |
| $\sigma_L^S$ | Start of transformation loading | 600 MPa |
| $\sigma_L^E$ | End of transformation loading | 670 MPa |
| $\sigma_U^S$ | Start of transformation unloading | 288 MPa |
| $\sigma_U^E$ | End of transformation unloading | 254 MPa |
| $\varepsilon^L$ | Maximum transformation strain | 6.3% |
| $\varepsilon_V^L$ | Maximum volumetric transformation strain | 6.3% |

elastic modulus of 2MPa and a uniform thickness of 2 mm. For the aortic leaflets, elastic modulus of 0.6 MPa and uniform thickness of 1.5 mm was adopted [172, 182]. Calcifications were modeled using a stiffer elastic material with perfect plasticity (E = 4 MPa, $\nu = 0.3$, Yield stress = 0.6 MPa) [175, 193]. Spring elements were added at each node of the aortic wall to incorporate the impact of surrounding structures in the model.

In each 3D aortic root model, the region of the atrioventricular conduction system was identified as previously described [193]. Briefly, the inferior border of the membranous septum was identified in the pre-operative MDCT images through three dedicated landmarks (Fig 7.2a). Two of these landmarks were selected at the beginning and at the end of the inferior border of the membranous septum, namely $p_1$ and $p_3$, with $p_1$ closer to the NCC and $p_3$ closer to the RCC. An additional point ($p_2$) was selected in between to better track the course of the inferior border of the membranous septum as this is often not a straight line. Starting from these anatomical landmarks, the region of the atrioventricular conduction system was defined by the area between the inferior border of the membranous septum (extended towards the RCC by a $25^o$ angle) and the plane 15 mm below the annulus (Fig 7.2a).

### 7.2.2 Computer simulation strategy and output variables

Finite-element (FE) simulations were performed using Abaqus/Explicit (v2017, Dassault Systemes Simulia Corp, Johnson, RI). The computer simulation strategy can be subdivided in three steps. In the first step, the device was crimped into the catheter (6 mm diameter), using a cylindrical surface. In the second step, the device was positioned coaxially within the aortic root (Fig 7.2b), and the catheter was retracted leading to the expansion of the device. The default general contact with finite sliding between all the surfaces was used, assuming a coefficient of friction of 0.7 between the valve frame and

**Table 7.3:** Patients selected for the study. The 'received device' column refers to the device that was implanted in each patient during TAVR. The last two columns report clinical outcomes in form of paravalvular AR and conduction abnormalities. '-' indicates that no conduction abnormalities occurred after TAVR.

| Patient | Age at TAVR | Gender | Received device (size) | Post-TAVR Paravalvular AR | Post-TAVR Conduction abnormalities |
|---|---|---|---|---|---|
| 1 | 79 | M | Evolut R (29) | Mild | - |
| 2 | 89 | F | Evolut R (29) | Mild | - |
| 3 | 76 | M | Evolut R (29) | Trace | - |
| 4 | 86 | F | Evolut R (29) | Mild | - |
| 5 | 78 | M | Evolut R (29) | Mild to moderate | - |
| 6 | 77 | F | CoreValve (29) | Mild to moderate | - |
| 7 | 88 | F | CoreValve (29) | Mild to moderate | Total AVB |
| 8 | 77 | F | CoreValve (29) | Trace | LBBB |
| 9 | 80 | F | CoreValve (29) | Mild | LBBB |
| 10 | 84 | F | CoreValve (29) | Trace | LBBB |
| 11 | 74 | F | Lotus (25) | None | - |
| 12 | - | F | Lotus (23) | None | - |

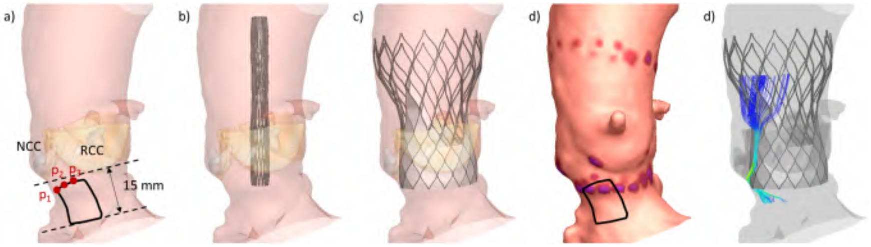

**Figure 7.2:** Computer simulation strategy. a) Patient-specific 3D reconstruction of the aortic root and the region of the atrioventricular conduction system (in red the 3 anatomical landmarks identified using pre-operative MDCT images); b) positioning of the crimped device within the aortic root; c) deployment of the device using FEA computer simulation; d) extraction of contact pressure output within the region of the atrioventricular conduction system; e) CFD simulation and predicted regurgitant jets.

the aortic model. In all patients, the device was implanted at approximately 4 mm below the aortic annulus (Fig 7.2c). In order to evaluate the risk of occurrence of new conduction abnormalities, the maximum contact pressure and the contact pressure index (i.e. the percentage of this region of interest subjected to contact pressure) within the region of the atrioventricular conduction system were extracted (Fig 7.2d). The contact pressure index was calculated according to the following formula:

$$\frac{Area_{ROI(whereCP>0)}}{Area_{ROI}}100 \tag{7.1}$$

In equation 7.1 ROI is the region of the atrioventricular conduction system and CP is the contact pressure.

As third step, a static computational fluid-dynamics (CFD) simulation was performed using the ico-FOAM solver available in OpenFOAM (OpenFOAM, v2.1.1, OpenCFD Ltd., Bracknell, UK). Ico-FOAM is a transient solver for laminar flow. Briefly, the deformed geometries (aortic root and device) were extracted from the FE analysis and a skirt was added to the TAVR device. The fluid domain was extended with cylindrical flow extensions of 8 diameters at the inlet (aortic side) and 3 diameters at the outlet (ventricular side). The extended flow domain was discretized using hexahedral elements and refined within the region of interest (i.e. the lumen within the rigid aortic root wall). The blood was modeled as Newtonian fluid ($\rho$ = 1060 $kg/m^3$, $\mu$ = 3.5 $10^{-3}$ Pa s). No slip condition was described at the aortic wall. A fixed transaortic pressure difference of 32 mmHg was imposed to calculate the inlet flow and the location and the velocity of regurgitant jets (Fig 7.2e). The imposed pressure difference value is the average of the post-operative end-diastolic transaortic pressure difference retrospectively observed in a sample of 20 patients [176]. This value is in line with the post-operative end-diastolic transaortic pressure difference observed by Sinning et al. in a cohort of 146 patients (33.8±12.3 mmHg) [149]. This analysis was previously validated for prediction of paravalvular AR after implantation of a CoreValve System [176].

### 7.2.3 Experimental design

The central composite design (CCD) was applied to determine the best combination of the frame parameters to reduce conduction abnormalities and paravalvular AR after TAVR. To this regard, the inflow portion of the CoreValve frame has a large diameter and provides high radial force to ensure anchoring and apposition to the aortic root, favouring a good sealing against paravalvular AR. On the other hand, high radial force can have a negative effect on the conduction system and generate conduction abnormalities. Further details on the rationale behind the design of the CoreValve System can be found in Appendix B. Given the fact that both diameter and cell dimensions contributes to the radial strength of the frame, we decided to optimize those two geometrical parameters at the inflow portion of the frame: the valve diameter at 4 mm above the ventricular inflow ($X_1$, mm) and the height of the first row of cells at the ventricular inflow ($X_2$, mm) (Fig 7.1b). Initial value for $X_1$ is 29.0 mm and for $X_2$ is 8.0 mm. The initial design space was limited by X1±10% and X2±20%. The parameter levels are coded as -$\lambda$, -1, 0 (central point), +1 and +$\lambda$, with $\alpha$ equals to $\sqrt{2}$. Independent variables and their levels for the CCD used in the initial design space are shown in Table 7.4. The designs of the frame obtained with the different combination of the geometrical parameters ($X_1$ and $X_2$) based on the initial design space are shown in Fig 7.3.

**Table 7.4:** Tested levels of experimental variables $X_1$ and $X_2$ in the initial design space.

| **Parameter** | | **Initial coded levels of variables** | | | | |
|---|---|---|---|---|---|---|
| | | -$\lambda$ | -1 | 0 | +1 | +$\lambda$ |
| Valve diameter at 4 mm above the ventricular inflow (mm) | $X_1$ | 24.9 | 26.1 | 29.0 | 31.9 | 33.1 |
| Height of the first row of cells at the ventricular inflow (mm) | $X_2$ | 5.7 | 6.4 | 8.0 | 9.6 | 10.3 |

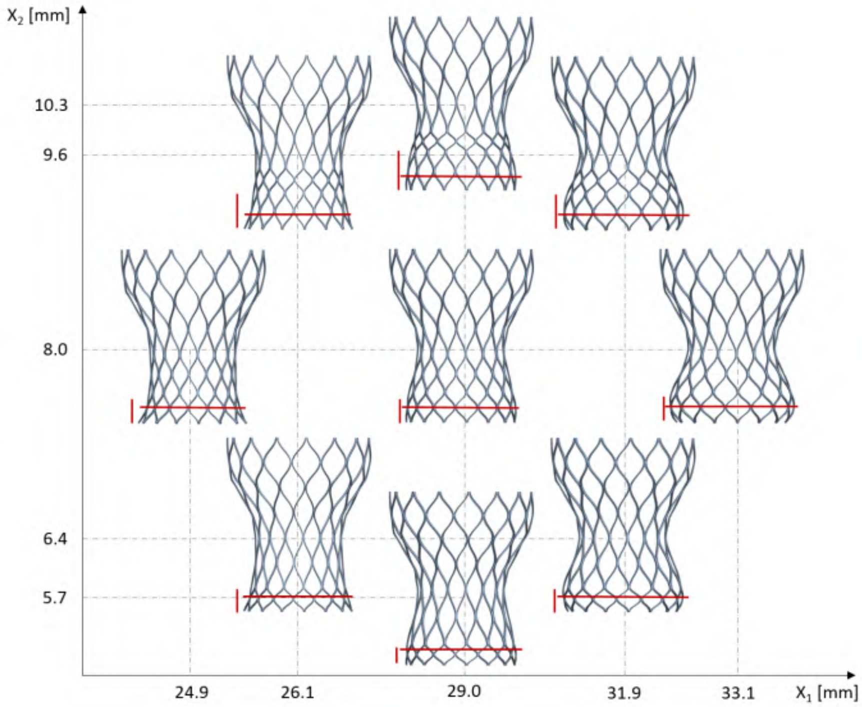

**Figure 7.3:** Frame designs obtained with the experimental variables $X_1$ and $X_2$ from the initial design space. Geometrical parameters X1 and X2 are represented in red.

A qualitative analysis of the effects of the two parameters on the outputs showed that high $X_1$ and $X_2$ parameters were associated with low values of the outputs (Fig 7.4). Therefore, subsequent refinement of the design space was performed in that region. This refined design space was used during the entire study. Independent variables and their levels for the CCD used in the refined design space are shown in Table 7.5.

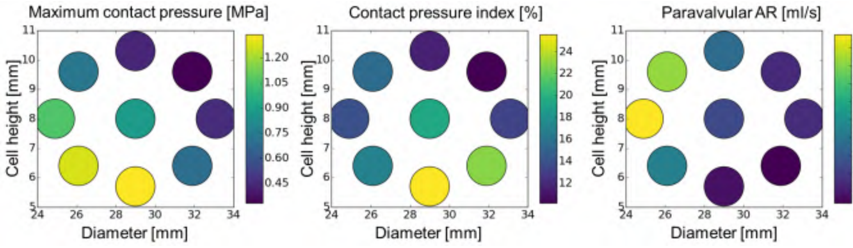

**Figure 7.4:** Experimental value of maximum contact pressure, contact pressure index and paravalvular AR at the CCD design data points.

**Table 7.5:** Tested levels of experimental variables $X_1$ and $X_2$in the refined design space.

| **Parameter** | | **Initial coded levels of variables** | | | | |
|---|---|---|---|---|---|---|
| | | $-\lambda$ | -1 | 0 | +1 | $+\lambda$ |
| Valve diameter at 4 mm above the ventricular inflow (mm) | $X_1$ | 28.4 | 29.0 | 30.5 | 31.9 | 32.5 |
| Height of the first row of cells at the ventricular inflow (mm) | $X_2$ | 7.7 | 8.0 | 8.8 | 9.6 | 9.9 |

### 7.2.4 Response surface methodology

A second-order polynomial response surface model (RSM) was used to fit the predicted outputs that are the maximum contact pressure and the contact pressure index (FE outputs) and the paravalvular AR (CFD output). As the study aim was to minimize the outputs predicted from the implantation of each device in all patients, their value averaged over all patients was considered. The fitting was based on the minimization of the residual error measured by sum of squared deviations between the actual and the estimated response. The second-order polynomial equation has been assumed as:

$$Y = B_0 + \sum_{i=1}^{2} B_i X_i + \sum_{i=1}^{2} B_{ii} X_i^2 + \sum_{i<j}^{2} B_{ij} X_i X_j \pm \varepsilon_r \tag{7.2}$$

with $Y$ the value of one output parameter averaged over the 12 patients, B the coefficients, $X$ the experimental variables and $\varepsilon_r$ the error associated with the model. Only the most significant terms from the polynomial equation were selected using the Exhaustive Search method. The quality of the model was assessed by coefficients of determination: $R^2$, *adjusted* $R^2$, *predicted* $R^2$, and residuals. $R^2$ represents a pure correlation between measured and predicted values and is indicative of the response variation explained by the model. *Adjusted* $R^2$ is used to compare the explanatory power of the model, and its value increases only if an added term improves the model. The *predicted* $R^2$ assesses the predictive power of the model for new observations. This coefficient was calculated by systematically removing each observation from the data set, estimating the regression equation and determining how well the model predicted the removed observation [237]. Residual plots present the difference between the actual and the predicted values and were used to assess whether the coefficients predictions were biased. All analyses were performed in Isight (Dassault Systemes Simulia Corp, Johnson, RI).

### 7.2.5 Optimization strategy

The Nonlinear Programming by Quadratic Lagrangian (NLPQL) was adopted as optimization algorithm, under the assumption that the objective functions are continuously differentiable [238]. The three objective functions were rescaled to have a value between 0 and 1 (eq. 7.3) and combined into a single-objective function using a weighted sum method (eq. 7.4 ):

$$y_i = \frac{x_i}{max(x)} \tag{7.3}$$

$$\sum_{i=1}^{3} w_i O_i(X_1, X_2) \tag{7.4}$$

In equation (7.3) $x_i$ is a value of one output and $y_i$ is the corresponding rescaled value. In equation (7.4), $w_i$ is the weight of each objective and $O_i$ are the objectives (RSM functions). In this study, the single-objective function built to minimize the maximum contact pressure ($O_1$), the contact pressure index ($O_2$) and the paravalvular AR ($O_3$) was:

$$0.5 O_1(X_1, X_2) + 0.5 O_2(X_1, X_2) + 1.0 O_3(X_1, X_2) \tag{7.5}$$

The weight factors accounted for the fact that maximum contact pressure ($O_1$) and contact pressure index ($O_2$) are both predictors of new conduction abnormalities. Lastly, the performance of the device with the optimal parameters was compared with the performance of the initial device in each patient. The one-tailed Wilcoxon rank test in SPSS (version 22.0, IBM Corporation, New York) was performed to verify whether the improvement in the predicted outcomes was statistically significant. The predicted maximum contact pressure, contact pressure index and paravalvular AR are reported as mean (standard deviation).

Fig 7.5 summarizes the workflow of the method used in this study.

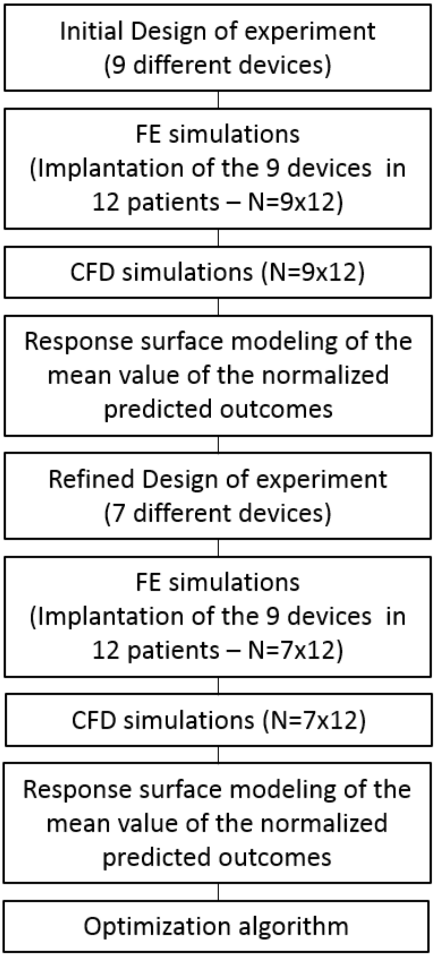
Initial Design of experiment (9 different devices)
FE simulations (Implantation of the 9 devices in 12 patients – N=9x12)
CFD simulations (N=9x12)
Response surface modeling of the mean value of the normalized predicted outcomes
Refined Design of experiment (7 different devices)
FE simulations (Implantation of the 9 devices in 12 patients – N=7x12)
CFD simulations (N=7x12)
Response surface modeling of the mean value of the normalized predicted outcomes
Optimization algorithm

**Figure 7.5:** Pipeline that has been followed in this study.

## 7.3 RESULTS

In total, 16 devices were created in this study: 9 devices based on the initial design space and 7 additional ones based on the refined design space. Of note, to limit the number of simulations, 2 configurations from the initial design space were included in the refined design space. Each device was implanted in 12 patients (FE simulation) and, subsequently, a CFD simulation was performed for each patient to derive the paravalvular AR (Fig 7.5). Therefore, this study counted 192 FE simulations and same amount of CFD simulations.

Average time for FE simulation was 53 minutes on a cluster with 16 computing cores (@ 4.0 GHz and 63.0 GB RAM for each node). All CFD simulations were performed on 2 cores (@ 3.2 GHz and 15.2 GB RAM for each node). Average time was 3 hours and 50 minutes.

### 7.3.1 Mesh sensitivity analysis of the device model

A selection of 8 different mesh sizes was used to perform mesh sensitivity analysis on the device radial force during the crimping and expansion phases. Because of small differences observed in the expanded and crimped device configurations after 3 cycles (crimping-expansion-crimping), only cycle 1 was used for the analysis. The radial force analysis was limited to the functional range of diameters (20.5 - 28.5 mm). Results from cycle 1 are shown in Fig 7.6. The radial force obtained with each mesh was extracted and the mean relative difference with respect to the finest mesh (Mesh_8, considered as 'the gold standard') calculated. Results are reported in Table 7.6. Slightly higher radial force was obtained with the coarsest mesh (Mesh_1, mean relative difference >5%). Small differences were observed among all the other meshes. Therefore, Mesh_2 was chosen for the device model.

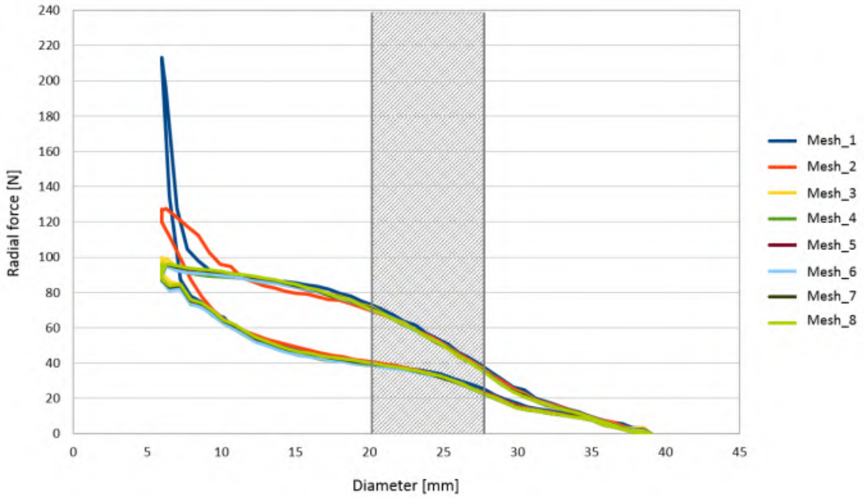

**Figure 7.6:** Radial force curves of one cycle (crimping-expansion) obtained with different mesh sizes. Mesh_1 is the coarsest mesh, Mesh_8 is the finest mesh. Functional diameters range within the grey area.

**Table 7.6:** Mesh sensitivity analysis of the device model. The selected mesh is highlighted in bold.

| **Mesh** | **Mesh_1** | **Mesh_2** | **Mesh_3** | **Mesh_4** | **Mesh_5** | **Mesh_6** | **Mesh_7** | **Mesh_8** |
|---|---|---|---|---|---|---|---|---|
| N elements | 1470 | 2670 | 3870 | 4590 | 5070 | 5550 | 6270 | 6990 |
| Mean relative differences in radial force (%) | 5.7% | 1.3% | 0.2% | 0.8% | 0.5% | 1.1% | 0.3% | - |

### 7.3.2 Goodness of fit

The CCD was used to provide good fitting with a second-order polynomial function. RSM polynomial models for maximum contact pressure ($O_1$), contact pressure index ($O_2$) and paravalvular AR ($O_3$) are respectively:

$$O_1 = 3.57 - 0.08X_1 - 0.01X_2^2$$
$$O_2 = 70.38 - 3.92X_2 - 0.02X_1^2$$
$$O_3 = 0.23 + 4.15X_2 - 0.11X_1X_2$$

The coefficient of determination $R^2$, *adjusted* $R^2$ and *predicted* $R^2$ of the models are reported in Table 7.7.

**Table 7.7:** Quality of the RSM models.

| **RSM models** | $R^2$ | ***Adjusted*** $R^2$ | ***Predicted*** $R^2$ |
|---|---|---|---|
| $O_1$ | 0.92 | 0.89 | 0.81 |
| $O_2$ | 0.94 | 0.93 | 0.86 |
| $O_3$ | 0.89 | 0.86 | 0.74 |

The coefficient of determination $R^2$ for all models was higher than 0.89, which indicates a good approximation of the actual function at the design points used for its construction (Fig 7.7a). The *predicted* $R^2$ [0.74-0.86] was in reasonable agreement with the *adjusted* $R^2$ [0.86-0.93], indicating good predictive power of the model. Residual plots (Fig 7.7b) indicated that the coefficients prediction was not biased.

The models have high $R^2$, *adjusted* $R^2$, *predicted* $R^2$ and random distribution of residual errors. These results indicate a good fit of the experimental data and high precision in predicting maximum contact pressure, contact pressure index and paravalvular AR. Therefore, the polynomial models were used for further analysis.

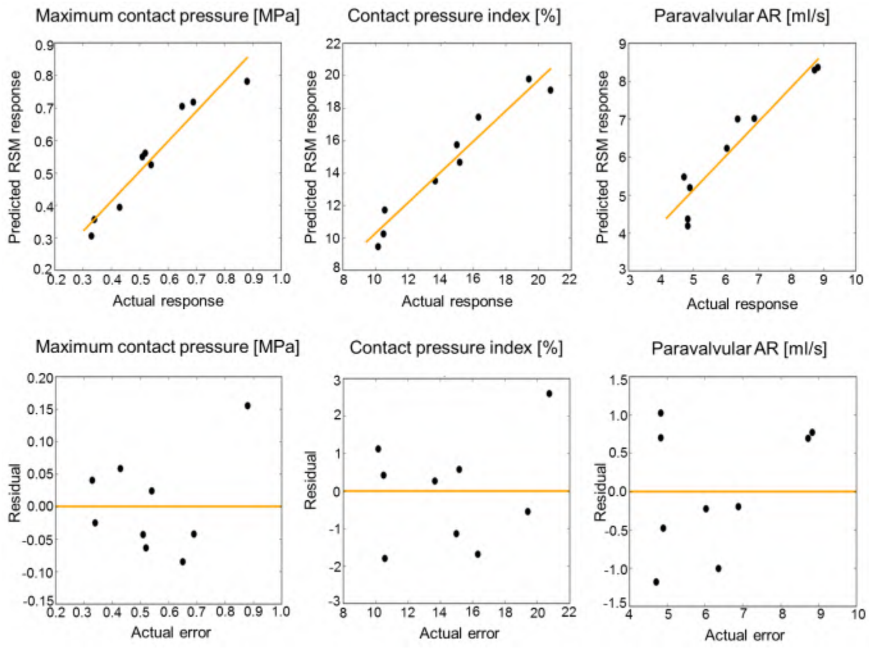

**Figure 7.7:** a) Plot of the actual and predicted responses and b) of the actual and residual errors at each design point (black dots). Residuals are defined as the difference between the actual and the predicted responses.

### 7.3.3 Effects of the geometrical parameters

Two-dimensional contour plots of the RSM models are shown in Fig 7.8. High values of maximum contact pressure were observed for low $X_1$ and $X_2$. The diameter at the ventricular inflow of the device ($X_1$) influences its profile. Small diameters determine a sharp profile of the frame, while large diameters make the profile rounder (Fig 7.9a). Therefore, small diameters are associated with local spots of contact with high maximum contact pressure. In addition, short cells ($X_2$) at the ventricular inflow of the frame increase the radial force, contributing to high maximum contact pressure on the aortic wall at the region of the ventricular inflow of the device.

The RSM model of the contact pressure index showed a comparable behavior as for the maximum contact pressure. High values of contact pressure index were observed for low $X_1$ and $X_2$. The diameter ($X_1$) and, therefore, the profile of the frame, strongly influences the level at which the device anchors to the aortic annular region. Large diameters (round profile) favor a higher anchoring level compared to small diameters (sharp profile). As the contact pressure index is a measure of the area of contact between the device and the aortic wall within the region of the atrioventricular conduction system, large diameters (high anchoring level) reduce the area of contact and are

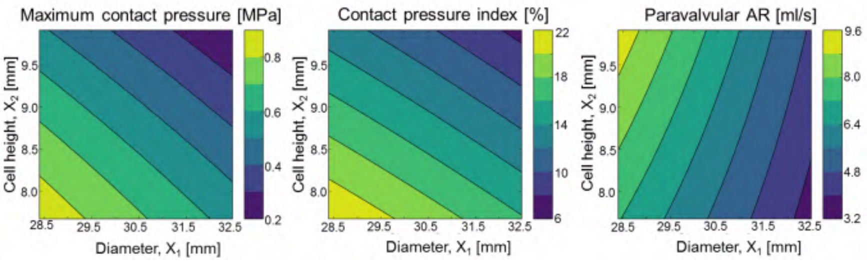

**Figure 7.8:** Contour plot of the response surface models of the maximum contact pressure, contact pressure index and paravalvular AR, respectively from the left to the right.

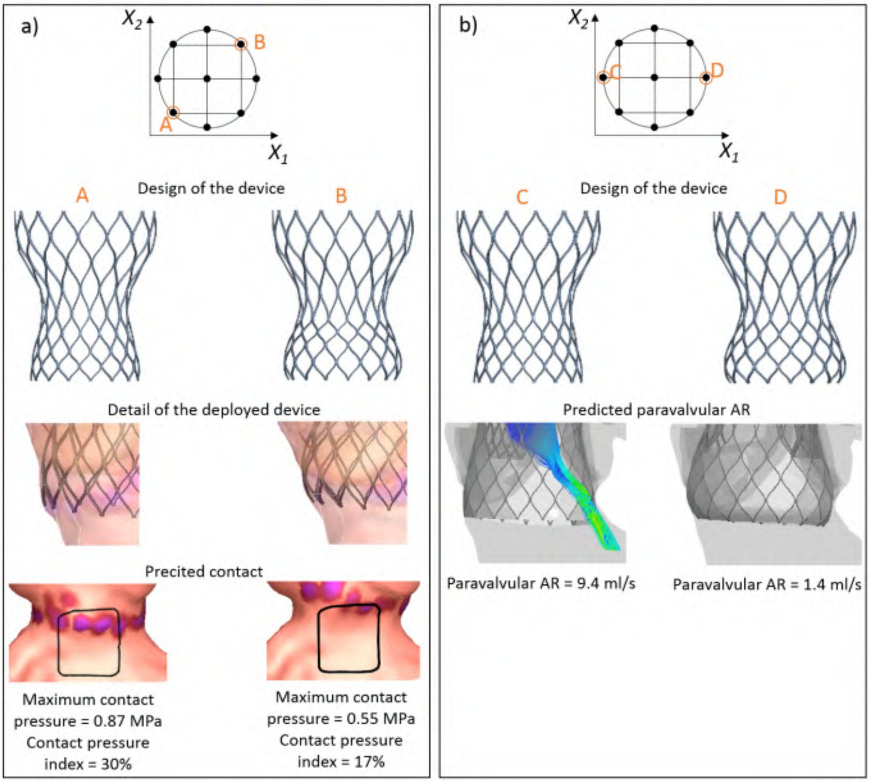
a)
X₂
X₁
A
B
Design of the device
Detail of the deployed device
Precited contact
Maximum contact pressure = 0.87 MPa Contact pressure index = 30%
Maximum contact pressure = 0.55 MPa Contact pressure index = 17%
b)
C
D
Predicted paravalvular AR
Paravalvular AR = 9.4 ml/s
Paravalvular AR = 1.4 ml/s

**Figure 7.9:** Representative examples of the effect of the geometrical parameters on maximum contact pressure and contact pressure index (a), and paravalvular AR (b). At the top, a schematic representation of the CCD. a) A device with low $X_1$ and low $X_2$ (A) results in high maximum contact pressure and contact pressure index. Whereas, a device with high $X_1$ and $X_2$ (B) results in low contact within the region of the atrioventricular conduction system. b) A device with low $X_1$ (C) results in high paravalvular AR, whereas high $X_1$ (D) prevents paravalvular AR.

associated with low values of contact pressure index. On the contrary, the devices with small diameter (sharp profile) often anchor at the level of the atrioventricular conduction system, resulting in high contact pressure index value (Fig 7.9a). Also, short cells ($X_2$), associated with higher radial force, favor the expansion of the frame, contributing to an increase in contact and, hence, the contact pressure index.

With respect to the paravalvular AR, large diameters ($X_1$) and short cells ($X_2$) favor a better apposition of the device to the aortic root, reducing paravalvular AR (Fig 7.9b). However, the diameter seems to have a larger influence on the output compared to the height of the cells.

### 7.3.4 Optimization results

Fig 7.10 reports the optimization history with NLPQL algorithm for the three objectives $O_1$, $O_2$, $O_3$. The orange line indicates the position where the minimum is located (Run 13). The starting point corresponds to the initial design parameters: $X_1 = 29.0$ mm and $X_2 = 8.0$ mm. The optimal parameters are: $X_1 = 31.9$ mm and $X_2 = 9.6$ mm. The optimized device is shown in Fig 7.11.

Fig 7.12 reports the maximum contact pressure, contact pressure index and paravalvular AR obtained in each patient after implantation of the device with the initial and the optimized design.

The optimized device was associated with lower maximum contact pressure and contact pressure index in all patients. The mean value of maximum contact pressure associated with the optimized device was almost 3-fold lower compared to the initial device (0.33 vs 0.88 MPa). Similarly, the mean value of contact pressure index was 2-fold lower (10% vs 19%). The standard deviation slightly decreased as well with the optimized device. With regard to paravalvular AR, the average value decreased from 6.9 ml/s to 4.9 ml/s with the optimized device. However, in some patients paravalvular AR slightly increased with the optimized device. Nevertheless, the Wilcoxon rank test confirmed that improvement in maximum contact pressure, contact pressure index as well as paravalvular AR is statistically significant (p value was found $\leq 0.001$ and $\leq 0.05$ for the contact pressure-related parameters and for AR respectively).

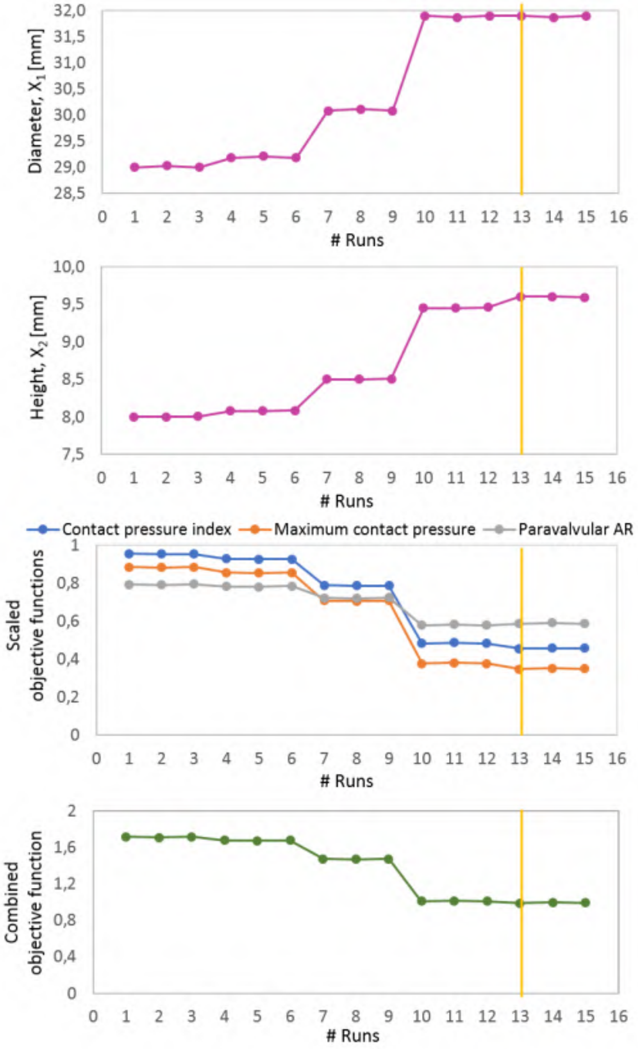

**Figure 7.10:** Optimization history of the objectives-function. The location of the minimum is indicated by the orange line.

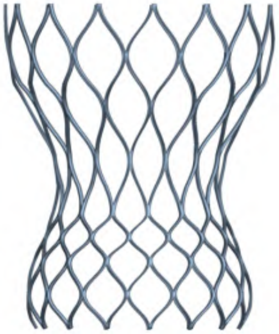

**Figure 7.11:** Optimal frame design.

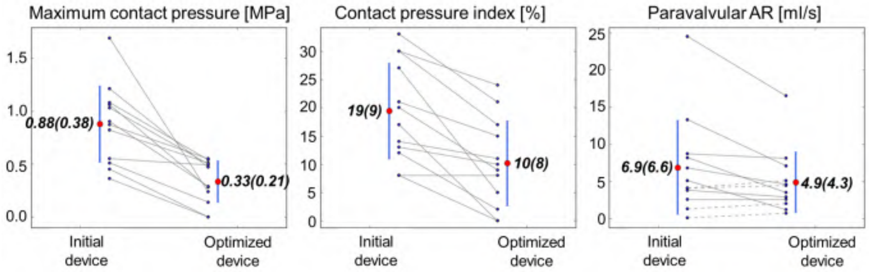

**Figure 7.12:** Comparison of performance between the optimized and initial designs. Continuous grey lines represent a decrease in maximum contact pressure, contact pressure index or paravalvular AR in the same patient. Dotted grey lines represent an increase in maximum contact pressure, contact pressure index or paravalvular AR in the same patient. Mean (standard deviation) are represented by the red dot and the blue bar respectively.

## 7.4 DISCUSSION

This proof-of-concept study presents an optimization workflow based on patient-specific computer simulation to improve the TAVR device performance in reducing paravalvular AR and conduction abnormalities after TAVR. The central composite design along with the NLPQL algorithm were adopted to optimize two geometrical parameters of a CoreValve-like device: the diameter at 4 mm above the ventricular inflow and the height of the first row of cells. The effect of the design parameters on the objectives was studied using RSM. Results suggest that large diameters and high height of the first row of cells favor a better apposition of the device to the aortic wall avoiding paravalvular AR, and lead to an anchoring level above the location of the atrioventricular conduction system preventing conduction abnormalities. The optimized device showed improved performance in all patients. Maximum contact pressure and contact pressure index that are predictive for conduction abnormalities lowered with the optimized device. Paravalvular AR was also reduced in 83% of the patients (10/12). Furthermore, good improvement in the design was achieved with only small changes to the geometry which will not change the mechanics or add difficulties in manufacturing.

Even though the combination of optimized parameters showed to improve the device performance in terms of contact pressure and paravalvular AR, whether the tapered configuration at the inlet of the frame significantly impacts the valve hemodynamics should be carefully investigated.

In this study the optimization of the frame geometrical parameters was performed using the central composite design together with the NLPQL algorithm. The central composite design is a relatively simple design which can provide good fitting with RSM polynomial functions. It is widely used in optimization studies to efficiently investigate the effect of several parameters on the objectives and to screen the most relevant parameters. However, a different design of experiment (e.g. full factorial, fractional factorial, hypercube...) can be alternatively adopted. Subsequently, given the obtained smooth surface of the objective function, we chose the NLPQL as optimization algorithm. Solving multi-objective problems by single-objective algorithms, as NLPQL, however implies to assume up front the weighting between the objectives, which might add inaccuracy to the model. While single-objective algorithms lead efficiently to a single solution, multi-objective optimization algorithms which treat each objective separately are a good alternative to obtain a set of equally optimal solutions (i.e. non-dominated Pareto solutions). Afterwards, tradeoff between the objectives needs to be evaluated in order to choose the desired solution. Multi-objective algorithms allow to deal with multiple 'conflicting' objectives at the price of increased complexity. However, given the aim of this study to show the potential of combining patient-specific computer simulation and optimization strategy to improve the geometry of a device and reduce postoperative complications, we believe the use of the NLPQL algorithm is appropriate.

Most of the existing optimization studies applied to stent geometries, employed computer simulation to improve mechanical properties (stress distribution, radial strength, fatigue resistance) or hemodynamic properties (flow disturbances, wall shear stress). However, optimization was based on mechanical tests performed on solely unit stent models [227], or simplified 3D stent models [230, 233, 234] neglecting the interaction with the arterial tissues. Putra et al [232] adopted computational fluid dynamics simulation to optimize a simplified and idealized two-dimensional stent geometry under the influence of the vessel wall deformation. Li et al [228] accounted for the interaction of the stent with simplified plaque and artery in the optimization of a stent life prediction and stent expansion. Recently, Bosi et al. [186], combined patient-specific modeling with optimization techniques to tune the material parameters of the aortic root in their TAVR simulation workflow.

To the best of our knowledge, this is the first study that adopts full three-dimensional patient-specific models to optimize stent geometrical parameters of a TAVR device, minimizing clinical complications. With this approach, the performance of the device can be evaluated in models resembling anatomical variability among patients eligible for TAVR, (aortic root variability, amount and location of calcifications, tricuspid or bicuspid aortic valve) before entering the clinical phase.

This proof-of-concept study shows that patient-specific computer simulations can be used to optimize the design of a TAVR device reducing the costs and the time of the design and development phase of a new device, as well as the level of risk during the clinical studies.

This is a valuable approach with the potential to be extended to medical devices in general. The objectives can also be extended to any other clinical outcome as long as computational modelling and simulation can accurately predict those outcomes. In this study, the optimized device is quite similar to the CoreValve system, for which the strategy for predicting paravalvular AR and conduction abnormalities was previously validated [175, 176, 193]. Due to the similarity between the CoreValve and the device variants modelled in this study, we believe the previous validation work remains valid for these new devices.

While in this study we focused on three key functional post-deployment variables (maximum contact pressure, contact pressure area and paravalvular regurgitation), this approach can be used to optimize any geometrical parameter that plays a relevant role in the performance of the device (i.e. stress distribution, durability of the device).

**Study limitations**

Although device optimization based on patient-specific computer simulation has many advantages in the stent design, this study has certain limitations. First, significant computational resources are required to perform this kind of study. A total of 16 devices were created and virtually implanted in 12 patients, resulting in 192 FEA simulations and same amount of CFD simulations. Additionally, iterative repositioning of the device was necessary in some cases to reach comparable implantation depth of the device in each patient. In fact, the obtained optimal device is implantation depth-specific. Whether it remains the optimal solution at different implantation depths needs to be verified. Second, a limited number of patients was enrolled in the study. Despite the fact that only 12 patients were used, they were representative of the population eligible for TAVR, and assumed sufficient for a proof-of-concept study.

In future, automatization of the entire process is planned, with inclusion of more patients to ensure optimal device performance. Last, this study focused on the prediction of three post-procedural outcomes, but other parameters that play an important role in the performance and durability of the device should be evaluated. For example, the crimping feasibility of those devices should be checked to ensure that the device is not damaged. A mechanical analysis of the stress distribution on the device frame and device leaflets should be performed to guarantee high performance and device durability. Also, mechanical factors that might affect the stress/strain distribution on the aortic wall to avoid negative outcomes (i.e. annulus rupture) should be included in the optimization study.

## 7.5 CONCLUSIONS

In this study, we proposed a framework to improve the design of a representative TAVR frame using patient-specific computer models able to predict post-operative outcomes. Results show that this approach can effectively evaluate and optimize the performance of a TAVR device on a virtual TAVR population. The proposed approach can help to speed up the initial design and development phase of new devices and lower the risk during clinical studies.

# III

# Conclusions

CHAPTERS

**8 Conclusions and future perspectives 141**

CHAPTER 8

# CONCLUSIONS AND FUTURE PERSPECTIVES

The work described in this thesis provides novel strategies to investigate, predict and hopefully avoid complications after TAVR. The application of this computational tool has led to a number of useful clinical insights that are summarized in this chapter, followed by some suggestions for future research.

## 8.1 CONCLUSIONS

Computational patient-specific models of TAVR have been increasingly developed since the first in human procedure in 2002. However, at the beginning of this project four years ago, only few studies had investigated TAVR. Existing studies were based on few patient-specific models and validation with *in vitro* or *in vivo* data was rarely performed. This work continues the validation and development of the computational framework (TAVIguide) developed at FEops, which allows to reproduce TAVR in patient-specific models and serves as a solid basis to investigate the interaction between the device and the arterial wall and predict the risk of postprocedural complications. At the onset of this thesis, the framework was validated for prediction of frame deformation, calcium displacement and paravalvular regurgitation after implantation of the first-generation CoreValve. However, further validation was needed. During this study, a new strategy to predict the risk of new conduction abnormalities has been developed and validated. Furthermore, TAVIguide has been used in combination with optimization algorithms, showing the potential of such approach to test the device in a virtual population and achieve on optimal design in a shorter period.

### 8.1.1 Clinical investigation using computational modeling

A new strategy to predict conduction abnormalities after TAVR has been presented in Chapter 4. Conduction abnormalities have been assumed to be a direct consequence of the contact pressure exerted by the implanted device on the AV conduction system. Statistical analysis showed that both contact pressure and area of contact are good predictors for new conduction abnormalities, confirming that both an extended area of pressure and a small spot at very high pressure on the conduction system may damage the conduction system. Validation on a relatively large population of 164 patients demonstrated that this strategy is applicable to both self-expandable and mechanically-expandable devices.

The key factor in our analysis is the identification of the anatomical region of the AV conduction system in each model. This represents, at the same time, the main challenge as the AV bundles themselves are not directly visible from MDCT. In this study, we used the inferior border of the membranous septum as landmark for the location of the AV system. However, the quality of MDCT images is a potential bottleneck for the successful application of this strategy in each and every patient. As the inferior border of the membranous septum is located at the AV crest, both the left ventricle and the right heart need to be sufficiently filled with contrast. In some patients, calcifications extend to the AV crest, making the landmark identification more difficult. Also, motion artefacts are not rare considering the elder and frail population. Other predictors have been proposed from clinical studies (e.g. calcifications in the LVOT, deep device implantation, oversizing of the balloon, distance between the membranous septum and the aortic annulus). However, the advantage of the described strategy is that the risk of conduction abnormalities comes as the result of the interaction between the device and patient-specific anatomical structures and at the same time it accounts for anatomical inter-patient variability of the location of the AV conduction system.

Next to conduction abnormalities, TAVIguide has been developed to predict paravalvular AR. The software was previously validated in 60 patients using the self-expandable CoreValve device [176]. A second validation of the framework in 63 patients, described in Chapter 5, confirmed previous findings. Numerical results showed to accurately distinguish patients at risk of 'none-to-mild' AR from patients at risk of 'moderate-to-severe' AR after implantation of a CoreValve device. Also, numerical results reported in

Chapter 6, showed that this strategy is applicable to both self-expandable and mechanically-expandable devices. Additionally, computer simulations revealed that the rotation of the device within the aortic root affects the paravalvular jets. In fact, when alignment between the native and the prosthetic commissures was reached, lower AR was observed. Currently, clinicians cannot control the alignment of the device during implantation as the prosthetic leaflets are not visible from fluoroscopy. However, this finding can be of interest in the development of future devices. Adding markers to the frame in correspondence of the commissures might be a simple improvement that makes the commissures visible during fluoroscopy and gives the clinicians the awareness of the device rotation.

The above validated strategies have been subsequently used to have a deep insight into sizing and positioning of the mechanically-expandable Lotus device in patients with equivocal aortic root dimensions. The Lotus valve can be precisely positioned, but the selection of the appropriate size remains challenging. As the sizing matrix of the Lotus is based upon multiple aortic root dimensions, it often occurs that two sizes can be selected. For these cases, there is a lack in the procedural guidelines and the device size selection is based on the experience of the clinician. Numerical results revealed that device size has a bigger impact than the implantation depth in the risk of paravalvular AR. Also, in some patients results revealed that low implantation and larger device size increases the risk of conduction abnormalities. However, in some other cases the risk of conduction abnormalities depended from multiple factors: location and amount of calcifications and location of the AV conduction system. This study demonstrates the advantage of using patient-specific computer modeling as a solid tool to correctly size and position the device to avoid postoperative complications, therefore functioning as support tool for the clinician during the procedural planning phase.

### 8.1.2 Optimization of new devices

A new strategy to optimize the design of a TAV through patient-specific finite element and fluid dynamics simulation is presented in Chapter 7. Several designs of a CoreValve-like device have been investigated by varying two geometrical parameters and their performance has been evaluated in a virtual population in terms of predicted paravalvular AR and conduction abnormalities. The design was then optimized to reduce predicted complications in all patients. Numerical results confirmed that the selected optimal device had improved performance in all patients. This is a proof-of-concept study that shows the potential of combining patient-specific simulation with optimization algorithm to perform in-silico clinical trials that could be conducted prior to the actual first-in-human clinical study. In this way, risks for patients and manufacturers can be significantly reduced. In addition, combining patient-specific computational modelling and simulation with device optimization techniques can help to develop better devices in a shorter time period. In this proof-of-concept study, the geometrical parameters to be optimized were chosen up front. However, the optimization study of a real device should include a screening phase where several parameters are investigated, and the most relevant ones selected. Similarly, the optimization algorithm should be chosen with care. Nevertheless, this is valuable and versatile approach that allows to optimize any geometrical parameter, aiming to improve the device performance in terms of mechanical property (e.g. stress peaks, durability...) as well as reduction of postoperative complications. To perform such analysis, the accuracy of the computational model and simulation need to be verified first. In this study, the optimized device is quite similar to the CoreValve system, for which the strategy for predicting paravalvular AR and conduction abnormalities was previously validated [175, 176, 193]. Due to the similarity between the CoreValve and the device variants modelled in this study, the previous validation work was assumed valid for these new devices. In case the analysis is applied to a new device, a prototype is needed as well as few in-animal implantations to validate the strategy. The major limitation in this study relies in the significant computational costs. However, automatization of the workflow would save a lot of resources (time and money).

## 8.2 CONSIDERATIONS AND FUTURE PERSPECTIVE

The described patient-specific computational modeling is based on a number of modeling assumptions that should be further investigated. In the first place the material models of the aortic root tissues have been assumed linear elastic even though anatomical structures are known to have a more complex anisotropic hyperelastic mechanical response. Linearization is justified by previous studies that reported comparable accuracy of TAVR simulations in terms of aortic root deformation using a simple linear elastic model or a more complex hyperelastic material [167, 182]. Even though a previous study demonstrated that the used parameters allow for accurate prediction of the interactions between the aorta and the TAVR device [175], further fine-tuning of the material could be performed using a larger population. Different strategies can be adopted to tune the parameters: an iterative process of back-calculations using pre and postoperative data from the patients as done previously [175] or optimization algorithms as recently proposed by Bosi et al [186]. The former approach allows a better understanding of the influence of a single parameter on the final result. However, it is difficult to control and very time consuming. On the other hand, the latter approach allows to evaluate the influence of single parameters as well as of their interaction on the final result. As it can be based on an automated workflow, it can be faster and new data can be easily included. Furthermore, as more and more younger patients will be treated with TAVR, the option to have a set of modeling parameters for a specific range of age (e.g. less stiff and thick aortic wall or aortic leaflets) should be considered.

Secondly, the accuracy of the calcification volumes on the aortic leaflets should be accurately verified. In fact, as the segmentation of calcium nodules depends on the quality of the enhanced-MDCT images (e.g. contrast level), calcium nodules can be over- or under-estimated. Calcifications influence the deployed device deformation and have been correlated with paravalvular gaps. Therefore, they should be modeled with care. To this goal, calcium volume extracted from enhanced-MDCT images could be compared with calcium volume quantified with the Agaston score in non-contrast images. Alternatively, pre-operative cardiac MDCT images of a patient selected for SAVR could be used to model calcifications on the aortic leaflets. Then, the reconstructed calcium volumes could be compared with the actual calcifications isolated from the valve removed during SAVR.

The clinical findings described in this work, can be used as a starting point for further research topics. To overcome some limitations of the work described in this thesis, some suggestions are listed below.

As mentioned, patient-computer modeling and simulation requires considerable resources in terms of time and money. The advent of machine learning might be adopted to fasten the entire workflow. For instance, in this study, the annular plane, annular dimensions as well as the landmarks used for the location of the AV conduction system of each patient are manually selected from MDCT images using Mimics. A well-trained model could automatically identify all those features from MDCT images, even when the image quality is not optimal. Furthermore, such model could reduce inter-operator variability and ensure consistency in measurements and landmarking. Additionally, this model could be trained to identify relevant features to discern patients with tricuspid and bicuspid aortic valve. Currently, some hospitals do not consider TAVR for patients with bicuspid aortic valve. However, the identification of a bicuspid valve is challenging and highly subjective. In this context, machine learning could be of great support for clinicians in the pre-procedural planning phase.

Besides the support in the preoperative phase, TAVIguide could be of great help during the procedure, providing the optimal/target device position for the specific patient. Fusion of simulation results with pre-operative imaging modalities could be performed to address this. However, the computational time necessary to perform the simulations remains a limiting factor for a wide-spread usage of this technology. Ideally, predictive modelling should be performed real-time. One way of doing this is using machine learning to predict risk on complications directly from MDCT images. Alternatively, a large database of simulated cases could be used to directly predict device deformation and/or complications for a new patients, for example by identifying patients with similar characteristics (i.e. nearest neighbour approach).

Maximum contact pressure and contact pressure area were identified as predictors for new conduction abnormalities, and cut-off values have been proposed to distinguish patients at high-risk from patients at low-risk of developing conduction abnormalities. However, it should be considered to combine the two predictors into a unique variable to facilitate the interpretation of numerical results from a clinical point of view, and to improve the overall accuracy of prediction. Also, prediction of conduction abnormalities has been evaluated at the end of the device deployment. However, damages to the conduction system might occur already peri-procedurally. Therefore, it would be interesting to evaluate the contact pressure during the entire deployment simulation.

Some existing studies speculated that elevated stresses in the region of the left ventricular outflow tract [182] or in the interventricular triangle confined by the non- and the left-coronary cusp could activate a tissue inflammatory response which might contribute to the development of conduction abnormalities after TAVR [187]. However, numerical results were not compared with clinical data. In future, it would be interesting to investigate the stress distribution within the region of the AV conduction system and evaluate this parameter as a possible predictor for conduction abnormalities.

Despite the continuous improvements of TAVR devices, some complications remain crucial after the procedure. Coronary obstruction and annulus rupture are rare but fatal complications and should be avoided. With the main goal of using TAVIguide as a tool to guide the clinician towards safe and efficient procedures, a complete overview of possible TAVR complications should be provided. This could favor especially unexperienced clinicians (e.g. clinicians at the beginning of their career, or clinicians who deal with a low volume of TAVR cases). Therefore, future research could focus on further extension of TAVIguide to include the prediction of coronary occlusion and annulus rupture.

The described computational workflow focused on conduction abnormalities and paravalvular regurgitation. As such, TAV leaflets were not modeled. Some studies showed that high stress on the TAV leaflets can compromise the short- and long-term performance of the device by causing a central regurgitation jet, inducing a faster deterioration or restenosis. Therefore, the inclusion of the TAV leaflets in the device model and mechanical analysis on the TAV leaflets might be of interest for future research.

Last, FSI simulations might provide a more complete scenario of the mutual interactions between the blood flow, the aortic root tissues and the implanted device. This might be of interest for further investigation on the hemodynamics after TAV implantation and therefore to evaluate the device performance in longer-term. However, the overall complexity of FSI simulations and its computational costs should not be underestimated.

# IV

# Appendices

Chapters

**A Model implementation step-by-step** **151**

**B Rationale behind the CoreValve System design** **157**

APPENDIX A

# MODEL IMPLEMENTATION STEP-BY-STEP

## SEGMENTATION PHASE (MIMICS)

Patient-specific cardiac anatomies are segmented starting from preoperative MDCT images, using the dedicated software Mimics (v18, Materialise, Leuven). When a preoperative 4D MDCT dataset is available, the end-systolic phase of the cardiac cycle is used. During the segmentation phase, two different greyscale thresholds are adopted to discriminate between the aortic lumen and the calcium nodules (on the aortic wall and leaflets). These thresholds depend from the quality of the images (e.g. pixel size, contrast), therefore thresholds are adapted in each patient-specific dataset to guarantee a precise definition of the border of each structure. The aortic lumen consists of the LVOT, the aortic root, coronary arteries (if visible) and ascending aorta. The aortic lumen is adjusted so that calcifications on the aortic wall are located on the outside of the segmented aortic region. Starting from the mask of the aortic lumen, 'Morphology and Boolean operations' available in Mimics are used to segment the visible parts of the healthy valve tissue. Subsequently, the triangulated surface of the 3D model of the structures is exported from Mimics to an *in-house* software (TAVIguide, FEops, Gent, Belgium) and used as the starting point for the native leaflet reconstruction.

### Landmarking phase (Mimics)

Next to the segmentation of the anatomical structures, six landmarks necessary to finalize the 3D model reconstruction are identified. To this scope, a reslice plane parallel to the annular plane is defined. From the resliced transversal view, the landmarks at the location of the three basal attachment points of the aortic valve leaflets are detected. On the other side, the resliced coronal view is used to detect the three landmarks at the location of the inferior border of the membranous septum.

### Aortic root meshing (TAVIguide)

In this phase, the attachment edge of the leaflets is manually picked on the aortic root model. A template aortic valve mesh consisting of prism elements is then adopted to shape the native leaflets, fitting the portion of the native valve previously segmented. The leaflets are shaped and positioned so that they intersect with the segmented calcium nodules located on the valve. Then, the elements at the intersection are extruded to completely embed the calcifications and reconstruct their volume.

A tie constraint is defined at the attachment edge of the leaflets as well as at the portion of calcifications adjacent to the aortic wall, to connect the valve geometry to the aorta.

The aorta is modelled with a triangulated mesh. To account for the surrounding tissues and to dampen the motion of the aorta, springs and dashpots are defined at each node of the aorta mesh. The thickness of the leaflets is assumed to be constant and equal to 1.5 mm, based on the data reported by Grande et al. [239]. As the thickness at each site on each aortic leaflet increases significantly with age (e.g. mean thickness of the cusp nodule was 0.67 mm in patients with age <20 years, 0.87 mm in patients with age between 20 and 59 and 1.42 mm in patients older than 60 years) [240], this high thickness is representative for the elder population who underwent TAVR.

### Material calibration

Linear elastic material models are used to approximate the mechanical behavior of the aorta and of the native leaflets. This approximation allows to reduce the complexity of the model and thus of the parameter calibration step. On the other hand, a linear elastic-plastic material model with perfect plasticity is used for the calcifications to simulate calcium fracture.

The material model of each anatomical region, the thickness of the aortic wall, the spring stiffness and the coefficient of friction for the contact definition were calibrated with an iterative process of back-calculations using pre and postoperative MSCT of 39 patients who received either a CoreValve or a Sapien XT device. Reasonable initial values were taken from literature. No other limits or priority rank were assumed. The analysis was performed manually: based on the evaluation of the FEA results, parameters were changed and simulations repeated until accurate results in terms of frame deformation and calcium displacement were obtained. Normally, one (or two parameters) were (simultaneously) modified after one iteration. The analysis consisted in more than 30 iterations. The calibration process is shown in Fig. A.1.

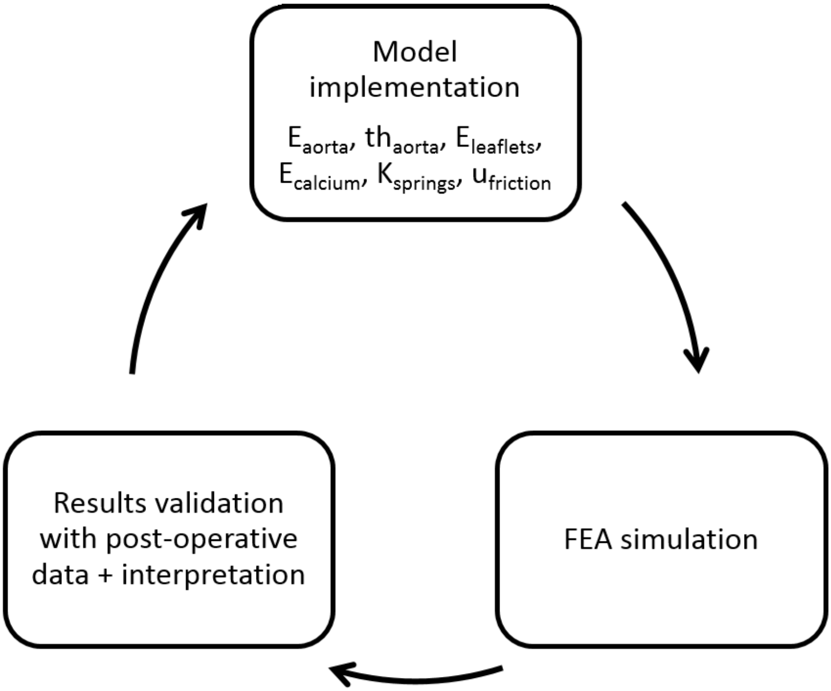
Model implementation
$E_{aorta}$, $th_{aorta}$, $E_{leaflets}$, $E_{calcium}$, $K_{springs}$, $u_{friction}$
FEA simulation
Results validation with post-operative data + interpretation

**Figure A.1:** Diagram representing the iterative process of material calibration.

The optimal material parameters resulted from the calibration process are summarized in Table A.1.

**Table A.1:** Optimal material parameters from the calibration analysis.

| | |
|---|---|
| Aorta | E=2.0 MPa, $\nu$=0.45 |
| Leaflets | E=0.6 MPa, $\nu$=0.3 |
| Calcifications | E=4.0 MPa, $\nu$=0.3, $\sigma_{yield}$=0.6 MPa |

### Bioprosthetic devices

The Medtronic CoreValve devices were reconstructed starting from microCT images received from the manufacturer. The parameters of the Nitinol material were iteratively calibrated by matching finite element models of the radial force bench test with experimental radial force from tests performed on the samples.

The braided Lotus valve was constructed based on technical drawings received from Boston Scientific. Also, the details of the Nitinol material model were provided by the manufacturer. The accuracy of the models was evaluated comparing the radial force obtained with finite element models and experimental radial force bench test that was provided by the manufacturer.

The prosthetic leaflets of the devices are not modeled. As they have negligible impact on the mechanics of the prosthesis, they are excluded from the finite element models. The crimped configuration of the devices was obtained by applying radial displacement to the crimper, represented as a simplified cylinder.

### FEA simulation setup (Abaqus)

The crimped devices and the crimper cylinder are imported in TAVIguide and positioned coaxially to the aortic root. FEA simulations are performed in Abaqus Explicit (v6.12). In the first step of the FEA analysis, the native aortic valve is opened to ensure no intersection between its elements and the frame of the device. To this purpose, a cylinder with a very small diameter placed coaxially to the aortic root is expanded radially until its diameter is slightly larger than the device frame to force the aortic valve to open.

The second step consists in the prosthesis deployment. The deployment strategy of the CoreValve and the Lotus device is different. The deployment of the CoreValve device consists in 2 steps. First, to mimic the insertion of the catheter with the crimped device, the CoreValve is pushed to the outside of the aorta's curvature. Secondly, the prosthesis sheath is moved axially to allow the frame expansion. Of note, as done in clinical practice, the nodes at the bottom inflow of the device are the first nodes to expand. In this step a friction coefficient of 0.7 is applied between the frame and the surrounding anatomy (aorta and aortic valve). This high friction compensates the fact that the skirt of the prosthesis is neglected in the model, thus reducing the area of contact (and friction) between the prosthesis and the patient anatomy. Furthermore, this high friction helps to obtain a non-uniform distribution of the prosthesis strut that was observed in post-operative MDCT images. On the other hand, the deployment of the mechanically-expandable Lotus is achieved by shortening the prosthesis, at the location of the posts, to a predefined length of 19 mm.

A final step of the FEA analysis allows the device frame to fully settle into the patient-specific anatomy and the remaining dynamics movements to come to rest. During this step, only the contact between the aorta, aortic valve and device is active. No displacements or loads are applied in this step.

### CFD SIMULATION SETUP (OPENFOAM)

CFD simulations are performed in icoFOAM, an open-source solver available within OpenFOAM (v2.1). The output of the FEA simulation represents the input for the CFD simulation. The prosthetic skirt is reconstructed on the deformed device frame. The region of interest for the fluid domain is discretized with hexahedral elements and refined within the region of interest (i.e. lumen within the aortic root wall). The aortic wall is assumed to be rigid and coronaries are not included in the lumen.

The flow is modeled as incompressible (constant density of 1060 $kg/m^3$, viscosity of 0.0035 Ps s), laminar and Newtonian. No slip condition (i.e. flow at zero velocity) is defined at the aortic wall. A constant static pressure of 32 mmHg is applied at the inlet (aortic side), while zero pressure is applied at the outlet (i.e. ventricular side). The imposed diastolic pressure gradient is the result of previous measurements performed in 20 patients after the treatment. This value is in line with the end-diastolic gradient observed by Sinning et al. in a cohort of 146 patients [148].

# APPENDIX B

# RATIONALE BEHIND THE COREVALVE SYSTEM DESIGN

The Medtronic CoreValve System has a long frame with a diamond-cell configuration (Fig. B.1). The frame can be subdivided in three levels, each serving a specific purpose [241]. The outflow portion (i.e. highest level towards the aortic side) has the largest diameter and high hoop strength to seat at the sino-tubular junction and to provide support in the device positioning, as well as in the alignment within the aortic root. The waist portion (i.e. at the level of the coronary sinuses) is the narrowest one and it hosts the bioprosthetic leaflets. This portion boasts very high hoop strength, to limit the frame deformation, favoring maximum valve opening (i.e. effective orifice area) in systole and leaflet coaptation in diastole. High commissures are designed to reduce the stresses on the leaflet, therefore improving the long-term performance of the valve (e.g. areas of high stresses can induce collagen deterioration leading progressively to valve failure). Even though the high commissures extend beyond the coronary ostia, the narrow waist ensures enough space between the device frame and the coronary ostia, reducing the risk of coronary obstruction. Furthermore, the smallest cell dimension (i.e. 12 Fr) accommodates a 10 Fr catheter, facilitating the access to the coronaries in case a future percutaneous coronary intervention is needed. The inflow portion of the frame (i.e. lowest level towards the LVOT) has a larger diameter and high radial force to open the native valve leaflets and anchor the frame within the aortic annulus. The flatter landing zone ensures the maximum over-sizing within the implant depth range. Furthermore, a long porcine skirt is sutured to the frame in this portion, to favor optimal sealing and prevent paravalvular regurgitation. Porcine pericardium is about half of the thickness of the bovine pericardium, allowing for low profile delivery access.

The CoreValve System is designed for a supra-annular position (Fig. B.2), to maximize the flow in systole and the leaflet coaptation in diastole. The target implantation depth is about 3-5 mm below the annular plane. To this purpose, the junction nodes (i.e. where two cells join each other) are used as a reference during deployment. In fact, when the device is in the crimped configuration, the nodes appears as a band through the delivery system. The target implantation depth is just below the first node (Fig. B.2).

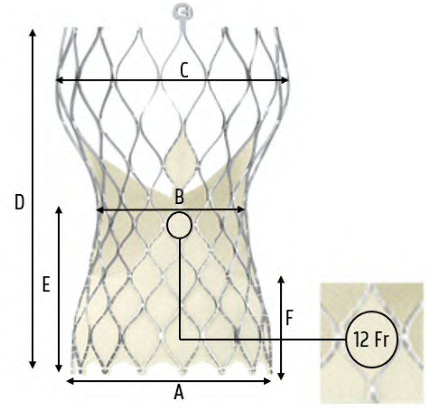

| | |
|---|---|
| A. Inflow diameter | 29 mm |
| B. Waist diameter | 23 mm |
| C. Outflow diameter | 34 mm |
| D. Frame height | 45 mm |
| E. Commissure height | 26 mm |
| F. Skirt height | 13 mm |

**Figure B.1:** Design and dimensions of frame of the Evolut R 29 mm.

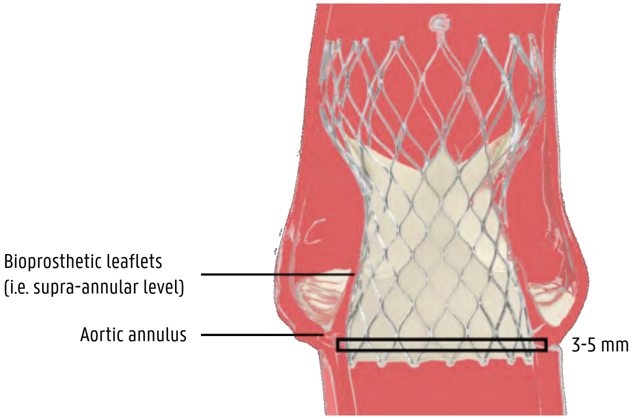

**Figure B.2:** Illustration of the CoreValve System in supra-annular position. The black rectangle shows the target implantation depth 3 to 5 mm below the aortic annulus.

# BIBLIOGRAPHY

[1] R. L. Osnabrugge, D. Mylotte, S. J. Head, N. M. Van Mieghem, V. T. Nkomo, C. M. LeReun, A. J. Bogers, N. Piazza and A. P. Kappetein, 'Aortic stenosis in the elderly: Disease prevalence and number of candidates for transcatheter aortic valve replacement: A meta-analysis and modeling study', *J Am Coll Cardiol*, vol. 62, no. 11, pp. 1002–12, 2013.

[2] A. Cribier, H. Eltchaninoff, A. Bash, N. Borenstein, C. Tron, F. Bauer, G. Derumeaux, F. Anselme, F. Laborde and M. B. Leon, 'Percutaneous transcatheter implantation of an aortic valve prosthesis for calcific aortic stenosis: First human case description', *Circulation*, vol. 106, no. 24, pp. 3006–8, 2002.

[3] G. M. Deeb, M. J. Reardon, S. Chetcuti, H. J. Patel, P. M. Grossman, S. J. Yakubov, N. S. Kleiman, J. S. Coselli, T. G. Gleason, J. S. Lee, J. Hermiller J. B., J. Heiser, W. Merhi, 3. Zorn G. L., P. Tadros, N. Robinson, G. Petrossian, G. C. Hughes, J. K. Harrison, B. Maini, M. Mumtaz, J. Conte, J. Resar, V. Aharonian, T. Pfeffer, J. K. Oh, H. Qiao, D. H. Adams and J. J. Popma, '3-year outcomes in high-risk patients who underwent surgical or transcatheter aortic valve replacement', *J Am Coll Cardiol*, vol. 67, no. 22, pp. 2565–74, 2016.

[4] M. J. Mack, M. B. Leon, C. R. Smith, D. C. Miller, J. W. Moses, E. M. Tuzcu, J. G. Webb, P. S. Douglas, W. N. Anderson, E. H. Blackstone, S. K. Kodali, R. R. Makkar, G. P. Fontana, S. Kapadia, J. Bavaria, R. T. Hahn, V. H. Thourani, V. Babaliaros, A. Pichard, H. C. Herrmann, D. L. Brown, M. Williams, M. J. Davidson, L. G. Svensson and J. Akin, '5-year outcomes of transcatheter aortic valve replacement or surgical aortic valve replacement for high surgical risk patients with aortic stenosis (partner 1): A randomised controlled trial', *The Lancet*, vol. 385, no. 9986, pp. 2477–2484, 2015.

[5] T. E. Feldman, M. J. Reardon, V. Rajagopal, R. R. Makkar, T. K. Bajwa, N. S. Kleiman, A. Linke, D. J. Kereiakes, R. Waksman, V. H. Thourani, R. C. Stoler, G. J. Mishkel, D. G. Rizik, V. S. Iyer, T. G. Gleason, D. Tchetche, J. D. Rovin, M. Buchbinder, I. T. Meredith, M. Gotberg, H. Bjursten, C. Meduri, M. H. Salinger, D. J. Allocco and K. D. Dawkins, 'Effect of mechanically expanded vs self-expanding transcatheter aortic valve replacement on mortality and major adverse clinical events in high-risk patients with aortic stenosis: The reprise iii randomized clinical trial', *Jama*, vol. 319, no. 1, pp. 27–37, 2018.

[6] N. Buzzatti, A. Castiglioni, E. Agricola, M. Barletta, S. Stella, F. Giannini, D. Regazzoli, A. Mangieri, M. Ancona, P. Spagnolo, A. Chieffo, M. Montorfano, O. Alfieri, A. Colombo and A. Latib, 'Five-year evolution of mild aortic regurgitation following transcatheter aortic valve implantation: Early insights from a single-centre experience', *Interact Cardiovasc Thorac Surg*, vol. 25, no. 1, pp. 75–82, 2017.

[7] S. K. Kodali, M. R. Williams, C. R. Smith, L. G. Svensson, J. G. Webb, R. R. Makkar, G. P. Fontana, T. M. Dewey, V. H. Thourani, A. D. Pichard, M. Fischbein, W. Y. Szeto, S. Lim, K. L. Greason, P. S. Teirstein, S. C. Malaisrie, P. S. Douglas, R. T. Hahn, B. Whisenant, A. Zajarias, D. Wang, J. J. Akin, W. N. Anderson and M. B. Leon, 'Two-year outcomes after transcatheter or surgical aortic-valve replacement', *New England Journal of Medicine*, vol. 366, no. 18, pp. 1686–1695, 2012.

[8] M. B. Leon, C. R. Smith, M. J. Mack, R. R. Makkar, L. G. Svensson, S. K. Kodali, V. H. Thourani, E. M. Tuzcu, D. C. Miller, H. C. Herrmann, D. Doshi, D. J. Cohen, A. D. Pichard, S. Kapadia, T. Dewey, V. Babaliaros, W. Y. Szeto, M. R. Williams, D. Kereiakes, A. Zajarias, K. L. Greason, B. K. Whisenant, R. W. Hodson, J. W. Moses, A. Trento, D. L. Brown, W. F. Fearon, P. Pibarot, R. T. Hahn, W. A. Jaber, W. N. Anderson, M. C. Alu and J. G. Webb, 'Transcatheter or surgical aortic-valve replacement in intermediate-risk patients', *New England Journal of Medicine*, vol. 374, no. 17, pp. 1609–1620, 2016.

[9] H. K. Marieb E.N., 'Anatomy & Physiology', 4th. Boston: Pearson, 2010.

[10] E. I. Charitos and H.-H. Sievers, 'Anatomy of the aortic root: Implications for valve-sparing surgery', *Annals of Cardiothoracic Surgery*, vol. 2, no. 1, pp. 53–56, 2013.

[11] K. Hanneman, F. P. Chan, R. S. Mitchell, D. C. Miller and D. Fleischmann, 'Pre- and postoperative imaging of the aortic root', *Radiographics*, vol. 36, no. 1, pp. 19–37, 2016.

[12] W. C. Roberts, 'The structure of the aortic valve in clinically isolated aortic stenosis: An autopsy study of 162 patients over 15 years of age', *Circulation*, vol. 42, no. 1, pp. 91–7, 1970.

[13] M. A. Silver and W. C. Roberts, 'Detailed anatomy of the normally functioning aortic valve in hearts of normal and increased weight', *Am J Cardiol*, vol. 55, no. 4, pp. 454–61, 1985.

[14] J. H. Chen and C. A. Simmons, 'Cell-matrix interactions in the pathobiology of calcific aortic valve disease: Critical roles for matricellular, matricrine, and matrix mechanics cues', *Circ Res*, vol. 108, no. 12, pp. 1510–24, 2011.

[15] I. Vesely, 'The role of elastin in aortic valve mechanics', *J Biomech*, vol. 31, no. 2, pp. 115–23, 1998.

[16] A. C. Braverman, H. Guven, M. A. Beardslee, M. Makan, A. M. Kates and M. R. Moon, 'The bicuspid aortic valve', *Curr Probl Cardiol*, vol. 30, no. 9, pp. 470–522, 2005.

[17] P. W. Fedak, S. Verma, T. E. David, R. L. Leask, R. D. Weisel and J. Butany, 'Clinical and pathophysiological implications of a bicuspid aortic valve', *Circulation*, vol. 106, no. 8, pp. 900–4, 2002.

[18] W. C. Roberts, 'The congenitally bicuspid aortic valve: A study of 85 autopsy cases', *The American Journal of Cardiology*, vol. 26, no. 1, pp. 72–83, 1970.

[19] H. Y. Sabet, W. D. Edwards, H. D. Tazelaar and R. C. Daly, 'Congenitally bicuspid aortic valves: A surgical pathology study of 542 cases (1991 through 1996) and a literature review of 2,715 additional cases', *Mayo Clin Proc*, vol. 74, no. 1, pp. 14–26, 1999.

[20] A. Angelini, S. Y. Ho, R. H. Anderson, W. A. Devine, J. R. Zuberbuhler, A. E. Becker and M. J. Davies, 'The morphology of the normal aortic valve as compared with the aortic valve having two leaflets', *J Thorac Cardiovasc Surg*, vol. 98, no. 3, pp. 362–7, 1989.

[21] H.-. H. Sievers and C. Schmidtke, 'A classification system for the bicuspid aortic valve from 304 surgical specimens', *The Journal of Thoracic and Cardiovascular Surgery*, vol. 133, no. 5, pp. 1226–1233, 2007.

[22] H. I. Michelena, V. A. Desjardins, J. F. Avierinos, A. Russo, V. T. Nkomo, T. M. Sundt, P. A. Pellikka, A. J. Tajik and M. Enriquez-Sarano, 'Natural history of asymptomatic patients with normally functioning or minimally dysfunctional bicuspid aortic valve in the community', *Circulation*, vol. 117, no. 21, pp. 2776–84, 2008.

[23] D. Mylotte, T. Lefevre, L. Sondergaard, Y. Watanabe, T. Modine, D. Dvir, J. Bosmans, D. Tchetche, R. Kornowski, J. M. Sinning, P. Theriault-Lauzier, C. J. O'Sullivan, M. Barbanti, N. Debry, J. Buithieu, P. Codner, M. Dorfmeister, G. Martucci, G. Nickenig, P. Wenaweser, C. Tamburino, E. Grube, J. G. Webb, S. Windecker, R. Lange and N. Piazza, 'Transcatheter aortic valve replacement in bicuspid aortic valve disease', *J Am Coll Cardiol*, vol. 64, no. 22, pp. 2330–9, 2014.

[24] M. Lindroos, M. Kupari, J. Heikkila and R. Tilvis, 'Prevalence of aortic valve abnormalities in the elderly: An echocardiographic study of a random population sample', *J Am Coll Cardiol*, vol. 21, no. 5, pp. 1220–5, 1993.

[25] B. F. Stewart, D. Siscovick, B. K. Lind, J. M. Gardin, J. S. Gottdiener, V. E. Smith, D. W. Kitzman and C. M. Otto, 'Clinical factors associated with calcific aortic valve disease. cardiovascular health study', *J Am Coll Cardiol*, vol. 29, no. 3, pp. 630–4, 1997.

[26] S. L. Lin, C. P. Liu, S. T. Young, M. Lin and C. W. Chiou, 'Age-related changes in aortic valve with emphasis on the relation between pressure loading and thickened leaflets of the aortic valves', *Int J Cardiol*, vol. 103, no. 3, pp. 272–9, 2005.

[27] V. T. Nkomo, J. M. Gardin, T. N. Skelton, J. S. Gottdiener, C. G. Scott and M. Enriquez-Sarano, 'Burden of valvular heart diseases: A population-based study', *Lancet*, vol. 368, no. 9540, pp. 1005–11, 2006.

[28] T. van Bemmel, V. Delgado, J. J. Bax, J. Gussekloo, G. J. Blauw, R. G. Westendorp and E. R. Holman, 'Impact of valvular heart disease on activities of daily living of nonagenarians: The leiden 85-plus study a population based study', *BMC Geriatr*, vol. 10, p. 17, 2010.

[29] B. Vaes, N. Rezzoug, A. Pasquet, P. Wallemacq, G. Van Pottelbergh, C. Mathei, J. L. Vanoverschelde and J. Degryse, 'The prevalence of cardiac dysfunction and the correlation with poor functioning among the very elderly', *Int J Cardiol*, vol. 155, no. 1, pp. 134–43, 2012.

[30] R. Danielsen, T. Aspelund, T. B. Harris and V. Gudnason, 'The prevalence of aortic stenosis in the elderly in iceland and predictions for the coming decades: The ages–reykjavík study', *International Journal of Cardiology*, vol. 176, no. 3, pp. 916–922, 2014.

[31] S. T. Gould, N. J. Darling and K. S. Anseth, 'Small peptide functionalized thiol-ene hydrogels as culture substrates for understanding valvular interstitial cell activation and de novo tissue deposition', *Acta Biomater*, vol. 8, no. 9, pp. 3201–9, 2012.

[32] X. Gu and K. S. Masters, 'Regulation of valvular interstitial cell calcification by adhesive peptide sequences', *Journal of biomedical materials research. Part A*, vol. 93, no. 4, pp. 1620–1630, 2010.

[33] A. M. Kloxin, J. A. Benton and K. S. Anseth, 'In situ elasticity modulation with dynamic substrates to direct cell phenotype', *Biomaterials*, vol. 31, no. 1, pp. 1–8, 2010.

[34] T. A. Pawade, D. E. Newby and M. R. Dweck, 'Calcification in aortic stenosis', *Journal of the American College of Cardiology*, vol. 66, no. 5, p. 561, 2015.

[35] X. Y. Jin, J. R. Pepper and D. G. Gibson, 'Effects of incoordination on left ventricular force-velocity relation in aortic stenosis', *Heart*, vol. 76, no. 6, pp. 495–501, 1996.

[36] R. Yotti and J. Bermejo, 'Left ventricular hypertrophy in aortic valve stenosis: Friend or foe?', *Heart*, vol. 97, no. 4, p. 269, 2011.

[37] R. A. Nishimura, C. M. Otto, R. O. Bonow, B. A. Carabello, 3. Erwin J. P., L. A. Fleisher, H. Jneid, M. J. Mack, C. J. McLeod, P. T. O'Gara, V. H. Rigolin, 3. Sundt T. M. and A. Thompson, '2017 aha/acc focused update of the 2014 aha/acc guideline for the management of patients with valvular heart disease: A report of the american college of cardiology/american heart association task force on clinical practice guidelines', *J Am Coll Cardiol*, vol. 70, no. 2, pp. 252–289, 2017.

[38] R. A. Nishimura, C. M. Otto, R. O. Bonow, B. A. Carabello, 3. Erwin J. P., R. A. Guyton, P. T. O'Gara, C. E. Ruiz, N. J. Skubas, P. Sorajja, 3. Sundt T. M., J. D. Thomas, J. L. Anderson, J. L. Halperin, N. M. Albert, B. Bozkurt, R. G. Brindis, M. A. Creager, L. H. Curtis, D. DeMets, R. A. Guyton, J. S. Hochman, R. J. Kovacs, E. M. Ohman, S. J. Pressler, F. W. Sellke, W. K. Shen, W. G. Stevenson and C. W. Yancy, '2014 aha/acc guideline for the management of patients with valvular heart disease: A report of the american college of cardiology/american heart association task force on practice guidelines', *J Thorac Cardiovasc Surg*, vol. 148, no. 1, e1–e132, 2014.

[39] J. Ross J. and E. Braunwald, 'Aortic stenosis', *Circulation*, vol. 38, no. 1 Suppl, pp. 61–7, 1968.

[40] R. Ramaraj and V. L. Sorrell, 'Degenerative aortic stenosis', *BMJ : British Medical Journal*, vol. 336, no. 7643, pp. 550–555, 2008.

[41] P. Pibarot and J. G. Dumesnil, 'Prosthetic heart valves: Selection of the optimal prosthesis and long-term management', *Circulation*, vol. 119, no. 7, pp. 1034–48, 2009.

[42] G. D. Dangas, J. I. Weitz, G. Giustino, R. Makkar and R. Mehran, 'Prosthetic heart valve thrombosis', *Journal of the American College of Cardiology*, vol. 68, no. 24, pp. 2670–2689, 2016.

[43] D. H. Adams, J. J. Popma, M. J. Reardon, S. J. Yakubov, J. S. Coselli, G. M. Deeb, T. G. Gleason, M. Buchbinder, J. Hermiller, N. S. Kleiman, S. Chetcuti, J. Heiser, W. Merhi, G. Zorn, P. Tadros, N. Robinson, G. Petrossian, G. C. Hughes, J. K. Harrison, J. Conte, B. Maini, M. Mumtaz, S. Chenoweth and J. K. Oh, 'Transcatheter aortic-valve replacement with a self-expanding prosthesis', *New England Journal of Medicine*, vol. 370, no. 19, pp. 1790–1798, 2014.

[44] K. S. Jee, Y. S. Kim, K. D. Park and Y. H. Kim, 'A novel chemical modification of bioprosthetic tissues using l-arginine', *Biomaterials*, vol. 24, no. 20, pp. 3409–16, 2003.

[45] W. K. Lee, K. D. Park, Y. H. Kim, H. Suh, J. C. Park, J. E. Lee, K. Sun, M. J. Baek, H. M. Kim and S. H. Kim, 'Improved calcification resistance and biocompatibility of tissue patch grafted with sulfonated peo or heparin after glutaraldehyde fixation', *J Biomed Mater Res*, vol. 58, no. 1, pp. 27–35, 2001.

[46] C. Seiler, 'Management and follow up of prosthetic heart valves', *Heart*, vol. 90, no. 7, pp. 818–824, 2004.

[47] D. Cheng, J. Pepper, J. Martin, R. Stanbridge, F. D. Ferdinand, W. R. Jamieson, P. Stelzer, G. Berg and G. Sani, 'Stentless versus stented bioprosthetic aortic valves: A systematic review and meta-analysis of controlled trials', *Innovations (Phila)*, vol. 4, no. 2, pp. 61–73, 2009.

[48] L. W. Wollersheim, W. W. Li, A. Kaya, B. J. Bouma, A. H. Driessen, W. J. van Boven, J. van der Meulen and B. A. de Mol, 'Stentless vs stented aortic valve bioprostheses in the small aortic root', *Seminars in Thoracic and Cardiovascular Surgery*, vol. 28, no. 2, pp. 390–397, 2016.

[49] D. Karangelis, A. Mazine, A. Roubelakis, C. Alexiou, S. Fragoulis, C. D. Mazer, B. Yanagawa, D. Latter and D. Bonneau, 'What is the role of sutureless aortic valves in today's armamentarium?', *Expert Rev Cardiovasc Ther*, vol. 15, no. 2, pp. 83–91, 2017.

[50] D. Ross, 'The pulmonary autograft: History and basic techniques', *Semin Thorac Cardiovasc Surg*, vol. 8, no. 4, pp. 350–7, 1996.

[51] F. Nappi, A. Nenna, C. Spadaccio and M. Chello, 'Pulmonary autograft in aortic position: Is everything known?', *Translational Pediatrics*, vol. 6, no. 1, pp. 11–17, 2017.

[52] T. Carrel, 'Aortic valve and/or aortic root replacement using an aortic homograft', *Multimed Man Cardiothorac Surg*, vol. 2009, no. 626, mmcts.2009.003905, 2009.

[53] G. Manoharan, M. S. Spence, J. Rodes-Cabau and J. G. Webb, 'St jude medical portico valve', *EuroIntervention*, vol. 8 Suppl Q, Q97–101, 2012.

[54] M. J. Reardon, D. H. Adams, N. S. Kleiman, S. J. Yakubov, J. S. Coselli, G. M. Deeb, T. G. Gleason, J. S. Lee, J. B. Hermiller, S. Chetcuti, J. Heiser, W. Merhi, G. L. Zorn, P. Tadros, N. Robinson, G. Petrossian, G. C. Hughes, J. K. Harrison, B. Maini, M. Mumtaz, J. V. Conte, J. R. Resar, V. Aharonian, T. Pfeffer, J. K. Oh, H. Qiao and J. J. Popma, '2-year outcomes in patients undergoing surgical or self-expanding transcatheter aortic valve replacement', *Journal of the American College of Cardiology*, vol. 66, no. 2, pp. 113–121, 2015.

[55] C. M. Barker and M. J. Reardon, 'The corevalve us pivotal trial', *Seminars in Thoracic and Cardiovascular Surgery*, vol. 26, no. 3, pp. 179–186, 2014.

[56] T. G. Gleason, M. J. Reardon, J. J. Popma, G. M. Deeb, S. J. Yakubov, J. S. Lee, N. S. Kleiman, S. Chetcuti, J. Hermiller J. B., J. Heiser, W. Merhi, 3. Zorn G. L., P. Tadros, N. Robinson, G. Petrossian, G. C. Hughes, J. K. Harrison, J. V. Conte, M. Mumtaz, J. K. Oh, J. Huang and D. H. Adams, '5-year outcomes of self-expanding transcatheter versus surgical aortic valve replacement in high-risk patients', *J Am Coll Cardiol*, vol. 72, no. 22, pp. 2687–2696, 2018.

[57] 3. Zorn G. L., S. H. Little, P. Tadros, G. M. Deeb, T. G. Gleason, J. Heiser, N. S. Kleiman, J. K. Oh, J. J. Popma, D. Adams, J. Huang and M. J. Reardon, 'Prosthesis-patient mismatch in high-risk patients with severe aortic stenosis: A randomized trial of a self-expanding prosthesis', *J Thorac Cardiovasc Surg*, vol. 151, no. 4, 1014–22, 1023.e1–3, 2016.

[58] S. V. Arnold, M. R. Reynolds, K. Wang, E. A. Magnuson, S. J. Baron, K. M. Chinnakondepalli, M. J. Reardon, P. N. Tadros, G. L. Zorn, B. Maini, M. A. Mumtaz, J. M. Brown, R. M. Kipperman, D. H. Adams, J. J. Popma and D. J. Cohen, 'Health status after transcatheter or surgical aortic valve replacement in patients with severe aortic stenosis at increased surgical risk: Results from the corevalve us pivotal trial', *JACC Cardiovasc Interv*, vol. 8, no. 9, pp. 1207–1217, 2015.

[59] M. J. Reardon, N. M. Van Mieghem, J. J. Popma, N. S. Kleiman, L. Sondergaard, M. Mumtaz, D. H. Adams, G. M. Deeb, B. Maini, H. Gada, S. Chetcuti, T. Gleason, J. Heiser, R. Lange, W. Merhi, J. K. Oh, P. S. Olsen, N. Piazza, M. Williams, S. Windecker, S. J. Yakubov, E. Grube, R. Makkar, J. S. Lee, J. Conte, E. Vang, H. Nguyen, Y. Chang, A. S. Mugglin, P. W. Serruys and A. P. Kappetein, 'Surgical or transcatheter aortic-valve replacement in intermediate-risk patients', *N Engl J Med*, vol. 376, no. 14, pp. 1321–1331, 2017.

[60] H. G. Thyregod, D. A. Steinbruchel, N. Ihlemann, H. Nissen, B. J. Kjeldsen, P. Petursson, Y. Chang, O. W. Franzen, T. Engstrom, P. Clemmensen, P. B. Hansen, L. W. Andersen, P. S. Olsen and L. Sondergaard, 'Transcatheter versus surgical aortic valve replacement in patients with severe aortic valve stenosis: 1-year results from the all-comers notion randomized clinical trial', *J Am Coll Cardiol*, vol. 65, no. 20, pp. 2184–94, 2015.

[61] H. G. H. Thyregod, N. Ihlemann, T. H. Jorgensen, H. Nissen, B. J. Kjeldsen, P. Petursson, Y. Chang, O. W. Franzen, T. Engstrom, P. Clemmensen, P. B. Hansen, L. W. Andersen, D. A. Steinbruchel, P. S. Olsen and L. Sondergaard, 'Five-year clinical and echocardiographic outcomes from the nordic aortic valve intervention (notion) randomized clinical trial in lower surgical risk patients', *Circulation*, 2019.

[62] L. Sondergaard, D. A. Steinbruchel, N. Ihlemann, H. Nissen, B. J. Kjeldsen, P. Petursson, A. T. Ngo, N. T. Olsen, Y. Chang, O. W. Franzen, T. Engstrom, P. Clemmensen, P. S. Olsen and H. G. Thyregod, 'Two-year outcomes in patients with severe aortic valve stenosis randomized to transcatheter versus surgical aortic valve replacement: The all-comers nordic aortic valve intervention randomized clinical trial', *Circ Cardiovasc Interv*, vol. 9, no. 6, 2016.

[63] H. G. Thyregod, D. A. Steinbruchel, N. Ihlemann, T. A. Ngo, H. Nissen, B. J. Kjeldsen, Y. Chang, P. B. Hansen, P. S. Olsen and L. Sondergaard, 'No clinical effect of prosthesis-patient mismatch after transcatheter versus surgical aortic valve replacement in intermediate- and low-risk patients with severe aortic valve stenosis at mid-term follow-up: An analysis from the notion trial', *Eur J Cardiothorac Surg*, vol. 50, no. 4, pp. 721–728, 2016.

[64] S. R. Kapadia, M. B. Leon, R. R. Makkar, E. M. Tuzcu, L. G. Svensson, S. Kodali, J. G. Webb, M. J. Mack, P. S. Douglas, V. H. Thourani, V. C. Babaliaros, H. C. Herrmann, W. Y. Szeto, A. D. Pichard, M. R. Williams, G. P. Fontana, D. C. Miller, W. N. Anderson, J. J. Akin, M. J. Davidson and C. R. Smith, '5-year outcomes of transcatheter aortic valve replacement compared with standard treatment for patients with inoperable aortic stenosis (partner 1): A randomised controlled trial', *Lancet*, vol. 385, no. 9986, pp. 2485–91, 2015.

[65] S. R. Kapadia, E. M. Tuzcu, R. R. Makkar, L. G. Svensson, S. Agarwal, S. Kodali, G. P. Fontana, J. G. Webb, M. Mack, V. H. Thourani, V. C. Babaliaros, H. C. Herrmann, W. Szeto, A. D. Pichard, M. R. Williams, W. N. Anderson, J. J. Akin, D. C. Miller, C. R. Smith and M. B. Leon, 'Long-term outcomes of inoperable patients with aortic stenosis randomly assigned to transcatheter aortic valve replacement or standard therapy', *Circulation*, vol. 130, no. 17, pp. 1483–92, 2014.

[66] M. B. Leon, C. R. Smith, M. Mack, D. C. Miller, J. W. Moses, L. G. Svensson, E. M. Tuzcu, J. G. Webb, G. P. Fontana, R. R. Makkar, D. L. Brown, P. C. Block, R. A. Guyton, A. D. Pichard, J. E. Bavaria, H. C. Herrmann, P. S. Douglas, J. L. Petersen, J. J. Akin, W. N. Anderson, D. Wang and S. Pocock, 'Transcatheter aortic-valve implantation for aortic stenosis in patients who cannot undergo surgery', *N Engl J Med*, vol. 363, no. 17, pp. 1597–607, 2010.

[67] R. R. Makkar, G. P. Fontana, H. Jilaihawi, S. Kapadia, A. D. Pichard, P. S. Douglas, V. H. Thourani, V. C. Babaliaros, J. G. Webb, H. C. Herrmann, J. E. Bavaria, S. Kodali, D. L. Brown, B. Bowers, T. M. Dewey, L. G. Svensson, M. Tuzcu, J. W. Moses, M. R. Williams, R. J. Siegel, J. J. Akin, W. N. Anderson, S. Pocock, C. R. Smith and M. B. Leon, 'Transcatheter aortic-valve replacement for inoperable severe aortic stenosis', *N Engl J Med*, vol. 366, no. 18, pp. 1696–704, 2012.

[68] C. R. Smith, M. B. Leon, M. J. Mack, D. C. Miller, J. W. Moses, L. G. Svensson, E. M. Tuzcu, J. G. Webb, G. P. Fontana, R. R. Makkar, M. Williams, T. Dewey, S. Kapadia, V. Babaliaros, V. H. Thourani, P. Corso, A. D. Pichard, J. E. Bavaria, H. C. Herrmann, J. J. Akin, W. N. Anderson, D. Wang and S. J. Pocock, 'Transcatheter versus surgical aortic-valve replacement in high-risk patients', *New England Journal of Medicine*, vol. 364, no. 23, pp. 2187–2198, 2011.

[69] M. J. Mack, M. B. Leon, V. H. Thourani, R. Makkar, S. K. Kodali, M. Russo, S. R. Kapadia, S. C. Malaisrie, D. J. Cohen, P. Pibarot, J. Leipsic, R. T. Hahn, P. Blanke, M. R. Williams, J. M. McCabe, D. L. Brown, V. Babaliaros, S. Goldman, W. Y. Szeto, P. Genereux, A. Pershad, S. J. Pocock, M. C. Alu, J. G. Webb and C. R. Smith, 'Transcatheter aortic-valve replacement with a balloon-expandable valve in low-risk patients', *New England Journal of Medicine*, vol. 0, no. 0, null,

[70] A. Vahanian, O. Alfieri, F. Andreotti, M. J. Antunes, G. Barón-Esquivias, H. Baumgartner, M. A. Borger, T. P. Carrel, M. De Bonis, A. Evangelista, V. Falk, B. Iung, P. Lancellotti, L. Pierard, S. Price, H.-J. Schäfers, G. Schuler, J. Stepinska, K. Swedberg, J. Takkenberg, U. O. Von Oppell, S. Windecker, J. L. Zamorano, M. Zembala, J. J. Bax, H. Baumgartner, C. Ceconi, V. Dean, C. Deaton, R. Fagard, C. Funck-Brentano, D. Hasdai, A. Hoes, P. Kirchhof, J. Knuuti, P. Kolh, T. McDonagh, C. Moulin, B. A. Popescu, Ž. Reiner, U. Sechtem, P. A. Sirnes, M. Tendera, A. Torbicki, A. Vahanian, S. Windecker, B. A. Popescu, L. Von Segesser, L. P. Badano, M. Bunc, M. J. Claeys, N. Drinkovic, G. Filippatos, G. Habib, A. P. Kappetein, R. Kassab, G. Y. H. Lip, N. Moat, G. Nickenig, C. M. Otto, J. Pepper, N. Piazza, P. G. Pieper, R. Rosenhek, N. Shuka, E. Schwammenthal, J. Schwitter, P. T. Mas, P. T. Trindade and T. Walther, 'Guidelines on the management of valvular heart disease (version 2012)the joint task force on the management of valvular heart disease of the european society of cardiology (esc) and the european association for cardio-thoracic surgery (eacts)', *European Heart Journal*, vol. 33, no. 19, pp. 2451–2496, 2012.

[71] B. A. Carabello, 'Should severe aortic stenosis be operated on before symptom onset? aortic valve replacement should be operated on before symptom onset', *Circulation*, vol. 126, no. 1, pp. 112–7, 2012.

[72] P. K. Shah, 'Should severe aortic stenosis be operated on before symptom onset? severe aortic stenosis should not be operated on before symptom onset', *Circulation*, vol. 126, no. 1, pp. 118–25, 2012.

[73] T. Taniguchi, T. Morimoto, H. Shiomi, K. Ando, N. Kanamori, K. Murata, T. Kitai, Y. Kawase, C. Izumi, T. Kato, K. Ishii, K. Nagao, Y. Nakagawa, M. Toyofuku, N. Saito, K. Minatoya, T. Kimura and C. A. R. Investigators, 'Sudden death in patients with severe aortic stenosis: Observations from the current as registry', *Journal of the American Heart Association*, vol. 7, no. 11, e008397, 2018.

[74] D. H. Kang, S. J. Park, J. H. Rim, S. C. Yun, D. H. Kim, J. M. Song, S. J. Choo, S. W. Park, J. K. Song, J. W. Lee and P. W. Park, 'Early surgery versus conventional treatment in asymptomatic very severe aortic stenosis', *Circulation*, vol. 121, no. 13, pp. 1502–9, 2010.

[75] D. T. Murphy, P. Blanke, S. Alaamri, C. Naoum, R. Rubinshtein, G. Pache, B. Precious, A. Berger, R. Raju, D. Dvir, D. A. Wood, J. Webb and J. A. Leipsic, 'Dynamism of the aortic annulus: Effect of diastolic versus systolic ct annular measurements on device selection in transcatheter aortic valve replacement (tavr)', *J Cardiovasc Comput Tomogr*, vol. 10, no. 1, pp. 37–43, 2016.

[76] O. Husser, A. Holzamer, M. Resch, D. H. Endemann, J. Nunez, V. Bodi, C. Schmid, G. A. J. Riegger, H. Gössmann, O. Hamer, C. Stroszczynski, A. Luchner, M. Hilker and C. Hengstenberg, 'Prosthesis sizing for transcatheter aortic valve implantation — comparison of three dimensional transesophageal echocardiography with multislice computed tomography', *International Journal of Cardiology*, vol. 168, no. 4, pp. 3431–3438, 2013.

[77] O. K. Khalique, S. K. Kodali, J. M. Paradis, T. M. Nazif, M. R. Williams, A. J. Einstein, G. D. Pearson, K. Harjai, K. Grubb, I. George, M. B. Leon and R. T. Hahn, 'Aortic annular sizing using a novel 3-dimensional echocardiographic method: Use and comparison with cardiac computed tomography', *Circ Cardiovasc Imaging*, vol. 7, no. 1, pp. 155–63, 2014.

[78] M. Gumsheimer, S. Stortecky, B. Gahl, B. Langhammer, T. Carrel, L. Buellesfeld, C. Huber and H. Most, 'Validation of 3d-reconstructed computed tomography images using osirix(r) software for pre-transcatheter aortic valve implantation aortic annulus sizing', *Interact Cardiovasc Thorac Surg*, vol. 25, no. 2, pp. 198–205, 2017.

[79] S. Stortecky, D. Heg, S. Gloekler, P. Wenaweser, S. Windecker and L. Buellesfeld, 'Accuracy and reproducibility of aortic annulus sizing using a dedicated three-dimensional computed tomography reconstruction tool in patients evaluated for transcatheter aortic valve replacement', *EuroIntervention*, vol. 10, no. 3, pp. 339–46, 2014.

[80] T. Podlesnikar, E. A. Prihadi, P. J. van Rosendael, E. M. Vollema, F. van der Kley, A. de Weger, N. Ajmone Marsan, F. Naji, Z. Fras, J. J. Bax and V. Delgado, 'Influence of the quantity of aortic valve calcium on the agreement between automated 3-dimensional transesophageal echocardiography and multidetector row computed tomography for aortic annulus sizing', *The American Journal of Cardiology*, vol. 121, no. 1, pp. 86–93, 2018.

[81] A. Mediratta, K. Addetia, D. Medvedofsky, R. J. Schneider, E. Kruse, A. P. Shah, S. Nathan, J. D. Paul, J. E. Blair, T. Ota, H. H. Balkhy, A. R. Patel, V. Mor-Avi and R. M. Lang, '3d echocardiographic analysis of aortic annulus for transcatheter aortic valve replacement using novel aortic valve quantification software: Comparison with computed tomography', *Echocardiography*, vol. 34, no. 5, pp. 690–699, 2017.

[82] E. A. Prihadi, P. J. van Rosendael, E. M. Vollema, J. J. Bax, V. Delgado and N. Ajmone Marsan, 'Feasibility, accuracy, and reproducibility of aortic annular and root sizing for transcatheter aortic valve replacement using novel automated three-dimensional echocardiographic software: Comparison with multi–detector row computed tomography', *Journal of the American Society of Echocardiography*, vol. 31, no. 4, 505–514.e3, 2018.

[83] S. Queirós, P. Morais, C. Dubois, J.-U. Voigt, W. Fehske, A. Kuhn, T. Achenbach, J. C. Fonseca, J. L. Vilaça and J. D'Hooge, 'Validation of a novel software tool for automatic aortic annular sizing in three-dimensional transesophageal echocardiographic images', *Journal of the American Society of Echocardiography*, vol. 31, no. 4, 515–525.e5, 2018.

[84] H. Jilaihawi, N. Doctor, M. Kashif, T. Chakravarty, A. Rafique, M. Makar, A. Furugen, M. Nakamura, J. Mirocha, M. Gheorghiu, J. Stegic, K. Okuyama, D. J. Sullivan, R. Siegel, J. K. Min, S. V. Gurudevan, G. P. Fontana, W. Cheng, G. Friede, T. Shiota and R. R. Makkar, 'Aortic annular sizing for transcatheter aortic valve replacement using cross-sectional 3-dimensional transesophageal echocardiography', *Journal of the American College of Cardiology*, vol. 61, no. 9, pp. 908–916, 2013.

[85] A. C. T. Ng, V. Delgado, F. van der Kley, M. Shanks, N. R. L. van de Veire, M. Bertini, G. Nucifora, R. J. van Bommel, L. F. Tops, A. de Weger, G. Tavilla, A. de Roos, L. J. Kroft, D. Y. Leung, J. Schuijf, M. J. Schalij and J. J. Bax, 'Comparison of aortic root dimensions and geometries before and after transcatheter aortic valve implantation by 2- and 3-dimensional transesophageal echocardiography and multislice computed tomography;clinical perspective', *Circulation: Cardiovascular Imaging*, vol. 3, no. 1, p. 94, 2010.

[86] W. Tsang, M. G. Bateman, L. Weinert, G. Pellegrini, V. Mor-Avi, L. Sugeng, H. Yeung, A. R. Patel, A. J. Hill, P. A. Iaizzo and R. M. Lang, 'Accuracy of aortic annular measurements obtained from three-dimensional echocardiography, ct and mri: Human in vitro and in vivo studies', *Heart*, vol. 98, no. 15, pp. 1146–52, 2012.

[87] B. Vaquerizo, M. Spaziano, J. Alali, D. Mylote, P. Theriault-Lauzier, R. Alfagih, G. Martucci, J. Buithieu and N. Piazza, 'Three-dimensional echocardiography vs. computed tomography for transcatheter aortic valve replacement sizing', *European Heart Journal Cardiovascular Imaging*, vol. 17, no. 1, pp. 15–23, 2016.

[88] P. Bernhardt, C. Rodewald, J. Seeger, B. Gonska, D. Buckert, M. Radermacher, V. Hombach, W. Rottbauer and J. Wohrle, 'Non-contrast-enhanced magnetic resonance angiography is equal to contrast-enhanced multislice computed tomography for correct aortic sizing before transcatheter aortic valve implantation', *Clin Res Cardiol*, vol. 105, no. 3, pp. 273–8, 2016.

[89] J. J. Popma, T. G. Gleason, S. J. Yakubov, J. K. Harrison, J. K. Forrest, B. Maini, C. E. Ruiz, D. S. Pinto, M. Costa, J. Resar, J. Conte, J. Crestanello, Y. Chang, J. K. Oh, M. J. Reardon and D. H. Adams, 'Relationship of annular sizing using multidetector computed tomographic imaging and clinical outcomes after self-expanding corevalve transcatheter aortic valve replacement', *Circ Cardiovasc Interv*, vol. 9, no. 7, 2016.

[90] S. H. Ewe, A. C. Ng, J. D. Schuijf, F. van der Kley, A. Colli, M. Palmen, A. de Weger, N. A. Marsan, E. R. Holman, A. de Roos, M. J. Schalij, J. J. Bax and V. Delgado, 'Location and severity of aortic valve calcium and implications for aortic regurgitation after transcatheter aortic valve implantation', *Am J Cardiol*, vol. 108, no. 10, pp. 1470–7, 2011.

[91] R. Koos, A. H. Mahnken, G. Dohmen, K. Brehmer, R. W. Gunther, R. Autschbach, N. Marx and R. Hoffmann, 'Association of aortic valve calcification severity with the degree of aortic regurgitation after transcatheter aortic valve implantation', *Int J Cardiol*, vol. 150, no. 2, pp. 142–5, 2011.

[92] A. Dashkevich, P. Blanke, M. Siepe, G. Pache, M. Langer, C. Schlensak and F. Beyersdorf, 'Preoperative assessment of aortic annulus dimensions: Comparison of noninvasive and intraoperative measurement', *Ann Thorac Surg*, vol. 91, no. 3, pp. 709–14, 2011.

[93] T. Walther, H. Möllmann, A. van Linden and J. Kempfert, 'Transcatheter aortic valve implantation transapical: Step by step', *Seminars in Thoracic and Cardiovascular Surgery*, vol. 23, no. 1, pp. 55–61, 2011.

[94] C. Bleakley and M. J. Monaghan, 'The pivotal role of imaging in tavr procedures', *Curr Cardiol Rep*, vol. 20, no. 2, p. 9, 2018.

[95] I. Sherifi, A. M. S. Omar, M. Varghese, M. Weiner, A. Anyanwu, J. C. Kovacic, S. Sharma, A. Kini and P. P. Sengupta, ‘Comparison of transesophageal and transthoracic echocardiography under moderate sedation for guiding transcatheter aortic valve replacement’, *Echo Res Pract*, vol. 5, no. 2, pp. 79–87, 2018.

[96] P. Schoenhagen, U. Numburi, S. S. Halliburton, P. Aulbach, M. von Roden, M. Y. Desai, L. L. Rodriguez, S. R. Kapadia, E. M. Tuzcu and B. W. Lytle, ‘Three-dimensional imaging in the context of minimally invasive and transcatheter cardiovascular interventions using multidetector computed tomography: From pre-operative planning to intra-operative guidance’, *Eur Heart J*, vol. 31, no. 22, pp. 2727–40, 2010.

[97] J. V. Conte, J. Hermiller, J. R. Resar, G. M. Deeb, T. G. Gleason, D. H. Adams, J. J. Popma, S. J. Yakubov, D. Watson, J. Guo, G. L. Zorn and M. J. Reardon, ‘Complications after self-expanding transcatheter or surgical aortic valve replacement’, *Seminars in Thoracic and Cardiovascular Surgery*, vol. 29, no. 3, pp. 321–330, 2017.

[98] J. J. Popma, D. H. Adams, M. J. Reardon, S. J. Yakubov, N. S. Kleiman, D. Heimansohn, J. Hermiller, G. C. Hughes, J. K. Harrison, J. Coselli, J. Diez, A. Kafi, T. Schreiber, T. G. Gleason, J. Conte, M. Buchbinder, G. M. Deeb, B. Carabello, P. W. Serruys, S. Chenoweth and J. K. Oh, ‘Transcatheter aortic valve replacement using a self-expanding bioprosthesis in patients with severe aortic stenosis at extreme risk for surgery’, *Journal of the American College of Cardiology*, vol. 63, no. 19, pp. 1972–1981, 2014.

[99] T. G. Gleason, J. T. Schindler, D. H. Adams, M. J. Reardon, N. S. Kleiman, L. R. Caplan, J. V. Conte, G. M. Deeb, J. Hughes G. C., S. Chenoweth and J. J. Popma, ‘The risk and extent of neurologic events are equivalent for high-risk patients treated with transcatheter or surgical aortic valve replacement’, in *J Thorac Cardiovasc Surg*, vol. 152, 2016, pp. 85–96.

[100] U. Gerckens, C. Tamburino, S. Bleiziffer, J. Bosmans, P. Wenaweser, S. Brecker, J. Guo and A. Linke, ‘Final 5-year clinical and echocardiographic results for treatment of severe aortic stenosis with a self-expanding bioprosthesis from the advance study’, *European Heart Journal*, vol. 38, no. 36, pp. 2729–2738, 2017.

[101] J. J. Popma, G. M. Deeb, S. J. Yakubov, M. Mumtaz, H. Gada, D. O'Hair, T. Bajwa, J. C. Heiser, W. Merhi, N. S. Kleiman, J. Askew, P. Sorajja, J. Rovin, S. J. Chetcuti, D. H. Adams, P. S. Teirstein, G. L. Zorn, J. K. Forrest, D. Tchétché, J. Resar, A. Walton, N. Piazza, B. Ramlawi, N. Robinson, G. Petrossian, T. G. Gleason, J. K. Oh, M. J. Boulware, H. Qiao, A. S. Mugglin and M. J. Reardon, 'Transcatheter aortic-valve replacement with a self-expanding valve in low-risk patients', *New England Journal of Medicine*, vol. 0, no. 0, null,

[102] G. Athappan, E. Patvardhan, E. M. Tuzcu, L. G. Svensson, P. A. Lemos, C. Fraccaro, G. Tarantini, J. M. Sinning, G. Nickenig, D. Capodanno, C. Tamburino, A. Latib, A. Colombo and S. R. Kapadia, 'Incidence, predictors, and outcomes of aortic regurgitation after transcatheter aortic valve replacement: Meta-analysis and systematic review of literature', *J Am Coll Cardiol*, vol. 61, no. 15, pp. 1585–95, 2013.

[103] W. Klimek-Piotrowska, M. K. Holda, M. Koziej, K. Salapa, K. Piatek and J. Holda, 'Geometry of koch's triangle', *Europace*, vol. 19, no. 3, pp. 452–457, 2017.

[104] T. Kawashima and H. Sasaki, 'A macroscopic anatomical investigation of atrioventricular bundle locational variation relative to the membranous part of the ventricular septum in elderly human hearts', *Surg Radiol Anat*, vol. 27, no. 3, pp. 206–13, 2005.

[105] ——, 'Gross anatomy of the human cardiac conduction system with comparative morphological and developmental implications for human application', *Ann Anat*, vol. 193, no. 1, pp. 1–12, 2011.

[106] A. D. Kistin, 'Observations on the anatomy of the atrioventricular bundle (bundle of his) and the question of other muscular atrioventricular connections in normal human hearts', *Am Heart J*, vol. 37, no. 6, pp. 847–67, 1949.

[107] N. Piazza, Y. Onuma, E. Jesserun, P. P. Kint, A. M. Maugenest, R. H. Anderson, P. P. de Jaegere and P. W. Serruys, 'Early and persistent intraventricular conduction abnormalities and requirements for pacemaking after percutaneous replacement of the aortic valve', *JACC Cardiovasc Interv*, vol. 1, no. 3, pp. 310–6, 2008.

[108] M. Brignole, A. Auricchio, G. Baron-Esquivias, P. Bordachar, G. Boriani, O. A. Breithardt, J. Cleland, J. C. Deharo, V. Delgado, P. M. Elliott, B. Gorenek, C. W. Israel, C. Leclercq, C. Linde, L. Mont, L. Padeletti, R. Sutton and P. E. Vardas, '2013 esc guidelines on cardiac pacing and cardiac resynchronization therapy: The task force on cardiac pacing and resynchronization therapy of the european society of cardiology (esc). developed in collaboration with the european

heart rhythm association (ehra)', *Europace*, vol. 15, no. 8, pp. 1070–118, 2013.

[109] A. E. Epstein, J. P. DiMarco, K. A. Ellenbogen, 3. Estes N. A., R. A. Freedman, L. S. Gettes, A. M. Gillinov, G. Gregoratos, S. C. Hammill, D. L. Hayes, M. A. Hlatky, L. K. Newby, R. L. Page, M. H. Schoenfeld, M. J. Silka, L. W. Stevenson, M. O. Sweeney, C. M. Tracy, A. E. Epstein, D. Darbar, J. P. DiMarco, S. B. Dunbar, 3. Estes N. A., J. Ferguson T. B., S. C. Hammill, P. E. Karasik, M. S. Link, J. E. Marine, M. H. Schoenfeld, A. J. Shanker, M. J. Silka, L. W. Stevenson, W. G. Stevenson and P. D. Varosy, '2012 accf/aha/hrs focused update incorporated into the accf/aha/hrs 2008 guidelines for device-based therapy of cardiac rhythm abnormalities: A report of the american college of cardiology foundation/american heart association task force on practice guidelines and the heart rhythm society', *J Am Coll Cardiol*, vol. 61, no. 3, e6–75, 2013.

[110] K. Boerlage-Van Dijk, K. M. Kooiman, Z. Y. Yong, E. M. Wiegerinck, P. Damman, B. J. Bouma, J. G. Tijssen, J. J. Piek, R. E. Knops and J. Baan J., 'Predictors and permanency of cardiac conduction disorders and necessity of pacing after transcatheter aortic valve implantation', *Pacing Clin Electrophysiol*, vol. 37, no. 11, pp. 1520–9, 2014.

[111] N. Dumonteil, I. T. Meredith, D. J. Blackman, D. Tchetche, D. Hildick-Smith, M. S. Spence, D. L. Walters, J. Harnek, S. G. Worthley, G. Rioufol, T. Lefevre, T. Modine, N. Van Mieghem, V. M. Houle, D. J. Allocco and K. D. Dawkins, 'Insights into the need for permanent pacemaker following implantation of the repositionable lotus valve for transcatheter aortic valve replacement in 250 patients: Results from the reprise ii trial with extended cohort', *EuroIntervention*, vol. 13, no. 7, pp. 796–803, 2017.

[112] O. O. Fadahunsi, A. Olowoyeye, A. Ukaigwe, Z. Li, A. N. Vora, S. Vemulapalli, E. Elgin and A. Donato, 'Incidence, predictors, and outcomes of permanent pacemaker implantation following transcatheter aortic valve replacement: Analysis from the u.s. society of thoracic surgeons/american college of cardiology tvt registry', *JACC Cardiovasc Interv*, vol. 9, no. 21, pp. 2189–2199, 2016.

[113] B. Fujita, M. Kutting, M. Seiffert, S. Scholtz, S. Egron, E. Prashovikj, J. Borgermann, T. Schafer, W. Scholtz, R. Preuss, J. Gummert, U. Steinseifer and S. M. Ensminger, 'Calcium distribution patterns of the aortic valve as a risk factor for the need of permanent pacemaker implantation after transcatheter aortic valve implantation', *Eur Heart J Cardiovasc Imaging*, vol. 17, no. 12, pp. 1385–1393, 2016.

[114] C. S. Gensas, A. Caixeta, D. Siqueira, L. A. Carvalho, R. Sarmento-Leite, J. A. Mangione, P. A. Lemos, A. S. Colafranceschi, P. Caramori, M. C. Ferreira, A. Abizaid and J. Brito F. S., 'Predictors of permanent pacemaker requirement after transcatheter aortic valve implantation: Insights from a brazilian registry', *Int J Cardiol*, vol. 175, no. 2, pp. 248–52, 2014.

[115] B. Gonska, J. Seeger, M. Kessler, A. von Keil, W. Rottbauer and J. Wohrle, 'Predictors for permanent pacemaker implantation in patients undergoing transfemoral aortic valve implantation with the edwards sapien 3 valve', *Clin Res Cardiol*, vol. 106, no. 8, pp. 590–597, 2017.

[116] M. Kessler, B. Gonska, J. Seeger, W. Rottbauer and J. Wohrle, 'Predictors of permanent pacemaker implantation after transfemoral aortic valve implantation with the lotus valve', *Am Heart J*, vol. 192, pp. 57–63, 2017.

[117] G. D. Lenders, V. Collas, J. M. Hernandez, V. Legrand, H. D. Danenberg, P. den Heijer, I. E. Rodrigus, B. P. Paelinck, C. J. Vrints and J. M. Bosmans, 'Depth of valve implantation, conduction disturbances and pacemaker implantation with corevalve and corevalve accutrak system for transcatheter aortic valve implantation, a multi-center study', *Int J Cardiol*, vol. 176, no. 3, pp. 771–5, 2014.

[118] J. Lopez-Aguilera, J. M. Segura Saint-Gerons, F. Mazuelos Bellido, J. Suarez de Lezo, S. Ojeda Pineda, M. Pan Alvarez-Ossorio, M. A. Romero Moreno, D. Pavlovic, S. Espejo Perez and J. Suarez de Lezo, 'Atrioventricular conduction changes after corevalve transcatheter aortic valve implantation', *Rev Esp Cardiol (Engl Ed)*, vol. 69, no. 1, pp. 28–36, 2016.

[119] A. Maan, M. M. Refaat, E. K. Heist, J. Passeri, I. Inglessis, L. Ptaszek, G. Vlahakes, J. N. Ruskin, I. Palacios, T. Sundt and M. Mansour, 'Incidence and predictors of pacemaker implantation in patients undergoing transcatheter aortic valve replacement', *Pacing Clin Electrophysiol*, vol. 38, no. 7, pp. 878–86, 2015.

[120] V. Mauri, A. Reimann, D. Stern, M. Scherner, E. Kuhn, V. Rudolph, S. Rosenkranz, K. Eghbalzadeh, K. Friedrichs, T. Wahlers, S. Baldus, N. Madershahian and T. K. Rudolph, 'Predictors of permanent pacemaker implantation after transcatheter aortic valve replacement with the sapien 3', *JACC Cardiovasc Interv*, vol. 9, no. 21, pp. 2200–2209, 2016.

[121] C. Monteiro, A. D. L. Ferrari, P. R. A. Caramori, L. A. F. Carvalho, D. A. A. Siqueira, L. Thiago, M. Perin, V. C. Lima, E. Guerios and F. S. Brito Junior, 'Permanent pacing after transcatheter aortic valve implantation: Incidence, predictors and evolution of left ventricular function', *Arq Bras Cardiol*, vol. 109, no. 6, pp. 550–559, 2017.

[122] T. M. Nazif, J. M. Dizon, R. T. Hahn, K. Xu, V. Babaliaros, P. S. Douglas, M. F. El-Chami, H. C. Herrmann, M. Mack, R. R. Makkar, D. C. Miller, A. Pichard, E. M. Tuzcu, W. Y. Szeto, J. G. Webb, J. W. Moses, C. R. Smith, M. R. Williams, M. B. Leon and S. K. Kodali, 'Predictors and clinical outcomes of permanent pacemaker implantation after transcatheter aortic valve replacement: The partner (placement of aortic transcatheter valves) trial and registry', *JACC Cardiovasc Interv*, vol. 8, no. 1 Pt A, pp. 60–9, 2015.

[123] C. A. Raelson, J. Gabriels, J. Ruan, J. E. Ip, G. Thomas, C. F. Liu, J. W. Cheung, B. B. Lerman, A. Patel and S. M. Markowitz, 'Recovery of atrioventricular conduction in patients with heart block after transcatheter aortic valve replacement', *J Cardiovasc Electrophysiol*, vol. 28, no. 10, pp. 1196–1202, 2017.

[124] G. C. Siontis, P. Juni, T. Pilgrim, S. Stortecky, L. Bullesfeld, B. Meier, P. Wenaweser and S. Windecker, 'Predictors of permanent pacemaker implantation in patients with severe aortic stenosis undergoing tavr: A meta-analysis', *J Am Coll Cardiol*, vol. 64, no. 2, pp. 129–40, 2014.

[125] S. Zaman, L. McCormick, R. Gooley, H. Rashid, S. Ramkumar, D. Jackson, S. Hui and I. T. Meredith, 'Incidence and predictors of permanent pacemaker implantation following treatment with the repositionable lotus transcatheter aortic valve', *Catheter Cardiovasc Interv*, vol. 90, no. 1, pp. 147–154, 2017.

[126] L. Gaede, W. K. Kim, C. Liebetrau, O. Dorr, J. Sperzel, J. Blumenstein, A. Berkowitsch, T. Walther, C. Hamm, A. Elsasser, H. Nef and H. Mollmann, 'Pacemaker implantation after tavi: Predictors of av block persistence', *Clin Res Cardiol*, vol. 107, no. 1, pp. 60–69, 2018.

[127] O. Husser, C. Pellegrini, T. Kessler, C. Burgdorf, H. Thaller, N. P. Mayr, A. M. Kasel, A. Kastrati, H. Schunkert and C. Hengstenberg, 'Predictors of permanent pacemaker implantations and new-onset conduction abnormalities with the sapien 3 balloon-expandable transcatheter heart valve', *JACC Cardiovasc Interv*, vol. 9, no. 3, pp. 244–254, 2016.

[128] A. Hamdan, V. Guetta, R. Klempfner, E. Konen, E. Raanani, M. Glikson, O. Goitein, A. Segev, I. Barbash, P. Fefer, D. Spiegelstein, I. Goldenberg and E. Schwammenthal, 'Inverse relationship between membranous septal length and the risk of atrioventricular block in patients undergoing transcatheter aortic valve implantation', *JACC Cardiovasc Interv*, vol. 8, no. 9, pp. 1218–1228, 2015.

[129] R. Hein-Rothweiler, D. Jochheim, K. Rizas, A. Egger, H. Theiss, A. Bauer, S. Massberg and J. Mehilli, 'Aortic annulus to left coronary distance as a predictor for persistent left bundle branch block after tavi', *Catheter Cardiovasc Interv*, vol. 89, no. 4, E162–e168, 2017.

[130] Y. Maeno, Y. Abramowitz, H. Kawamori, Y. Kazuno, S. Kubo, N. Takahashi, G. Mangat, K. Okuyama, M. Kashif, T. Chakravarty, M. Nakamura, W. Cheng, J. Friedman, D. Berman, R. R. Makkar and H. Jilaihawi, 'A highly predictive risk model for pacemaker implantation after tavr', *JACC Cardiovasc Imaging*, vol. 10, no. 10 Pt A, pp. 1139–1147, 2017.

[131] J. G. Almeida, S. M. Ferreira, P. Fonseca, T. Dias, C. Guerreiro, A. R. Barbosa, P. Teixeira, M. Carvalho, W. Ferreira, N. D. Ferreira, M. Oliveira, H. Goncalves, P. Braga, J. Ribeiro, J. Primo and V. G. Ribeiro, 'Association between implantation depth assessed by computed tomography and new-onset conduction disturbances after transcatheter aortic valve implantation', *J Cardiovasc Comput Tomogr*, vol. 11, no. 5, pp. 332–337, 2017.

[132] L. van Gils, D. Tchetche, T. Lhermusier, M. Abawi, N. Dumonteil, R. Rodriguez Olivares, J. Molina-Martin de Nicolas, P. R. Stella, D. Carrie, P. P. De Jaegere and N. M. Van Mieghem, 'Transcatheter heart valve selection and permanent pacemaker implantation in patients with pre-existent right bundle branch block', *J Am Heart Assoc*, vol. 6, no. 3, 2017.

[133] G. Tarantini, V. Gasparetto, M. Napodano, C. Fraccaro, G. Gerosa and G. Isabella, 'Valvular leak after transcatheter aortic valve implantation: A clinician update on epidemiology, pathophysiology and clinical implications', *Am J Cardiovasc Dis*, vol. 1, no. 3, pp. 312–20, 2011.

[134] K. Yared, T. Garcia-Camarero, L. Fernandez-Friera, M. Llano, R. Durst, A. A. Reddy, W. W. O'Neill and M. H. Picard, 'Impact of aortic regurgitation after transcatheter aortic valve implantation: Results from the revival trial', *JACC Cardiovasc Imaging*, vol. 5, no. 5, pp. 469–77, 2012.

[135] K. Shibayama, H. Mihara, H. Jilaihawi, J. Berdejo, K. Harada, Y. Itabashi, R. Siegel, R. R. Makkar and T. Shiota, '3d assessment of features associated with transvalvular aortic regurgitation after tavr: A real-time 3d tee study', *JACC Cardiovasc Imaging*, vol. 9, no. 2, pp. 114–23, 2016.

[136] E. Altiok, M. Frick, C. G. Meyer, G. Al Ateah, A. Napp, A. Kirschfink, M. Almalla, S. Lotfi, M. Becker, L. Herich, W. Lehmacher and R. Hoffmann, 'Comparison of two- and three-dimensional transthoracic echocardiography to cardiac magnetic resonance imaging for assessment of paravalvular regurgitation after transcatheter aortic valve implantation', *Am J Cardiol*, vol. 113, no. 11, pp. 1859–66, 2014.

[137] A. P. Kappetein, S. J. Head, P. Genereux, N. Piazza, N. M. van Mieghem, E. H. Blackstone, T. G. Brott, D. J. Cohen, D. E. Cutlip, G. A. van Es, R. T. Hahn, A. J. Kirtane, M. W. Krucoff, S. Kodali, M. J. Mack, R. Mehran, J. Rodes-Cabau, P. Vranckx, J. G. Webb, S. Windecker, P. W. Serruys and M. B. Leon, 'Updated standardized endpoint definitions for transcatheter aortic valve implantation: The valve academic research consortium-2 consensus document (varc-2)', *Eur J Cardiothorac Surg*, vol. 42, no. 5, S45–60, 2012.

[138] G. R. Hartlage, V. C. Babaliaros, V. H. Thourani, S. Hayek, C. Chrysohoou, N. Ghasemzadeh, A. E. Stillman, S. D. Clements, J. N. Oshinski and S. Lerakis, 'The role of cardiovascular magnetic resonance in stratifying paravalvular leak severity after transcatheter aortic valve replacement: An observational outcome study', *J Cardiovasc Magn Reson*, vol. 16, p. 93, 2014.

[139] S. Orwat, G. P. Diller, G. Kaleschke, G. Kerckhoff, A. Kempny, R. M. Radke, B. Buerke, M. Burg, C. Schulke and H. Baumgartner, 'Aortic regurgitation severity after transcatheter aortic valve implantation is underestimated by echocardiography compared with mri', *Heart*, vol. 100, no. 24, pp. 1933–8, 2014.

[140] R. D. Sellers, M. J. Levy, K. Amplatz and C. W. Lillehei, 'Left retrograde cardioangiography in acquired cardiac disease: Technic, indications and interpretations in 700 cases', *Am J Cardiol*, vol. 14, pp. 437–47, 1964.

[141] M. Frick, C. G. Meyer, A. Kirschfink, E. Altiok, M. Lehrke, K. Brehmer, S. Lotfi and R. Hoffmann, 'Evaluation of aortic regurgitation after transcatheter aortic valve implantation: Aortic root angiography in comparison to cardiac magnetic resonance', *EuroIntervention*, vol. 11, no. 12, pp. 1419–27, 2016.

[142] M. A. Sherif, M. Abdel-Wahab, H. W. Beurich, B. Stocker, D. Zachow, V. Geist, R. Tolg and G. Richardt, 'Haemodynamic evaluation of aortic regurgitation after transcatheter aortic valve implantation using cardiovascular magnetic resonance', *EuroIntervention*, vol. 7, no. 1, pp. 57–63, 2011.

[143] W. A. Zoghbi, J. B. Chambers, J. G. Dumesnil, E. Foster, J. S. Gottdiener, P. A. Grayburn, B. K. Khandheria, R. A. Levine, G. R. Marx, J. Miller F. A., S. Nakatani, M. A. Quinones, H. Rakowski, L. L. Rodriguez, M. Swaminathan, A. D. Waggoner, N. J. Weissman and M. Zabalgoitia, 'Recommendations for evaluation of prosthetic valves with echocardiography and doppler ultrasound: A report from the american society of echocardiography's guidelines and standards committee and the task force on prosthetic valves, developed in conjunction with the american college of cardiology cardiovascular imaging committee, cardiac imaging committee of the american heart association, the european association of echocardiography, a registered branch of the european society of cardiology, the japanese society of echocardiography and the canadian society of echocardiography, endorsed by the american college of cardiology foundation, american heart association, european association of echocardiography, a registered branch of the european society of cardiology, the japanese society of echocardiography, and canadian society of echocardiography', *J Am Soc Echocardiogr*, vol. 22, no. 9, 975–1014, quiz 1082–4, 2009.

[144] W. A. Zoghbi, M. Enriquez-Sarano, E. Foster, P. A. Grayburn, C. D. Kraft, R. A. Levine, P. Nihoyannopoulos, C. M. Otto, M. A. Quinones, H. Rakowski, W. J. Stewart, A. Waggoner and N. J. Weissman, 'Recommendations for evaluation of the severity of native valvular regurgitation with two-dimensional and doppler echocardiography', *J Am Soc Echocardiogr*, vol. 16, no. 7, pp. 777–802, 2003.

[145] H. B. Ribeiro, F. Le Ven, E. Larose, A. Dahou, L. Nombela-Franco, M. Urena, R. Allende, I. Amat-Santos, L. Ricapito Mde, C. Thebault, M. A. Clavel, R. Delarochelliere, D. Doyle, E. Dumont, J. G. Dumesnil, P. Pibarot and J. Rodes-Cabau, 'Cardiac magnetic resonance versus transthoracic echocardiography for the assessment and quantification of aortic regurgitation in patients undergoing transcatheter aortic valve implantation', *Heart*, vol. 100, no. 24, pp. 1924–32, 2014.

[146] H. B. Ribeiro, S. Orwat, S. S. Hayek, E. Larose, V. Babaliaros, A. Dahou, F. Le Ven, S. Pasian, R. Puri, O. Abdul-Jawad Altisent, F. Campelo-Parada, M. A. Clavel, P. Pibarot, S. Lerakis, H. Baumgartner and J. Rodes-Cabau, 'Cardiovascular magnetic resonance to evaluate aortic regurgitation after transcatheter aortic valve replacement', *J Am Coll Cardiol*, vol. 68, no. 6, pp. 577–585, 2016.

[147] E. Salaun, A. Jacquier, A. Theron, R. Giorgi, M. Lambert, N. Jaussaud, S. Hubert, F. Collart, J. L. Bonnet, G. Habib, T. Cuisset and D. Grisoli, 'Value of cmr in quantification of paravalvular aortic regurgitation after tavi', *Eur Heart J Cardiovasc Imaging*, vol. 17, no. 1, pp. 41–50, 2016.

[148] J. M. Sinning, C. Hammerstingl, M. Vasa-Nicotera, V. Adenauer, S. J. Lema Cachiguango, A. C. Scheer, S. Hausen, A. Sedaghat, A. Ghanem, C. Muller, E. Grube, G. Nickenig and N. Werner, 'Aortic regurgitation index defines severity of peri-prosthetic regurgitation and predicts outcome in patients after transcatheter aortic valve implantation', *J Am Coll Cardiol*, vol. 59, no. 13, pp. 1134–41, 2012.

[149] J. M. Sinning, A. Stundl, S. Pingel, M. Weber, A. Sedaghat, C. Hammerstingl, M. Vasa-Nicotera, F. Mellert, W. Schiller, J. Kovac, A. Welz, E. Grube, N. Werner and G. Nickenig, 'Pre-procedural hemodynamic status improves the discriminatory value of the aortic regurgitation index in patients undergoing transcatheter aortic valve replacement', *JACC Cardiovasc Interv*, vol. 9, no. 7, pp. 700–11, 2016.

[150] P. Pibarot, R. T. Hahn, N. J. Weissman and M. J. Monaghan, 'Assessment of paravalvular regurgitation following tavr: A proposal of unifying grading scheme', *JACC Cardiovasc Imaging*, vol. 8, no. 3, pp. 340–60, 2015.

[151] R. T. Hahn, P. Pibarot, J. Webb, J. Rodes-Cabau, H. C. Herrmann, M. Williams, R. Makkar, W. Y. Szeto, M. L. Main, V. H. Thourani, E. M. Tuzcu, S. Kapadia, J. Akin, T. McAndrew, K. Xu, M. B. Leon and S. K. Kodali, 'Outcomes with post-dilation following transcatheter aortic valve replacement: The partner i trial (placement of aortic transcatheter valve)', *JACC: Cardiovascular Interventions*, vol. 7, no. 7, pp. 781–789, 2014.

[152] T. M. Waterbury, G. S. Reeder, S. V. Pislaru, A. K. Cabalka, C. S. Rihal and M. F. Eleid, 'Techniques and outcomes of paravalvular leak repair after transcatheter aortic valve replacement', *Catheter Cardiovasc Interv*, vol. 90, no. 5, pp. 870–877, 2017.

[153] O. F. Ali, C. Schultz, A. Jabbour, M. Rubens, T. Mittal, R. Mohiaddin, S. Davies, C. Di Mario, R. Van der Boon, A. S. Ahmad, M. Amrani, N. Moat, P. P. T. De Jaegere and M. Dalby, 'Predictors of paravalvular aortic regurgitation following self-expanding medtronic corevalve implantation: The role of annulus size, degree of calcification, and balloon size during pre-implantation valvuloplasty and implant depth', *International Journal of Cardiology*, vol. 179, pp. 539–545, 2015.

[154] E. Y. Koh, K. Y. Lam, N. R. Bindraban, R. Cocchieri, R. N. Planken, K. T. Koch, J. Baan J., B. A. de Mol and H. A. Marquering, 'Aortic valve calcification as a predictor of location and severity of paravalvular regurgitation after transcatheter aortic valve implantation', *Interact Cardiovasc Thorac Surg*, vol. 20, no. 3, pp. 345–50, 2015.

[155] L. Azzalini, B. B. Ghoshhajra, S. Elmariah, J. J. Passeri, I. Inglessis, I. F. Palacios and S. Abbara, 'The aortic valve calcium nodule score (avcns) independently predicts paravalvular regurgitation after transcatheter aortic valve replacement (tavr)', *Journal of Cardiovascular Computed Tomography*, vol. 8, no. 2, pp. 131–140, 2014.

[156] R. Bekeredjian, D. Bodingbauer, N. P. Hofmann, S. Greiner, M. Schuetz, N. A. Geis, H. U. Kauczor, M. Bryant, E. Chorianopoulos, S. T. Pleger, D. Mereles, H. A. Katus and G. Korosoglou, 'The extent of aortic annulus calcification is a predictor of postprocedural eccentricity and paravalvular regurgitation: A pre- and postinterventional cardiac computed tomography angiography study', *J Invasive Cardiol*, vol. 27, no. 3, pp. 172–80, 2015.

[157] L. F. Di Martino, W. B. Vletter, B. Ren, C. Schultz, N. M. Van Mieghem, O. I. Soliman, M. Di Biase, P. P. de Jaegere and M. L. Geleijnse, 'Prediction of paravalvular leakage after transcatheter aortic valve implantation', *Int J Cardiovasc Imaging*, vol. 31, no. 7, pp. 1461–8, 2015.

[158] G. Feuchtner, F. Plank, T. Bartel, S. Mueller, J. Leipsic, T. Schachner, L. Müller, G. Friedrich, A. Klauser, M. Grimm and N. Bonaros, 'Prediction of paravalvular regurgitation after transcatheter aortic valve implantation by computed tomography: Value of aortic valve and annular calcification', *The Annals of Thoracic Surgery*, vol. 96, no. 5, pp. 1574–1580, 2013.

[159] P. Fonseca, B. Figueiredo, C. Almeida, J. Almeida, N. Bettencourt, F. Sampaio, N. Ferreira, H. Goncalves, P. Braga and V. G. Ribeiro, 'Aortic valve calcium volume predicts paravalvular regurgitation and the need for balloon post-dilatation after transcatheter aortic valve implantation', *J Interv Cardiol*, vol. 29, no. 1, pp. 117–23, 2016.

[160] B. E. Stahli, T. D. Nguyen-Kim, C. Gebhard, L. Erhart, T. Frauenfelder, F. C. Tanner, V. Falk, U. Landmesser, F. Nietlispach, T. F. Luscher, W. Maier and R. K. Binder, 'Prosthesis-specific predictors of paravalvular regurgitation after transcatheter aortic valve replacement: Impact of calcification and sizing on balloon-expandable versus self-expandable transcatheter heart valves', *J Heart Valve Dis*, vol. 24, no. 1, pp. 10–21, 2015.

[161] A. Unbehaun, M. Pasic, M. Kukucka, A. Mladenow, N. Solowjowa, S. Dreysse, T. Drews, A. Penkalla, R. Hetzer and S. Buz, 'Transapical aortic valve implantation: Predictors of leakage and impact on survival: An update', *The Annals of Thoracic Surgery*, vol. 98, no. 4, pp. 1308–1315, 2014.

[162] E. Van Belle, F. Juthier, S. Susen, A. Vincentelli, B. Iung, J. Dallongeville, H. Eltchaninoff, M. Laskar, P. Leprince, M. Lievre, C. Banfi, J. L. Auffray, C. Delhaye, P. Donzeau-Gouge, K. Chevreul, J. Fajadet, A. Leguerrier, A. Prat, M. Gilard and E. Teiger, 'Postprocedural aortic regurgitation in balloon-expandable and self-expandable transcatheter aortic valve replacement procedures: Analysis of predictors and impact on long-term mortality: Insights from the france2 registry', *Circulation*, vol. 129, no. 13, pp. 1415–27, 2014.

[163] K. Takagi, A. Latib, R. Al-Lamee, M. Mussardo, M. Montorfano, F. Maisano, C. Godino, A. Chieffo, O. Alfieri and A. Colombo, 'Predictors of moderate-to-severe paravalvular aortic regurgitation immediately after corevalve implantation and the impact of postdilatation', *Catheter Cardiovasc Interv*, vol. 78, no. 3, pp. 432–43, 2011.

[164] E. Sirois, Q. Wang and W. Sun, 'Fluid simulation of a transcatheter aortic valve deployment into a patient-specific aortic root', *Cardiovasc Eng Tech*, vol. 2, no. 3, pp. 186–195, 2011.

[165] Q. Wang, E. Sirois and W. Sun, 'Patient-specific modeling of biomechanical interaction in transcatheter aortic valve deployment', *J Biomech*, vol. 45, no. 11, pp. 1965–71, 2012.

[166] C. Capelli, G. M. Bosi, E. Cerri, J. Nordmeyer, T. Odenwald, P. Bonhoeffer, F. Migliavacca, A. M. Taylor and S. Schievano, 'Patient-specific simulations of transcatheter aortic valve stent implantation', *Med Biol Eng Comput*, vol. 50, no. 2, pp. 183–92, 2012.

[167] C. Russ, R. Hopf, S. Hirsch, S. Sundermann, V. Falk, G. Szekely and M. Gessat, 'Simulation of transcatheter aortic valve implantation under consideration of leaflet calcification', *Conf Proc IEEE Eng Med Biol Soc*, vol. 2013, pp. 711–4, 2013.

[168] F. Auricchio, M. Conti, S. Morganti and A. Reali, 'Simulation of transcatheter aortic valve implantation: A patient-specific finite element approach', *Comput Methods Biomech Biomed Engin*, vol. 17, no. 12, pp. 1347–57, 2014.

[169] S. Morganti, M. Conti, M. Aiello, A. Valentini, A. Mazzola, A. Reali and F. Auricchio, 'Simulation of transcatheter aortic valve implantation through patient-specific finite element analysis: Two clinical cases', *J Biomech*, vol. 47, no. 11, pp. 2547–55, 2014.

[170] P. S. Gunning, T. J. Vaughan and L. M. McNamara, 'Simulation of self expanding transcatheter aortic valve in a realistic aortic root: Implications of deployment geometry on leaflet deformation', *Ann Biomed Eng*, vol. 42, no. 9, pp. 1989–2001, 2014.

[171] Q. Wang, S. Kodali, C. Primiano and W. Sun, 'Simulations of transcatheter aortic valve implantation: Implications for aortic root rupture', *Biomech Model Mechanobiol*, vol. 14, no. 1, pp. 29–38, 2015.

[172] J. Bailey, N. Curzen and N. W. Bressloff, 'Assessing the impact of including leaflets in the simulation of tavi deployment into a patient-specific aortic root', *Comput Methods Biomech Biomed Engin*, vol. 19, no. 7, pp. 733–44, 2016.

[173] M. Bianchi, R. P. Ghosh, G. Marom, M. J. Slepian and D. Bluestein, 'Simulation of transcatheter aortic valve replacement in patient-specific aortic roots: Effect of crimping and positioning on device performance', *Conf Proc IEEE Eng Med Biol Soc*, vol. 2015, pp. 282–5, 2015.

[174] S. Morganti, N. Brambilla, A. S. Petronio, A. Reali, F. Bedogni and F. Auricchio, 'Prediction of patient-specific post-operative outcomes of tavi procedure: The impact of the positioning strategy on valve performance', *J Biomech*, vol. 49, no. 12, pp. 2513–9, 2016.

[175] C. J. Schultz, R. Rodriguez-Olivares, J. Bosmans, T. Lefèvre, G. De Santis, N. Bruining, V. Collas, T. Dezutter, B. Bosmans, Z. Rahhab, N. E. Faquir, Y. Watanabe, P. Segers, B. Verhegghe, B. Chevalier, N. M. Van Mieghem, M. De Beule, P. Mortier and P. P. T. de Jaegere, 'Patient-specific image-based computer simulation for the prediction of valve morphology and calcium displacement after tavi with the medtronic corevalve and the edwards sapien valve', *EuroIntervention*, vol. 11, no. 9, pp. 1044–1052, 2016.

[176] P. de Jaegere, G. De Santis, R. Rodriguez-Olivares, J. Bosmans, N. Bruining, T. Dezutter, Z. Rahhab, N. El Faquir, V. Collas, B. Bosmans, B. Verhegghe, C. Ren, M. Geleinse, C. Schultz, N. van Mieghem, M. De Beule and P. Mortier, 'Patient-specific computer modeling to predict aortic regurgitation after transcatheter aortic valve replacement', *JACC: Cardiovascular Interventions*, vol. 9, no. 5, pp. 508–512, 2016.

[177] F. Sturla, M. Ronzoni, M. Vitali, A. Dimasi, R. Vismara, G. Preston-Maher, G. Burriesci, E. Votta and A. Redaelli, 'Impact of different aortic valve calcification patterns on the outcome of transcatheter aortic valve implantation: A finite element study', *J Biomech*, vol. 49, no. 12, pp. 2520–30, 2016.

[178] M. Bianchi, G. Marom, R. P. Ghosh, H. A. Fernandez, J. Taylor J. R., M. J. Slepian and D. Bluestein, 'Effect of balloon-expandable transcatheter aortic valve replacement positioning: A patient-specific numerical model', *Artif Organs*, vol. 40, no. 12, E292–e304, 2016.

[179] B. Bosmans, N. Famaey, E. Verhoelst, J. Bosmans and J. Vander Sloten, 'A validated methodology for patient specific computational modeling of self-expandable transcatheter aortic valve implantation', *J Biomech*, vol. 49, no. 13, pp. 2824–2830, 2016.

[180] E. A. Ovcharenko, K. U. Klyshnikov, A. E. Yuzhalin, G. V. Savrasov, A. N. Kokov, A. V. Batranin, V. I. Ganyukov and Y. A. Kudryavtseva, 'Modeling of transcatheter aortic valve replacement: Patient specific vs general approaches based on finite element analysis', *Comput Biol Med*, vol. 69, pp. 29–36, 2016.

[181] W. Wu, D. Pott, B. Mazza, T. Sironi, E. Dordoni, C. Chiastra, L. Petrini, G. Pennati, G. Dubini, U. Steinseifer, S. Sonntag, M. Kuetting and F. Migliavacca, 'Fluid-structure interaction model of a percutaneous aortic valve: Comparison with an in vitro test and feasibility study in a patient-specific case', *Ann Biomed Eng*, vol. 44, no. 2, pp. 590–603, 2016.

[182] A. Finotello, S. Morganti and F. Auricchio, 'Finite element analysis of tavi: Impact of native aortic root computational modeling strategies on simulation outcomes', *Med Eng Phys*, vol. 47, pp. 2–12, 2017.

[183] K. Vahidkhah, M. Abbasi, M. Barakat, P. N. Azadani, A. Tandar, D. Dvir and A. N. Azadani, 'Effect of reduced cardiac output on blood stasis on transcatheter aortic valve leaflets: Implications for valve thrombosis', *EuroIntervention*, vol. 13, no. 7, pp. 811–819, 2017.

[184] K. Vahidkhah and A. N. Azadani, 'Supra-annular valve-in-valve implantation reduces blood stasis on the transcatheter aortic valve leaflets', *J Biomech*, vol. 58, pp. 114–122, 2017.

[185] K. Vahidkhah, S. Javani, M. Abbasi, P. N. Azadani, A. Tandar, D. Dvir and A. N. Azadani, 'Blood stasis on transcatheter valve leaflets and implications for valve-in-valve leaflet thrombosis', *Ann Thorac Surg*, vol. 104, no. 3, pp. 751–759, 2017.

[186] G. M. Bosi, C. Capelli, M. H. Cheang, N. Delahunty, M. Mullen, A. M. Taylor and S. Schievano, 'Population-specific material properties of the implantation site for transcatheter aortic valve replacement finite element simulations', *J Biomech*, vol. 71, pp. 236–244, 2018.

[187] O. M. McGee, P. S. Gunning, A. McNamara and L. M. McNamara, 'The impact of implantation depth of the lotus valve on mechanical stress in close proximity to the bundle of his', *Biomech Model Mechanobiol*, 2018.

[188] M. Bianchi, G. Marom, R. P. Ghosh, O. M. Rotman, P. Parikh, L. Gruberg and D. Bluestein, 'Patient-specific simulation of transcatheter aortic valve replacement: Impact of deployment options on paravalvular leakage', *Biomech Model Mechanobiol*, 2018.

[189] W. Mao, Q. Wang, S. Kodali and W. Sun, 'Numerical parametric study of paravalvular leak following a transcatheter aortic valve deployment into a patient-specific aortic root', *J Biomech Eng*, vol. 140, no. 10, 2018.

[190] H. S. Kandail, S. D. Trivedi, A. C. Shaikh, T. K. Bajwa, D. P. O'Hair, A. Jahangir and J. LaDisa J. F., 'Impact of annular and supra-annular corevalve deployment locations on aortic and coronary artery hemodynamics', *J Mech Behav Biomed Mater*, vol. 86, pp. 131–142, 2018.

[191] S. Tzamtzis, J. Viquerat, J. Yap, M. J. Mullen and G. Burriesci, 'Numerical analysis of the radial force produced by the medtronic-corevalve and edwards-sapien after transcatheter aortic valve implantation (tavi)', *Med Eng Phys*, vol. 35, no. 1, pp. 125–30, 2013.

[192] J. Brouwer, L. Gheorghe, V. J. Nijenhuis, J. M. Ten Berg, B. Rensing, J. A. S. van der Heyden and M. J. Swaans, 'Insight on patient specific computer modeling of transcatheter aortic valve implantation in patients with bicuspid aortic valve disease', *Catheter Cardiovasc Interv*, 2018.

[193] G. Rocatello, N. El Faquir, G. De Santis, F. Iannaccone, J. Bosmans, O. De Backer, L. Sondergaard, P. Segers, M. De Beule, P. de Jaegere and P. Mortier, 'Patient-specific computer simulation to elucidate the role of contact pressure in the development of new conduction abnormalities after catheter-based implantation of a self-expanding aortic valve', *Circ Cardiovasc Interv*, vol. 11, no. 2, e005344, 2018.

[194] D. Mylotte, R. L. Osnabrugge, S. Windecker, T. Lefevre, P. De Jaegere, R. Jeger, P. Wenaweser, F. Maisano, N. Moat and L. Sondergaard, 'Tct-752 transcatheter aortic valve replacement in europe: The 2013 update', *Journal of the American College of Cardiology*, vol. 62, no. 18, B229, 2013.

[195] V. H. Thourani, S. Kodali, R. R. Makkar, H. C. Herrmann, M. Williams, V. Babaliaros, R. Smalling, S. Lim, S. C. Malaisrie, S. Kapadia, W. Y. Szeto, K. L. Greason, D. Kereiakes, G. Ailawadi, B. K. Whisenant, C. Devireddy, J. Leipsic, R. T. Hahn, P. Pibarot, N. J. Weissman, W. A. Jaber, D. J. Cohen, R. Suri, E. M. Tuzcu, L. G. Svensson, J. G. Webb, J. W. Moses, M. J. Mack, D. C. Miller, C. R. Smith, M. C. Alu, R. Parvataneni, J. D'Agostino R. B. and M. B. Leon, 'Transcatheter aortic valve replacement versus surgical valve replacement in intermediate-risk patients: A propensity score analysis', *Lancet*, vol. 387, no. 10034, pp. 2218–25, 2016.

[196] R. M. van der Boon, P. Houthuizen, M. Urena, T. T. Poels, N. M. van Mieghem, G. R. Brueren, S. Altintas, R. J. Nuis, P. W. Serruys, L. A. van Garsse, R. T. van Domburg, J. R. Cabau, P. P. de Jaegere and F. W. Prinzen, 'Trends in the occurrence of new conduction abnormalities after transcatheter aortic valve implantation', *Catheter Cardiovasc Interv*, vol. 85, no. 5, E144–52, 2015.

[197] P. Houthuizen, L. A. Van Garsse, T. T. Poels, P. de Jaegere, R. M. van der Boon, B. M. Swinkels, J. M. Ten Berg, F. van der Kley, M. J. Schalij, J. Baan J., R. Cocchieri, G. R. Brueren, A. H. van Straten, P. den Heijer, M. Bentala, V. van Ommen, J. Kluin, P. R. Stella, M. H. Prins, J. G. Maessen and F. W. Prinzen, 'Left bundle-branch block induced by transcatheter aortic valve implantation increases risk of death', *Circulation*, vol. 126, no. 6, pp. 720–8, 2012.

[198] C. Moris and J. M. Rubin, 'Conduction disorders and transcatheter aortic valve. clinically relevant or just a mild complication?', *Rev Esp Cardiol (Engl Ed)*, vol. 66, no. 9, pp. 692–4, 2013.

[199] J. J. Bax, V. Delgado, V. Bapat, H. Baumgartner, J. P. Collet, R. Erbel, C. Hamm, A. P. Kappetein, J. Leipsic, M. B. Leon, P. MacCarthy, N. Piazza, P. Pibarot, W. C. Roberts, J. Rodes-Cabau, P. W. Serruys, M. Thomas, A. Vahanian, J. Webb, J. L. Zamorano and S. Windecker, 'Open issues in transcatheter aortic valve implantation. part 2: Procedural issues and outcomes after transcatheter aortic valve implantation', *Eur Heart J*, vol. 35, no. 38, pp. 2639–54, 2014.

[200] R. J. Nuis, N. M. Van Mieghem, C. J. Schultz, A. Tzikas, R. M. Van der Boon, A. M. Maugenest, J. Cheng, N. Piazza, R. T. van Domburg, P. W. Serruys and P. P. de Jaegere, 'Timing and potential mechanisms of new conduction abnormalities during the implantation of the medtronic corevalve system in patients with aortic stenosis', *Eur Heart J*, vol. 32, no. 16, pp. 2067–74, 2011.

[201] G. K. Massing and T. N. James, 'Anatomical configuration of the his bundle and bundle branches in the human heart', *Circulation*, vol. 53, no. 4, pp. 609–21, 1976.

[202] N. Piazza, P. de Jaegere, C. Schultz, A. E. Becker, P. W. Serruys and R. H. Anderson, 'Anatomy of the aortic valvar complex and its implications for transcatheter implantation of the aortic valve', *Circ Cardiovasc Interv*, vol. 1, no. 1, pp. 74–81, 2008.

[203] T. Kawashima and F. Sato, 'Visualizing anatomical evidences on atrioventricular conduction system for tavi', *Int J Cardiol*, vol. 174, no. 1, pp. 1–6, 2014.

[204] W. J. Youden, 'Index for rating diagnostic tests', *Cancer*, vol. 3, no. 1, pp. 32–5, 1950.

[205] N. Piazza, R. J. Nuis, A. Tzikas, A. Otten, Y. Onuma, H. Garcia-Garcia, C. Schultz, R. van Domburg, G. A. van Es, R. van Geuns, P. de Jaegere and P. W. Serruys, 'Persistent conduction abnormalities and requirements for pacemaking six months after transcatheter aortic valve implantation', *EuroIntervention*, vol. 6, no. 4, pp. 475–84, 2010.

[206] M. Urena, M. Mok, V. Serra, E. Dumont, L. Nombela-Franco, R. DeLarochelliere, D. Doyle, A. Igual, E. Larose, I. Amat-Santos, M. Cote, H. Cuellar, P. Pibarot, P. de Jaegere, F. Philippon, B. Garcia del Blanco and J. Rodes-Cabau, 'Predictive factors and long-term clinical consequences of persistent left bundle branch block following transcatheter aortic valve implantation with a balloon-expandable valve', *J Am Coll Cardiol*, vol. 60, no. 18, pp. 1743–52, 2012.

[207] G. Mouillet, N. Lellouche, P. Lim, K. Meguro, M. Yamamoto, J. F. Deux, J. L. Monin, E. Bergoend, J. L. Dubois-Rande and E. Teiger, 'Patients without prolonged qrs after tavi with corevalve device do not experience high-degree atrio-ventricular block', *Catheter Cardiovasc Interv*, vol. 81, no. 5, pp. 882–7, 2013.

[208] E. Pereira, N. Ferreira, D. Caeiro, J. Primo, L. Adao, M. Oliveira, H. Goncalves, J. Ribeiro, E. Santos, D. Leite, N. Bettencourt, P. Braga, L. Simoes, L. Vouga and V. Gama, 'Transcatheter aortic valve implantation and requirements of pacing over time', *Pacing Clin Electrophysiol*, vol. 36, no. 5, pp. 559–69, 2013.

[209] N. Smith, A. de Vecchi, M. McCormick, D. Nordsletten, O. Camara, A. F. Frangi, H. Delingette, M. Sermesant, J. Relan, N. Ayache, M. W. Krueger, W. H. Schulze, R. Hose, I. Valverde, P. Beerbaum, C. Staicu, M. Siebes, J. Spaan, P. Hunter, J. Weese, H. Lehmann, D. Chapelle and R. Rezavi, 'Euheart: Personalized and integrated cardiac care using patient-specific cardiovascular modelling', *Interface Focus*, vol. 1, no. 3, pp. 349–64, 2011.

[210] P. Kirchhof, K. R. Sipido, M. R. Cowie, T. Eschenhagen, K. A. Fox, H. Katus, S. Schroeder, H. Schunkert and S. Priori, 'The continuum of personalized cardiovascular medicine: A position paper of the european society of cardiology', *Eur Heart J*, vol. 35, no. 46, pp. 3250–7, 2014.

[211] R. A. Nishimura, C. M. Otto, R. O. Bonow, B. A. Carabello, J. P. Erwin, R. A. Guyton, P. T. O'Gara, C. E. Ruiz, N. J. Skubas, P. Sorajja, T. M. Sundt and J. D. Thomas, '2014 aha/acc guideline for the management of patients with valvular heart disease: Executive summary', *A Report of the American College of Cardiology/American Heart Association Task Force on Practice Guidelines*, vol. 129, pp. 2440–2492, 2014.

[212] B. Bosmans, V. Collas, E. Verhoelst, B. Paelinck, J. Vander Sloten and J. Bosmans, 'Morphological characteristics and calcification of the native aortic valve and the relation to significant aortic regurgitation after corevalve tavi', *J Heart Valve Dis*, vol. 25, no. 4, pp. 410–416, 2016.

[213] L. van Gils, J. Wohrle, D. Hildick-Smith, S. Bleiziffer, D. J. Blackman, M. Abdel-Wahab, U. Gerckens, S. Brecker, V. Bapat, T. Modine, O. I. Soliman, A. Nersesov, D. Allocco, V. Falk and N. M. Van Mieghem, 'Importance of contrast aortography with lotus transcatheter aortic valve replacement: A post hoc analysis from the respond post-market study', *JACC Cardiovasc Interv*, vol. 11, no. 2, pp. 119–128, 2018.

[214] V. M. Collas, B. P. Paelinck, I. E. Rodrigus, C. J. Vrints and J. M. Bosmans, 'Aortic regurgitation after transcatheter aortic valve implantation (tavi); angiographic, echocardiographic and hemodynamic assessment in relation to one year outcome', *International Journal of Cardiology*, vol. 194, pp. 13–20, 2015.

[215] B. Ren, C. Schultz, L. van Gils, N. M. Van Mieghem, P. P. de Jaegere, T. W. Galema, W. B. Vletter, M. L. Geleijnse, L. F. Di Martino, O. I. Soliman and M. Di Biase, 'Relation between calcium burden, echocardiographic stent frame eccentricity and paravalvular leakage after corevalve transcatheter aortic valve implantation', *European Heart Journal - Cardiovascular Imaging*, vol. 18, no. 6, pp. 648–653, 2017.

[216] C. J. Schultz, T. L. B. Slots, G. Yong, J.-P. Aben, N. M. Van Mieghem, M. J. Swaans, Z. Rahhab, N. E. Faquir, R. J. van Geuns, G. Mast, F. Zijlstra and P. P. T. de Jaegere, 'An objective and reproducible method for quantification of aortic regurgitation after tavi', *EuroIntervention*, vol. 10, no. 3, pp. 355–363, 2014.

[217] J. Bailey, N. Curzen and N. W. Bressloff, 'The impact of imperfect frame deployment and rotational orientation on stress within the prosthetic leaflets during transcatheter aortic valve implantation', *J Biomech*, vol. 53, pp. 22–28, 2017.

[218] G. C. M. Siontis, F. Praz, T. Pilgrim, D. Mavridis, S. Verma, G. Salanti, L. Søndergaard, P. Jüni and S. Windecker, 'Transcatheter aortic valve implantation vs. surgical aortic valve replacement for treatment of severe aortic stenosis: A meta-analysis of randomized trials', *European Heart Journal*, vol. 37, no. 47, pp. 3503–3512, 2016.

[219] P. Blanke, J. Reinohl, C. Schlensak, M. Siepe, G. Pache, W. Euringer, A. Geibel-Zehender, C. Bode, M. Langer, F. Beyersdorf and M. Zehender, 'Prosthesis oversizing in balloon-expandable transcatheter aortic valve implantation is associated with contained rupture of the aortic root', *Circ Cardiovasc Interv*, vol. 5, no. 4, pp. 540–8, 2012.

[220] N. Debry, A. Sudre, I. Elquodeimat, C. Delhaye, G. Schurtz, A. Bical, M. Koussa, K. Fattouch and T. Modine, 'Prognostic value of the ratio between prosthesis area and indexed annulus area measured by multislice-ct for transcatheter aortic valve implantation procedures', *J Geriatr Cardiol*, vol. 13, no. 6, pp. 483–8, 2016.

[221] M. A. Sherif, M. Abdel-Wahab, B. Stöcker, V. Geist, D. Richardt, R. Tölg and G. Richardt, 'Anatomic and procedural predictors of paravalvular aortic regurgitation after implantation of the medtronic corevalve bioprosthesis', *Journal of the American College of Cardiology*, vol. 56, no. 20, pp. 1623–1629, 2010.

[222] A. G. Cerillo, M. Mariani, S. Berti and M. Glauber, 'Sizing the aortic annulus', *Ann Cardiothorac Surg*, vol. 1, no. 2, pp. 245–56, 2012.

[223] D. J. Blackman, I. T. Meredith, N. Dumonteil, D. Tchetche, D. Hildick-Smith, M. S. Spence, D. L. Walters, J. Harnek, S. G. Worthley, G. Rioufol, T. Lefevre, V. M. Houle, D. J. Allocco and K. D. Dawkins, 'Predictors of paravalvular regurgitation after implantation of the fully repositionable and retrievable lotus transcatheter aortic valve (from the reprise ii trial extended cohort)', *Am J Cardiol*, vol. 120, no. 2, pp. 292–299, 2017.

[224] T. M. Morrison, M. L. Dreher, S. Nagaraja, L. M. Angelone and W. Kainz, 'The role of computational modeling and simulation in the total product life cycle of peripheral vascular devices', *Journal of medical devices*, vol. 11, no. 2, p. 024 503, 2017.

[225] S. Pant, N. W. Bressloff and G. Limbert, 'Geometry parameterization and multidisciplinary constrained optimization of coronary stents', *Biomech Model Mechanobiol*, vol. 11, no. 1-2, pp. 61–82, 2012.

[226] S. Pant, G. Limbert, N. P. Curzen and N. W. Bressloff, 'Multiobjective design optimisation of coronary stents', *Biomaterials*, vol. 32, no. 31, pp. 7755–73, 2011.

[227] G. Alaimo, F. Auricchio, M. Conti and M. Zingales, 'Multi-objective optimization of nitinol stent design', *Med Eng Phys*, vol. 47, pp. 13–24, 2017.

[228] H. Li, T. Liu, M. Wang, D. Zhao, A. Qiao, X. Wang, J. Gu, Z. Li and B. Zhu, 'Design optimization of stent and its dilatation balloon using kriging surrogate model', *BioMedical Engineering OnLine*, vol. 16, no. 1, p. 13, 2017.

[229] H. Li, T. Qiu, B. Zhu, J. Wu and X. Wang, 'Design optimization of coronary stent based on finite element models', *ScientificWorldJournal*, vol. 2013, p. 630 243, 2013.

[230] T. J. Gundert, A. L. Marsden, W. Yang and J. LaDisa J. F., 'Optimization of cardiovascular stent design using computational fluid dynamics', *J Biomech Eng*, vol. 134, no. 1, p. 011 002, 2012.

[231] F. Migliavacca, L. Petrini, V. Montanari, I. Quagliana, F. Auricchio and G. Dubini, 'A predictive study of the mechanical behaviour of coronary stents by computer modelling', *Med Eng Phys*, vol. 27, no. 1, pp. 13–8, 2005.

[232] N. K. Putra, P. S. Palar, H. Anzai, K. Shimoyama and M. Ohta, 'Multiobjective design optimization of stent geometry with wall deformation for triangular and rectangular struts', *Med Biol Eng Comput*, 2018.

[233] H. Li, J. Gu, M. Wang, D. Zhao, Z. Li, A. Qiao and B. Zhu, 'Multi-objective optimization of coronary stent using kriging surrogate model', *Biomed Eng Online*, vol. 15, no. Suppl 2, p. 148, 2016.

[234] N. Li, H. Zhang and H. Ouyang, 'Shape optimization of coronary artery stent based on a parametric model', *Finite Elem. Anal. Des.*, vol. 45, no. 6-7, pp. 468–475, 2009.

[235] S. Kodali, P. Pibarot, P. S. Douglas, M. Williams, K. Xu, V. Thourani, C. S. Rihal, A. Zajarias, D. Doshi, M. Davidson, E. M. Tuzcu, W. Stewart, N. J. Weissman, L. Svensson, K. Greason, H. Maniar, M. Mack, S. Anwaruddin, M. B. Leon and R. T. Hahn, 'Paravalvular regurgitation after transcatheter aortic valve replacement with the edwards sapien valve in the partner trial: Characterizing patients and impact on outcomes', *Eur Heart J*, vol. 36, no. 7, pp. 449–56, 2015.

[236] M. Gessat, L. Altwegg, T. Frauenfelder, A. Plass and V. Falk, 'Cubic hermite bezier spline based reconstruction of implanted aortic valve stents from ct images', *Conf Proc IEEE Eng Med Biol Soc*, vol. 2011, pp. 2667–70, 2011.

[237] D. M. Allen, 'The relationship between variable selection and data agumentation and a method for prediction', *Technometrics*, vol. 16, no. 1, pp. 125–127, 1974.

[238] K. Schittkowski, 'Nlpql: A fortran subroutine solving constrained nonlinear programming problems', *Annals of Operations Research*, vol. 5, no. 2, pp. 485–500, 1986.

[239] K. J. Grande, R. P. Cochran, P. G. Reinhall and K. S. Kunzelman, 'Stress variations in the human aortic root and valve: The role of anatomic asymmetry', *Ann Biomed Eng*, vol. 26, no. 4, pp. 534–45, 1998.

[240] Y. Sahasakul, W. D. Edwards, J. M. Naessens and A. J. Tajik, 'Age-related changes in aortic and mitral valve thickness: Implications for two-dimensional echocardiography based on an autopsy study of 200 normal human hearts', *The American Journal of Cardiology*, vol. 62, no. 7, pp. 424–430, 1988.

[241] A. Halapas, M. Chrissoheris, N. Bouboulis, J. Nicolaou, S. Pattakos and K. Spargias, 'Update on current tavi technology, indications, screening, and outcomes', *Continuing Cardiology Education*, vol. 2, no. 1, pp. 37–46, 2016.